

Exploring cellular stress responses: HspB1 and autophagy

By

© Joseph-Patrick William Edward Clarke

A thesis submitted to the School of Graduate Studies in partial fulfillment of the requirements for  
the degree of Doctor of Philosophy

Division of BioMedical Sciences

Faculty of Medicine

Memorial University of Newfoundland

May 2016

## **Abstract**

Through an understanding of the innate mechanisms that neurons undertake when they undergo episodes of stress, we can develop effective strategies and treatments that ultimately prevent neuron death and promote neuron survival and neurite growth. In this study, the overall objectives were to investigate how the innate cellular mechanisms of both the heat stress response and autophagy promote survival in neurons during episodes of cell stress.

Chapter 2 focuses upon the interaction dynamics between heat shock protein B1 (HspB1) and filamentous actin (F-actin) in stressed cells. This study demonstrates that under non-stressed conditions HspB1 interacts with F-actin as a non-phosphorylated protein, but after heat stress, both phosphorylated and non-phosphorylated forms of HspB1 interact with F-actin. Furthermore, by inhibiting HspB1 phosphorylation during heat stress, there is attenuation in the interaction between phosphorylated HspB1 and F-actin. This study was the first to show the interaction differences between the phosphorylated and non-phosphorylated forms of HspB1 with F-actin using an endogenous HspB1 expressing model.

Chapter 3 explores the interaction between HspB1 and death-associated protein 6 (Daxx) in dorsal root ganglion (DRG) neurons, and how this interaction could influence autophagic activity. This study demonstrates that high glucose cell stress in DRG neurons affects the mRNA expression and the cellular localization of Daxx, HspB1 and B-cell lymphoma 2 protein (Bcl-2). Subsequent changes in autophagic activity associated with the changes found in Daxx, HspB1 or Bcl-2 expression, however, were not detected. Overall, the experimental results observed in this study can be used as a basis for further research into this topic.

Chapter 4, 5 and 6 focus on how the process of autophagy affects DRG neuron survival and neurite growth. These studies demonstrate that adult rat DRG neurons activate autophagy when exposed to the stressful conditions of nutrient starvation and hydrogen peroxide. Furthermore, treatment with 3-methyladenine (3-MA) inhibits both endogenous and stress activated autophagy, while treatment with rapamycin does not further activate autophagy past levels obtained by stressful conditions. Additionally, inhibition of autophagy with 3-MA resulted in a reduction in cell survival, neurite growth, branching and initiation from the cell soma. Overall, these results suggest that autophagic activity plays a significant role in DRG survival and neurite growth.

## Acknowledgements

First and foremost, I wish to wholeheartedly thank my supervisor and mentor Dr. Karen M. Mearow. Without her support, encouragement and advice I would not be where I am today; finishing my Ph.D. and ready to further my career in scientific research. Thank you for allowing me the opportunities to attend top tier conferences, to publish my findings from my research, and to complete my Ph.D. in your laboratory. It may not have been a smooth sail throughout my entire time in your lab, but thanks to your extreme patience and focus you were able to guide me to the light at the end of the tunnel. Again, thank you.

I would also like to extend a warm thank you to Firoozeh Nafar. Without her support, encouragement, and advice I do not think I would have survived during my Ph.D. She was an immense help technically and a great friend.

I must also thank my past lab mates for their support, encouragement and advice. Thank you Mike, Megan, Neva and Brad for your technical support, encouragement, advice and friendship. It was a great professional and personal experience working with you all.

I wish to also thank Dr.'s Jules Doré and Daniel MacPhee, who served as members of my supervisory committee for their guidance, encouragement, advice and support.

I would like to acknowledge the support of the National Sciences and Engineering Research Council for funding my experiments and Ph.D.

Finally, I would like to thank my parents. I thank them for their unwavering support and encouragement throughout my Ph.D. Without them, I would not be where I am today.

## Table of Contents

Abstract.....	i
Acknowledgements.....	iii
List of Figures.....	xi
List of Tables.....	xiii
List of Abbreviations.....	xiv
List of Appendices.....	xvii
Chapter 1: Introduction.....	1
1.1    Endogenously activated cellular mechanisms that promote survival during stress.....	1
1.1.1    Heat shock protein response.....	2
1.1.1.1    Small heat shock proteins.....	3
1.1.1.1.1    Heat shock protein B1 (HspB1).....	4
1.1.1.1.1.1    HspB1 domains and structure.....	5
1.1.1.1.1.2    HspB1 phosphorylation.....	6
1.1.1.1.1.3    Cell survival and HspB1.....	9
1.1.1.1.1.4    Neuron survival and HspB1.....	11
1.1.1.1.1.5    Neurite growth and HspB1.....	12
1.1.1.1.1.5.1    Microfilament growth and stability with HspB1.....	13
1.1.1.1.1.6    HspB1 and DRG neuron survival.....	17
1.1.1.1.1.7    Peripheral neuropathy and HspB1.....	18
1.1.2    The potential involvement of HspB1 in other cell stress pathways.....	19
1.1.3    Autophagy.....	25

1.1.3.1	Mammalian target of rapamycin (mTOR).....	26
1.1.3.1.1	Regulation of mTOR activity .....	30
1.1.3.2	The autophagic process .....	31
1.1.3.3	Pharmacological modulation of autophagy .....	35
1.1.3.3.1	Autophagic flux .....	36
1.1.3.4	Autophagy and neurodegenerative diseases .....	37
	Hypothesis and Objectives.....	39
	Co-authorship statement .....	42
	Chapter 2: Cell stress promotes the association of phosphorylated HspB1 with F-actin.....	44
2.1	Abstract .....	44
2.2	Introduction .....	45
2.3	Materials and Methods .....	48
2.3.1	Reagents and Antibodies.....	48
2.3.2	Cell Cultures and Treatments.....	48
2.3.3	In vitro F/G-Actin and Biotinylated-Phalloidin Pull-down .....	50
2.3.4	Pull-Down Assay – cellular samples .....	51
2.3.5	Biochemical Analysis of Protein Fractions and Pull-Downs.....	52
2.3.6	Immunocytochemistry of PC12 Cells.....	53
2.3.7	3-Dimensional Imaging of Cellular Expression .....	53
2.3.8	Densitometric and Statistical Analysis .....	54
2.4	Results .....	54
2.4.1	Cellular distribution of total HspB1 and phosphorylated HspB1 .....	54
2.4.2	Biochemical Assessment of HspB1 and F-actin distribution with stress: .....	63

2.4.3	Determining the interaction(s) of HspB1 and F-actin.....	68
2.4.3.1	Pull-Down and Immunoprecipitation assays.....	68
2.5	Discussion .....	79
2.5.1	HspB1 interactions with actin.....	79
2.5.2	Role of HspB1 and actin interactions in unstressed cells: .....	80
2.5.3	Role of HspB1 in cytoskeletal protection: .....	82
2.6	Conclusions:.....	85
2.7	Acknowledgements:.....	86
 Chapter 3: Exploring the Link between HspB1, Daxx, Bcl-2 and Autophagic Activity in DRG		
Neurons.....		
3.1	Abstract .....	87
3.2	Introduction .....	88
3.3	Materials and Methods.....	90
3.3.1	Reagents and Antibodies.....	90
3.3.2	Ethics Statement.....	91
3.3.3	DRG Isolation and Plating .....	91
3.3.4	Quantitative Real-Time PCR (qRT-PCR) of DRG Neurons .....	93
3.3.5	Immunocytochemistry of DRG Neurons .....	94
3.3.6	Immunohistochemistry of DRG Neurons .....	95
3.3.7	Densitometric Analysis.....	95
3.4	Results .....	96
3.4.1	HspB1, Daxx, Bcl-2, HMGB1 and LC3B are endogenously expressed in adult DRG neurons.....	96

3.4.2	A High Glucose Environment Alters HspB1, Daxx and Bcl-2 RNA Expression in DRG Neurons .....	101
3.4.3	Expression and Localization of Daxx and HspB1 is Altered in DRG Neurons Treated with High Glucose - Immunocytochemistry .....	101
3.5	Discussion .....	104
3.6	Acknowledgements: .....	109
Chapter 4: Autophagy Inhibition in Endogenous and Nutrient Deprived Conditions Reduces DRG Neuron Survival and Neurite Growth <i>In Vitro</i> .....		
DRG Neuron Survival and Neurite Growth <i>In Vitro</i> .....		
4.1	Abstract .....	110
4.2	Introduction .....	110
4.3	Materials and Methods .....	113
4.3.1	Reagents and Antibodies.....	113
4.3.2	Ethics Statement.....	115
4.3.3	DRG Isolation and Plating .....	115
4.3.4	MTS Cell Viability Assay.....	116
4.3.5	Isolation and Biochemical Analysis of Protein Fractions.....	116
4.3.6	Immunocytochemistry of DRG Neurons .....	117
4.3.7	Densitometric and Statistical Analysis .....	118
4.4	Results .....	119
4.4.1	Nutrient Deprivation Alters Constitutive Autophagy in DRG Neurons.....	119
4.4.2	Autophagy Inhibition Reduces DRG Neuron Viability.....	120
4.4.3	Inhibiting Autophagy Decreases Autophagy Related Proteins in DRG Neurons.	127
4.4.4	DRG Growth Morphology Is Negatively Altered With Autophagy Inhibition....	135

4.5	Discussion .....	147
4.5.1	Autophagy and Neuronal Cell Survival.....	147
4.5.2	Modulation of Autophagy.....	150
4.5.3	Autophagy and Neurite Growth.....	151
4.6	Conclusion.....	155
4.7	Acknowledgements .....	155
Chapter 5: Autophagy Inhibition in Endogenous and Increased Reactive Oxygen Species		
Conditions Reduces DRG Neuron Survival and Growth <i>In Vitro</i> .....		
5.1	Abstract .....	156
5.2	Introduction .....	156
5.3	Materials and Methods.....	158
5.3.1	Reagents and Antibodies.....	158
5.3.2	Ethics Statement.....	160
5.3.3	DRG Isolation and Plating.....	160
5.3.4	MTS Cell Viability Assay.....	161
5.3.5	Isolation and Biochemical Analysis of Protein Fractions.....	161
5.3.6	Immunocytochemistry and Oxidative Stress Analysis of DRG Neurons.....	162
5.3.7	Densitometric and Statistical Analysis .....	163
5.4	Results .....	164
5.4.1	H <sub>2</sub> O <sub>2</sub> Causes Oxidative Stress in DRG Neurons .....	164
5.4.2	Autophagy Inhibition in Conjunction with H <sub>2</sub> O <sub>2</sub> Treatment Reduces DRG Neuron Viability.....	167

5.4.3	Inhibiting Autophagy in Conjunction with H <sub>2</sub> O <sub>2</sub> Treatment Decreases Autophagy Related Proteins in DRG Neurons.....	168
5.4.4	DRG Growth Morphology Is Negatively Altered With Autophagy Inhibition in Conjunction with H <sub>2</sub> O <sub>2</sub> Treatment .....	171
5.5	Discussion .....	176
5.5.1	Autophagy and Neuronal Cell Survival.....	179
5.5.2	Autophagy and Neurite Growth.....	180
5.6	Conclusion.....	181
5.7	Acknowledgements .....	181
Chapter 6: Autophagy Inhibition Alters DRG Neurite Growth Initiation <i>In Vitro</i> .....		182
6.1	Abstract .....	182
6.2	Introduction .....	182
6.3	Materials and Methods.....	184
6.3.1	Reagents and Antibodies.....	184
6.3.2	Ethics Statement.....	186
6.3.3	DRG Isolation, Plating and Immunocytochemistry .....	186
6.4	Results .....	187
6.4.1	Inhibition of Autophagy Suppresses DRG Neurite Growth Initiation.....	187
6.4.2	Autophagy Inhibition Reduces IB <sub>4</sub> -Positive DRG Neurite Growth .....	195
6.5	Discussion .....	196
6.6	Conclusion.....	202
6.7	Acknowledgements .....	203
Chapter 7: Discussion and Future Directions .....		204

7.1	Research Outcomes and Future Directions .....	204
7.1.1	The effect(s) of stress induced HspB1 phosphorylation on its interaction(s) with filamentous actin .....	204
7.1.2	The potential role HspB1 has on the process of autophagy .....	208
7.1.3	The effects of autophagy on DRG neuron survival and neurite growth .....	210
7.2	Conclusion.....	213
	References.....	215
	Appendix.....	242

## List of Figures

Figure 1.1: Structure, phosphorylation and oligomerization of HspB1.....	7
Figure 1.2: Diagrammatic representation of HspB1 interactions with actin. ....	15
Figure 1.3: The potential interaction between HspB1, Daxx and Autophagy. ....	22
Figure 1.4: mTORC1 and mTORC2 cellular effects. ....	28
Figure 1.5: The process and pharmacological regulation of autophagy. ....	33
Figure 2.1: Cellular localization of HspB1 and F-actin in control PC12 cells. ....	56
Figure 2.2: Cellular localization of HspB1 and F-actin in PC12 cells subsequent to a heat shock. .....	58
Figure 2.3: Cellular localization of HspB1 and F-actin in PC12 cells subsequent to a heat shock in the presence of a p38-MAPK inhibitor. ....	60
Figure 2.4: HspB1 is phosphorylated and redistributed to the cytoskeletal fraction during cellular stress. ....	66
Figure 2.5: Specificity of the phalloidin pull-down for F-actin. ....	70
Figure 2.6: HspB1 is associated with F-actin. ....	72
Figure 2.7: Densitometric analyses of the amounts of F-actin and HspB1 in the precipitated complexes. ....	74
Figure 2.8: Changes in the relative amounts of the association of F-actin and HspB1. ....	77
Figure 3.1: Expression of HspB1, Bcl-2, HMGB1 and LC3B in adult rat DRG neurons.....	97
Figure 3.2: Expression of HspB1, Bcl-2, HMGB1 and LC3B and Daxx in adult rat DRG neurons. ....	99
Figure 3.3: mRNA expression of HspB1, Daxx and Bcl-2 is altered with high glucose treatment in DRG neurons. ....	102
Figure 3.4: Confocal imaging of endogenous localization and expression of HspB1, Daxx, Bcl-2, HMGB1 and LC3B in untreated and high glucose treated DRG neurons. ....	105
Figure 4.1: Constitutive autophagy in adult DRG neurons can be modulated with nutrient deprivation and pharmacological treatment. ....	121
Figure 4.2: Constitutive autophagy in adult DRG neurons can be modulated with nutrient deprivation and pharmacological treatment. ....	123
Figure 4.3: Alterations in constitutive autophagy with nutrient deprivation and pharmacological treatment are a result of changes in autophagic flux. ....	125
Figure 4.4: DRG cell viability is reduced with treatment of either 3-MA or BA1 in control and nutrient deprived conditions. ....	128
Figure 4.5: Autophagy related proteins are reduced with 3-MA treatment in nutrient control conditions. ....	131
Figure 4.6: Autophagy is activated by nutrient deprivation conditions, while inhibited with subsequent 3-MA treatment. ....	133
Figure 4.7: DRG neurite length and branching complexity are reduced with autophagy inhibition in nutrient control conditions. ....	137
Figure 4.8: DRG neurite growth is reduced after 3, 16 and 24 hr treatment with 3-MA in nutrient control conditions. ....	139
Figure 4.9: DRG neurite length and branching complexity are reduced with autophagy inhibition in nutrient deprived (HBSS) conditions. ....	141
Figure 4.10: DRG neurite growth is reduced after 3, 16 and 24 hr treatment with 3-MA in nutrient deprived (HBSS) conditions. ....	143

Figure 4.11: Autophagy inhibition reduces autophagosome occurrence in DRG neurites.....	145
Figure 5.1: H <sub>2</sub> O <sub>2</sub> treatment causes oxidative stress in DRG neurons. ....	165
Figure 5.2: Autophagy is activated with increased reactive oxygen species, and inhibited with 3-MA treatment. ....	169
Figure 5.3: DRG neurite length and branching complexity are reduced with autophagy inhibition in increased reactive oxygen species conditions.....	172
Figure 5.4: DRG neurite growth is reduced after 3, 16 and 24 hr treatment with 3-MA in increased reactive oxygen species conditions.....	174
Figure 5.5: Autophagy inhibition reduces autophagosome occurrence in DRG neurites.....	177
Figure 6.1: DRG neurite initiation and branching complexity are reduced with autophagy inhibition. ....	189
Figure 6.2: DRG neurite growth initiation is reduced after 24 hr treatment with 3-MA or BA1. ....	191
Figure 6.3: Autophagy inhibition reduces autophagosomes in DRG neurites.....	193
Figure 6.4: Qualitative measurement of neurite growth in soluble laminin treated IB <sub>4</sub> and non-IB <sub>4</sub> DRG neurons. ....	197
Figure 6.5: Qualitative measurement of neurite growth characteristics in soluble laminin treated small, medium and large DRG neurons.....	199

## List of Tables

Table 1.1: Mutations in HspB1 implicated to cause Charcot-Marie-Tooth disease. ....	20
Table 2.1: List of primary and secondary antibodies, with experimental dilutions, used for immunoblotting (IB), immunocytochemistry (IC) and immunoprecipitation (IP). ....	49
Table 3.1: List of primary and secondary antibodies, with experimental dilutions, used for immunoblotting (IB), immunocytochemistry (IC) and immunohistochemistry (IHC). ....	92
Table 4.1: List of primary and secondary antibodies, with experimental dilutions, used either for immunoblotting (IB) or immunocytochemistry (ICC). ....	114
Table 5.1: List of primary and secondary antibodies, with experimental dilutions, used either for immunoblotting (IB) or immunocytochemistry (ICC). ....	159
Table 6.1: List of primary and secondary antibodies, with experimental dilutions, used either for immunoblotting (IB) or immunocytochemistry (ICC). ....	185

## List of Abbreviations

3D	3 dimensional
3-MA	3-methyladenine
4E-BP1	eukaryotic translation initiation factor binding protein 1
AD	Alzheimer's disease
ADP	adenosine diphosphate
Akt	protein kinase B
AMP	adenosine monophosphate
AMPK $\alpha$	5' adenosine monophosphate-activated protein kinase
APP	amyloid precursor protein
AraC	cytosine arabinoside
Arp2/3	actin-related protein 2/3
ASB	actin stabilization buffer
ATG	autophagy-related protein
BA1	bafilomycin-A1
BAD	Bcl-2-associated death promoter
BCA	bicinchoninic acid
Bcl-2	B-cell lymphoma 2
BDNF	brain-derived neurotrophic factor
BH3	Bcl-2 homology 3
BSA	Bovine serum albumin
CCAC	Canadian Council on Animal Care
cDNA	complimentary DNA
CMT	Charcot-Marie-Tooth disease
CNS	central nervous system
Ct	cycle threshold
DAPI	4',6-diamidino-2-phenylindole
Daxx	death-associated protein 6
DnaJ	heat shock factor 40
DMEM	Dulbecco's Modified Eagle Medium
DNMT	DNA methyltransferase
DPN	diabetic peripheral neuropathy
DRG	dorsal root ganglion
DTT	dithiothreitol
eIF	eukaryotic initiation factor
eIF4E	eukaryotic initiation factor 4E
ETS1	E-twenty-six 1 protein
F-actin	filamentous actin
FdU	5-fluoro-2'-deoxyuridine
FKBP12	tacrolimus (FK506) binding protein 12
FRB	FKBP12-rapamycin binding domain
G-actin	globular actin
GSK3 $\beta$	glycogen synthase kinase-3 $\beta$
GTP	guanosine triphosphate

HBSS	Hank's Balance Salt Solution
HD	Huntington's disease
HDAC	histone deacetylase
HMGB1	high-mobility group protein B1
HS	heat shock
HSE	heat shock element
HSF	heat shock factor
HSP	heat shock protein
HspA	heat shock factor 70; Hsp70
HspA8	heat shock cognate 70; Hsc70
HspB1	heat shock protein B1; Hsp27
HspB1-AA	pseudo-non-phosphorylated HspB1 with alanine mutations
HspB1-EE	pseudo-phosphorylated HspB1 with glutamic acid mutations
HspB5	$\alpha$ B-crystallin
HspB6	heat shock protein 20; Hsp20
HspB8	heat shock protein 22; Hsp22
HspC	heat shock factor 90; Hsp90
HspH	heat shock factor 110; Hsp110
Htt	Huntingtin protein
HV PMTs	high voltage photomultipliers
IACC	Institutional Animal Care Committee of Memorial University of Newfoundland
IB <sub>4</sub>	isolectin B <sub>4</sub>
IB	immunoblot
ICC	immunocytochemistry
IHC	immunohistochemistry
IP	immunoprecipitation
LAMP-2A	lysosomal-associated membrane protein type 2A
LBB	lectin binding buffer
LC3B	microtubule-associated protein 1A/1B light chain 3B; MAP1LC3B; ATG8
mHtt	mutant Htt
MKK2	mitogen-activated protein kinase-associated protein kinase 2
MOMP	mitochondrial outer membrane permeabilization
mTOR	mammalian target of rapamycin
mTORC1/2	mTOR complex 1/2
MTS	3-(4,5-dimethylthiazol-2-yl)-5-(3-carboxymethoxyphenyl)-2-(4-sulfophenyl)-2H-tetrazolium
NGF	nerve growth factor
p38-MAPK	p38 mitogen activated protein kinase
PBS	phosphate buffered saline
PC12	neuroendocrine rat pheochromocytoma PC12 cells
PE-LC3B	phosphatidylethanolamine-LC3B
pHspB1	phosphorylated HspB1
PI3K	phosphoinositide 3-kinase
PKC $\delta$	protein kinase C delta
PMS	phenazine methosulfate
PNS	peripheral nervous system

polyQ	polyglutamine
qRT-PCR	Quantitative Real-Time PCR
Rapa	rapamycin
RAPTOR	regulatory-associated protein of mTOR
Rheb	ras homolog enriched in brain
RhoA-GEF	ras homolog gene family, member A guanosine exchange factor
RNAi	RNA interference
ROD	relative optical density
ROS	reactive oxygen species
SDS	sodium dodecyl sulfate
SDS-PAGE	SDS-polyacrylamide gel electrophoresis
shRNA	short hairpin RNA
siRNA	small interfering RNA
STZ	streptozotocin
SQSTM1	sequesterome 1
tBid	truncated BH3 interacting-domain death agonist
TBS	Tris-Buffered Saline
TBST	TBS supplemented with 0.025% Tween 20, pH 7.2
TSC2	tuberous sclerosis protein 2
ULK1	Unc-51 like autophagy activating kinase 1
UPR	ubiquitin proteasome response
UPS	ubiquitin proteasome system
V-ATPase	vacuolar-type H <sup>+</sup> -ATPase

## List of Appendices

Appendix A: Cytoskeleton, Inc. <i>In vitro</i> actin binding protein assay biochemistry kit: G- and F-actin preparation protocol. ....	242
Appendix B: Qiagen RNeasy® Plus Micro kit: cellular RNA isolation protocol. ....	244
Appendix C: Agilent 6000 Nano kit: RNA integrity determination protocol. ....	246
Appendix D: Invitrogen SuperScript® III First-Strand Synthesis System: complimentary DNA (cDNA) reaction protocol. ....	249
Appendix E: Promega Cell Titer 96® AQueous MTS Reagent and PMS: Cell viability quantification using the MTS colorimetric technique. ....	251
Appendix F.1: ThermoFisher Scientific CellROX® Green Reagent for oxidative stress detection: Oxidative stress quantification protocol. ....	253
Appendix G.2: ThermoFisher Scientific CellROX® Green Reagent for oxidative stress detection: DRG neuron images showing that H <sub>2</sub> O <sub>2</sub> causes oxidative stress after 30 mins of treatment. ....	255
Appendix H.3: ThermoFisher Scientific CellROX® Green Reagent for oxidative stress detection: DRG neuron images showing that H <sub>2</sub> O <sub>2</sub> causes oxidative stress after 1 hr of treatment. ....	257
Appendix I.4: ThermoFisher Scientific CellROX® Green Reagent for oxidative stress detection: DRG neuron images showing that H <sub>2</sub> O <sub>2</sub> causes oxidative stress after 2 hr of treatment. ....	259
Appendix J.5: ThermoFisher Scientific CellROX® Green Reagent for oxidative stress detection: DRG neuron images showing that H <sub>2</sub> O <sub>2</sub> causes oxidative stress after 3 hr of treatment. ....	261

## **Chapter 1: Introduction**

### **1.1 Endogenously activated cellular mechanisms that promote survival during stress**

Endogenous protective cellular responses to internal or external stress stimuli are essential to the survival and growth of cells. Different types of protective cellular responses can vary vastly, with distinct responses being elicited depending upon the type, severity and duration of the stress stimulus. In addition, before a protective cellular response can be activated, the cellular stress stimulus needs to surpass a predetermined cellular threshold; not until this cellular threshold has been surpassed will a cell induce a corresponding response.

Upon surpassing a cellular threshold, or a threshold whereby a cell decides to mount a concentrated cellular response to a cell stress, cellular stress responses activate and can include: the unfolded protein response (UPR); the DNA damage response; the oxidative stress response; the heat shock response; and autophagy (Fulda et al., 2010). Depending on the responses activated, cells will undergo a multitude of changes in order to counterbalance the damage that has occurred. Without the activation of protective responses, cells will ultimately undergo stress-induced cell death, culminating in the activation of either the programmed cell death mechanisms of apoptosis, autophagic cell death, necroptosis and pyroptosis, or the un-programmed cell death mechanism of necrosis (Fulda et al., 2010).

The following sections of the introduction will focus on areas with relevance to the heat shock response and autophagy. An emphasis upon HspB1 and its protective effects on cytoskeletal proteins in neurons and its potential involvement in autophagy activation will be described initially, while autophagy, with a focus upon its role in DRG neuronal survival and neurite growth, will follow.

### 1.1.1 Heat shock protein response

Once a cellular stress threshold has been surpassed, one endogenously activated protective mechanism is the heat shock response. This response was first observed and characterized in the salivary gland puff of *Drosophila busckii*, and was discovered to involve the transcription and translation of a set of cytoprotective, molecular chaperone proteins later characterized as heat shock proteins (Ritossa, 1962; Tissieres et al., 1974). The name “heat shock protein” (HSP) is a bit of a misnomer, as further experimentation has shown that the heat shock response can be activated by a variety of stress stimuli, such as heat stress, oxidative stress, heavy metals, toxins and bacterial infections (Hightower, 1991).

The activation of the heat shock response is a sensitive and rapid process, often being induced in response to a mild, non-lethal stress. Interestingly, the induction of a heat shock response to a mild stress, prior to a potentially lethal cellular insult, has been shown to have a greater protective effect than with no prior mild stress (Chretien and Landry, 1988). This protective effect is referred to as thermotolerance, and is of interest in devising strategies to use this response to protect against major cellular insults (Hightower, 1991; Quigney et al., 2003).

Upon cellular stress, the activation of the heat shock response involves the transcriptional activation of HSP genes by heat shock factors (HSFs). Briefly, at least 4 HSFs are known to exist (HSF-1, HSF-2, HSF-3 and HSF-4), and under homeostatic conditions they exist in a repressed monomeric state in the cytoplasm through a complex with either DnaJ/Hsp70 or Hsp90 (Shi et al., 1998; Zou et al., 1998). Upon the introduction of a cellular stress, HSF proteins are post-translationally modified, causing them to form homotrimers that translocate to the nucleus

where they bind to HSP promoter regions, called heat shock elements (HSEs), and consequently promote the transcription of HSPs (Kim et al., 2005; Wang et al., 2006b; Yunoki et al., 2013).

Translated heat shock proteins are classified by both their molecular weight and their dependence on ATP to function. Specifically, new nomenclature guidelines refer to high molecular weight (> 40kDa), ATP energy dependent HSPs as HspH/Hsp110, HspC/Hsp90 and HspA/Hsp70, while low molecular weight (12 – 42kDa), non-ATP dependent HSPs are termed DnaJ/Hsp40/, HspB1/Hsp27, HspB5/ $\alpha$ B-crystallin and HspB6/Hsp20 (Kampinga et al., 2009; Vos et al., 2008). Regardless of the HSP involved, HSPs promote cellular survival through their endogenous interactions with cytoplasmic proteins (such as the cytoskeletal proteins actin, tubulin and neurofilaments), and through their chaperoning and folding of nascent and damaged polypeptides (Ehrnsperger et al., 1997; Lavoie et al., 1995; Lee et al., 1997).

#### **1.1.1.1 Small heat shock proteins**

The family of the low molecular weight, non-ATP energy dependent HSPs (or small HSPs) consists of a group of 10 distinct proteins (HspB1-B10), whereby several members can be induced in response to cell stress (e.g. HspB1 and HspB5), while others cannot (e.g. HspB6) (Head et al., 1994; Sugiyama et al., 2000). Structurally, small HSPs all share a conserved C-terminal  $\alpha$ -crystallin domain, a C-terminal domain that contains a (I/V/L)X(I/V/L) hydrophobic tripeptide motif and a flexible tail, while some members also contain a variable N-terminal domain, with both a hydrophobic proline/phenylalanine rich (W/F)(D/E)PF motif and N-terminal phospho-serine sites (Haslbeck et al., 2005; Pasta et al., 2004; Sudnitsyna et al., 2012; Theriault et al., 2004). The N-terminal motif and phospho-serine sites, within the members that contain them, are thought to be utilized to modify HSP tertiary structure, influencing their protein

interaction dynamics and oligomerization, while the conserved C-terminal motif is thought to interact with the  $\alpha$ -crystallin core of neighboring HSPs, further modulating their oligomerization (Kim et al., 1998; Sudnitsyna et al., 2012; van Montfort et al., 2001b; Welsh and Gaestel, 1998). Differing sizes of oligomers of small HSPs, from dimers to larger oligomeric complexes, have been shown to assemble and are believed to exert the specific effects of small HSPs on cells during the heat stress response, mainly by either chaperoning damaged proteins, controlling the redox state of the cell or regulating cytoskeletal dynamics (Haslbeck et al., 2005; Welsh and Gaestel, 1998).

#### **1.1.1.1.1 Heat shock protein B1 (HspB1)**

Of the 10 proteins that make up the group of small HSPs, HspB1 (also called Hsp27) was the first to be characterized and purified, and thus is one of the most studied (Arrigo et al., 1988; Arrigo and Welch, 1987). HspB1 is constitutively expressed in many tissues, and is particularly abundant in heart, liver, colon, prostate and muscle tissues, where it can reach up to 3 mg/g of total protein, and is found in varying concentrations in central and peripheral nervous tissues (Arrigo, 2012; Franklin et al., 2005; Kato et al., 1992). HspB1 primarily acts as an ATP-independent molecular chaperone that attenuates protein aggregation by trapping and storing denatured polypeptides in a refolding competent state. The molecular chaperone activity of HspB1 was defined in experiments where it was shown that HspB1 could refold urea-denatured citrate synthase and  $\alpha$ -glucosidase in an ATP-independent manner *in vitro* (Jakob et al., 1993). Refolding or proteolytic elimination of HspB1-trapped denatured polypeptides, however, is not directly performed by HspB1, but rather performed in association with the ATP-dependent

protein folding machinery and the ubiquitin proteasome system (UPS) (Ehrnsperger et al., 1997; Parcellier et al., 2003).

#### **1.1.1.1.1 HspB1 domains and structure**

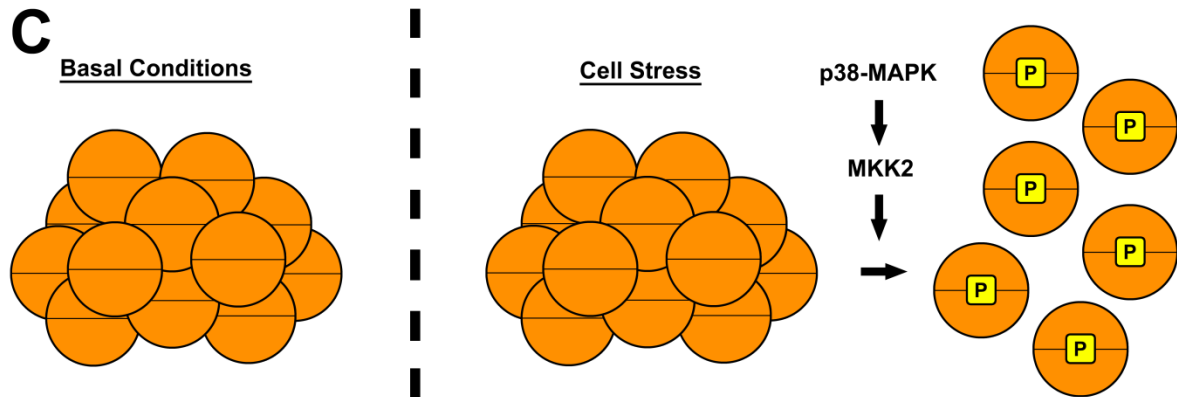
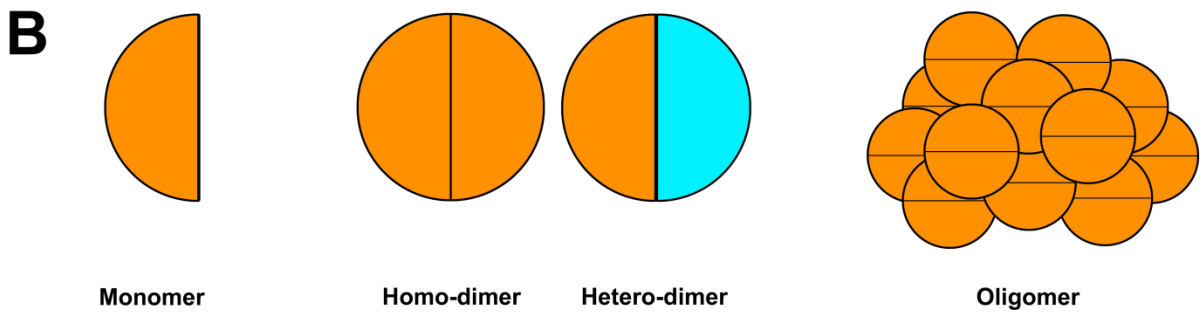
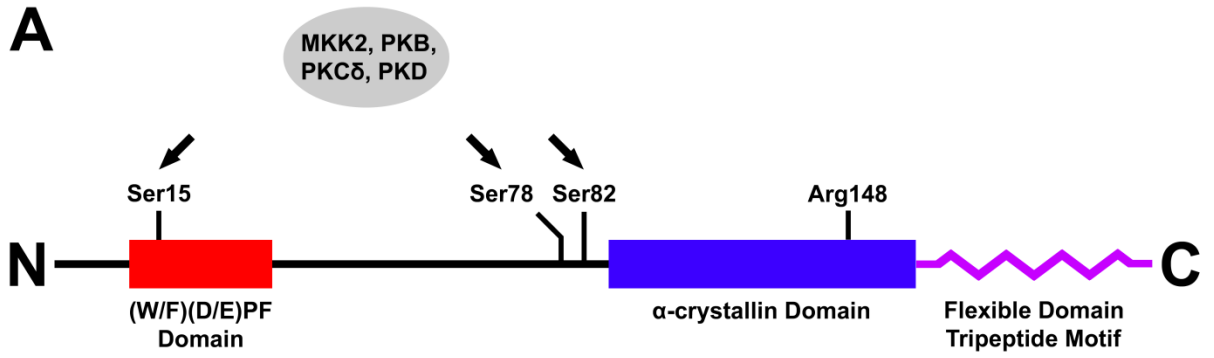
Under normal conditions, HspB1 forms large cytosolic oligomers (having a molecular mass of approximately 700 kDa) of approximately 24 monomers that can undergo dynamic changes in response to physiological alterations of the cellular environment, causing both the formation of smaller oligomeric structures and changes in oligomeric cellular distribution (Guo et al., 2012; Lambert et al., 1999). HspB1 structurally consists of the C-terminal  $\alpha$ -crystallin domain, the tripeptide motif and a flexible C-terminal tail, while also containing an N-terminal domain with both the hydrophobic motif and N-terminal serine phosphorylation sites. The  $\alpha$ -crystallin domain is an integral structural motif of all small HSP proteins, and this domain allows HspB1 to form oligomers with itself, as well as weak hetero-oligomers with other small HSPs (e.g. HspB5 or HspB6), through intermolecular interactions between the  $\beta$ -sheets of its tertiary structure (van Montfort et al., 2001a; van Montfort et al., 2001b). Interestingly, the  $\alpha$ -crystallin domain contains a conserved arginine (Arg148) that is important in maintaining the structural integrity of HspB1 oligomers, as a mutation of this residue can lead to an inability to form large oligomeric structures (Chavez Zobel et al., 2005). Additionally, molecular interactions between hydrophobic sequences in the N-terminus of adjacent HspB1 proteins further stabilize the oligomeric structures, as studies on the N-terminal deletion of the (W/F)(D/E)PF motif have shown a reduced ability of HspB1 to form oligomers larger than dimers (Lambert et al., 1999; Theriault et al., 2004).

#### **1.1.1.1.2 HspB1 phosphorylation**

Alterations in HspB1 oligomeric structure and distribution (i.e. cytosolic vs. nuclear) are also thought to be associated with changes in its N-terminal phosphorylation state (Mehlen et al., 1995; Rogalla et al., 1999). HspB1 can be phosphorylated via a myriad of tissue specific kinases (Fig. 1.1A), such as mitogen-activated protein kinase-associated protein kinase 2 (MKK2), protein kinase B (Akt), protein kinase C delta (PKC $\delta$ ), and protein kinase D (Kostenko and Moens, 2009). Specifically, HspB1 can be phosphorylated by MKK2 at three serines (Ser) in the human protein (Ser15, Ser78 and Ser82), and two serines in the rodent protein [(Ser15 and Ser86 (rat), Ser90 (hamster) or Ser82 (mouse)] in many cell types (Huot et al., 1995; Kostenko and Moens, 2009; Stokoe et al., 1992). Typically, when cell stress occurs, p38 mitogen activated protein kinase (p38-MAPK) becomes activated and subsequently activates MKK2, causing MKK2 to phosphorylate HspB1, and this phosphorylation ultimately causes an alteration in the HspB1 quaternary structure, promoting the formation of smaller HspB1 oligomers over larger ones (Fig. 1.1C). The change in quaternary structure is thought to occur as a result of Ser82 phosphorylation, as the use of HspB1 phosphorylation mutants (serine to alanine non-phosphorylated mutants, and serine to aspartic acid or glutamic acid constitutively phosphorylated mutants) have indicated that specific phosphorylation of Ser15, or Ser78 in human HspB1 protein does not induce changes in HspB1 oligomerization (Theriault et al., 2004). Additionally, while the N-terminal (W/F)(D/E)PF motif of HspB1 can interact with an exposed hydrophobic surface on an adjacent HspB1  $\alpha$ -crystallin domain, thus promoting stabilization of larger oligomeric structures, this interaction can be modulated by Ser82 phosphorylation, causing destabilization of large oligomers into smaller species (Theriault et al., 2004).

**Figure 1.1: Structure, phosphorylation and oligomerization of HspB1.**

**A.** The structure of HspB1 is comprised of an N-terminal hydrophobic (W/F)(D/E)PF domain, an  $\alpha$ -crystallin domain and a C-terminal flexible tail with a (I/V/L)X(I/V/L) hydrophobic tripeptide motif. In addition, human HspB1 contains phospho-serine sites at Ser15, Ser78 and Ser82 that can be subsequently phosphorylated by multiple kinases (e.g. MKK2, PKB, PKC $\delta$  and PKD) during cell stress. Further, any alteration of Arg148 in the  $\alpha$ -crystallin domain leads to the loss in the structural integrity of HspB1 oligomers. **B.** The base monomeric structure of HspB1 predominantly forms homo-oligomers through its interaction with the  $\alpha$ -crystallin domain on other HspB1 proteins (e.g. dimers, trimers, tetramers and large oligomers). However, HspB1 can also interact with other HSPs (e.g. HspB5 or HspB6) through their  $\alpha$ -crystallin domain and form hetero-oligomers. **C.** At basal conditions, HspB1 predominantly forms large non-phosphorylated oligomers, but when cell stress occurs, forms smaller oligomers through the phosphorylation of its phospho-serine sites, specifically Ser82.



The plasticity of HspB1 oligomerization through its phosphorylation is of particular interest as it is believed that by changing its oligomerization HspB1 can act as a sensor of the physiological state of the cell (Arrigo, 2013). In doing so, HspB1 thus has the ability to act as a sensor that can adapt and choose appropriate binding proteins, thereby allowing the cell to mount an appropriate protective response to the physiological cell stress (Arrigo and Gibert, 2012; Hayes et al., 2009; Jovcevski et al., 2015; Lelj-Garolla and Mauk, 2006). Additionally, HspB1 can form homo- and hetero-oligomers with other HSPs (Fig. 1.1B), and the alterations in their formation caused by phosphorylation can further affect the ability of HspB1 to interact with specific protein targets or generate the recognition of new targets (Aquilina et al., 2013; Sun et al., 2004).

#### **1.1.1.1.1.3 Cell survival and HspB1**

Promotion of cell survival by HspB1 has been primarily attributed to its ability to chaperone damaged proteins, but it has also been found to involve its promotion of anti-oxidation, anti-apoptosis, cytoskeleton stabilization and protein aggregate clearance in stressed cells (Arrigo et al., 2005; Preville et al., 1999; Qi et al., 2014b; Williams and Mearow, 2011). Additionally, HspB1 has been found to promote cell survival by modulating nuclear transcription and cytosolic translation activity, as well as intracellular signaling pathways (Cuesta et al., 2000; Mearow et al., 2002; Qi et al., 2014a; Wettstein et al., 2013). It is generally believed that large unphosphorylated multimers relay a majority of the positive cellular effects of HspB1, while smaller phosphorylated oligomers are thought to relay some positive effects, but their mechanisms and targets are still being discovered (Arrigo and Gibert, 2012; Bruey et al., 2000b). Furthermore, the specific species of HspB1 that confers chaperone activity is currently unknown,

as some studies suggest large oligomers are predominantly chaperone-like, while others suggest smaller oligomeric species (Jovceviski et al., 2015; Lelj-Garolla and Mauk, 2006).

Whether through the use of large un-phosphorylated multimers or smaller phosphorylated oligomers, it has been shown that HspB1 can interact directly with nuclear and cytosolic proteins, modifying their activity and modulating cell survival through chaperoning and anti-aggregation effects. For instance, mitochondrial outer membrane permeabilization (MOMP) during cell stress can result in the release of cytochrome C into the cytosol, subsequently causing apoptosis induction (Renault et al., 2013). HspB1 has been shown to prevent MOMP by inhibiting the translocation of the truncated Bcl-2 homology 3 (BH3) interacting-domain death agonist protein (tBid) to the mitochondrial membrane, thus preventing the release of cytochrome C (Paul et al., 2002). HspB1 can also directly sequester any cytochrome C that has been released, thereby preventing its initiation of apoptosis (Bruey et al., 2000a). In addition, HspB1 can act upstream of mitochondrial dysfunction, directly interacting with and increasing the activation of PKB, ultimately functioning to inhibit apoptosis (Dodge et al., 2006; Mearow et al., 2002; O'Shaughnessy et al., 2007; Wu et al., 2007).

Interestingly, depending on the environment and pathology of the cell, the effects of HspB1 on cell survival can be disadvantageous as well. For instance, aberrant up-regulation of endogenous HspB1 expression in cancer cells has been found to lead to increased tumor growth, motility and invasiveness, as well as tumor dissemination to form metastatic colonies (Cordonnier et al., 2015; Gibert et al., 2012; Straume et al., 2012). HspB1 is believed to influence cancer cell survival by blocking apoptosis, chaperoning damaged proteins, stabilizing the cell cytoskeleton and counteracting the oncogene-induced senescence (Kanagasabai et al., 2010; O'Callaghan-Sunol et al., 2007).

#### **1.1.1.1.4 Neuron survival and HspB1**

The occurrence of stressful stimuli in post-mitotic neurons of the central (CNS) and peripheral (PNS) nervous tissues poses a unique problem as neurons cannot be replaced after damage or cell death, nor can they dilute out the effects of cell damage via cell division. In the search for therapeutic treatment targets, HspB1 has arisen as a potential candidate protein to study in order to aid in neuron survival. For example, HspB1 has been suggested to aid in neuronal cell survival in Huntington's disease (HD) by either decreasing mutant Huntingtin (mHtt) aggregation through its chaperoning capability or by prohibiting the activation of apoptosis by mHtt (Chiou et al., 2008; Perrin et al., 2007; Wyttenbach et al., 2002).

Although HspB1 has been shown to have positive effects on neuronal survival, its ability to do so in neuronal cells that do not endogenously produce HspB1 has intrigued many to study it in neurodegenerative diseases. Specifically, HspB1 is not expressed in neurons of the cerebral cortex, but has been found in purkinje cells of the cerebellum, pyramidal and granular cells of the hippocampus and dentate gyrus, anterior horn motor neurons of the spinal cord, DRG neurons and in all glial cells, such as astrocytes, oligodendrocytes, Schwann cells and microglia (Fragoso et al., 2003; Goldbaum et al., 2009; King et al., 2009; Kirbach and Golenhofen, 2011; Quraishe et al., 2008; Williams et al., 2005).

The potential protective influence of HspB1 is being studied in models of Alzheimer's disease (AD) to determine whether it aids in mitigating disease effects and helps in neuronal survival. Specifically, AD is caused by both the abnormal processing of the amyloid precursor protein (APP) to create the amyloid- $\beta$  protein, as well as the hyperphosphorylation of the microtubule stabilization protein tau, causing the formation of insoluble protein aggregates of both proteins

(Calero et al., 2015; Pedersen and Sigurdsson, 2015). Studies have shown that HspB1 is incorporated with extracellular amyloid- $\beta$  plaques in post-mortem brain tissue from AD patients, while in HspB1 overexpressing models, it has been shown to ameliorate the cognitive effects of AD, as well as reduce processing of amyloid- $\beta$  (Conway et al., 2014; Ojha et al., 2011a; Shinohara et al., 1993; Toth et al., 2013; Wilhelmus et al., 2006b). Additionally, HspB1 has been shown to associate with tau *in vitro*, leading to an improvement in neuron cell survival (Nemes et al., 2004; Shimura et al., 2004). In both instances, it is still being studied how HspB1 relays its positive effects, but theories suggest that HspB1 modulates the aggregation of both amyloid- $\beta$  and tau through its chaperone activity, thereby inhibiting their detrimental effects on other intracellular proteins and signaling pathways (Choi et al., 2015; Ojha et al., 2011b; Shimura et al., 2004; Wilhelmus et al., 2006a).

#### **1.1.1.1.1.5 Neurite growth and HspB1**

In addition to maintaining neuronal cell survival at the somal level, the maintenance of axonal and dendritic processes during cell stress is of equal importance. Neurons project neuronal processes from their cell body in order to enable them to communicate either with other neurons, such as in the CNS, or with peripheral nerve endings of the somatic and autonomic nervous system, such as in the PNS. Depending upon the neuron localization, however, can dramatically vary the neuronal process length, from microns to a meter in length. In order for neuronal processes to grow, a proper extracellular environment of growth factors and extracellular matrix proteins need to be present in order to initiate morphological changes via pro-growth signaling pathways (Polleux and Snider, 2010). Even with proper extracellular support and intracellular signaling, however, neuronal processes will not grow without an appropriate regulation of their

microfilament, microtubule and neurofilament cytoskeleton, as those structures facilitate the extension, branching and turning of growing neurites (Polleux and Snider, 2010). In parallel to a properly structured and stable cytoskeletal foundation, the transportation of proteins and organelles along the growing neuronal process to their distal tips of active growth is essential in accommodating their metabolic and protein needs for growth. Growing evidence suggests that HspB1 mediates the effective growth of neuronal processes and proper transportation of cytosolic constituents by modulating the cytoskeletal dynamics of microfilaments, microtubules and neurofilaments through its direct and indirect interactions with their core proteins, actin, tubulin and neurofilament, respectively (Benn et al., 2002; Costigan et al., 1998; Williams and Mearow, 2011; Williams et al., 2005, 2006).

#### **1.1.1.1.5.1 Microfilament growth and stability with HspB1**

Of the three cytoskeletal elements found in neurons, the interaction(s) between HspB1 and microfilaments are the most widely studied. Filamentous actin (F-actin) is important in neuronal survival as it imparts cellular flexibility, allowing cells to change their shape in response to varying extracellular and intracellular conditions, and is essential in the regulation of neuronal process elongation and guidance through its formation of mesh-like lamellipodia and filopodial linear bundles at the leading edge of growing neurites [reviewed in (Dent et al., 2011)]. Current studies *in vitro* have shown that HspB1, in its non-phosphorylated form, may act either as an F-actin capping protein (Fig. 1.2B), binding to the growing (barbed; +) end of F-actin and preventing its polymerization, or act as a globular actin (G-actin) binding protein (Fig. 1.2A), preventing the association of actin monomers into growing actin filaments (Benndorf et al., 1994; During et al., 2007; Guay et al., 1997; Lavoie et al., 1995; Pichon et al., 2004). Studies

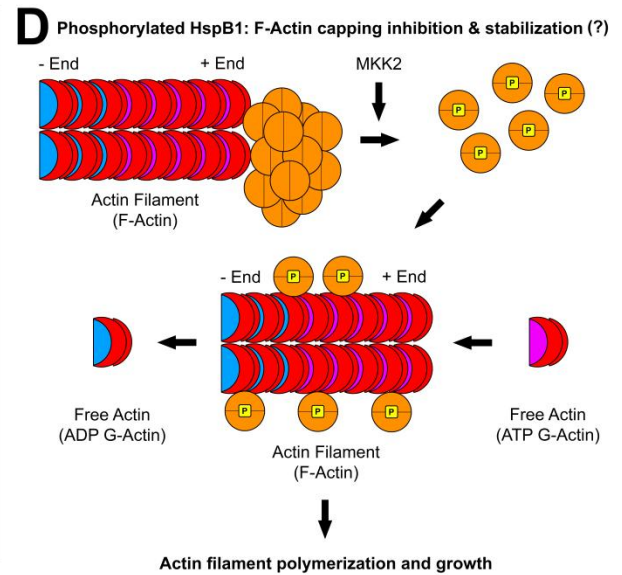
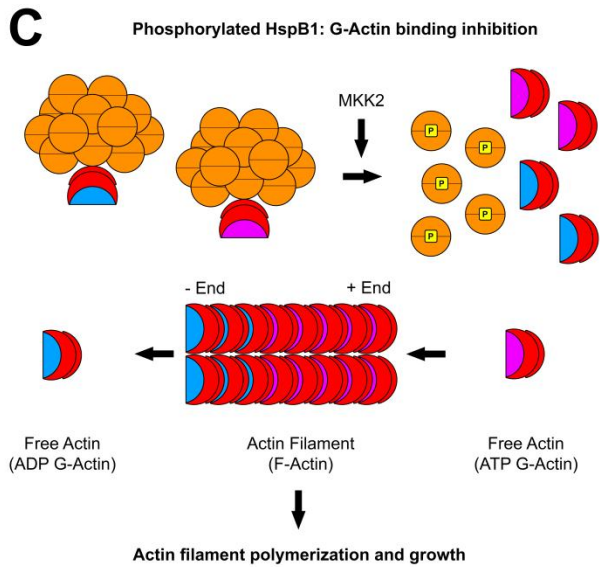
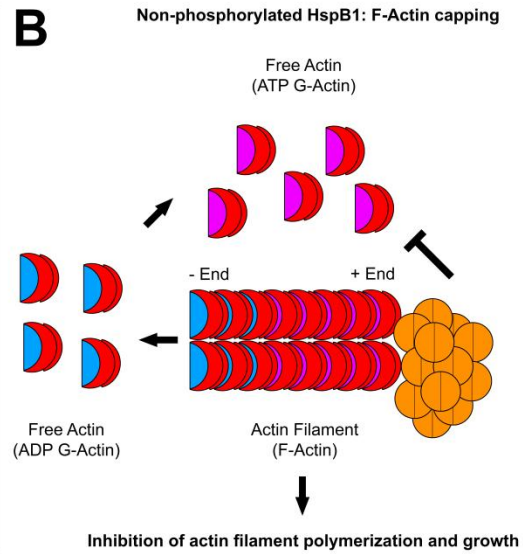
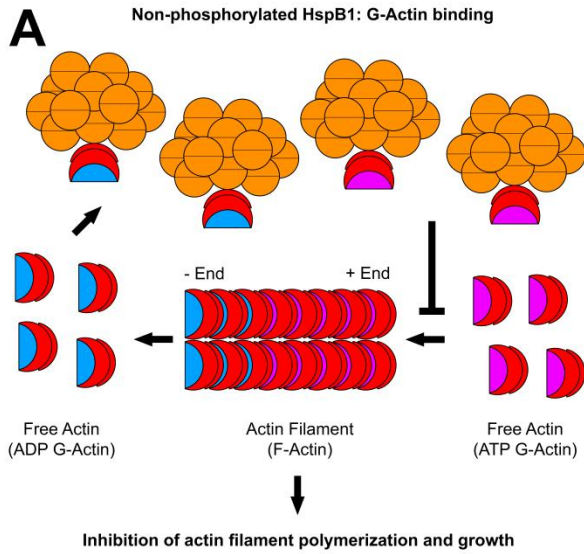
have also demonstrated that during cell stress HspB1 increases the stability of F-actin and promotes cell survival, while other studies have suggested that HspB1 can chaperone denatured actin filaments caused by cell stress, preventing their aggregation and promoting their repolymerization (Lavoie et al., 1993; Pivovarova et al., 2005; Schafer et al., 1999; Van Why et al., 2003). Additionally, HspB1 has been found to localize at the leading edge of lamellipodium in migrating cells, further suggesting that HspB1 either caps F-actin, or influences the binding of F-actin with focal adhesions, possibly through its interaction with the actin binding protein filamin (Pichon et al., 2004).

Upon phosphorylation, studies have demonstrated that HspB1 loses its F-actin capping/G-actin binding capability, thereby allowing actin filaments to polymerize and grow (Benndorf et al., 1994; Doshi et al., 2010) (Fig. 1.2C and D). Some studies, however, hypothesize that phosphorylated HspB1 can still bind to the actin filament, by potentially associating with the sides of F-actin, thereby improving their stability and preventing them from depolymerizing during cell stress (Graceffa, 2011; Mounier and Arrigo, 2002) (Fig. 1.2D). Alternatively, phosphorylated HspB1 may influence other signaling pathways that can modulate actin binding protein activity (Graceffa, 2011; Mounier and Arrigo, 2002).

In addition to potentially regulating the growth dynamics of F-actin through direct interactions with the actin filament, studies have shown that HspB1 potentially regulates F-actin growth through its binding proteins. For instance, a recent study in cortical neurons demonstrated that by overexpressing HspB1 there was a reduction in the translation of the ras homolog gene family member A guanosine exchange factor (RhoA-GEF), leading to the promotion in neurite extension as RhoA-GEF regulates the activity of cofilin, an F-actin depolymerization protein (Sun et al., 2013). Additionally, HspB1 has been found to be a binding

**Figure 1.2: Diagrammatic representation of HspB1 interactions with actin.**

Filamentous actin continuously undergoes a state of homeostatic polymerization and depolymerization called treadmilling, whereby cytosolic ADP bound G-Actin (blue images) initially exchanges its ADP for ATP (purple images) and then associates with the growing, barbed (+) end of an actin filament. Once bound to the filament, actin hydrolyzes its bound ATP to ADP, and is treadmilled along the filament toward the non-growing, pointed (-) end where it falls off and returns to the G-actin pool. Non-phosphorylated, oligomeric HspB1 is thought to alter this process through either its binding with cytosolic G-Actin (**A**), or through a direct binding to the growing end of the actin filament (**B**); the resulting effect in either case is an inhibition and stabilization of actin filament growth. Upon HspB1 phosphorylation, however, HspB1 loses its inhibitory effect on G-actin (**C**) and the actin filament (**D**), resulting in renewed actin filament polymerization and growth. Additionally, it is thought that smaller phosphorylated oligomeric species of HspB1 can bind to the actin filament, potentially aiding in its stabilization and growth (**D**).



partner of ArpC1a, a subunit of the actin-related protein 2/3 (Arp2/3) complex, and thereby may influence the branching of actin filaments, as the Arp2/3 complex nucleates branches off existing actin filaments, ultimately forming mesh-like lamellipodia (Jia et al., 2010).

#### **1.1.1.1.1.6 HspB1 and DRG neuron survival**

Neuronal cell exposure to stressful stimuli is unavoidable, but how well neurons moderate potential damage ultimately determines if they will survive or not. This situation is most apparent in DRG neurons of the PNS. Dorsal root ganglia are located at all spinal levels (cervical, thoracic, lumbar and sacral), and consist of a heterogeneous population of DRG neurons that are further subdivided based upon their neurochemistry, morphology, trophic requirements and sensory modalities (Averill et al., 1995; Gavazzi et al., 1999; Petruska et al., 2000; Priestley et al., 2002). DRG neurons have been further subdivided into large-, medium- and small-diameter neurons and are identified based upon the expression of either the p75 neurotrophin receptor, tropomyosin-related kinase (Trk) receptor, calcitonin gene-related peptide, or the isolectin B4 (Averill et al., 1995; Priestley et al., 2002). The main goal of DRG neurons is to convey somatosensory information about touch, nociception, proprioception and temperature from the periphery to the CNS through a single extensive axon, reaching up to a meter in length (Devor, 1999). DRG neurons are able to accomplish this as they grow bifurcating axons, whereby one axon projects to the dorsal horn of the spinal cord, forming either the dorsal column-medial lemniscus pathway, the lateral and anterior spinothalamic tracts, or the anterior and posterior spinocerebellar tracts, depending on the sensory modality being conveyed, while a second axon projects toward the periphery to innervate skin, muscle or visceral organ afferent nerve endings (Devor, 1999).

Damage to the distal tips of DRG axons, either through chemical, mechanical or thermal means (e.g. cutting or burning of the skin), can lead to the degeneration of the peripheral axon back to the neuron in the DRG, a process referred to as axonal die-back or Wallerian degeneration (Raff et al., 2002; Wang et al., 2012). If the damage is dealt with accordingly, however, damaged DRG axons are then able to regrow back to their afferent targets.

Many DRG neurons endogenously express HspB1, which has been postulated to be involved in DRG neuritogenesis, neurite extension, neurite growth patterning and neuron survival after stress (Costigan et al., 1998; Dodge et al., 2006; Lewis et al., 1999; Williams and Mearow, 2011; Williams et al., 2005, 2006). HspB1 colocalizes with actin in lamellipodia and focal adhesions at the early stages of neurite growth in DRG neurons, and in neuronal processes, branch points and growth cones at later stages (Williams et al., 2005). Additionally, it has been shown that by silencing HspB1 expression in DRG neurons or by modulating the phosphorylation of HspB1, aberrant neurite growth can occur (Dodge et al., 2006; Williams and Mearow, 2011; Williams et al., 2006). Interestingly, studies have also shown that by increasing HspB1 expression, DRG neurons are more susceptible to survive peripheral nerve injury, as well as protect DRG neurons from diabetic damage (Korngut et al., 2012; Pourhamidi et al., 2011). It is postulated that HspB1 is able to exert a positive effect on DRG neuron survival and growth through its effects on actin filament dynamics, apoptosis and protein chaperoning and refolding.

#### **1.1.1.1.7 Peripheral neuropathy and HspB1**

The small heat shock protein HspB1 is a multifunctional molecular chaperone protein that participates in a multitude of cellular processes in order to aid in cell survival and growth. Like other cellular proteins, the ability of HspB1 to properly function depends significantly on its

proper transcription and translation in relation to specific cellular stress cues. However, like other proteins, genetic mutations in HspB1 can alter its cellular function and as a result have been shown to manifest into cellular disease. For instance, a study found that five nucleotide missense mutations in HspB1 are associated with the peripheral neuropathy Charcot-Marie-Tooth disease (CMT) (Houlden et al., 2008). Specifically, CMT is an autosomal dominant peripheral sensorimotor neuropathy associated with slowly progressive weakness and atrophy of distal muscles in the feet and/or hands, with occasional and predominant distal sensory loss and reduced tendon reflexes (Ekins et al., 2015). There are multiple subtypes of CMT, but missense mutations in HspB1 have been associated predominantly with CMT2F (Table 1.1), which accounts for approximately 20-40% of all CMT patients and mainly affects peripheral axons (Evgrafov et al., 2004; Houlden et al., 2008). A recent study has demonstrated that the CMT2F causing HspB1 mutants stabilize the microtubule network in peripheral axons of DRG neurons by interacting directly with tubulin (Almeida-Souza et al., 2011). However, it is thought that the microtubule stabilization conferred by mutant HspB1 is aberrant and transient, causing microtubules to spend more time in a stationary phase, and less time growing or shrinking, thereby affecting their growth dynamics (Almeida-Souza et al., 2011). Moreover, when a threshold of stabilization and depolymerization is reached, depolymerization is then favored and microtubules rapidly depolymerize because stabilization is not intact, causing a loss in axonal stability and transport (Almeida-Souza et al., 2011).

### **1.1.2 The potential involvement of HspB1 in other cell stress pathways**

Once cell stress has surpassed a specific threshold, protective cellular stress responses become activated and promote cell survival and growth. Thus far, HspB1, specifically in relation to the

**Table 1.1: Mutations in HspB1 implicated to cause Charcot-Marie-Tooth disease.**

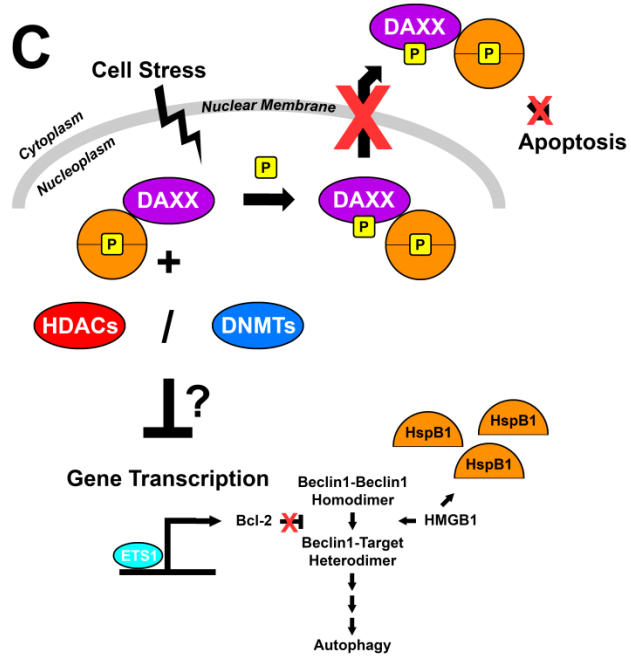
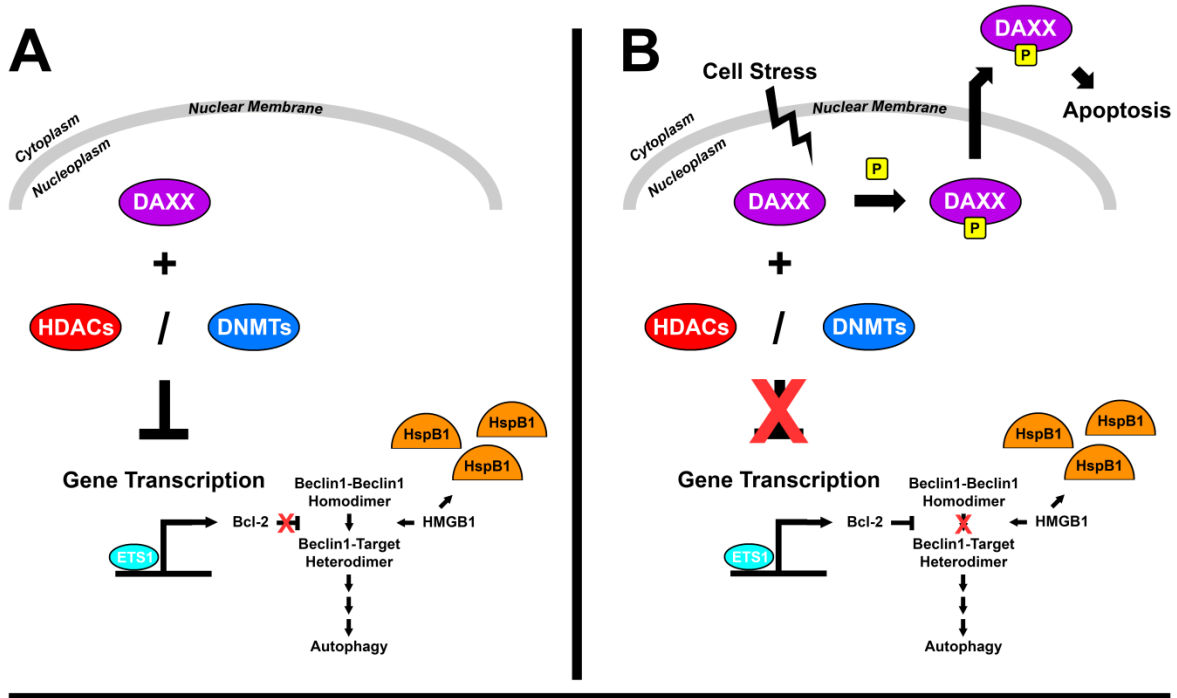
<b>Amino Acid Mutation</b>	<b>Nucleotide Change</b>	<b>Mutation Location</b>
<b>R127 →W127</b>	<b>C379 →T379</b>	$\alpha$ -crystallin domain
<b>S135 →F135</b>	<b>C404 →T404</b>	$\alpha$ -crystallin domain
<b>R136 →W136</b>	<b>C406 →T406</b>	$\alpha$ -crystallin domain
<b>T151 →I151</b>	<b>C452 →T452</b>	$\alpha$ -crystallin domain
<b>P182 →L182</b>	<b>C545 →T545</b>	C-terminal tail

the heat shock response, has been described and its cellular benefits and detrimental effects have been outlined. What has been described thus far, however, is an isolation of a specific response. Endogenously, multiple responses activate and act in unison in order to mitigate multiple adverse cellular effects, globally influencing cell survival and growth. Yet, these responses do not all work independently of each other, but rather directly or indirectly influence each other, modifying each response in order to fine tune a specific response to a specific cellular insult. For instance, even though HspB1 influences cytoskeletal dynamics and protein aggregation, its interactions with other proteins involved in other cellular processes can maximize its influence on cell survival. Specifically, in addition to binding cytochrome C, recent studies have also shown that HspB1 influences apoptosis through the binding of Daxx (Charette and Landry, 2000; Charette et al., 2000) (Fig. 1.3C). Under normal conditions, Daxx (death-associated protein 6) functions as a nuclear transcriptional co-repressor through its interactions with various transcriptional and nuclear factors (Fig. 1.3A), such as histone deacetylases and DNA methyltransferases (Ecsedy et al., 2003; Hollenbach et al., 2002; Michaelson et al., 1999; Muromoto et al., 2004). After cell stress, however, Daxx becomes phosphorylated and localizes to the cytoplasm (Fig. 1.3B) where it activates apoptosis (Yang et al., 1997). Studies have suggested that phosphorylated dimers of HspB1 can inhibit the cytosolic localization of Daxx (Fig. 1.3C), and also bind to cytosolic Daxx, thereby inhibiting apoptosis induction (Charette and Landry, 2000; Charette et al., 2000).

In addition to preventing apoptosis, the interaction between nuclear Daxx and HspB1 may also indirectly influence the process of autophagy (discussed in section 1.1.3), and thus further promote cell survival during cell stress. Briefly, a study found that Daxx can inhibit the nuclear transcriptional activation of E-twenty-six 1 (ETS1), causing a transcriptional repression in its

**Figure 1.3: The potential interaction between HspB1, Daxx and Autophagy.**

**A.** Under normal conditions Daxx has been shown to act as a nuclear transcriptional co-repressor that may indirectly affect the autophagic process through its repression of Bcl-2 transcription. Bcl-2 competitively binds to Beclin1 homodimers with HMGB1, promoting homodimer formation and autophagy inhibition. However, when HMGB1 binds to Beclin1 it promotes heterodimerization of Beclin1 to its target proteins, which then promotes autophagy initiation. **B.** Upon cellular stress, Daxx becomes phosphorylated and as result loses its transcription regulation of Bcl-2 activity; this in effect promotes the inhibition of the autophagic process. Additionally, phosphorylated Daxx loses its nuclear localization, as it transports to the cellular cytosol where it promotes apoptosis. **C.** Phosphorylated dimers of HspB1 are thought to interact with both nuclear and cytosolic phosphorylated Daxx and help mitigate its effects during stress. Studies have shown that this interaction prevents apoptosis initiation, and there may be reasons to believe that this interaction may also influence autophagy initiation. In addition, HMGB1 has been shown to transcriptionally regulate HspB1, and thus may further affect phosphorylated Daxx localization and effects during stress. HDACs: histone deacetylases; DNMTs: DNA methyltransferases.



target genes (Fig. 1.3A), specifically Bcl-2 (Li et al., 2000). Interestingly, Bcl-2 is essential in the process of autophagy as it stabilizes the homodimerization of Beclin1 via binding to a BH3 domain within Beclin1 (Fig. 1.3A), thereby impeding the ability of Beclin1 to form heterodimers with its target proteins, and thus activating autophagy (He et al., 2013; Maejima et al., 2013; Pattingre et al., 2005). Linking Daxx to autophagy, during non-stressed conditions Daxx could potentially repress Bcl-2 transcription and thus increase the probability that Beclin1 will form heterodimers with its target proteins, subsequently activating endogenous autophagy (Fig. 1.3A). This process, theoretically, could also be influenced by HspB1 during stressed conditions, as its interaction with phosphorylated Daxx may prevent the transcriptional inhibition loss of phosphorylated Daxx, and thus allow Daxx to continue to inhibit Bcl-2 (Fig. 1.3C).

In addition to Bcl-2, the high-mobility group protein B1 (HMGB1) protein competes for Beclin1 binding, as its binding promotes Beclin1 heterodimerization (Fig. 1.3), thus favoring autophagy induction (Kang et al., 2010). Under non-stressed conditions, HMGB1 acts as a chromosomal architectural factor, sustaining chromosome structure and stability; however, under stress conditions, HMGB1 translocates to the cytosol, where it interacts with Beclin1 and promotes autophagy (Kang et al., 2010; Tian et al., 2010). Interestingly, HMGB1 can also function as a nuclear DNA-binding protein (Fig. 1.3), capable of regulating the expression of HspB1 (Narumi et al., 2015; Tang et al., 2011). Therefore, HMGB1 could indirectly influence its own interaction with Beclin1 through the control of HspB1, and theoretically, the expression of Bcl-2 (Fig. 1.3C).

### 1.1.3 Autophagy

In response to cellular stress, most damaged intracellular proteins are either refolded using heat shock proteins, are selectively degraded by the UPR, or are bulk-degraded using the lysosome. Autophagy (derived from the Greek meaning *auto-* “self” and *phagein* “to eat”) is an evolutionary conserved eukaryotic cellular process that serves as the mechanism by which aged and damaged cytoplasmic proteins and organelles, as well as cytosolic bacteria and viruses, are delivered in bulk to the lysosome (Klionsky and Codogno, 2013). Autophagy was first observed in rat bile canaliculi hepatocytes using electron microscopy visualization, whereby dense cytosolic bodies considerably increased in number and displaced toward the center of the cytoplasm, near the nucleus, upon glucagon treatment (Ashford and Porter, 1962). Further observations found that the displaced bodies also contained mitochondria and other cytoplasmic components that were in a state of incipient deterioration, therefore further suggesting that the dense cytosolic bodies were potentially lysosomes (Ashford and Porter, 1962). A further study demonstrated that the dense cytosolic bodies, confirmed to be lysosomes, largely disappeared and were replaced by vacuoles of larger size that still contained lysosomal enzyme activity (Deter and De Duve, 1967). What was later discovered from these initial experiments was that the lysosomes were not replaced, but rather the formation of a new vacuole had occurred and subsequently fused with the lysosome (Deter et al., 1967). This new vacuole was later shown to be a double membrane vesicle that expanded to engulf cytoplasmic proteins and organelles, now referred to as the autophagosome (Baba et al., 1994; Dunn, 1990; Kirisako et al., 1999).

The ultimate goal of autophagy is to engulf cytosolic constituents and transport them to the lysosome, where acidic lysosomal hydrolases degrade the constituents into their basic building materials (proteins → amino acids), which are then released back into the cytosol for the

formation of new cellular materials (Parzych and Klionsky, 2014). This process can be activated to either clear unwanted constituents from the cell, or to meet the metabolic needs of the cell during episodes of nutrient deprivation, and thus helps maintain cellular homeostasis. Currently, three types of autophagy have been identified: macroautophagy, microautophagy and chaperone-mediated autophagy. Briefly, macroautophagy is characterized by the formation of the autophagosome, and can be further categorized based upon its selective cytosolic cargo (Shimizu et al., 2014). Microautophagy, however, involves the engulfing of cytoplasmic materials by lysosomal endocytosis, while chaperone-mediated autophagy involves the trafficking and uptake of specific cytoplasmic materials that contain the pentapeptide sequence KFERQ using the heat shock proteins HspA8 (heat shock cognate 70; Hsc70) and HspB8 (heat shock protein 22), and lysosomal-associated membrane protein type 2A (Cuervo and Wong, 2014; Li et al., 2012b). Among the types of autophagy, macroautophagy (hereafter referred to as autophagy) is believed to be responsible for the majority of intracellular protein degradation, and thus will be the focus in the following sections.

#### **1.1.3.1 Mammalian target of rapamycin (mTOR)**

Autophagy is typically induced by cellular stress, caused either by nutrient deprivation, oxidative stress or UV radiation, but has also been associated with cellular development and differentiation, as well as with the defense against cellular pathogens (Mortimore and Schworer, 1977; Pei et al., 2015; Rich et al., 2003; Rieber and Rieber, 2008; Schworer et al., 1981; Zhao et al., 2010). This process, however, does not act as a singular event, but involves many iterations of the same process depending upon both the metabolic needs of the cell and its state of disrepair. The regulation of autophagy is tightly controlled, and primarily dependent upon the

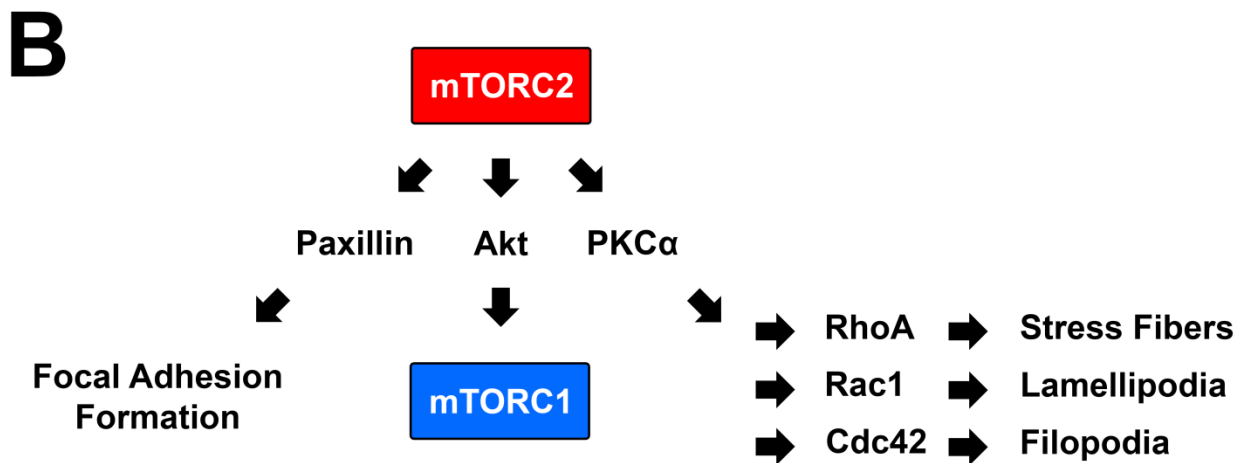
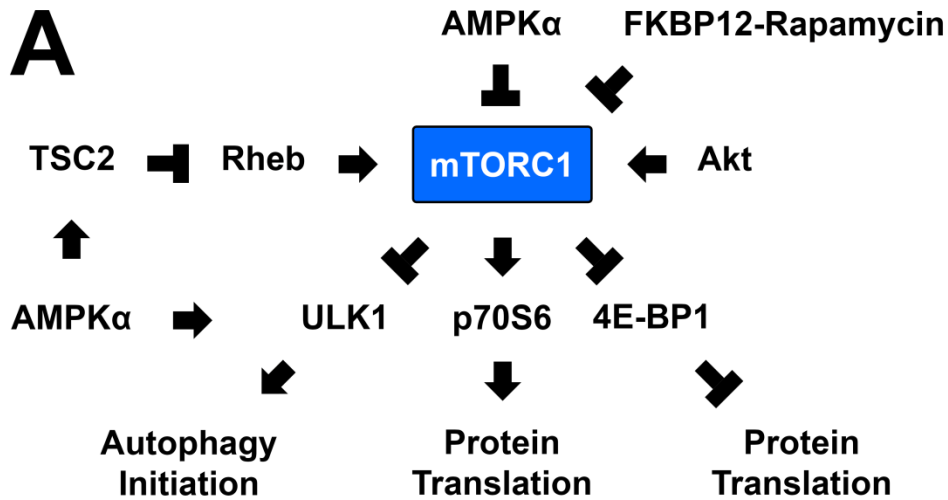
regulation of the mammalian target of rapamycin (mTOR) protein (Fig. 1.4A), as mTOR regulates the primary autophagy initiation protein, Unc-51 like autophagy activating kinase 1 (Egan et al., 2011a; Hosokawa et al., 2009).

Under normal conditions, in addition to inhibiting Unc-51 like autophagy activating kinase 1 (ULK1) activity, mTOR acts as a cytosolic serine/threonine protein kinase that promotes cell survival and growth through protein and lipid biosynthesis, mitochondrial biogenesis, lysosome biogenesis, ribosome biogenesis, cytoskeletal organization, and apoptosis and autophagy inhibition (Brown et al., 2007; Hannan et al., 2003; Jacinto et al., 2004; McDonald et al., 2008; Morita et al., 2013; Rocznik-Ferguson et al., 2012). The ability of mTOR to affect multiple cellular mechanisms is primarily through its ability to form two separate complexes [mTOR complex 1 (mTORC1) and mTOR complex 2 (mTORC2)] that affect separate downstream target proteins and processes (Sabatini, 2006). For instance, studies have demonstrated that mTORC1 modulates protein synthesis (Fig. 1.4A) through its phosphorylation of p70S6 kinase and eukaryotic translation initiation factor (eIF) binding protein 1 (4E-BP1), both of which modulate protein translation through phosphorylation of ribosomal protein S6 and eIF4E, respectively (Choo et al., 2008). Conversely, mTORC2 has been found to activate Akt, paxillin and PKC $\alpha$  through phosphorylation (Fig. 1.4B), thus subsequently modulating mTORC1 activity, the actin cytoskeletal network through the phosphorylation of the Rho guanosine triphosphate (GTP) hydrolases RhoA, Rac1 and Cdc42, and the formation of focal adhesions (Jacinto et al., 2004; Sarbassov et al., 2004).

**Figure 1.4: mTORC1 and mTORC2 cellular effects.**

**A.** Under normal conditions mTORC1 promotes protein translation and autophagy inhibition through its post-translational phosphorylation effects on the proteins p70S6 kinase, 4E-BP1 and ULK1. However, mTORC1 activity can be altered depending on the binding of allosteric inhibitors, such as FKBP12-rapamycin, or its phosphorylation by AMPK $\alpha$ , Akt, or Rheb binding.

**B.** Unlike mTORC1, under normal conditions mTORC2 primarily promotes the activation of Akt, and thus indirectly the activation of mTORC1. In addition, mTORC2 affects the formation of focal adhesions through the phosphorylation of paxillin, and the morphology of actin filaments, such as stress fiber, lamellipodia or filopodial formation, through the phosphorylation of PKC $\alpha$ .



#### 1.1.3.1.1 Regulation of mTOR activity

Studies have shown that autophagy initiation occurs only when mTORC1 is inhibited, and inhibition has been found to occur either by allosteric control of the mTORC1 complex or through phosphorylation of the mTOR catalytic domain (Chen et al., 1995; Cheng et al., 2004; Gwinn et al., 2008; Sabatini et al., 1994). For instance, allosteric inhibition of the mTORC1 complex can be accomplished through the binding of tacrolimus (FK506) binding protein 12 (Fig. 1.4A). Tacrolimus (FK506) binding protein 12 (FKBP12) is a peptidyl-prolyl-cis-trans isomerase that can associate with the *Streptomyces hygroscopicus* antifungal chemical rapamycin (also known as sirolimus), forming a FKBP12-rapamycin complex (Bierer et al., 1990; Schreiber and Crabtree, 1992). This complex is required before FKBP12 can bind to mTOR, but upon formation, binds to its specific binding domain (FKBP12-rapamycin binding domain; FRB) within the mTOR protein, inhibiting its activity (Chen et al., 1995; Sabatini et al., 1994). The specifics of how the FKBP12-rapamycin complex inhibits mTOR activity are unknown, but have been speculated to either directly affect mTOR kinase activity, or the subunit composition of mTORC1 (Hoeffler et al., 2008; Oshiro et al., 2004; Yip et al., 2010).

In addition to complex formation and allosteric control, the phosphorylation of mTOR can also modulate its activity. Under normal conditions, mTOR is activated through its phosphorylation at Ser1261 and Ser2448, and autophosphorylation of Ser2481 upon prior phosphorylation at Ser1261 (Acosta-Jaquez et al., 2009; Soliman et al., 2010). The full mechanism of mTOR phosphorylation and activation is still unknown, but current studies associate the direct binding of the lysosomal bound ras homolog enriched in brain (Rheb) to mTOR to initiate phosphorylation (Long et al., 2005a; Long et al., 2005b; Sato et al., 2009; Yadav et al., 2013). Rheb binding of mTOR phosphorylates Ser1261, which subsequently

stimulates the autophosphorylation of Ser2481 and the ability of Ser2448 to be phosphorylated by other cytosolic kinases, such as Akt (Long et al., 2005a; Long et al., 2005b; Sato et al., 2009).

In addition to the direct regulation of mTOR, its activity can be indirectly influenced through the modulation of its binding proteins. For instance, studies have found that the protein tuberous sclerosis complex 2 (TSC2) can hydrolyze GTP bound to Rheb (Fig. 1.4A), thus affecting its association and activation of mTOR (Inoki et al., 2003a). Additionally, in response to nutrient deprivation, the protein 5' adenosine monophosphate-activated protein kinase  $\alpha$  (AMPK $\alpha$ ) becomes activated upon adenosine monophosphate/diphosphate (AMP/ADP) binding, and subsequently phosphorylates both mTOR at Thr2446 (an inhibitory phosphorylation that affects the phosphorylation of Ser2448) and the mTOR complex protein RAPTOR (regulatory-associated protein of mTOR); RAPTOR phosphorylation influences its binding to the 14-3-3 protein, thereby reducing the association of RAPTOR with mTOR (Cheng et al., 2004; Gwinn et al., 2008). AMPK $\alpha$  can phosphorylate TSC2, activating its GTPase function, and can directly associate with and phosphorylate ULK1 on multiple serine and threonine sites (Fig. 1.4A), ultimately initiating autophagy (Egan et al., 2011a; Egan et al., 2011b; Inoki et al., 2003b; Kim and Lee, 2015; Lee et al., 2010).

### **1.1.3.2 The autophagic process**

Upon the inhibition of mTORC1, and the subsequent activation of ULK1, autophagy initiates by following a series of sequential steps, using a multitude of proteins, such as Beclin1 and autophagy-related proteins (ATGs), which help form the double lipid membrane autophagic vesicle, leading to the recycling of sequestered proteins and organelles at lysosomes. Occurring initially is the formation of a small membrane structure called the phagophore (Fig. 1.5A) that

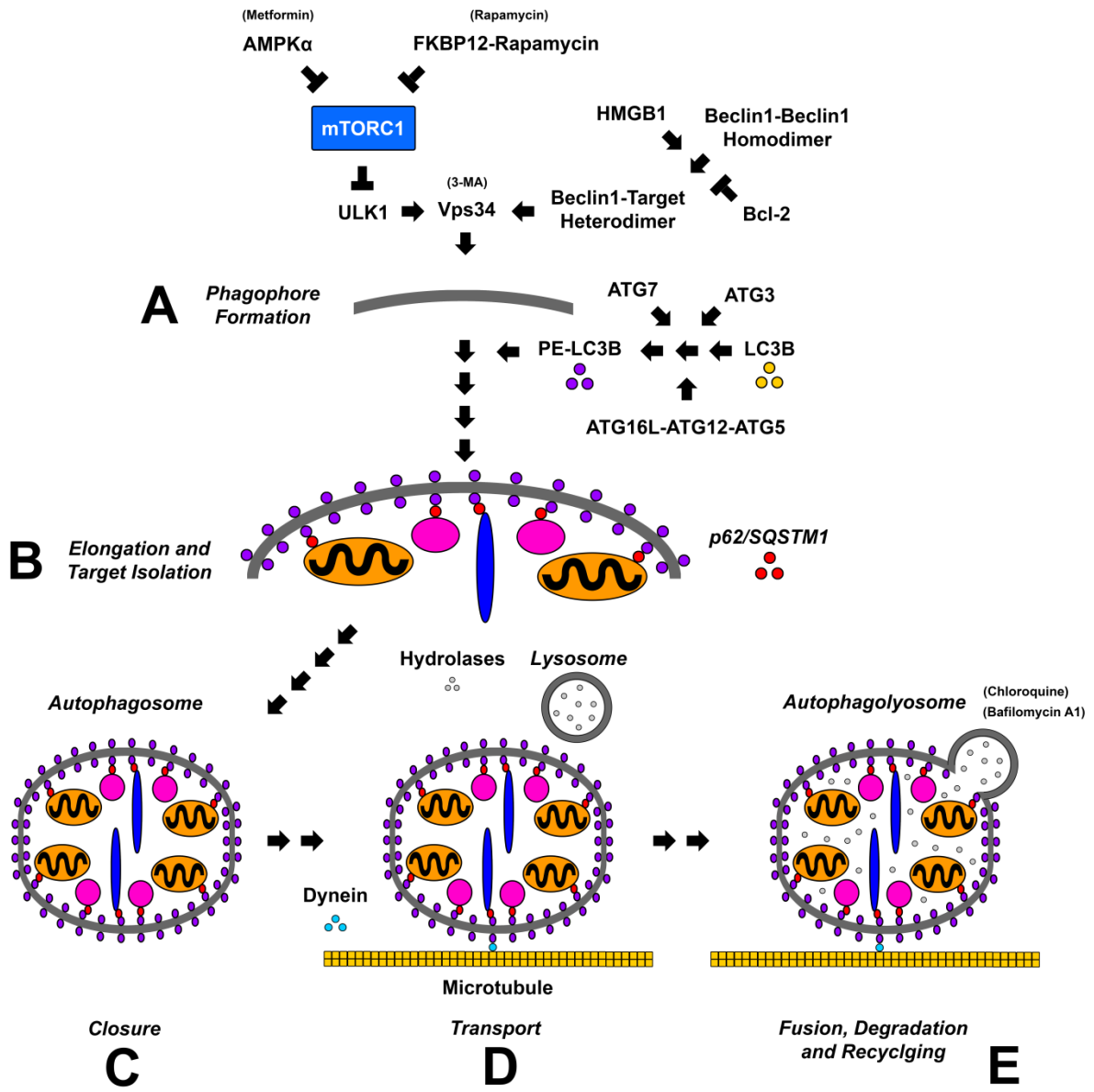
functions to localize all the proteins involved in the subsequent steps of autophagosome formation (Mizushima et al., 2001; Suzuki et al., 2001). How this structure is formed, however, is currently unknown, with the membrane involved in phagophore formation thought to originate from either the mitochondria, endoplasmic reticulum or Golgi body (Biazik et al., 2015).

After localization of autophagosomal specific proteins to the phagophore, elongation of the membrane then occurs, leading to the engulfment of cytosolic proteins and organelles. The full mechanism of elongation is still unknown, but it is thought that the protein microtubule-associated protein 1A/1B light chain 3B (MAP1LC3B; LC3B; ATG8) aids in the expansion and closure of autophagosomes (Saetre et al., 2015; Xie et al., 2008). LC3B is a soluble cytosolic protein with a molecular mass of ~17 kDa that is distributed ubiquitously in mammalian tissues and cultured cells (Xie et al., 2008). During autophagy, LC3B, referred to as LC3BI, is hydrolyzed at its the C-terminus by the cysteine protease ATG4B, and through a series of ubiquitin-like reactions involving the enzymes ATG3, ATG7 and the ATG16L-ATG12-ATG5 complex (Fig. 1.5B), becomes conjugated to the head group of the lipid phosphatidylethanolamine (Saetre et al., 2015; Xie et al., 2008). The lipidated form of LC3B, referred to as LC3BII, is then involved in autophagosome membrane expansion and fusion events (Saetre et al., 2015; Xie et al., 2008). LC3B has also been shown to be involved in substrate localization into the growing phagophore as studies have demonstrated that the protein p62/sequesterome 1 (p62/SQSTM1) interacts with both ubiquitinated proteins and organelles, and with LC3B (Pankiv et al., 2007; Shvets and Elazar, 2008; Shvets et al., 2008).

After formation of autophagosomes (Fig. 1.5C) subsequent transportation and fusion with lysosomes needs to occur in order for their cytosolic materials to be degraded and recycled. Studies have suggested that autophagosomes interact with dynein motors on the cellular

**Figure 1.5: The process and pharmacological regulation of autophagy.**

**A.** The activation of autophagy requires the inhibition of mTORC1, as mTORC1 regulates the activity of ULK1. Once activated, ULK1 activates the class III PI3K Vps34, and in conjunction with Beclin1 heterodimer binding, forms the initial autophagic membrane structure, the phagophore. This initial process can be modulated pharmacologically as rapamycin and metformin both contribute to the activation of phagophore formation, while 3-MA contributes to its inhibition. **B.** After the initial formation of the phagophore structure, cytosolic LC3B, in conjunction with the autophagy proteins ATG3, ATG7, and the ATG16L-ATG12-ATG5 complex, becomes lipidated with phosphatidylethanolamine and is incorporated into the phagophore membrane, contributing to its elongation. Further, p62/SQSTM1 binds to ubiquitinated proteins and organelles, and sequesters them inside the growing phagophore as p62/SQSTM1 binds directly to PE-LC3B. **C.** After elongation and sequestration of targeted proteins and organelles, the phagophore closes and is now referred to as an autophagosome. **D.** Protein and organelle loaded autophagosomes are then transported along microtubules by dynein motors toward cytosolic lysosomes. **E.** Upon localization to lysosomes, autophagosomes fuse with lysosomes, creating autophagolysosomes, whereby the captured constituents and the autophagosomes themselves are degraded by lysosomal hydrolases. The degraded products are then released back into the cytosol where they aid in cellular homeostasis (i.e. new protein and organelle production and ATP production). This final process can also be modulated pharmacologically as Chloroquine inhibits lysosomal hydrolase activity and Bafilomycin A1 inhibits the fusion between autophagosome and lysosome.



mitochondrial network to transverse toward lysosomes (Fig. 1.5D), while fusion with lysosomes is believed to be influenced by the Rab-GTPases (Ao et al., 2014; Fu and Holzbaur, 2014). Upon localization and fusion with lysosomes, the new vesicle created is referred to as an autophagolysosome, and its contents, as well as the original autophagosome, are degraded into their base materials (i.e. protein → amino acids) by lysosomal hydrolases (Fig. 1.5E).

### **1.1.3.3 Pharmacological modulation of autophagy**

Advancement of current theories and mechanistic pathways of autophagy have been aided by the use of pharmacological substrates that modulate specific proteins involved in the process. For instance, the use of the *Streptomyces hygroscopicus* antifungal chemical rapamycin, and subsequently synthesized rapamycin homologs (rapalogs), has been instrumental in determining that mTOR regulates the autophagic process, and has been used in many studies to determine the influence of autophagy on cell survival (Goldshmit et al., 2015; Ramirez et al., 2014). Additionally, studies using metformin, an oral anti-hyperglycemic medication, have shown that AMPK $\alpha$  inhibits mTOR and stimulates autophagy as metformin increases the intracellular concentration of AMP (Fig. 1.5), which subsequently activates AMPK $\alpha$  (Shi et al., 2012; Xie et al., 2011). Conversely, studies using 3-methyladenine (3-MA), a class III PI3 kinase inhibitor, have shown that the class III PI3 kinase protein Vps34 is involved in autophagosome elongation (Fig. 1.5) and its inhibition prohibits autophagosome formation (Caro et al., 1988; Su et al., 2011).

In addition to helping discover and modulate the proteins involved in autophagosome formation, pharmacological modulation of the lysosome has been employed to study its influence in autophagy. For example, chloroquine, an anti-malarial drug, has been shown to

increase the pH of the lysosome (Fig. 1.5), inhibiting both lysosomal hydrolases and the degradation of autophagosomes and their constituents (Mizui et al., 2010). Additionally, the vacuolar-type H<sup>+</sup>-ATPase (V-ATPase) inhibitor Bafilomycin A1 has been shown to inhibit the fusion between the autophagosome and lysosome (Fig. 1.5), thus suggesting that V-ATPase is involved in the autophagic process (Yamamoto et al., 1998).

#### **1.1.3.3.1 Autophagic flux**

The use of pharmacological agents to modulate autophagy not only has aided in further understanding the proteins involved in autophagy, but has also been used to understand autophagic flux. Autophagic flux denotes the entire dynamic process of autophagy, from autophagosome formation to degradation, and is used as a reliable indicator of autophagic activity in a cell (Jiang and Mizushima, 2015; Mizushima et al., 2010). A common misconception in the analysis of autophagy is the notion that increased numbers of autophagosomes in cells invariably corresponds to increased autophagic activity. Since autophagosomes act as an intermediate structure in the process, however, the observation of autophagosomes at any specific time point is a function of the balance between the rate of their generation and their degradation at lysosomes. Thus, in order to determine if individual changes in autophagosome numbers indicate a change in the overall process, flux needs to be determined. For example, compared to basal levels, autophagy activation is expected to result in an increase in autophagosome formation. However, if autophagolysosomal fusion or autophagosome degradation were blocked, even in the basal condition, autophagosome numbers would also increase. By using a combination of pharmacological modulation (i.e. rapamycin, 3-MA and Bafilomycin A1) and different experimental methodologies (i.e. Western immunoblotting,

immunocytochemistry, live-cell imaging), changes in autophagic flux can be determined to distinguish between basal levels, induction and repression of autophagy (Jiang and Mizushima, 2015; Mizushima et al., 2010).

#### **1.1.3.4 Autophagy and neurodegenerative diseases**

Basal autophagy occurs in neurons of the CNS and PNS, and contributes to their cellular homeostasis by catabolizing damaged and dysfunctional proteins and organelles, and supplying neurons with the materials to maintain their energy status (Kosacka et al., 2013; Liu et al., 2015; Portovedo et al., 2015). In addition, autophagy has been shown to improve neuron survival after episodes of cell stress. For example, studies have suggested that autophagy induction can help alleviate diabetic peripheral neuropathy (DPN), as well as protect neurons from death after cerebral ischemia (Carloni et al., 2010; Qu et al., 2014). Studies in DPN have demonstrated that the humoral immune system, which can be activated in diabetes, can modulate autophagy, and that this method of activation may represent an early cellular protective response (Townes et al., 2008a; Townes et al., 2005; Townes et al., 2008b). In addition to DPN, in Parkinson's disease cellular models, autophagy has been shown to promote the clearance of mutant  $\alpha$ -synuclein, as well as recycle dysfunctional mitochondria (Heo et al., 2015; Hu et al., 2016; Lazarou et al., 2015).

While studies suggest that autophagy may play a role in improving neurons affected by neurodegenerative disease, they also suggest that aberrant changes in autophagic flux are likely to contribute to the neurodegenerative processes of numerous CNS diseases. For example, it has been demonstrated that autophagy is transcriptionally up-regulated in AD, while autophagosome transportation and autophagolysosomal fusion is decreased in AD neurons (Lipinski et al., 2010;

Nixon et al., 2005). In other studies, the autophagy protein Beclin1 has also been found to be down-regulated in early AD, leading to the observations of decreased autophagy, altered APP processing and increased Amyloid- $\beta$  deposition (Jaeger et al., 2010; Pickford et al., 2008; Rohn et al., 2011).

Further studies in other neurodegenerative diseases, such as Huntington's disease and amyotrophic lateral sclerosis, have also indicated that aberrant changes in autophagy lead to neurodegeneration. For example, studies have suggested that the huntingtin protein interacts with ULK1, acting as a scaffold for the protein (Ochaba et al., 2014; Rui et al., 2015). In addition, the huntingtin protein has also been shown to compete with mTOR for ULK1 binding, thus inducing autophagy by inhibiting the interaction between ULK1 and mTORC1 (Rui et al., 2015). In Huntington's disease, however, expanded polyQ modified huntingtin protein loses its ability to interact with ULK1, and thus autophagy becomes attenuated, leading to further neurodegeneration (Zheng et al., 2010). With amyotrophic lateral sclerosis, however, a specific mechanism that may alter autophagic function is still unknown, with studies suggesting that genetic mutations in TANK binding kinase 1, optineurin and SigmaR1 cause the inhibition of autophagic flux and degradation, thereby promoting further neurodegeneration (Heo et al., 2015; Vollrath et al., 2014; Wild et al., 2011). Overall, more research is still needed in order to fully appreciate how autophagy promotes neuron survival, and how its dysfunction leads to neurodegeneration.

## Hypothesis and Objectives

The overall question I wished to investigate in this body of work was how the innate cellular mechanisms of neurons promote their survival during episodes of stress? In order to answer this question the work presented herein focused upon the cellular mechanisms of the heat shock response, with respect to HspB1, and autophagy, and how they influence cell survival. Three main questions were addressed in order to aid in answering how HspB1 and autophagy influence cell survival: Does the cell stress-specific phosphorylation of HspB1 influence its interaction dynamics with filamentous actin? Does HspB1 influence the process of autophagy during cell stress? Does autophagy influence DRG neuron survival and neurite growth during cell stress?

With regards to the first question, I proposed that the interaction dynamics between HspB1 and F-actin would alter based upon the phosphorylation state of HspB1. Previous *in vitro* studies have demonstrated interactions between actin and recombinant HspB1 (Datskevich et al., 2012; During et al., 2007; Graceffa, 2011; Mymrikov et al., 2012; Pivovarova et al., 2007), while similarly, a number of *in vivo* studies have shown interactions between actin and phosphorylated HspB1 using HspB1 phosphorylation constructs (Bryantsev et al., 2007; Doshi et al., 2009; Huot et al., 1996; Landry and Huot, 1995; Sun et al., 2011; Verschuure et al., 2002). Up to this point, however, *in vitro* and *in vivo* studies had not examined the interactions between HspB1 and filamentous actin endogenously. Therefore, I was interested in discovering whether endogenous HspB1, in a non-overexpressing cellular model, could interact with filamentous actin and whether phosphorylation modified this interaction.

The inclusion of autophagy into this project came from two independent studies. One study found an interaction between HspB1 and the nuclear transcriptional co-repressor protein Daxx *in*

*vitro*, where it was found that HspB1 interacted directly with Daxx during cell stress and inhibited its ability to activate apoptosis (Charette and Landry, 2000; Charette et al., 2000). The second study found that Daxx acts as a transcriptional co-repressor of Bcl-2, a protein directly involved in the process of autophagy (Li et al., 2000). Therefore, in this study I proposed that endogenous HspB1 interacted with Daxx and that this interaction influenced the process of autophagy through the transcriptional regulation of Bcl-2.

Finally, in continuing with autophagy research, I was interested in determining whether this endogenous cellular process was involved in the survival and neurite growth characteristics of DRG neurons. I proposed that negative modulation of the autophagic process in DRG neurons would decrease neuron survival and neurite growth characteristics. Previous research has shown that DRG neurons have an intrinsic capacity to regrow damaged axons under favorable environmental conditions (Tucker et al., 2005a, 2006). The cellular mechanisms of this regrowth, however, are not completely understood and therefore I wanted to determine whether autophagy played a role in this process. Furthermore, DRG axons can be subjected to daily stresses that could result in axonal damage, and I was interested in determining whether autophagy could play a role in the maintenance of neuronal function.

To study my hypotheses, three specific objectives were developed:

**Objective 1: To determine if endogenous HspB1 interacts with filamentous actin and whether phosphorylation influences this interaction.** Neuroendocrine rat pheochromocytoma PC12 cells were employed as a cellular model for inducing stress (using heat shock), with analyses carried out using biochemical (Western blotting and immunoprecipitation) and cellular (confocal microscopy) strategies. Results are presented in Chapter 2. This work has been published as Clarke J and Mearow KM, PLoSOne 2013, 8(7).

**Objective 2: To determine a link between HspB1, Daxx, Bcl-2 and autophagic activity.**

In these studies, dissociated adult rat DRG neurons were employed. Neurons were cultured under varying conditions and subsequent analyses were carried out using qRT-PCR western blotting/protein expression, as well as confocal microscopy. Results are presented in Chapter 3.

**Objective 3: To determine whether autophagy plays a role in DRG neuron survival and neurite growth.** Dissociated adult rat DRG neurons were cultured and exposed to stresses designed to induce autophagy: nutrient deprivation or H<sub>2</sub>O<sub>2</sub> exposure. Pharmacological manipulations were employed that might induce (rapamycin) or inhibit autophagy (3-methyl adenine and Bafilomycin A1). Cellular survival and modulation of neurite growth or neurite initiation were analyzed using biochemical (western blotting/protein expression) and cellular (confocal microscopy and image analysis) strategies. Results are presented in Chapters 4, 5 and 6.

## Co-authorship statement

I, Joseph-Patrick William Edward Clarke, am the principle author for all chapters that are contained with this thesis. However, each of these chapters has been co-authored by my supervisor Dr. Karen M. Mearow. The specific contributions of each author to each chapter are described below. The manuscript in chapter 2 is published (Clarke and Mearow, 2013) while the manuscript in chapter 4 has been submitted for review (Clarke and Mearow, 2016). The manuscripts in chapters 3, 5 and 6 are still in preparation for review.

Chapter 2, “Cell stress promotes the association of phosphorylated HspB1 with F-actin”. As the principle author I participated in the experimental design, performed the experimental work and data analyses, and contributed to the writing of the manuscript. Ms. Firoozeh Nafar provided technical assistance. Dr. Mearow edited the manuscript and was responsible for the experimental concept, design and overall supervision of the experiments, and participated in both confocal imaging and data analyses.

Chapter 3, “Exploring the Link between HspB1, Daxx, Bcl-2 and Autophagic Activity in DRG Neurons”. I participated in the experimental design and performed all experimental work, data analyses and writing for completion of this chapter. Ms. Firoozeh Nafar provided technical assistance, and Dr. Mearow participated in the experimental design and editing.

Chapter 4, “Autophagy Inhibition in Endogenous and Nutrient Deprived Conditions Reduces DRG Neuron Survival and Growth *In Vitro*”. As the principle author I participated in the experimental design, and performed the experimental work and data analyses, and contributed to the writing of the manuscript. Ms. Nafar and Mr. Brad Williams provided technical assistance. Dr. Mearow edited the manuscript and was responsible for the experimental concept, design and

overall supervision of the experiments, and participated in both confocal imaging and data analyses.

Chapter 5, “Autophagy Inhibition in Endogenous and Increased Reactive Oxygen Species Conditions Reduces DRG Neuron Survival and Growth *In Vitro*”. As the principle author I participated in the experimental design and performed all experimental work, data analyses and writing for completion of this chapter. Ms. Nafar and Mr. Williams provided technical assistance, and Dr. Mearow participated in the experimental design and editing of this chapter.

Chapter 6, “Autophagy Inhibition Alters DRG Neurite Growth Initiation *In Vitro*”. As the principle author I participated in the experimental design and performed all experimental work, data analyses and writing for completion of this manuscript. Ms. Nafar and Mr. Williams provided technical assistance, and Dr. Mearow participated in the experimental design and editing of this chapter.

## **Chapter 2: Cell stress promotes the association of phosphorylated HspB1 with F-actin**

A version was published as Clarke J and Mearow KM, PLoSOne 2013, 8(7)

### **2.1 Abstract**

Previous studies have suggested that the small heat shock protein, HspB1, has a direct influence on the dynamics of cytoskeletal elements, in particular, F-actin polymerization. In this study we have assessed the influence of HspB1 phosphorylation on its interaction(s) with F-actin. We first determined the distribution of endogenous non-phosphorylated HspB1, phosphorylated HspB1 and F-actin in undifferentiated neuroendocrine PC12 cells by immunocytochemistry and confocal microscopy. We then investigated a potential direct interaction between HspB1 with F-actin by precipitating F-actin directly with biotinylated-phalloidin followed by Western analyses; the reverse immunoprecipitation of HspB1 was also carried out. The phosphorylation influence of HspB1 in this interaction was investigated by using pharmacologic inhibition of p38-MAPK. In control cells, HspB1 interacts with F-actin as a predominantly non-phosphorylated protein, but subsequent to stress there is a redistribution of HspB1 to the cytoskeletal fraction and a significantly increased association of pHspB1 with F-actin. Our data demonstrate HspB1 is found in a complex with F-actin both in phosphorylated and non-phosphorylated forms, with an increased association of pHspB1 with F-actin after heat stress. Overall, our study combines both cellular and biochemical approaches to show cellular localization and direct demonstration of an interaction between endogenous HspB1 and F-actin using methodology that specifically isolates F-actin.

## 2.2 Introduction

The maintenance of cytoskeletal integrity is a key determinant in the survival and growth of cells during stressful cellular episodes, such as radiation, inflammation, or heat stress. In diseases such as the combined motor and sensory neuron disorder Charcot-Marie-Tooth disease or Alexander disease, perturbations in cytoskeletal integrity can lead to either an establishment or progression of the disease state (Fabrizi et al., 2007; Hsiao et al., 2005; Watson et al., 1994).

An intrinsic mechanism of importance in modulating cellular responses to stress involves the regulation of a set of highly conserved cellular proteins known as heat shock proteins. These proteins are modulated by cellular stressors and act predominantly as protein chaperones, with some proteins in this family having innate refolding mechanisms to refold damaged proteins (Nollen et al., 2001; Okada et al., 2004). Their cellular function is dependent upon many factors, such as increased protein expression, post-translation modifications, and altered oligomerization state and cellular distribution changes. These factors can be further regulated by cell-type specific, stress-activated pathways, such as the p38-MAPK and c-Jun N-terminal kinase pathways (Kostenko and Moens, 2009; Rouse et al., 1994)

Of particular interest is HspB1, which is a member of the class of small heat shock proteins (sHsps, 15-30 kDa). Like other heat shock proteins, HspB1 acts predominantly as a protein chaperone, but unlike the other heat shock proteins, does not display any innate refolding capabilities (Ehrensperger et al., 1997; Lee et al., 1997). HspB1 plays a role in a variety of cellular mechanisms, which can be modulated by its post-translational status (Bryantsev et al., 2007; Mehlen and Arrigo, 1994; Rogalla et al., 1999). It is phosphorylated by the stress-activated MAPK pathway involving the activation of MKK2 by p38-MAPK (Stokoe et al., 1992), as well as other kinases that have been implicated in HspB1 phosphorylation (Kostenko

and Moens, 2009). Phosphorylation of multimeric HspB1 on three conserved serines (human Ser15, 78 and 82; rodent Ser15 and 86; hamster Ser15 and 90) by MKK2 results in the formation of smaller oligomeric HspB1 structures that are thought to be the main structural units of HspB1 and potentially carry out its main functions (Ehrensperger et al., 1999; Kostenko and Moens, 2009; Landry et al., 1992). Additionally, changes in the conserved domains of HspB1 can alter the stability of the oligomeric structure of HspB1, and thus regulate its downstream effects on other proteins (Lambert et al., 1999; Rogalla et al., 1999; van Montfort et al., 2001b).

HspB1 is involved in the maintenance of cytoskeletal integrity and has been shown to interact with various elements including actin, tubulin, neurofilament, keratins and glial fibrillary acidic protein [reviewed in (Li et al., 2012a; Quinlan, 2002; Wettstein et al., 2012)]. The interactions between HspB1 and actin have been studied extensively in a variety of different experimental systems and HspB1 has been reported to interact variably with actin filaments or monomeric actin to influence actin polymerization and/or depolymerization (Doshi et al., 2009; During et al., 2007; Guay et al., 1997; Lavoie et al., 1995; Li et al., 2012a; Schneider et al., 1998; Seit-Nebi et al., 2013; Wettstein et al., 2012). The necessity of phosphorylation of HspB1 for its interactions with actin has been the subject of much discussion (Landry and Huot, 1995; Li et al., 2012a; Rogalla et al., 1999; Seit-Nebi et al., 2013; Wettstein et al., 2012). Models for HspB1 regulation of actin filament dynamics propose that non-phosphorylated monomeric HspB1 inhibits actin polymerization by acting as an actin-capping protein or by binding to and sequestering G-actin monomers, while phosphorylation reverses this effect (Doshi et al., 2010; During et al., 2007; Li et al., 2012a). A direct interaction between HspB1 and either G- or F-actin, however, has been questioned (Seit-Nebi et al., 2013).

*In vitro* studies have demonstrated interactions between actin and recombinant HspB1 (Datskevich et al., 2012; During et al., 2007; Graceffa, 2011; Mymrikov et al., 2012; Pivovarova et al., 2007). Similarly, a number of *in vivo* studies have shown interactions of HspB1 constructs with actin by immunoprecipitating tagged-HspB1 or colocalization at a cellular level of F-actin and HspB1, often employing cells overexpressing various constructs of HspB1 (Bryantsev et al., 2007; Doshi et al., 2009; Huot et al., 1996; Landry and Huot, 1995; Sun et al., 2011; Verschuure et al., 2002). We have also used a similar approach in examining the role of HspB1 and its phosphorylation status in contributing to neurite growth from primary sensory neurons (Williams and Mearow, 2011; Williams et al., 2006). We have observed co-localization of F-actin and HspB1 in neurons, and reported a higher level of localization of F-actin with a non-phosphorylatable HspB1 construct compared to pseudophosphorylated HspB1. In the present study, we were interested in determining whether there is a direct interaction of endogenous HspB1 with F-actin and whether HspB1 phosphorylation would influence this.

In this study we have employed PC12 cells that endogenously express HspB1 and modulated HspB1 phosphorylation status by inhibitor treatment in either a normal or stressed state. Immunocytochemistry, confocal microscopy and western blot analysis were employed to determine the cellular distribution of F-actin and HspB1 following cellular stress. By isolating F-actin specifically or HspB1 via pull-down assays, we investigated any association between the two proteins and the influence of HspB1 phosphorylation status on this association. Our results demonstrate that heat stress induces redistribution of HspB1 to the cytoskeletal protein fraction and that endogenous HspB1 is associated with F-actin regardless of the phosphorylation status of HspB1. HspB1 is phosphorylated on both serines 15 and 86 after stress and also interacts with F-actin. Immunocytochemistry and confocal imaging show a correspondence with the

biochemical analyses, and further suggest a differential compartmentalized distribution of phosphorylated and non-phosphorylated HspB1. Taken together, our data provide new evidence of a direct interaction of HspB1 specifically with F-actin that supports its role in modulating the actin cytoskeletal dynamics.

## **2.3 Materials and Methods**

### **2.3.1 Reagents and Antibodies**

Standard cell culture, lipofection reagents, streptavidin-coupled Dynabeads® (Cat. No. 112-05D), Dynabeads® Protein A (Cat. No. 100.01D) and Dynabeads® Protein G (Cat. No. 100.03D) were purchased from Invitrogen (Burlington, ON, CAN). *In vitro* actin binding protein assay biochemistry kit (Cat. No. BK013) was obtained from Cytoskeleton (Denver, CO). Biotinylated-phalloidin (Cat. No. P8716) was obtained from Sigma-Aldrich Canada Ltd. (Oakville, ON, CAN). The pharmacologic inhibitor of p38-MAPK, SB203580 (Cat. No. 559389) was purchased from Calbiochem (La Jolla, CA). Bicinchoninic acid (BCA) protein assay solutions, immunoblot reagents and membranes were purchased from ThermoFisher Scientific (Nepean, ON, CAN) and GE Healthcare (BaieD'Urfe, QC, CAN), respectively. Amaxa reagents were purchased from Amaxa Biosystems (Walkersville, MD). Primary and secondary antibodies used in this study are outlined in Table 2.1.

### **2.3.2 Cell Cultures and Treatments**

Neuroendocrine rat pheochromocytoma PC12 cells (ATTC CRL-1721.1; (Greene and Tischler, 1976)) were grown on collagen coated T-25 culture flasks and maintained at 37°C with

**Table 2.1: List of primary and secondary antibodies, with experimental dilutions, used for immunoblotting (IB), immunocytochemistry (IC) and immunoprecipitation (IP).**

<b>Antibody</b>	<b>Method</b>	<b>Dilution</b>	<b>Company</b>	<b>Cat. #</b>
Rabbit anti- $\beta$ -Actin	IB	1:500	Sigma-Aldrich	A2066
Rabbit anti-Hsp25	IB/IP	1:1000	Enzo Life Sciences	SPA-801-F
Rabbit anti-phosphoHsp27 (Ser15)	IB	1:1000	Enzo Life Sciences	SPA-525
Rabbit anti-phosphoHsp27 (Ser82)	IB ICC	1:1000 1:100	New England Biolabs	24065
Goat anti-rabbit IgG (H&L) HRP	IB	1:10000	ThermoFisher Scientific	31460
Mouse anti-Hsp27	ICC	1:100	Santa Cruz Biotech	SC-51956
Rabbit anti-phosphoHsp27 (Ser15)	ICC	1:100	ThermoFisher Scientific	PA1-018
Alexa Fluor® 488 Phalloidin	ICC	1:250	Invitrogen	A12379
Alexa Fluor® 405 Goat anti-Mouse IgG (H&L)	ICC	1:500	Invitrogen	31553
DyLight™ 647 Donkey anti-Rabbit IgG (H&L)	ICC	1:500	Jackson ImmunoResearch	P711-495- 152

5% CO<sub>2</sub> in Dulbecco's Modified Eagle Medium (DMEM), supplemented with 10% horse serum, 5% fetal bovine serum and 1% penicillin, streptomycin and glutamine. A total of 4 x 10<sup>6</sup> cells were used for each sample.

Cell cultures were exposed to 10µM SB203580 for 1 hr, after which cultures were either incubated for an additional 30 mins, or stressed with heat shock (HS) at 42°C for 30 mins (i.e., 1 hr inhibitor treatment → 30 mins heat stress → immediate collection of protein). Optimal inhibitor concentrations were determined empirically (Williams et al., 2005). Immediately after treatments, cells were collected and then lysed with actin stabilization buffer [ASB: 1% Triton-X 100, 0.1% sodium dodecyl sulfate (SDS), 10 mM ethylenediaminetetraacetic acid, 1% sodium deoxycholate, 200 pM sodium vanadate, 200 pM sodium fluoride, 1 complete protease inhibitor cocktail tablet, 0.5 mM ATP and Tris-Buffered Saline (TBS), pH 7.4]. After lysis, samples were either centrifuged at 15,000 x g for 10 min to be separated into Triton X-100 soluble (cytosolic; lysate) and Triton X-100 insoluble (cytoskeletal; pellet) samples, or were left as total lysate (crude sample).

### **2.3.3 In vitro F/G-Actin and Biotinylated-Phalloidin Pull-down**

Non-muscle actin was prepared *in vitro* into globular actin (G-Actin) or filamentous actin (F-actin), as per the manufacturer's protocol (See Appendix A), and then subsequently pulled-down with 5µg of biotinylated-phalloidin. Briefly, 2.5 µg and 5.0 µg samples of both G-Actin and F-actin were diluted to a total volume of 200 µL in TBS, and 5 µg of biotinylated-phalloidin was added to each sample. G-actin/biotinylated-phalloidin and untreated samples (actin-containing sample lacking phalloidin) were incubated for one hour at 4°C, with constant rotation on a bench-top rotator. F-actin/biotinylated-phalloidin and untreated samples (actin-containing

sample lacking phalloidin) were incubated for one hour at room temperature (~22°C), with constant rotation on a bench-top rotator. After one hour, 20 µL of streptavidin-coupled Dynabeads® were added only to the biotinylated-phalloidin treated samples and these were also incubated for one hour at 4°C (G-Actin sample) or room temperature (F-actin sample), with constant rotation on a bench-top rotator. Pull-down at this point was considered to be complete, and the samples were then isolated using a block magnet and 20 µL of 2X loading dye was added. Supernatants from pull-downs were collected and used for subsequent biochemical analysis to assess efficiency of the pull-down. Dynabead® pellets were washed three times with TBS, with the samples being used for biochemical analysis after the third wash. Immunoblots of pull-downs (phalloidin interacting samples), untreated supernatants (no biotinylated-phalloidin or Dynabeads® added) and supernatants after pull-down (non-phalloidin interacting samples) were then carried out. Specifically, 65 µL of untreated sample and supernatants after pull-down (approximately 1/3 of original volumes) were electrophoresed along with the precipitated samples and immunoblotted with anti-actin antibodies.

#### **2.3.4 Pull-Down Assay – cellular samples**

Previous studies have shown that biotinylated-phalloidin can be used to specifically pull-down F-actin from tissue (Fulga et al., 2007). By adapting this technique to our study, we performed pull-downs on Triton X-100 insoluble (cytoskeletal) protein samples resuspended in ASB, and crude total protein samples using biotinylated-phalloidin. Both samples were used in order to assess F-actin pull-down efficiency, which was ultimately determined to be similar (Fig. 2.4). Biotinylated-phalloidin (5.0 µg) was added to the protein samples and they were incubated for one hr at 4°C with constant rotation. Subsequently, 20 µL of streptavidin-coupled magnetic

Dynabeads® were added and this was incubated for an additional hour at 4°C with constant rotation. The magnetic beads were isolated using a block magnet and washed three times with phosphate buffer saline (PBS), pH 7.4, with the samples being used for biochemical analysis after the third wash. Pull-downs of HspB1 were performed similarly, using rabbit anti-HspB1 antibody (5.0 µg) and a 1:1 mixture of Dynabeads® A/G that were substituted for biotinylated-phalloidin and streptavidin-coupled magnetic Dynabeads®, respectively.

### **2.3.5 Biochemical Analysis of Protein Fractions and Pull-Downs**

Protein concentrations of lysates were determined using the BCA protein assay. Equivalent amounts of protein (20-25 µg) were electrophoresed in a 10% sodium dodecyl sulfate polyacrylamide gel (SDS-PAGE), separated, and transferred onto a nitrocellulose membrane; Ponceau Red staining was used to assess the equivalency of protein loading. Blots were then blocked either with 3% skim milk, or 5% bovine serum albumin (BSA) solution, depending on if phospho-specific antibodies were used or not, incubated at 4°C overnight with primary antibodies (Table 2.1) and developed the next day. Bands were detected using peroxidase conjugated secondary antibodies and SuperSignal® West Pico Chemiluminescent Substrate.

Analysis of the pull-down samples was carried out as follows. After the final wash of the pull-down pellets, the supernatants were discarded and loading dye with dithiothreitol (DTT) was added. These samples were pulse sonicated (3 pulses of 3 sec each with the power set to 35% of maximum using a model 16-850 Virsonic Cell Disrupter) and then separated once again using a block magnet. The supernatants were loaded onto a 10% SDS-PAGE and treated as outlined above.

### **2.3.6 Immunocytochemistry of PC12 Cells**

PC12 cells were cultured on collagen-coated 16-well chamber slides at ~1000 cells/well. Cells were treated with 10  $\mu$ M SB203580 (p38-MAPK inhibitor), with and without a heat stress at 42°C for 30 mins (1 hr inhibitor treatment  $\rightarrow$  30 mins heat stress  $\rightarrow$  immediate fixation of cells). After treatment, cells were fixed immediately using 4% paraformaldehyde in PBS for 20 mins, permeabilized in 0.1% Triton X-100, and blocked with 10% horse serum in PBS. Cells were incubated with primary antibodies at appropriate concentrations (Table 2.1) for 16-20 hrs at 4°C, rinsed with TBS supplemented with 0.025% Tween 20, pH 7.2 (TBST), and subsequently incubated with fluorophore-conjugated secondary antibodies at appropriate concentrations (Table 2.1) for 1-2 hr. Cells were washed again three times with TBST and cover-slipped with Gelvatol<sup>TM</sup>. Images were acquired in each of three channels (405nm, 488nm and 649nm) by laser scanning confocal microscopy with sequential Z-stage scanning (Olympus Fluoview 1000 confocal laser scanning microscope). Image acquisition for the different samples was carried out using similar scanning parameters [laser power, high voltage photomultipliers (HV PMTs), and number of optical slices]. Scanned stacks were compiled as individual images, and composite digital images were prepared in Adobe Photoshop CS (Adobe Systems Incorporated, San Jose, CA, USA).

### **2.3.7 3-Dimensional Imaging of Cellular Expression**

Immunocytochemical (ICC) confocal images were volume rendered in 3 dimensions (3D) using Imaris software (Bitplane Inc., South Windsor, CT). Confocal image stacks were initially saved as .oib files and then imported into Imaris. Images were cropped in 3D to focus on a region of interest and rendered employing the Surfaces tool within the Surpass module of Imaris.

Images were then saved as .tif files and Adobe Photoshop CS was used to prepare composite images.

### **2.3.8 Densitometric and Statistical Analysis**

Densitometric analyses of triplicate Western immunoblots were carried out using ImageJ and a calibrated grey value scale (NIH, Bethesda, Maryland); ratios of HspB1 expression (total and phosphorylated) were compared to actin expression. Densitometric analyses of confocal images (using average gray scale assessment) were also carried out using ImageJ, with average grey value expression of pSer15-HspB1, pSer86-HspB1 and total HspB1 being calculated. Statistical analyses were performed using GraphPad Prism 4 (GraphPad Software, San Diego, CA) with significance determined by one-way ANOVA and post hoc testing via Tukey's test.

## **2.4 Results**

### **2.4.1 Cellular distribution of total HspB1 and phosphorylated HspB1**

We initially examined the cellular distribution of HspB1, phospho-HspB1 and F-actin in control conditions compared to heat stress. PC12 cells were either not treated (vehicle control) or treated with the p38-MAPK inhibitor SB203580 (10  $\mu$ M) for 1 hr prior to stress; the cells were then heat-shocked for 30 min at 42°C, and fixed immediately. The distribution of HspB1, phospho-HspB1 and F-actin was visualized by confocal imaging. Cellular localization of HspB1 was determined with immunocytochemistry by using antibodies specific for pSer15-HspB1, pSer86-HspB1 and total HspB1, while F-actin was specifically visualized with fluorescently labeled Phalloidin.

In the control conditions, HspB1 was localized primarily throughout the cytosol, in a somewhat granular appearance. In some cells with lamellipodia, HspB1 was observed at the leading edges (Fig. 2.1A, arrows). Phosphorylated HspB1 was also detected throughout the cells, and at the leading edges of lamellipodia or ruffles (Fig. 2.1C, arrows). ICC of pHspB1-Ser15 is presented, although the pattern of pHspB1-Ser86 staining is similar. F-actin (as detected by Alexa-488 Phalloidin labeling) was observed at the cellular periphery outlining the cell boundaries (Fig. 2.1B, arrowhead), as well as being found in a more punctate distribution throughout the cell. There was co-localization observed between F-actin and HspB1, and to a certain extent with the pHspB1 (Fig. 2.1D).

The HS treatment resulted in the rounding of the cells and the collapse of the cytoskeleton and redistribution of HspB1 to a peri-nuclear location (Fig. 2.2A), a classical reaction of many cells to heat shock. Ruffles and membrane blebbing were observed on the surface of many of the cells (Fig. 2.2A-D). In these cells, there was again a distinct colocalization of the HspB1, pHspB1 and actin in a punctate or granular pattern within the cells, and associated with the membrane (Fig. 2.2A-C, arrows). There was an apparent increase in the amount of pHspB1 staining and this appeared to be colocalized with the F-actin (Fig. 2.2B-C, arrows).

In the presence of the p38-MAPK inhibitor (SB) plus HS (SB+HS), the pHspB1 staining was somewhat attenuated (Fig. 2.3C), appearing similar to the control condition. Many of the cells were rounded and the F-actin staining appeared less distinct than in the HS alone condition (Fig. 2.3B compared to Fig. 2.2B). There was still colocalization of the HspB1 and F-actin but closer examination of the cells revealed that there seemed to be an absence of the blebbing/ruffling that was apparent with HS alone; the staining of HspB1 and F-actin did not appear granular or punctate in nature (compare Fig. 2.2A to 2.3A, 2.2B to 2.3B).

**Figure 2.1: Cellular localization of HspB1 and F-actin in control PC12 cells.**

Low passage PC12 cells were cultured on collagen-coated coverslips, and processed for immunocytochemistry using antibodies directed against total HspB1 (Stressgen SPA801) or phospho-S15-HspB1 followed by fluorescently tagged secondary antibodies; F-actin was labelled using Alexa-488-phalloidin. Panel A-D: PC12 cells visualized with confocal microscopy; images represent the z-stack projections. A - HspB1 (blue); B - phalloidin (green); C - pS15-HspB1 (magenta); D - merged image. Panels E-K, L-R: three-dimensional rendering of immunostained surfaces as compiled by Imaris software of cells (boxes in D) selected from the low power view. E, L -HspB1 (blue); F, M - Phalloidin (green); G, N - pHspB1 (magenta); H, O - all 3 together; I, P - HspB1 + pHspB1; J, Q - HspB1 + Phalloidin; K, R - pHspB1 + Phalloidin. Scale bar – 50  $\mu\text{m}$ , D; 10  $\mu\text{m}$ , lower panels.

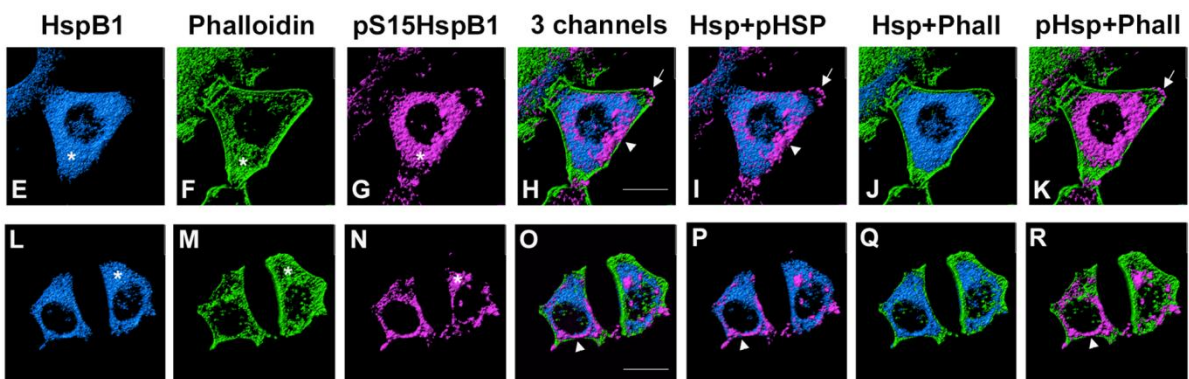
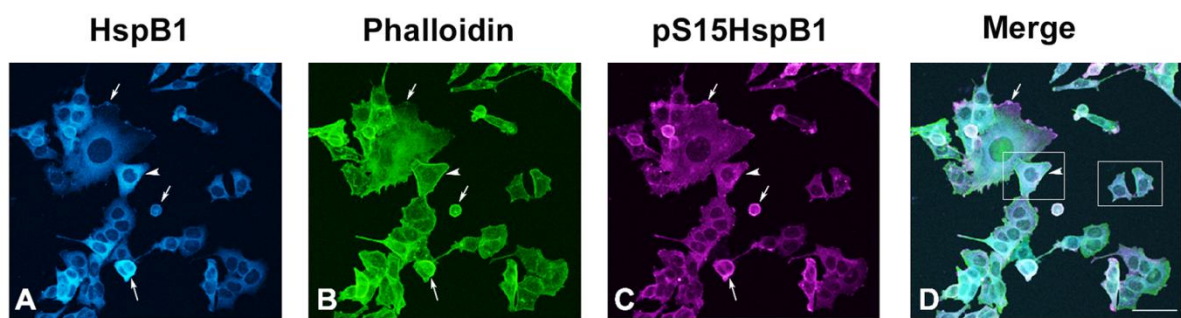


**Figure 2.2: Cellular localization of HspB1 and F-actin in PC12 cells subsequent to a heat shock.**

Low passage PC12 cells were cultured on collagen-coated coverslips and were subjected to a 30 min HS followed by immediate fixation. Processing for immunocytochemistry was performed using antibodies directed against total HspB1 or phospho-S15-HspB1 followed by fluorescently tagged secondary antibodies; F-actin was labelled using Alexa-488-phalloidin. Panel A-D: PC12 cells visualized with confocal microscopy; images represent the z-stack projections. A- HspB1 (blue); B - phalloidin (green); C - pS15-HspB1 (magenta); D - merged image. Panels E-K, L-R: three-dimensional rendering of immunostained surfaces as compiled by Imaris software of cells (boxes in D) selected from the low power view. E, L - HspB1 (blue); F, M - Phalloidin (green); G, N - pHspB1 (magenta); H, O - all 3 together; I, P - HspB1 + pHspB1; J, Q - HspB1 + Phalloidin; K, R - pHspB1 + Phalloidin. Scale bar – 10  $\mu$ m.

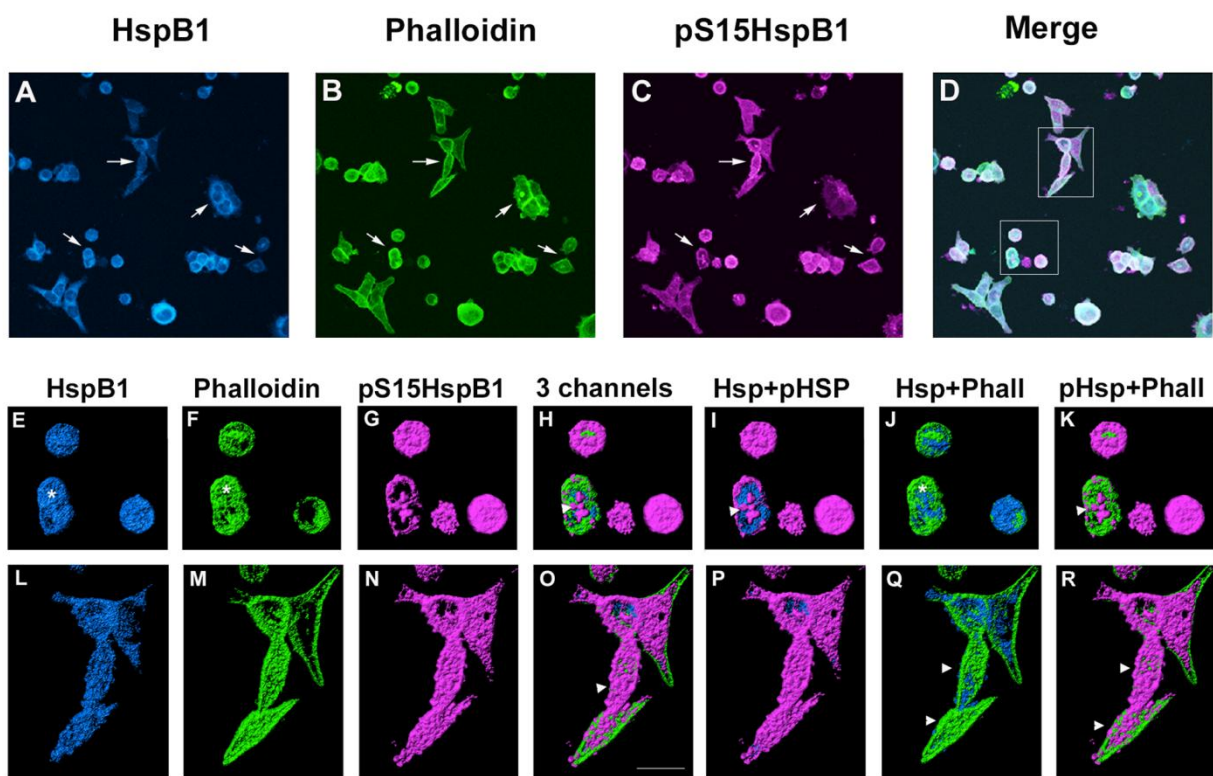
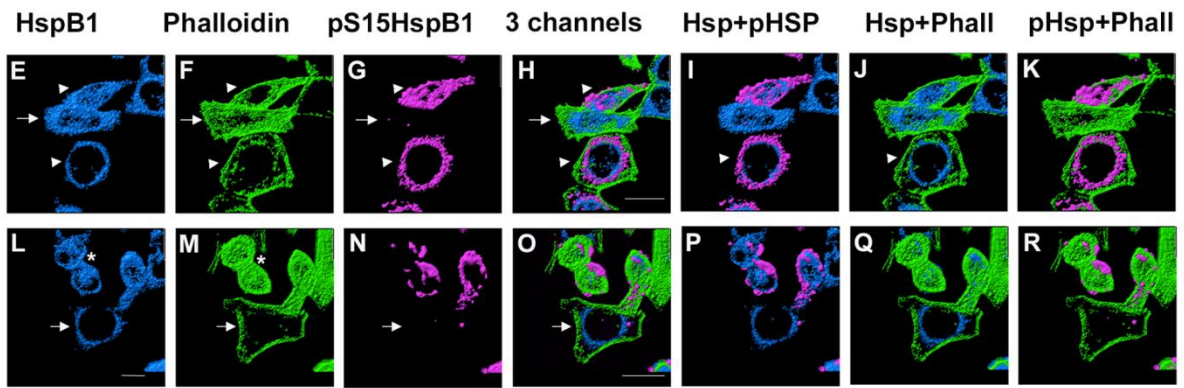
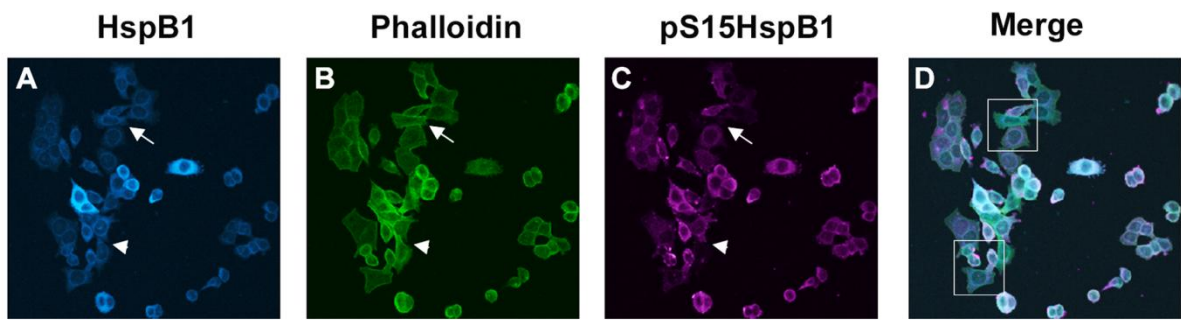


**Figure 2.3: Cellular localization of HspB1 and F-actin in PC12 cells subsequent to a heat shock in the presence of a p38-MAPK inhibitor.**

Low passage PC12 cells were cultured on collagen-coated coverslips, incubated with 10  $\mu$ M SB203580 for 1 hr prior to and during a 30 min HS, followed by immediate fixation. Processing for immunocytochemistry was performed using antibodies directed against total HspB1 (Stressgen SPA801) or phospho-S15-HspB1 followed by fluorescently tagged secondary antibodies; F-actin was labelled using Alexa-488-phalloidin. Panel A-D: PC12 cells visualized with confocal microscopy; images represent the z-stack projections. A - HspB1 (blue); B - phalloidin (green); C - pS15-HspB1 (magenta); D- merged image. Panels E-K, L-R: three-dimensional rendering of immunostained surfaces as compiled by Imaris software of cells (boxes in D) selected from the low power view. E, L -HspB1 (blue); F, M - Phalloidin (green); G, N - pHspB1 (magenta); H, O - all 3 together; I, P - HspB1 + pHspB1; J, Q - HspB1 + Phalloidin; K, R - pHspB1 + Phalloidin. Scale bar – 10  $\mu$ m.



Three-dimensional images of each channel separately and in combination provide a more informative view of the distribution of HspB1 and actin under each of the conditions. Representative cells (or groups of cells) were selected from the each of the images presented in Fig. 2.1-2.3 and 3-dimensional surfaces for each channel rendered using Imaris software. Confocal image stacks were obtained with sequential z-stage scanning over a 5-10 um top-bottom distance of the immunostained cultures, image stacks imported into Imaris software (Bitplane Corp), and 3D surfaces and cellular volumes displayed.

In cells selected from the control condition (Fig. 2.1E-R), HspB1 is distributed rather evenly throughout the cytoplasm, and colocalized with both F-actin and basal levels of pHspB1 for the most part. However, pHspB1 is also clearly observed at the leading edges of the cells (perhaps in focal contacts/adhesions) and co-localized with F-actin in these areas (Fig. 2.1J, Q). F-actin is associated with cortical areas (particularly noticeable in Fig. 2.1F, J and K) as well as being found distributed throughout in apparent colocalization with HspB1 and pHspB1. Note that the cortical F-actin does not appear to completely overlap with HspB1 in these examples (Fig. 2.1E, F, H and J).

With HS (Fig. 2.2E-R), many of the cells have rounded up, and in these cells both HspB1 and F-actin appear condensed and collapsed (Fig. 2.2E-K). There is an increased amount of pHspB1 and this appears associated mainly with the surfaces of the cells (Fig. 2.2G-I). In the second series of cells (Fig. 2.2L-R), the blebbing noted above is more clearly observed showing that pHspB1 and F-actin apparently associated with the surface of cell.

In cells subjected to HS in the presence of the inhibitor (Fig. 2.3E-R), the phosphorylation of HspB1 is attenuated, but what little is present is still associated with actin and membrane blebbing. In one cell, where the HspB1 has become mainly perinuclear, much of the F-actin

remains peripheral, although there is still some overlap with the perinuclear HspB1. In these cells, even where there is essentially no pHspB1 detectable, HspB1 and F-actin still colocalize.

Interestingly, in cells where there is no detectable pHspB1 (arrowheads, Fig. 2.3N-O), F-actin appears to be retained in a cortical organization though not associated with HspB1. In another example (Fig. 2.3F-G), in the absence of pHspB1, there is still colocalization with HspB1 and a more cellular distribution of the F-actin staining, perhaps indicative of the presence of smaller actin filaments.

These results show colocalization of HspB1 and F-actin in both control and stressed conditions, and suggest that HspB1 does not necessarily require phosphorylation in order to interact with F-actin.

Statistical analysis of the imaging data (described in the Methods) confirmed the qualitative expression differences, showing pHspB1 was significantly up-regulated with stress and this up-regulation attenuated by the inclusion of SB203580; there was no significant difference in the expression of total HspB1 in any condition (Supplementary Fig. 2.1).

#### **2.4.2 Biochemical Assessment of HspB1 and F-actin distribution with stress:**

To further investigate whether the immunocytochemical colocalization represents a molecular association of HspB1 with F-actin, we carried out a series of biochemical assays using analyses of protein lysates from cells treated as noted above (control, 30 min HS, SB, and SB+HS). Cells lysed immediately at the end of the experimental treatment (no recovery from HS) and the intracellular distribution of HspB1 and actin was determined by Western blotting of 3 different preparations: the Triton X-100 soluble (cytosolic lysate), Triton X-100 insoluble (cytoskeletal pellet) and unfractionated total cellular lysate.

**Supplementary Figure 2.1: Densitometric analyses of relative gray levels of PC12 cell ICC demonstrating the significant increase in pSer15-HspB1 and pSer86-HspB1 with heat shock.**

Relative densitometric quantification and statistical analyses of cells imaged by confocal microscopy analyzed using ImageJ. Values expressed are the average grey values for pSer15-HspB1, pSer86-HspB1 and total HspB1 (+/- S.E.M., n = 100). \*\*: P<0.01; \*\*\*: P<0.001

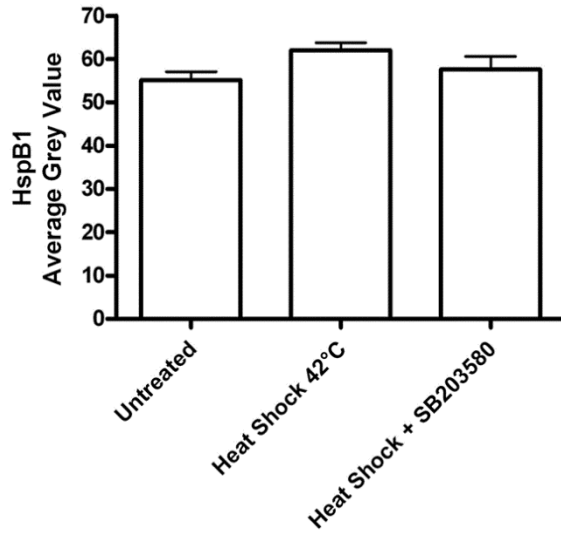
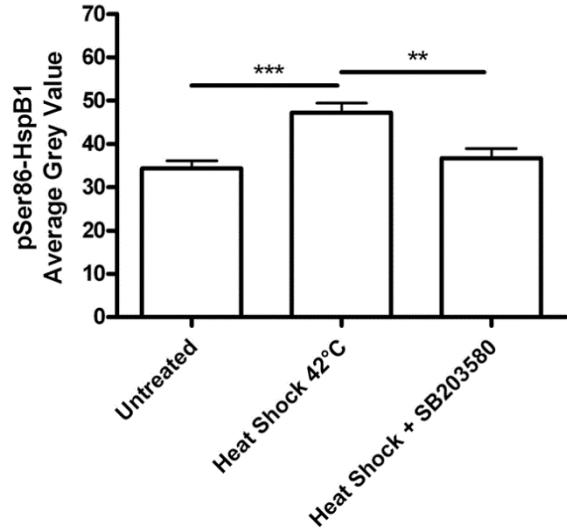
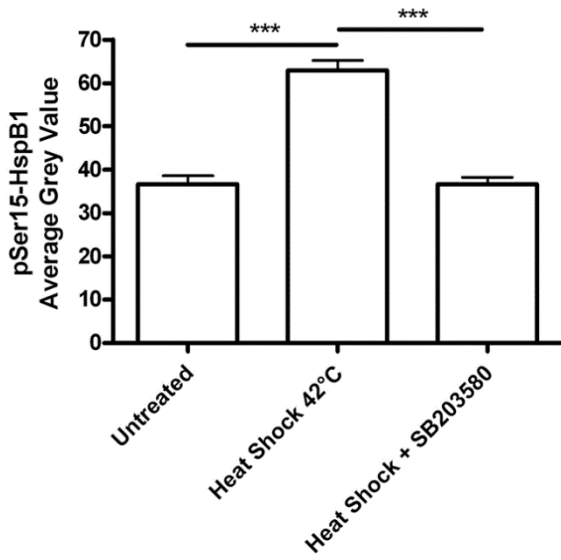
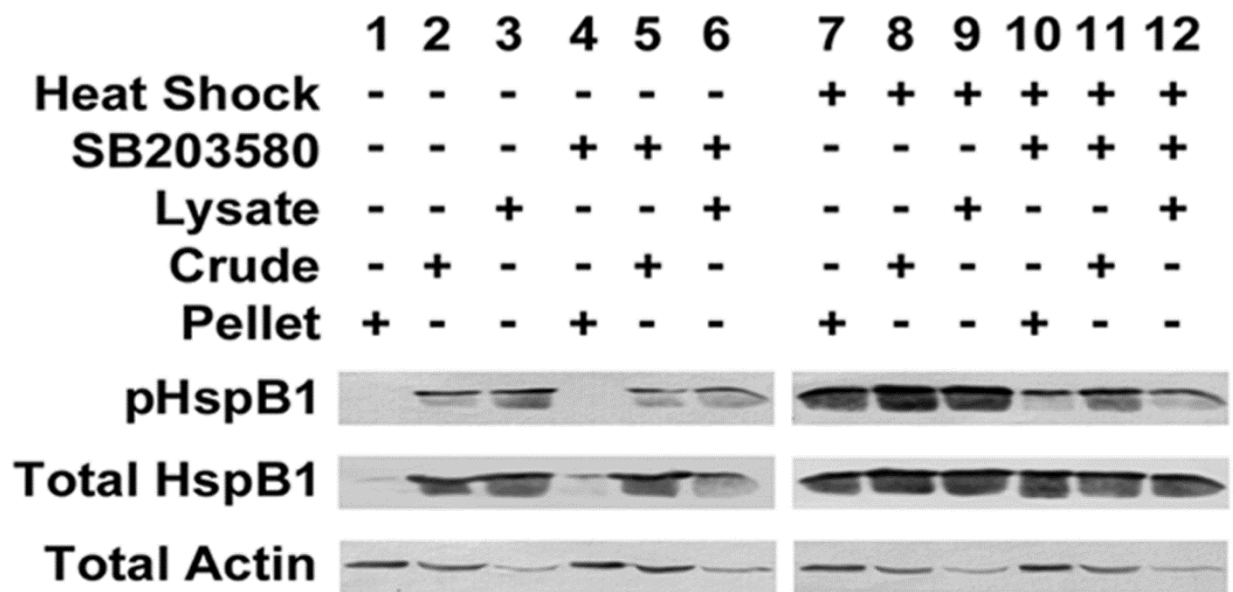


**Figure 2.4: HspB1 is phosphorylated and redistributed to the cytoskeletal fraction during cellular stress.**

PC12 cells were treated as described in the Methods, subsequently lysed and separated by cellular fractionation into Triton X-100 soluble (cytosolic; lysate) and Triton X-100 insoluble (cytoskeletal; pellet) samples, or were left as crude total protein samples. Untreated cells (Lanes 1-3); treated with 10  $\mu$ M SB203580 (Lanes 4-6); heat shocked cells (Lanes 7-9); cells treated with inhibitor and heat shock (Lanes 10-12). Western blots were sequentially probed with antibodies to pS15-HspB1, pS86-HspB1, HspB1 and actin; blots were stripped after analysis of each probe. Note the increased amount of HspB1 in the cytoskeletal fraction after HS, as well as the increased amount of phosphorylated HspB1.



Under control conditions, total HspB1 was primarily found in the cytosolic and crude total protein fractions, and there was also a low level of pHspB1 detected in these samples (Fig. 2.4). After HS, there was an increase in HspB1 in the cytoskeletal fraction (compare lane 1 with lane 7) associated with increased phosphorylation of HspB1. With the addition of the p38-MAPK inhibitor SB203580, HspB1 phosphorylation was attenuated as expected, but there appeared to be little effect on the redistribution of the HspB1 to the cytoskeletal fraction (Fig. 2.4). While HS does result in increased expression of HspB1 over a longer time frame [ $> 3$  hrs recovery after HS (Mearow et al., 2002)], in these experiments cells were sampled immediately after the termination of the HS treatment to assess early effects of HspB1 phosphorylation.

Actin was detected in all cell fractions with an increased expression in the cytoskeletal fraction (Fig. 2.4, e.g., lanes 1 vs. 3), but with little detectable difference in distribution with stress. Since the antibodies used to probe for actin detect both filamentous and globular actin, one cannot distinguish between the two species by Western blotting. However, it is generally accepted that the actin associated with the cytoskeletal fraction represents F-actin, while the cytosolic fraction represents globular actin (Kobayashi et al., 1982).

### **2.4.3 Determining the interaction(s) of HspB1 and F-actin**

#### **2.4.3.1 Pull-Down and Immunoprecipitation assays**

While HspB1 is reported to interact with actin, there has been little evidence of an interaction with F-actin specifically in a cellular model (in the absence of overexpression of tagged HspB1). We thus investigated whether there was an association of HspB1 with F-actin, and if so, whether the phosphorylation state of HspB1 influenced this interaction.

To specifically isolate F-actin we employed a biotinylated phalloidin pull down protocol. The efficacy and specificity of this approach was first assessed using solutions of polymerized F-actin and G-actin. As shown in Fig.2.5, the biotinylated phalloidin specifically pulled down F-actin (top panels), with no G-actin being observed in the precipitated samples (bottom panels).

Experimental samples were incubated with biotinylated-phalloidin followed by precipitation of the captured complexes with streptavidin-linked magnetic beads. Precipitated fractions were then subjected to SDS-PAGE and immunoblotted to detect pHspB1, total HspB1 and actin. Although we were primarily interested in the F-actin and HspB1 in the cytoskeletal fractions we initially performed the experiments on both the total cell lysate (N=2 experiments) and the cytoskeletal fraction (N = 3 experiments).

The Western blots of representative phalloidin pull-down experiments are presented in Fig. 2.6 (panels A, B) while Fig.2.7 presents the graphical analyses of these experiments from the total cell lysate (Fig. 2.7A) and the cytoskeletal fraction (Fig. 2.7B). As shown in Fig. 2.6A, pulldown of F-actin from the total cellular lysate captured HspB1 in the control situations and this was increased with HS. In the control situations, little of the HspB1 associated with the F-actin was phosphorylated. However, after HS, the fraction of pHspB1 associated with F-actin increased, and this was inhibited in the presence of SB203580.

Phalloidin pulldown from the Triton X-insoluble (cytoskeletal pellet) fraction, which should be enriched in F-actin, is shown in Fig. 2.6B. HspB1 was precipitated with the F-actin, although there were no significant differences between the untreated and HS conditions for either the F-actin or HspB1 (Fig. 2.7B). In contrast to the total cellular lysate, much of the HspB1 found in the complexes with F-actin was phosphorylated and was significantly increased with HS, and blocked with the inhibitor (Fig. 2.7B).

**Figure 2.5: Specificity of the phalloidin pull-down for F-actin.**

*In vitro* preparations (2.5 or 5.0  $\mu\text{g}$ ) of globular actin (G-actin) and filamentous actin (F-actin) were prepared using an *in vitro* actin-binding assay kit (Cytoskeleton) and incubated with 5.0  $\mu\text{g}$  biotinylated-phalloidin as described in the Methods section. The resulting solutions were separated into supernatant (non-phalloidin interacting) and pull-down (phalloidin interacting) samples and assayed by Western blotting. Additionally, untreated G- or F-actin samples were also probed. Note that biotinylated-phalloidin selectively precipitates F-actin, but not G-actin, and that this pull-down is reasonably efficient.

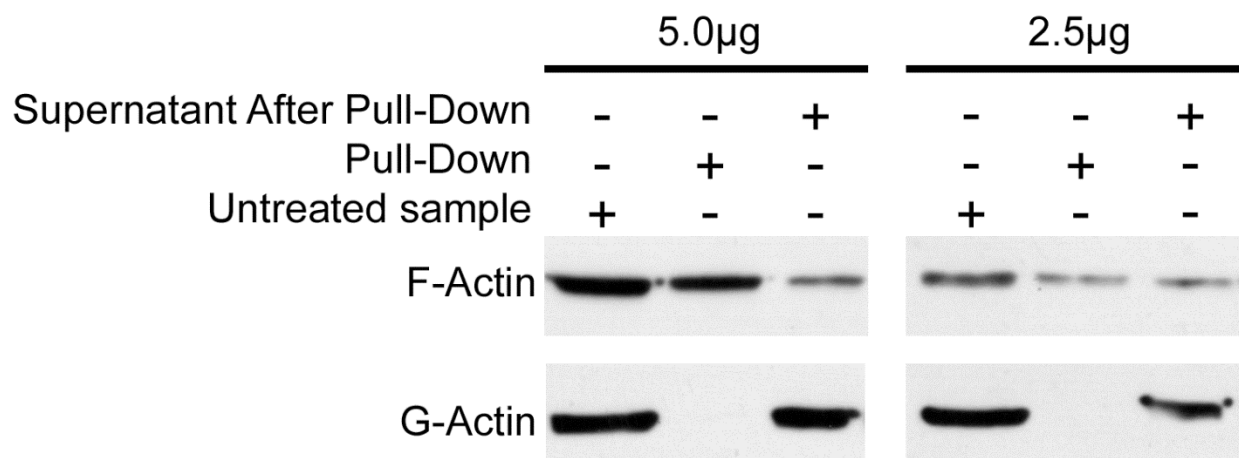


**Figure 2.6: HspB1 is associated with F-actin.**

Representative blots showing precipitation of F-actin complexes (with biotinylated phalloidin, A-B) and immunoprecipitations (IP) of HspB1 (C-D) from total cellular lysates (A, C) or the cytoskeletal pellet fraction (B, D). PC12 cells were treated as described in the Methods. Cell cultures were exposed to 10  $\mu$ M SB203580 for 1 hr, after which cultures were either incubated for an additional 30 mins, or stressed with heat shock at 42°C for 30 mins; control cells were not treated. Immediately after treatments, cells were collected, lysed with actin stabilization buffer; samples were separated for analysis as total cell lysate or further fractionated into the TritonX-100 insoluble cytoskeletal pellet. Samples were incubated with biotinylated-phalloidin followed by precipitation of the captured complexes with streptavidin-linked magnetic beads. Precipitated fractions were then subjected to SDS-PAGE and sequentially immunoblotted to detect pHspB1, total HspB1 and actin. Pulldown of F-actin also captures HspB1 in both the cell lysates (A) and the cytoskeletal fraction (B); similarly the HspB1 IPs also bring down actin and this is enhanced in the cytoskeletal fraction.

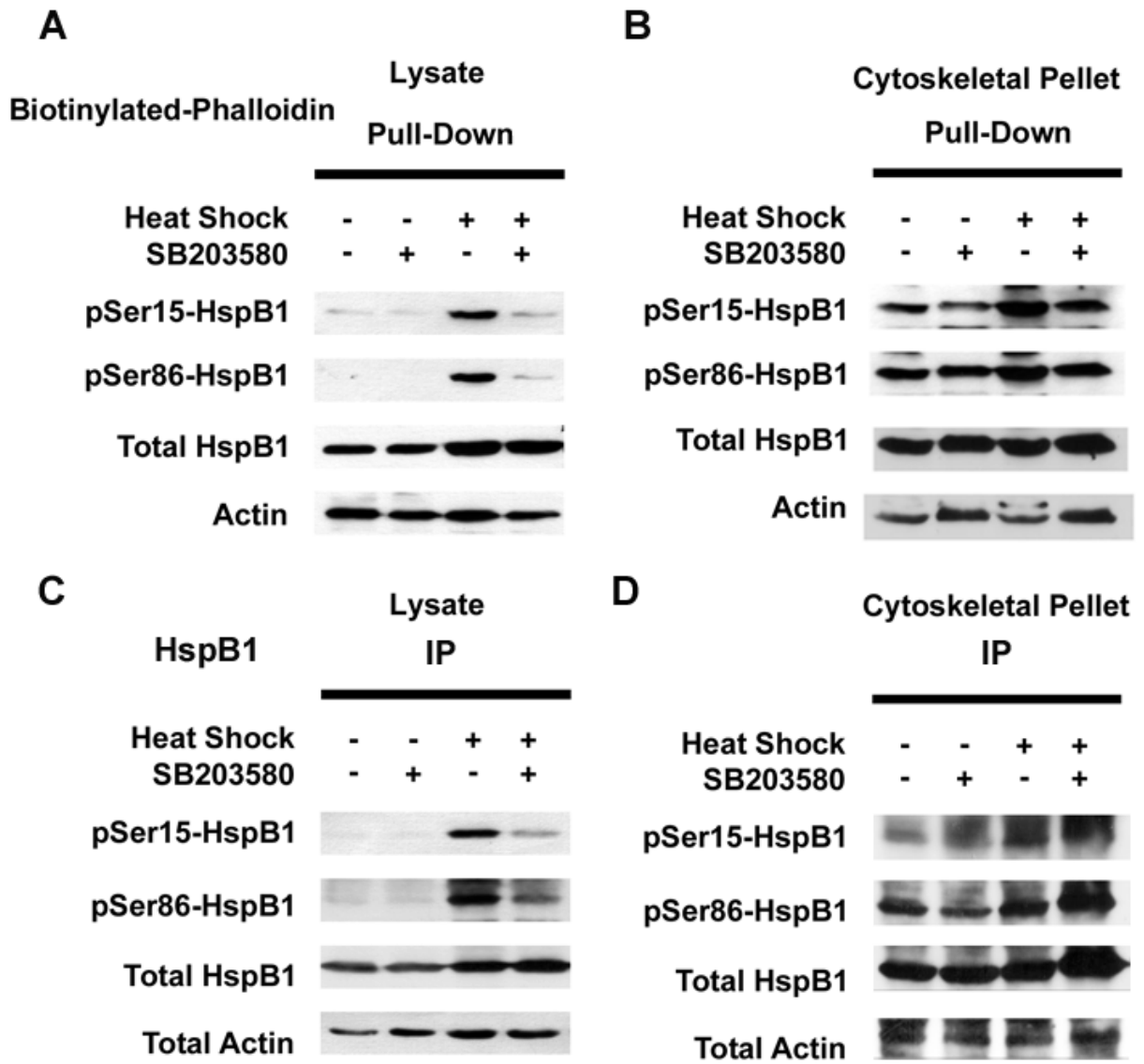
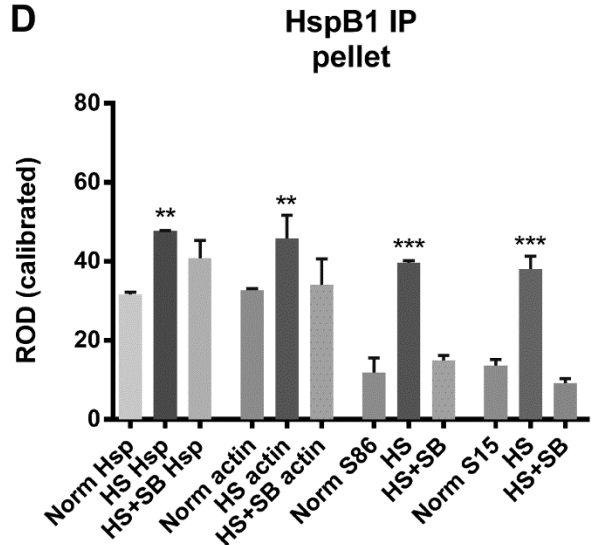
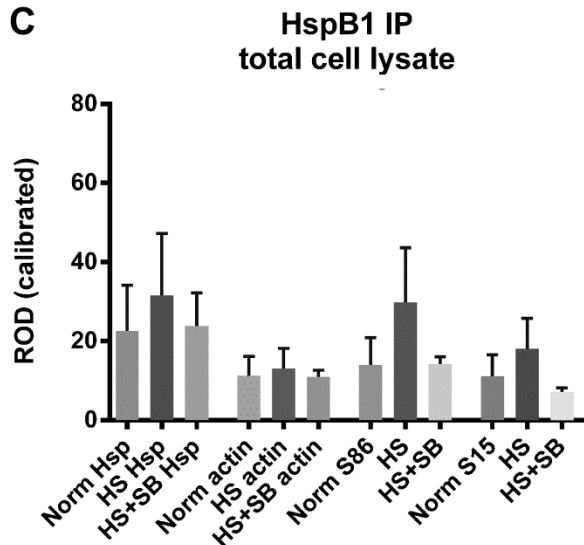
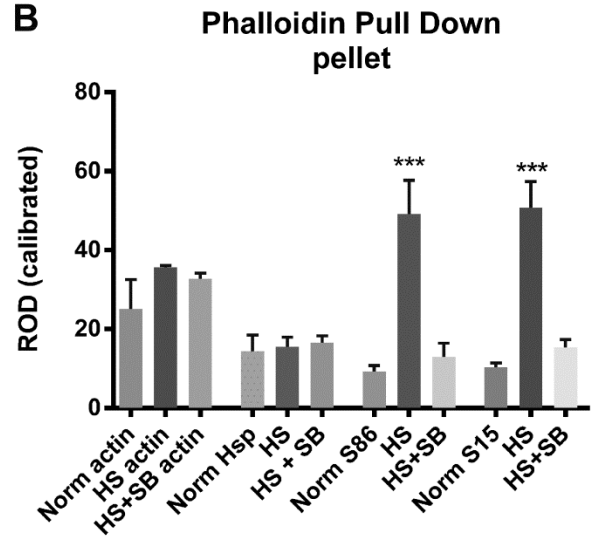
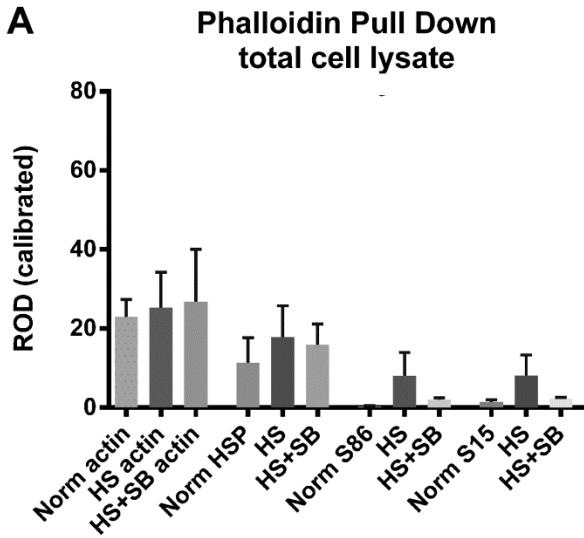


**Figure 2.7: Densitometric analyses of the amounts of F-actin and HspB1 in the precipitated complexes.**

Western blots were scanned and densitometric analysis of bands carried out using Image J and a calibrated gray scale standard. The bars are the mean relative optical density (ROD) ( $\pm$  SEM) of paired values for Actin , HspB1 (Hsp), pS86-HspB1 (S86) and pS15-HspB1 (S15) from each of 3 separate experiments for the cytoskeletal fraction samples (pellet) and from 2 separate experiments for total cell lysates. Panel A - Phalloidin pulldown from total cell lysates; B - Phalloidin pulldown from the cytoskeletal fraction; C - HspB1 IP from total cell lysates; D - HspB1 IP from the cytoskeletal fraction. Norm - control; HS - Heat Shock; HS + SB - Heat shock + SB203580. \*\* P < 0.01; \*\*\* P <0.001

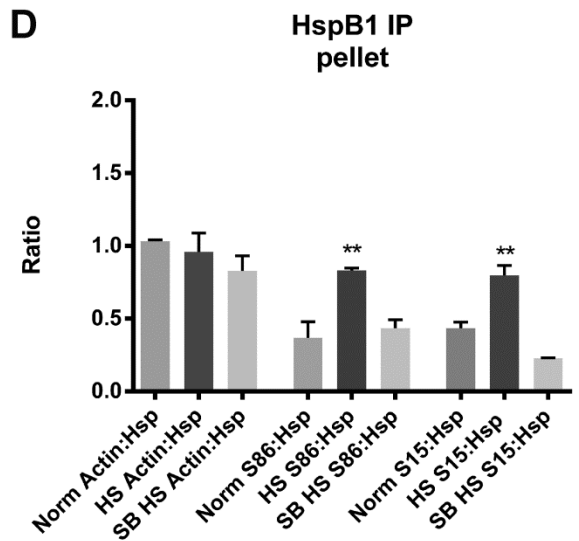
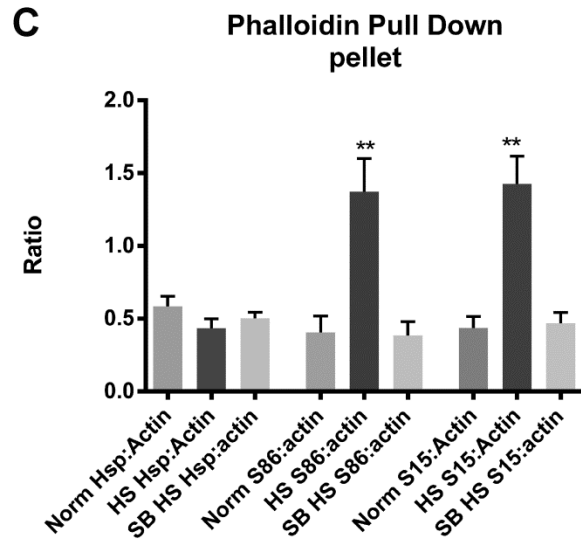
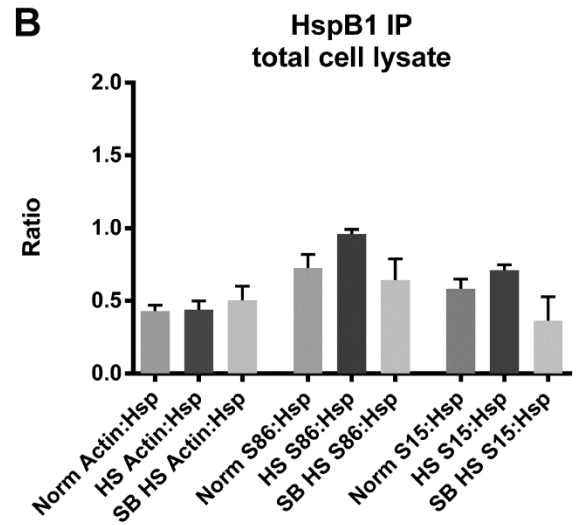
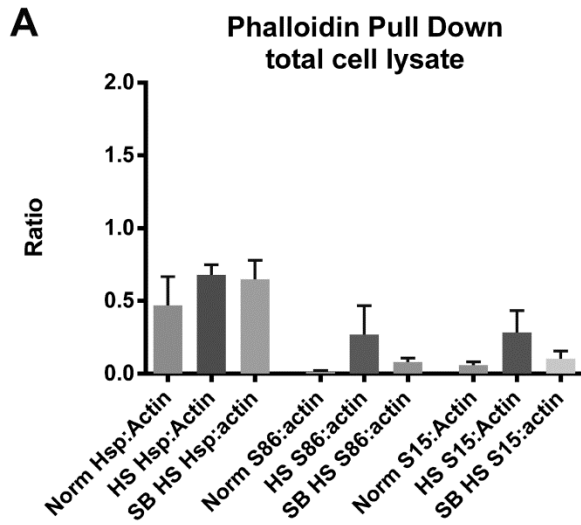


In order to provide some measure of specificity, since it was possible that large complexes in the cytoskeletal precipitates could be non-selectively ‘trapping’ HspB1, we carried out immunoprecipitation of HspB1 under the same conditions as noted above. The results of representative HspB1 IP experiments are presented in Fig. 2.6C-D, with graphical analyses presented in Fig. 2.7C-D. HspB1 immunoprecipitated from the cell lysates, with an increase in immunoprecipitated HspB1 found after HS (Fig. 2.6C). In the control conditions little of the HspB1 was phosphorylated (similar to what was observed for the F-actin pulldown), with increases in pHspB1 observed after HS and blocked in the presence of the inhibitor. Here we also observed actin being co-precipitated with the HspB1 (Fig. 2.6C). In the cytoskeletal fraction, as with the F-actin-specific pull-downs, IP of HspB1 showed that with HS there was a significant increase in the amount of HspB1 precipitated (Fig. 2.7D). This indicated a redistribution from the cytosol to the cytoskeletal fraction and concomitantly, also a significant increase in the amount of actin co-precipitating with HspB1 (Fig. 2.7D). pHspB1 was significantly increased after HS and this increase was attenuated by treatment with the inhibitor (Fig. 2.7D).

The ratios of HspB1 and pHspB1 relative to F-actin are presented graphically in Fig. 2.8 (Fig. 2.8A, C for F-actin; Fig. 2.8B, D for HspB1). With respect to the F-actin pulldown, the ratio of HspB1:actin does not differ between the total cell lysate and the pellet, however it is clear that HS significantly increases the fraction of phosphorylated HspB1 precipitated with F-actin (Fig. 2.8C). Although the ratio of actin:HspB1 differs between the cell lysates and the pellet, with more actin being associated with HspB1 in the cytoskeletal fraction, again there is a significant increase in the phosphorylated fraction of HspB1 with HS.

**Figure 2.8: Changes in the relative amounts of the association of F-actin and HspB1.**

Densitometric data of F-actin and HspB1 expression in pulldowns presented as ratios of HspB1:F-actin or Actin:HspB1, as well as the pHspB1:F-actin or pHspB1:HspB1. Panel A - ratios for Phalloidin pulldown from total cell lysate; B - ratios for HspB1 IP from total cell lysate; C - ratios for Phalloidin pulldown from cytoskeletal fraction (pellet); D - ratios for HspB1 from the cytoskeletal fraction. \*\* P <0.01



The results of the biotinylated pulldowns suggest that not only does HspB1 directly interact with F-actin, but also that a relatively large fraction of this HspB1 is phosphorylated in stressed cells. The HspB1 IP experiments also point to an interaction with F-actin selectively (results from the cytoskeletal fraction), although we cannot rule out an interaction of HspB1 also with non-filamentous actin (results from the total cell lysates, where both F- and G-actin should be present).

## **2.5 Discussion**

In this study, we investigated the interaction of HspB1 with cytoskeletal F-actin and the influence of phosphorylation on this association. We demonstrate cellular colocalization of HspB1 and F-actin as well as a molecular interaction between endogenous HspB1 and F-actin under both control and stressed conditions. Our pulldown and IP results indicate that HspB1 and F-actin are normally associated to some degree, but cell stress results in an enhanced interaction especially of pHspB1. Overall, our data provide support for a direct association of HspB1 with F-actin.

### **2.5.1 HspB1 interactions with actin**

HspB1 has been reported to interact variably with actin filaments or monomeric actin to influence actin polymerization and/or depolymerization (Doshi et al., 2009; During et al., 2007; Guay et al., 1997; Lavoie et al., 1995; Li et al., 2012a; Schneider et al., 1998; Seit-Nebi et al., 2013; Wettstein et al., 2012). *In vitro* studies have demonstrated interactions between actin and recombinant HspB1 (Datskevich et al., 2012; During et al., 2007; Graceffa, 2011; Mymrikov et al., 2012; Pivovarova et al., 2007). Similarly, a number of *in vivo* studies have shown

interactions of HspB1 constructs with actin by immunoprecipitating tagged-HspB1, or colocalization at a cellular level of F-actin and HspB1 often employing cells overexpressing various constructs of HspB1 (Bryantsev et al., 2007; Doshi et al., 2009; Huot et al., 1996; Landry and Huot, 1995; Verschuure et al., 2002). However, a direct interaction between HspB1 and either G- or F-actin has been questioned (Mymrikov et al., 2011; Seit-Nebi et al., 2013).

While there have been numerous studies describing an interaction between F-actin and HspB1 using purified solutions of each, there has been much less evidence of such interactions in a cellular system. Models for HspB1 regulation of actin filament dynamics propose that non-phosphorylated monomeric HspB1 inhibits actin polymerization by acting as an actin-capping protein or by binding to and sequestering G-actin monomers, while phosphorylation reverse this effect and allows for polymerization or filament elongation (During et al., 2007; Li et al., 2012a).

### **2.5.2 Role of HspB1 and actin interactions in unstressed cells:**

HspB1 interactions with actin and other cytoskeletal elements play a role in the dynamic regulation of the cytoskeleton that underlies cellular behavior. For example, HspB1 has been shown to be required for cellular migration in a variety of cell types: leukocytes, smooth muscle, neutrophils and fibroblasts (Jog et al., 2007; Landry and Huot, 1999; Nomura et al., 2007; Pichon et al., 2004). Its role in migration is via regulation of actin filament polymerization at the leading edge of the cell, as well as in focal adhesions that connect the actin cytoskeleton to the extracellular matrix. In addition to influencing cell migration, HspB1 also plays a role in axonal growth from neurons (Benn et al., 2002; Costigan et al., 1998; Williams and Mearow, 2011; Williams et al., 2005, 2006). We have suggested that the regulation of actin dynamics by HspB1 is important in axonal growth from primary neurons, and have previously demonstrated

colocalization of HspB1 with F-actin and tubulin in lamellipodia, filopodia and focal contacts at the earliest stages of sensory neurite growth as well as in mature axons and growth cones (Williams et al., 2005, 2006). Using phosphorylation mutants of HspB1, we have recently reported that phosphorylation (or the oligomerization) status of HspB1 does influence neurite growth and colocalization of HspB1 with F-actin in growth cones (Williams and Mearow, 2011). However the influence of phosphorylation was not clear cut as that observed in other cellular models. For example, HspB1-EE (fully phosphorylated and unable to be dephosphorylated) resulted in the lowest amount of total neurite growth which could be consistent with decreased actin polymerization. In contrast, the non-phosphorylatable construct (HspB1-AA) showed similar growth to the wild-type HspB1 but a more patchy colocalization with F-actin, an effect that is difficult to explain based on the models that suggested that nonphosphorylated HspB1 inhibits F-actin polymerization via sequestration of actin monomers (During et al., 2007) or capping of the barbed ends of actin filaments (Benndorf et al., 1994). Unlike the results observed in experiments with purified HspB1 and actin, the situation in the cellular context is much more complex, with HspB1 being able to be rapidly phosphorylated and dephosphorylated in response to the changing cellular environment.

The current study was undertaken as part of our efforts to understand interactions of actin and HspB1 in a cellular context using a model system more amenable to biochemical approaches. Here in the control cells, we observed that the cellular distribution of HspB1, pHspB1 and F-actin is consistent with a role in normal cellular attachment, spreading and cellular motility, being present in lamellipodia and at the leading edges of cells (Fig. 2.1). Specific isolation of F-actin from total cell lysates or the cytoskeletal fraction also precipitated HspB1. Non-phosphorylated HspB1 was observed in a complex with F-actin in the control cells, as was the

relatively small fraction of phosphorylated HspB1. In this situation the association of HspB1 and F-actin likely plays a role in the normal adhesion and motility of these PC12 cells, with phosphorylated HspB1 potentially supporting actin polymerization needed for cellular adhesion and migration (Pichon et al., 2004; Rousseau et al., 2000).

### **2.5.3 Role of HspB1 in cytoskeletal protection:**

Part of HspB1's protective role in stressed cells has been attributed to its interactions with actin, resulting in increased actin filament stability. During various stresses HspB1 has been reported to increase the stability of the actin cytoskeleton effectively preventing actin fragmentation (Lavoie et al., 1993; Lee et al., 2007; Schafer et al., 1999; Van Why et al., 2003; Vigilanza et al., 2008). HspB1 has been reported to interact with actin as a barbed end actin capping protein (Miron et al., 1991), and its actions in protecting the actin filament cytoskeleton have been attributed to this actin capping ability (Lavoie et al., 1993). It has also been suggested, however, that HspB1 impairs actin filament polymerization by sequestering actin monomers rather than by capping (During et al., 2007). Protection of the actin cytoskeleton by HspB1 appears to be dependent on the ability of HspB1 to bind to denatured actin filaments, preventing their aggregation and facilitating reformation (Pivovarova et al., 2005). In the actin-capping model, HspB1 was thought to cap actin filaments as a nonphosphorylated monomer and its phosphorylation resulted in dissociation from the actin filament and elongation (Benndorf et al., 1994; Guay et al., 1997; Landry and Huot, 1999; Lavoie et al., 1995; Miron et al., 1991). The actin sequestering model suggests that nonphosphorylated HspB1 binds actin monomers resulting in an increase in the G-actin pool and a subsequent decrease in actin filament levels; upon phosphorylation HspB1 dissociates from the actin monomers which are then available for

filament elongation (During et al., 2007). A recent *in vitro* study provides support for a model with HspB1 binding along the lengths of actin filaments, but not acting as a capping protein (Graceffa, 2011).

HspB1 is known to interact directly with actin *in vitro* as described above, but whether this is also true in cells has been unclear. While a number of studies have shown co-localization of HspB1 with F-actin and redistribution of both after various stimuli using confocal microscopy, few have concomitantly studied whether there is a biochemical association with F-actin. Furthermore, the majority of these investigations have employed cells in which HspB1 had been overexpressed (Bryantsev et al., 2002; Doshi et al., 2009; Landry and Huot, 1995; Lavoie et al., 1995; Pichon et al., 2004; Piotrowicz et al., 1998). Although there has been little evidence for a direct association of HspB1 and actin *in vivo*, recent studies have shown that actin exists in complexes of immunoprecipitated HspB1 (Doshi et al., 2009; Jia et al., 2010). One of these demonstrated that actin could be interacting with HspB1 based on immunoprecipitation of overexpressed tagged fish HspB1 from mammalian cells (Doshi et al., 2009). In this study, the interaction between fish HspB1 and actin after HS was observed to decrease by 3 hrs, but then increased by 24 hrs. In our study, we were primarily interested in the response of PC12 cells to a HS over the short term when phosphorylation of HspB1 increases rapidly; in PC12 cells in response to HS, pHsp is detectable as early as 5 min after a 15 min HS, with a maximum reached by 1 hr (Mearow et al., 2002). Unlike the former study, we observed association of HspB1 with F-actin in the control cells and an increased association of pHspB1 with F-actin immediately after the termination of the HS.

An elegant study by Jia and colleagues quite clearly demonstrates that endogenous HspB1 interacts not only with actin but also with several other cytoskeletal proteins and actin-binding

proteins (Jia et al., 2010). In our experiments, while we did not exhaustively investigate the presence of other proteins in the precipitated complexes, we did not detect the presence of tubulin, neurofilament, nestin or Daxx (data not shown), suggesting that interactions between HspB1 and the cytoskeleton may vary in different cells.

In our investigation, we performed pull-down and immunoprecipitation assays in order to determine any interaction between HspB1 and F-actin. Under all conditions HspB1 interacted with F-actin with seemingly high selectivity, based upon our approach of performing both direct precipitation of F-actin and the reverse approach of HspB1 IP. Our results show that HspB1 is found in a complex with F-actin both in non-phosphorylated and phosphorylated forms, with an increased association of pHspB1 with actin after stress. In the normal cells, the cellular distribution of HspB1, pHspB1 and F-actin is consistent with a role in cellular motility, being present in lamellipodia and at the leading edges of cells (Fig. 2.1). Upon HS, there was a relatively rapid (within 30 min) reorganization of the cytoskeleton accompanied by a redistribution and increased phosphorylation of HspB1 (Fig. 2.2). This is evident at the level of cellular localization (Fig. 2.1-2.3) and also at the biochemical level (Fig. 2.4, 2.6-2.8). Specific isolation of F-actin from total cell lysates or the cytoskeletal fraction also precipitated HspB1. Non-phosphorylated HspB1 was observed in a complex with F-actin in both the control and stressed cells. A relatively small fraction of HspB1 is phosphorylated in the control cells. In this situation according to the proposed models, phosphorylated HspB1 would support actin polymerization needed for cellular adhesion and migration (Pichon et al., 2004; Rousseau et al., 2000). After HS there is an increased phosphorylation and redistribution of HspB1 to the cytoskeletal fraction. It is clear that a significant fraction of the HspB1 pulled down with F-actin is phosphorylated on both the Ser15 and Ser86 sites, and that this is attenuated by the presence of

the p38-MAPK inhibitor, SB203580. The increase in phosphorylation and increased association with F-actin is consistent with the role of HspB1 in protecting actin filaments by inhibiting actin fragmentation (Lavoie et al., 1995; Schafer et al., 1999). The reverse pull-down experiments provide similar results. Immunoprecipitation of HspB1 also brings down actin and, in the cytoskeletal pellet at least, it is highly likely that this is also F-actin. With stress there is an increased amount of HspB1 precipitated, and an apparent corresponding increase in the amount of actin, although ratio of actin:HspB1 does not differ between conditions (Fig. 2.7 and 2.8).

These results are the first that we are aware of to combine both cellular and molecular approaches to show cellular localization and a direct demonstration of an interaction between endogenous HspB1 and F-actin, using a method that specifically isolates endogenous F-actin. However, based upon the reports of others, we also are aware that despite our evidence that we cannot rule out some other indirect interactor that plays a role in linking the response of the cytoskeleton to HspB1.

## **2.6 Conclusions:**

HspB1 is associated with the actin cytoskeleton in both control and heat-shocked cells. HspB1 phosphorylated on both the S15 and S86 sites is detectable by immunocytochemistry in normal cells and this is increased after HS, but attenuated by treatment with the p38-MAPK inhibitor. HspB1 is found distributed primarily throughout the cytoplasm in the normal cells and is redistributed after HS to the cytoskeletal fraction, where it is detected as colocalized with F-actin. HS results in the phosphorylation of HspB1, which also colocalizes with F-actin and is significantly increased in association with F-actin after stress. These results directly demonstrate

that HspB1 interacts with F-actin and that both phosphorylated and non-phosphorylated HspB1 are found to be present in F-actin complexes.

## **2.7 Acknowledgements:**

We thank members of the Mearow lab (especially F. Nafar) for their technical support and assistance in the course of this study.

## **Chapter 3: Exploring the Link between HspB1, Daxx, Bcl-2 and Autophagic Activity in DRG Neurons**

### **3.1 Abstract**

The understanding of how cells use endogenous mechanisms to oppose the detrimental effects of cell stress is quite complex. Influencing the complexity of how cell stress mechanisms work is how a multitude of individual proteins interact with each other to influence the overall process. This study investigates how the proteins HMGB1, HspB1, Daxx and Bcl-2 are linked to the activity of autophagy in DRG neurons. Cell stress was stimulated in DRG neurons by treating with a high D-glucose concentration, and the mRNA expression, immunocytochemical protein expression and cellular localization of HMGB1, HspB1, Daxx and Bcl-2 were assessed. In conjunction, the protein expression and cellular localization of the autophagosome-specific protein LC3B was also assessed. The results demonstrate that the endogenous mRNA expression of HspB1, Daxx and Bcl-2 is altered during cell stress with high glucose treatment, and this further corresponded to changes in their cellular localization and expression as observed with immunocytochemistry. Further, HMGB1 and LC3B cellular localization and expression did not change with D-glucose treatment. Overall, this study evaluated a link between HspB1, Daxx, Bcl-2 and HMGB1 that could potentially provide a control mechanism of autophagic activity during cell stress. Although the data presented does not suggest a specific pathway, it does allow for further research to be undertaken in order to further explore a potential mechanism.

### 3.2 Introduction

The survival of cells during and after stress is highly dependent upon the coordinated mechanistic properties of many endogenous intracellular proteins. During stress, these proteins may undergo a multitude of alterations including post-translational modifications, cellular localization changes, or protein expression and dynamic interaction variations. The specificity and selectivity of any cell survival protein alteration needs to be coordinately modulated so as to both react to a cell stress and not cause detrimental effects during cellular homeostasis. As such, cells have developed endogenous mechanisms that modify protective activities according to their needs.

Two protective cellular responses that are under constant cellular control are the heat shock response and autophagy. Both processes are endogenously active during cellular homeostasis and stress, and act to recycle old and damaged proteins and organelles. In the case of heat shock proteins, they provide proper chaperoning and folding of newly created proteins, and interact with various cellular proteins, modifying them according to the cellular state. For instance, *in vitro* studies have found that HspB1 can interact with Daxx, inhibiting its ability to activate apoptosis during cell stress (Charette and Landry, 2000; Charette et al., 2000). Under normal conditions, endogenously expressed Daxx acts as a transcriptional co-repressor, found to interact with transcriptional co-regulators including HDACs and DNMTs, and with a number of DNA-binding transcription factors, including ETS1 and the p53 family proteins (Ecsedy et al., 2003; Hollenbach et al., 2002; Michaelson et al., 1999; Muromoto et al., 2004). During cell stress conditions, however, Daxx has been found to translocate to the cytoplasm where it subsequently helps activate apoptosis through the activation of apoptosis signal-regulating kinase 1 (Yang et al., 1997).

Although HspB1 interacts with Daxx to prevent apoptosis during cell stress, studies have not yet considered the effects of HspB1 on modifying the transcriptional effects of Daxx. Of the transcriptional targets of Daxx co-repression discovered, bcl-2 is one of the most intriguing (Li et al., 2000). Aside from being an important anti-apoptotic protein, Bcl-2 also acts as a regulator of autophagic activity through its regulation of Beclin1 activity (He et al., 2013; Maejima et al., 2013; Pattingre et al., 2005). Beclin1 is an integral protein in autophagy initiation, and as such, is tightly controlled so as to control the activation of a further autophagic response. Under normal conditions, Bcl-2 and high-mobility HMGB1 are under constant competitive regulation of Beclin1, where Beclin1 activity is inhibited by Bcl-2 and activated by HMGB1 (Kang et al., 2010). This competitive regulation of autophagy allows for both an endogenous activity of the process, as well as prevents it from being inadvertently over-activated when a cell is not undergoing a stressful stimulus.

Although current studies have not focused on the influence of Daxx on autophagy, it could be hypothesized that if Daxx were transcriptionally regulating Bcl-2, it could also potentially be indirectly affecting autophagy. A further interesting point is the fact that HMGB1 also acts as a nuclear DNA-binding protein that is capable of regulating the expression of HspB1 (Narumi et al., 2015; Tang et al., 2011). Again, since HspB1 has been found to bind to Daxx, it is possible that the activity of Daxx itself, and thus the transcriptional repression of Bcl-2 and the activity of autophagy could be modulated by HspB1 activity and expression.

In this study, the possibility that HspB1, Daxx, Bcl-2 and HMGB1 form an interaction paradigm that controls autophagic activity during cell stress in DRG neurons was explored. DRG neurons were chosen as a model to study the interaction paradigm since cell stress in these neurons can lead to adverse cytoskeletal changes in their axons, causing disassembly and

granular degeneration of the axons, and ultimately cell death (Raff et al., 2002; Wang et al., 2012). DRG neurons, however, have a robust capacity to regrow damaged axons under favorable conditions, including the presence of neurotrophins and a positive extracellular matrix growth environment (Tucker et al., 2005a, 2006). As a result, a number of studies are now focusing on trying to determine early endogenous cellular indicators of stress that can be modulated to attenuate DRG neuropathy and promote recovery, with the process of autophagy being studied in particular [e.g., (Gavazzi et al., 1999; Saleh et al., 2013; Zochodne et al., 2008)].

The data from this study suggests that after a high glucose stress in DRG neurons, the mRNA expression of HspB1, Daxx and Bcl-2 alters, while immunocytochemistry and confocal imaging of glucose treated DRG neurons showed a potential correlation with qRT-PCR analyses. Additionally, imaging data also suggests a differential compartmentalized distribution of both Daxx and HspB1 after treatment. Taken together, the data provides preliminary insights into how HspB1, Daxx, Bcl-2 and HMGB1 affect each others expression, and how this in turn may affect autophagy during cell stress.

### **3.3 Materials and Methods**

#### **3.3.1 Reagents and Antibodies**

Neurobasal media, HBSS  $\text{Ca}^{2+}/\text{Mg}^{2+}$ , HBSS without  $\text{Ca}^{2+}$  or  $\text{Mg}^{2+}$ , B27 supplement, collagenase type II, natural mouse laminin and SuperScript™ III First-Strand Synthesis System for qRT-PCR were purchased from Invitrogen (Burlington, ON, CAN). Cytosine  $\beta$ -D-arabinofuranoside hydrochloride (AraC), 5'-fluoro-2'-deoxyuridine 5'-monophosphate sodium salt (FdU), trypsin, deoxyribonuclease and D-mannitol were purchased from Sigma-Aldrich Canada Ltd. (Oakville, ON, CAN). TaqMan® Gene Expression Assay, TaqMan® Gene

Expression Master Mix, BCA protein assay solutions, immunoblot reagents and membranes were purchased from ThermoFisher Scientific (Nepean, ON, CAN) and GE Healthcare (BaieD'Urfe, QC, CAN), respectively. Ovomuroid protease inhibitor was purchased from Worthington Biochemical Corp. (Lakewood, NJ, USA), AErrane (Isoflurane) from Baxter Corp. (Mississauga, ON, CAN), RNeasy® Plus Micro Kit from Qiagen (Toronto, ON, CAN), Agilent RNA 6000 Nano Kit from Agilent Technologies (Mississauga, ON, CAN) and D-glucose from EMD Millipore (Etobicoke, ON, CAN). Primary and secondary antibodies used in this study are outlined in Table 3.1.

### **3.3.2 Ethics Statement**

Animal procedures were approved by the Institutional Animal Care Committee of Memorial University of Newfoundland in accordance with the Canadian Council on Animal Care. The approved protocol was ACP#KM-14-07.

### **3.3.3 DRG Isolation and Plating**

DRG neuronal dissociation and plating were carried out according to our established protocols (Fudge and Mearow, 2013; Tucker et al., 2005b; Williams et al., 2005). Briefly, 4-5 week old adult male Sprague-Dawley rats were anaesthetized using isoflurane, and then sacrificed by rapid decapitation. Spinal columns were then removed, cut along the central sagittal plane of the spinal column, and individual DRGs were removed. Pooled DRGs were subjected to enzymatic (e.g. collagenase and trypsin) and mechanical dissociation. Dissociated cells were suspended in serum-free DRG medium (Neurobasal media, 2% B27 supplement, 1% AraC/0.1% FdU), and plated on pre-coated (2X poly-D-lysine and 2X 50ng/μL laminin) 12-well

**Table 3.1: List of primary and secondary antibodies, with experimental dilutions, used for immunoblotting (IB), immunocytochemistry (IC) and immunohistochemistry (IHC).**

<b>Antibody</b>	<b>Method</b>	<b>Dilution</b>	<b>Company</b>	<b>Cat. #</b>
Rabbit anti- $\beta$ -Actin	IB	1:500	Sigma-Aldrich	A2066
Rabbit anti-LC3B	IB ICC	1:1000 1:100	Cell Signaling Technology	2775
Mouse anti-Hsp27	ICC IHC	1:100 1:100	Santa Cruz Biotech	SC-51956
Rabbit anti-Hsp25	IB ICC	1:1000 1:100	Enzo Life Sciences	SPA-801-F
Mouse anti-neuronal class III $\beta$ -Tubulin (Tuj1)	ICC	1:100	Covance	MMS-435P
Rabbit anti-HMGB1	ICC IHC	1:100 1:100	Abcam	ab18256
Rabbit anti-Bcl-2	ICC IHC	1:50 1:50	Abcam	ab7973
Rabbit anti-Daxx	IB ICC	1:100 1:100	EMD Millipore	07-471
Goat anti-Daxx	IHC	1:50	Santa Cruz	SC-7001
Mouse RT97	IHC	1:1000	Developmental Studies Hybridoma Bank	
DAPI	ICC	1:500	Invitrogen	D1306
Alexa Fluor® 488 Goat anti-Mouse IgG (H&L)	ICC	1:250	Jackson ImmunoResearch	711-544-152
Alexa Fluor® 488 Donkey anti-Rabbit IgG (H&L)	ICC	1:250	Jackson ImmunoResearch	711-545-152
Alexa Fluor® 647 Donkey anti-Rabbit IgG (H&L)	ICC	1:250	Jackson ImmunoResearch	711-605-152

plates or 16-well slides. The cells were then left to grow for 24 hr at 37°C, supplemented with 5% CO<sub>2</sub>, before experimental treatments.

### **3.3.4 Quantitative Real-Time PCR (qRT-PCR) of DRG Neurons**

Isolated DRG neurons were cultured on poly-D-lysine and laminin coated 12-well plates for 24hr. Neurons were then treated with neurobasal media supplemented with an additional 20mM D-glucose, for a final media concentration of 45mM glucose. Alternatively, 20mM D-mannitol was added to separate wells as a negative control for osmotic pressure change due to the increase in glucose concentration in the experimental treatment media. Further, to account for any changes that may have occurred due to the extra media addition with D-glucose or D-mannitol treatment, extra media addition alone was also performed as a control. At 2, 4, 8, 16 and 24 hr post-treatment two separate cellular samples were collected and frozen at -80°C for later qRT-PCR analysis. For analysis, cells were thawed and RNA was isolated using RNeasy® Plus Micro kits, as per the manufacturers' protocol (See Appendix B). After RNA isolation, RNA integrity was determined using an Agilent RNA 6000 Nano kit, as per the manufacturers' protocol (See Appendix C). Samples with a RNA integrity above 9.0 were used in complimentary DNA (cDNA) reactions, using SuperScript™ III First-Strand Synthesis System for qRT-PCR, as per the manufacturers' protocol (See Appendix D). Finally, cDNA samples were then used for qRT-PCR, using TaqMan® Gene Expression single-tube assays, specifically analyzing the expression of HspB1, Daxx and Bcl-2. Expression of 18S rRNA was used as the endogenous qRT-PCR control to correct for sample loading. In order to compare data obtained from multiple qRT-PCR analyses, comparative cycle threshold (Ct) values were adjusted such

that the same values were used for all data sets (HspB1 threshold values in data from 2, 4, 8, 16 and 24 hr samples were adjusted to the same values).

For qRT-PCR calculations, data were calculated according to established methodology (Pfaffl, 2001). Briefly, adjusted expression data were first related to matched 18S rRNA expression (Ct of sample – Ct of 18S rRNA = delta Ct), and then further related to media addition samples (delta Ct of treated sample/delta Ct of media addition sample = delta/delta Ct) in order to determine the effect of the specific treatment (high glucose or mannitol). At this point the fold changes in expression for the treatments were determined (e.g.  $2^{-\text{sample delta/delta Ct}}$  = fold change in expression). Finally, the fold change in expression due specifically to high glucose addition, and not due to any change in osmotic pressure due to a sugar addition, were calculated by taking the difference between the fold change expression in high glucose samples and mannitol samples (fold change high glucose – fold change mannitol = specific fold change only due to high glucose). Fold change data was analyzed using Excel, and graphed using GraphPad Prism 6 (GraphPad Software, San Diego, CA, USA).

### **3.3.5 Immunocytochemistry of DRG Neurons**

Isolated DRG neurons were cultured on poly-D-lysine and laminin coated 16-well chamber slides at ~1000 cells/well for 24 hr. Neurons were then treated for an additional 24 hr with neurobasal media supplemented with an additional 20mM D-glucose for a final media concentration of 45mM glucose. After treatment, cells were fixed immediately with 4% paraformaldehyde in PBS, pH 7.4, for 20 min. Cells were washed twice with PBS and then permeabilized and blocked in a solution containing 0.1% Triton X-100 and 10% horse serum in PBS. Cells were then incubated with primary antibodies at appropriate concentrations (Table

3.1) for 16-20 hr at 4°C. After incubation, cells were rinsed with TBST, pH 7.2, and subsequently incubated with fluorophore-conjugated secondary antibodies at appropriate concentrations (Table 3.1) for 1-2 hr. Cells were washed again three times with TBST and cover-slipped with Gelvatol™.

Images for data analysis were acquired in each of three channels (405nm, 488nm and 649nm) by laser scanning confocal microscopy with sequential Z-stage scanning (Olympus Fluoview 1000 confocal laser scanning microscope). Image acquisition for the different samples was carried out using consistent scanning parameters (i.e. laser power, HV PMTs and number of optical slices). Scanned stacks were compiled as individual images and composite digital images were prepared using both Imaris software (Bitplane Inc., South Windsor, CT, USA) and Adobe Photoshop CS (Adobe Systems Incorporated, San Jose, CA, USA).

### **3.3.6 Immunohistochemistry of DRG Neurons**

Cervical or lumbar DRGs were isolated and frozen immediately into a mold using optimum cutting temperature (O.C.T.) compound and liquid nitrogen. Serial 8-10µm cryosections were obtained using a Leica cryostat and mounted directly onto Superfrost™ glass slides, such that any one slide has a selection of sections through the entire ganglia. Sections were fixed in 4% paraformaldehyde in PBS (pH 7.4) and processed for IHC according to established protocols [see (Fudge and Mearow, 2013)].

### **3.3.7 Densitometric Analysis**

Densitometric analysis of Western immunoblots was carried out using ImageJ and a calibrated grey value scale (NIH, Bethesda, MD, USA); ratios of total protein expression were

compared to total actin, while LC3BII expression was compared to LC3BI expression. Results were graphed using GraphPad Prism 6 (GraphPad Software, San Diego, CA, USA).

### **3.4 Results**

#### **3.4.1 HspB1, Daxx, Bcl-2, HMGB1 and LC3B are endogenously expressed in adult DRG neurons**

Immunohistochemistry on cryosections of dorsal root ganglia after immediate removal from the animal was used to examine the endogenous cellular expression of HspB1, Daxx, Bcl2, HMGB1 and LC3B in adult DRG neurons. Using IHC, neuronal expression of HspB1 was found to be variable, with some cells having relatively high expression and others having little or no detectable HspB1, while LC3B was detected in most cells, including non-neuronal cells (Fig. 3.1). At higher magnification, punctate staining for LC3 was detectable in several neurons, however, this did not appear to be related to the expression of HspB1 (Fig. 3.1; Fig 3.2A, B and C, arrowheads). Bcl-2 appeared to primarily be expressed in the non-neuronal or satellite cells that surround the DRG neurons (Fig. 3.1D arrows; Fig. 3.2D, arrows), while there was only a faint staining within the DRG neurons themselves (Fig. 3.2D, arrowheads). As for HMGB1, it was detected in both neurons and non-neuronal cells, with nuclear staining found in both cell types (Fig. 3.1G; Fig. 3.2G). While HMGB1 has been reported to regulate HspB1 expression, there were a number of neurons that show HMGB1, but little or no HspB1 (Fig. 3.1G-I, Fig. 3.2G-I). Daxx, like Bcl-2, also primarily labeled the non-neuronal, satellite cells (Fig. 3.2J, arrows) that surround the DRG neurons, with some limited staining within the neurons themselves (Fig. 3.2, arrowheads).

**Figure 3.1: Expression of HspB1, Bcl-2, HMGB1 and LC3B in adult rat DRG neurons**

Adult rat dorsal root ganglia were isolated and frozen immediately using O.C.T. compound and liquid nitrogen. Serial cryosections were then obtained and mounted onto glass slides, and processed for immunocytochemistry according to established protocols (see section 3.2.6). Cryosections were immunostained for LC3B, Bcl-2, HMGB1 and HspB1. A-C. LC3B was detectable in most cells, including neurons and satellite cells (peripheral staining around neurons). D-F. Satellite cells show strong Bcl-2 labeling (arrows), while neuronal labeling was less distinct. G-I. HMGB1 was expressed in the non-neuronal, satellite cells, with apparent nuclear labeling. Neuronal labeling was also present. B, E, H. Neuronal HspB1 expression was variable, with some cells having relatively high expression and others having little or no detectable HspB1. Scale - 50µm.

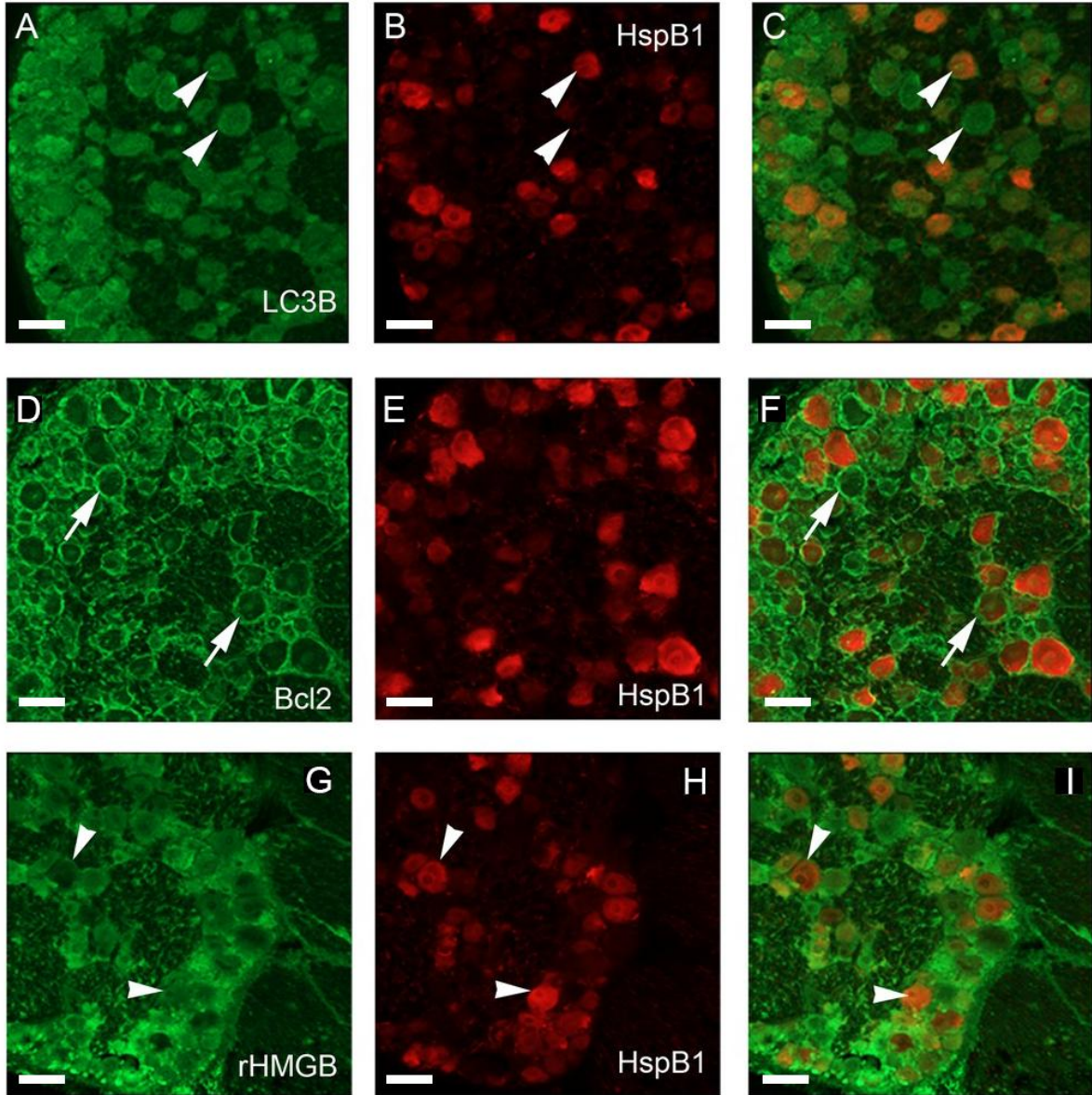
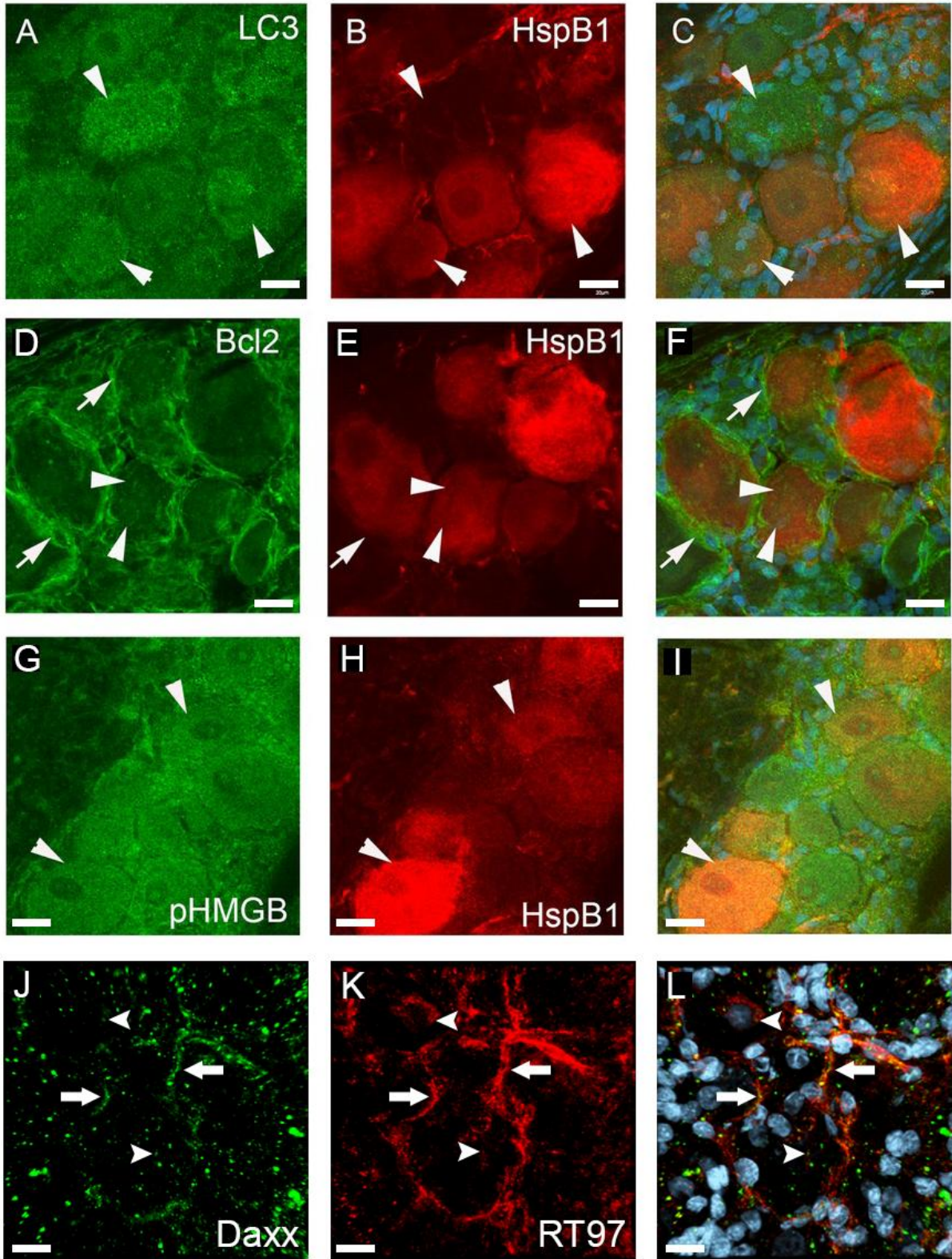


**Figure 3.2: Expression of HspB1, Bcl-2, HMGB1 and LC3B and Daxx in adult rat DRG neurons.**

Adult rat DRGs were isolated and frozen immediately using O.C.T. compound and liquid nitrogen. Serial cryosections were then obtained and mounted onto glass slides, and processed for immunocytochemistry according to established protocols (see section 3.2.6). Images represent high magnification images (40X) of cryosectioned adult rat DRG neurons immunostained for LC3B (A), Bcl-2 (D), HMGB1 (G) and HspB1 (B, E and H). A-I. Arrowheads indicate DRG neuron staining, while arrows indicate non-neuronal, satellite cell staining. J-L. Satellite cells show strong Daxx labeling (arrows), while neuronal labeling was less distinct (arrowheads). Scale - 20 $\mu$ m.



### **3.4.2 A High Glucose Environment Alters HspB1, Daxx and Bcl-2 RNA Expression in DRG Neurons**

After detecting the constitutive expression of HspB1, Daxx and Bcl-2 in DRG neurons the effect that high glucose stress may have on their expression levels was evaluated. Dissociated DRG neurons were treated either with glucose, mannitol or normal media over time frames of 2, 4, 8, 16 and 24 hr. After treatment, total RNA was isolated from samples and used in qRT-PCR analysis, as outlined in section 3.2.4.

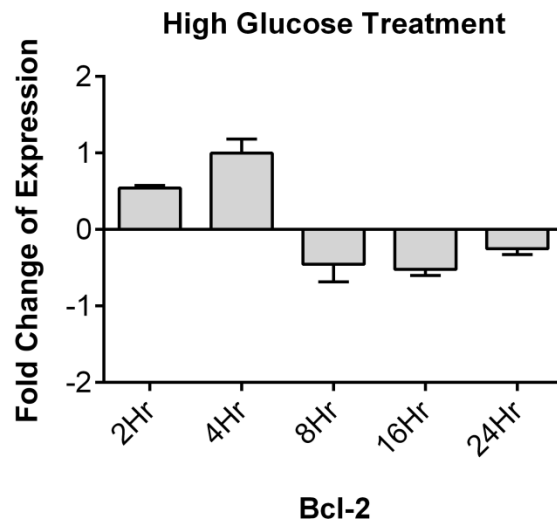
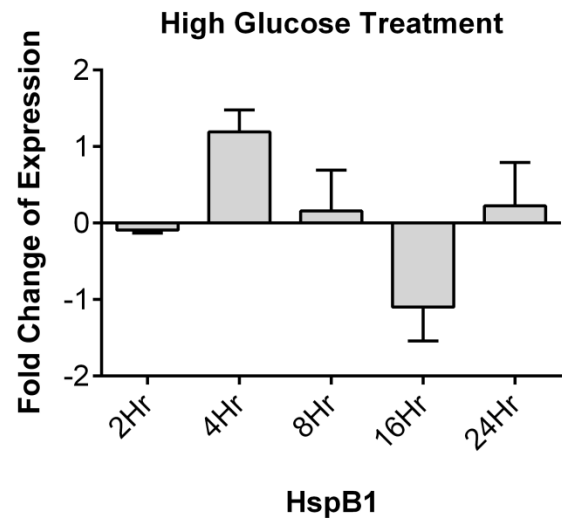
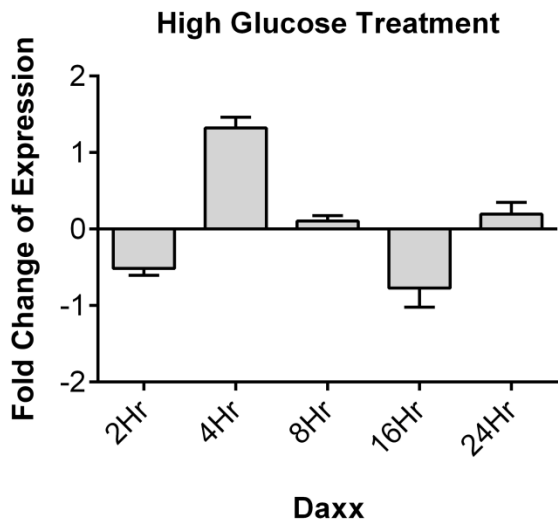
High glucose treatment, taking into consideration any changes due to an increase in osmotic pressure (i.e. mannitol control) or due to the changing of media, resulted in an increase in the expression of HspB1, Daxx and Bcl-2 after 4 hr of high glucose treatment (Fig. 3.3), although this was followed by a fluctuation in the expression of HspB1 and Daxx as shown in Fig 3.3. While Bcl-2 expression increased by 4 hr like HspB1 and Daxx, it then decreased below control levels by 8 hr, and remained at low levels for the duration of the experiment (Fig. 3.3).

### **3.4.3 Expression and Localization of Daxx and HspB1 is Altered in DRG Neurons Treated with High Glucose - Immunocytochemistry**

Quantitative RT-PCR results suggested a change in the mRNA expression of Daxx, HspB1 and Bcl-2 with high glucose treatment. Therefore, whether the changes observed in RNA expression corresponded to changes in cellular protein expression and localization in DRG neurons was next examined. Dissociated DRG neurons were plated in laminin-coated 16-well chamber slides and either left untreated (control), or treated with addition of glucose over a time frame of 24 hr, as outlined previously. Immunocytochemistry was carried out using antibodies

**Figure 3.3: mRNA expression of HspB1, Daxx and Bcl-2 is altered with high glucose treatment in DRG neurons.**

Isolated DRG neurons were cultured on poly-D-lysine and laminin coated 12-well plates for 24 hr. Neurons were then treated with neurobasal media supplemented with an additional D-glucose or D-mannitol. Controls to account for media addition were also performed. At 2, 4, 8, 16 and 24 hr post-treatment two separate cellular samples were collected, and RNA was extracted from them. The mRNA expression of HspB1, Daxx and Bcl-2 were analyzed using qRT-PCR, as described in section 3.2.4. The bars represent the mean fold change of expression ( $\pm$  SD) from each of N = 2 experimental replicates.



outlined in Table 3.1 and procedures outlined in section 3.2.5. Cultures were imaged using confocal microscopy and images were prepared using Imaris software and Adobe Photoshop CS.

Under normal conditions, the staining of Daxx was observed to be predominantly nuclear (Fig. 3.4C), while HspB1 was diffuse, with expression found in the cytosol, at the plasma membrane and in neurites (Fig. 3.4B, K and Q). Further, Bcl-2 staining, like Daxx, was also observed to be predominantly nuclear (Fig. 3.4X). In addition to Daxx, HspB1 and Bcl-2, the expression of HMGB1 was examined, as it had been suggested to both transcriptionally regulate HspB1 expression and act as a competitive regulator of autophagy with Bcl-2 (Kang et al., 2010; Narumi et al., 2015; Tang et al., 2011). In control conditions, HMGB1 expression was observed to be diffuse, with expression found in the cytosol, at the plasma membrane and in neurites (Fig. 3.4R). With respect to autophagy, the expression of LC3B was evaluated, as it is a marker of autophagosomes. Endogenous expression of autophagosomes was observed, as indicated by cytosolic LC3-positive autophagosomal puncta (Fig. 3.4J).

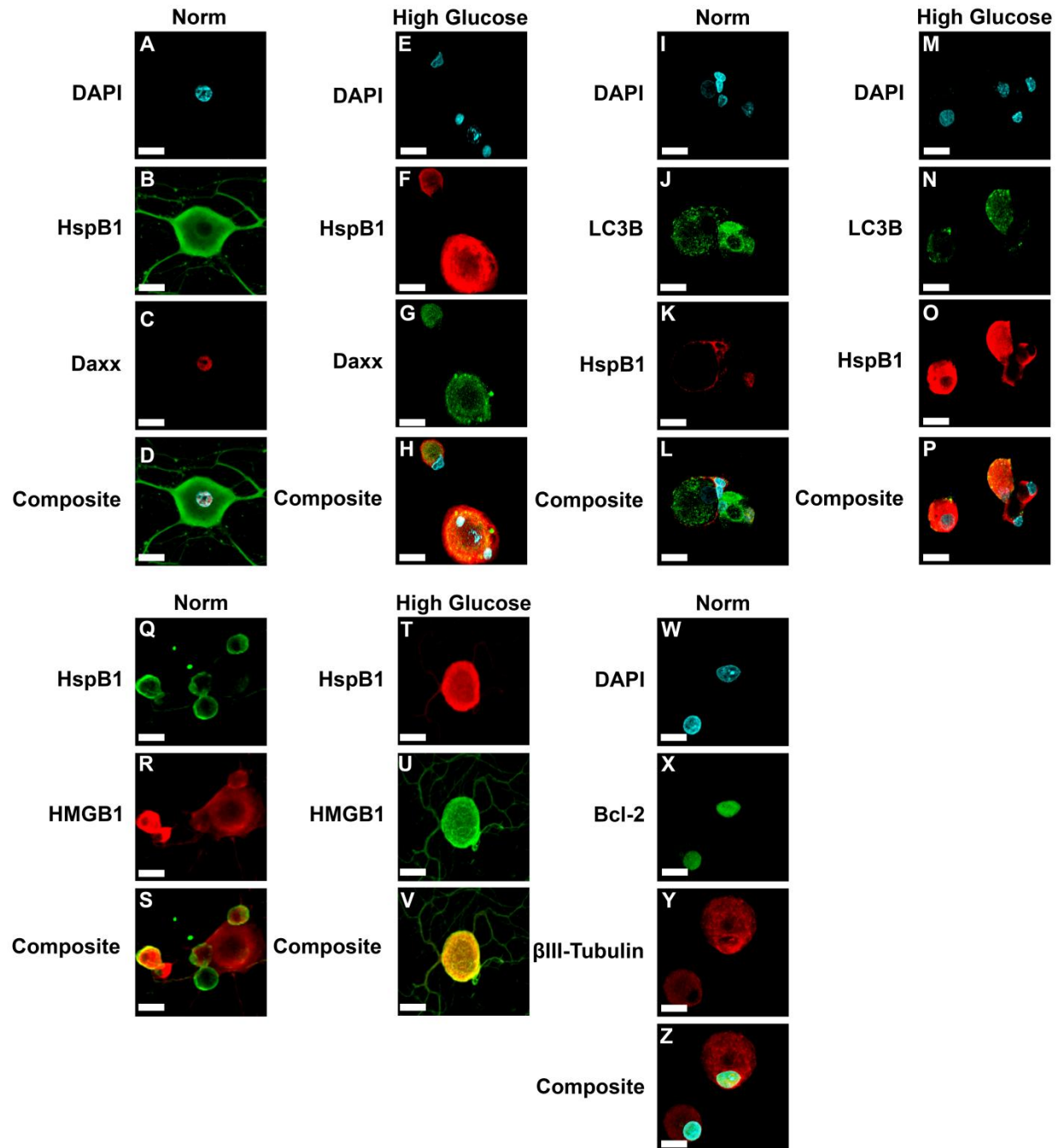
Upon treatment with glucose, Daxx became cytosolic and formed puncta (Fig. 3.4G), while HspB1 expression increased and became predominantly cytosolic and plasma membrane bound (Fig. 3.4F, O and T). HMGB1 expression did not change with glucose treatment (Fig. 3.4U), while Bcl-2 signal expression was undetected. The amount of LC3-positive autophagosomal puncta was not altered compared to the control condition (Fig. 3.4N).

### **3.5 Discussion**

The aim of this work was to evaluate a potential interaction between HspB1, Daxx, Bcl-2 and HMGB1 that might control autophagic activity during cell stress. Previous evidence has shown

**Figure 3.4: Confocal imaging of endogenous localization and expression of HspB1, Daxx, Bcl-2, HMGB1 and LC3B in untreated and high glucose treated DRG neurons.**

DRG neurons were cultured on poly-D-lysine and laminin coated 16-well culture slides, and processed for immunocytochemistry using antibodies directed against HspB1, Daxx, Bcl-2, HMGB1, LC3B and  $\beta$ III-Tubulin, followed by fluorescently tagged secondary antibodies. DAPI staining was additionally used to stain DRG nuclei. DRG neurons were visualized with confocal microscopy, and images represent z-stack projections. Scale - 30 $\mu$ m.



that HspB1 can bind to Daxx and modify its apoptosis inducing activity during cell stress (Charette and Landry, 2000; Charette et al., 2000). Separately, previous studies have shown that Bcl-2, in conjunction with HMGB1, regulates autophagy initiation through its interaction with Beclin1 (He et al., 2013; Kang et al., 2010; Maejima et al., 2013; Pattingre et al., 2005). Furthermore, Daxx has been reported to act as a transcriptional co-repressor, with Bcl-2 being a target of repression by Daxx (Li et al., 2000). Taken together, these studies outline a potential mechanism for the regulation of autophagy through the transcriptional activity of Bcl-2 by Daxx.

The study described herein was the first to assess whether such a mechanism potentially exists, using mature DRG neurons as a cellular model. DRG neurons were chosen as a number of studies have now focused upon how autophagic disruption or dysregulation can lead to axonopathies and eventual neurodegeneration (Button et al., 2015; Chu et al., 2009; Frake et al., 2015; Menzies et al., 2015; Ravikumar et al., 2010; Wong and Holzbaur, 2015; Yang et al., 2013). For instance, in diseases that affect DRG neurons, such as DPN, proper autophagic modulation may help alleviate physiological impairments associated with the diseases, such as neuropathic pain, as well as help improve the outcome of the diseases (Knoferle et al., 2010; Yang et al., 2014).

The data presented in this study suggests that the endogenous mRNA expression of HspB1, Daxx and Bcl-2 is altered during cell stress with high glucose treatment in DRG neurons, and this further corresponded to changes in their cellular localization and expression as observed with immunocytochemistry. Specifically, the early changes in mRNA expression of HspB1, Daxx and Bcl-2 suggest a specific cellular response to the high glucose stress, while later changes in mRNA expression, specifically for HspB1 and Daxx, could be a result of protein translation and a potential return back to cell homeostasis after cell stress. Interestingly, the later

changes found in Bcl-2 mRNA expression could be a direct result of Daxx dependent co-repression activity, as Bcl-2 mRNA expression does not return back to pretreatment levels.

Immunocytochemical observations on protein expression and localization before and after cell stress agree with published material regarding both Daxx and HspB1 (i.e. cytosolic Daxx localization and HspB1 plasma membrane localization), and further indicate a selective response to the high glucose treatment paradigm (Williams et al., 2005; Yang et al., 1997). Cellular protein expression and localization of Bcl-2 after high glucose treatment, however, was not detected in this study. The lack of detectable Bcl-2 cellular expression could either be a result of Daxx co-repression, or could be a result of poor antibody specificity. Alternatively, a recent study has suggested that pre-treatment with high glucose reduces the cellular expression of Bcl-2, thereby promoting apoptosis after lipopolysaccharide treatment in dendritic cells (Feng et al., 2014). Interestingly, immunohistochemistry of intact DRG neurons showed Bcl-2 expression confined to the satellite cells surrounding the neurons, with some less distinctive neuronal labeling.

Taking into consideration the conditions in which the DRG neurons were cultured and treated, we cannot rule out the fact that hyperglycemia and hyperinsulinemia may have been occurring well before treatments were carried out, and may be influencing the results we have obtained in this study. Normally, fasting blood glucose levels are calculated to be between 4mM and 5.5mM, with any level above 5.6mM regarded as a high glucose state (Komatsu et al., 2006). The DRG neurons in this study were initially cultured in 25mM glucose neurobasal media. As neurons do not regulate glucose uptake, and glucose is freely uptaken, high concentrations of glucose can cause cellular stress by either: increasing the formation of superoxide in the electron transport chain, potentially resulting in oxidative stress; glycosylating proteins, potentially

impairing their structure and function; or activating the polyol pathway, effectively reducing the concentrations of NADPH and NAD<sup>+</sup>, both of which are involved in preventing the formation of reactive oxygen species. Under the criteria for a normal glucose state, the DRG cultures in this study would be considered hyperglycemic, even before the addition of 20mM D-glucose. Furthermore, the cultures were also treated with B27 that has an insulin concentration of 4000ng/mL; a final concentration of 80ng/mL was used in DRG neuron cultures. This final concentration of insulin used is considered hyperinsulinemic as a normal fasting blood insulin level is calculated to be <1ng/mL (Komatsu et al., 2006). Although the cultures are hyperglycemia and hyperinsulinemic, these conditions have been used in previous studies and have not been reported to adversely affect DRG neuron survival and neurite growth (Williams and Mearow, 2011; Williams et al., 2005, 2006). This observation further attests to the resilient nature of DRG neurons and their ability to survive episodes of stress.

Overall, this study evaluated a link between HspB1, Daxx, Bcl-2 and HMGB1 that could potentially provide a control mechanism of autophagic activity during cell stress. Although the data presented does not suggest a specific pathway, it does allow for further research to be undertaken in order to further explore a potential mechanism.

### **3.6 Acknowledgements:**

We thank members of the Mearow lab (especially F. Nafar) for their technical support and assistance in the course of this study.

## **Chapter 4: Autophagy Inhibition in Endogenous and Nutrient Deprived Conditions Reduces DRG Neuron Survival and Neurite Growth *In Vitro***

A version was published as Clarke J and Mearow K, J. Neurosci. Res. 2016

### **4.1 Abstract**

Peripheral neuropathies can result in cytoskeletal changes in axons, ultimately leading to Wallerian degeneration and cell death. Recently, autophagy has been studied as a potential target for improving axonal survival and growth during peripheral nerve damage. This study investigates the influence of autophagy on adult DRG neuron survival and axonal growth in control and nutrient deprivation conditions. Constitutive autophagy was modulated using pharmacological activators (rapamycin) and inhibitors (3-methyladenine, Bafilomycin A1) in conjunction with either a nutrient stable environment (standard culture medium) or a nutrient deprived environment (HBSS + Ca<sup>2+</sup>/Mg<sup>2+</sup>). The results demonstrate that autophagy inhibition decreased cell viability and reduced neurite growth and branching complexity. While autophagy was upregulated with nutrient deprivation compared to the control, it was not further activated by rapamycin, suggesting a threshold level of autophagy. Overall, both cellular and biochemical approaches have been combined to show the influence of autophagy on adult DRG neuron survival and growth.

### **4.2 Introduction**

Peripheral neuropathies can lead to adverse cytoskeletal changes in axons of dorsal root ganglia (DRG) neurons, causing disassembly and granular degeneration of the axons, also known as axonal dieback or Wallerian degeneration, and ultimately cell death (Raff et al., 2002; Wang et al., 2012). Morphologically, neurons within the DRG send bifurcating axons to targets both in the central nervous system and the peripheral nervous system, with axons growing up to 20,000

times larger than the cell body in length and total surface area in order to reach their distal peripheral targets. Clinical manifestations of peripheral axonal dysfunction can include numbness, burning and tingling sensations, and intractable pain (Vinik et al., 2013). Further compounding DRG axonal dieback and cell death is the fact that DRG neurons are post-mitotic, and thus surviving neurons do not divide once cell loss has occurred, thereby exacerbating peripheral effects. DRG neurons, however, have a robust capacity to regrow damaged axons under favorable conditions, including the presence of neurotrophins and a positive extracellular matrix growth environment (Tucker et al., 2005a, 2006). As a result, many studies have focused upon devising strategies that promote axonal regrowth to peripheral targets after neuropathies through the introduction of positive growth factors, such as nerve growth factor (NGF) (Averill et al., 2004; Karamoysoyli et al., 2008; Lindsay, 1988; Tosaki et al., 2008) and the extracellular matrix glycoprotein laminin (Fudge and Mearow, 2013; Plantman et al., 2008; Tucker and Mearow, 2008; Tucker et al., 2006; Zhu et al., 2010).

Since DRG axonal dieback and cell death occur after trauma, a number of studies are now focusing on trying to determine early endogenous cellular indicators of stress that can be modulated to attenuate neuropathy and promote recovery [e.g., (Gavazzi et al., 1999; Saleh et al., 2013; Zochodne et al., 2008)]. One process in particular that is being studied in neuropathy is autophagy, which is a regulated cellular process for the clearance and recycling of proteins and damaged organelles by the lysosome. It is necessary for cellular homeostasis and survival in response to stress, and is primarily activated by starvation and amino acid limitation [reviewed in (Russell et al., 2014; Singh and Cuervo, 2011)]. Autophagy involves the formation of double membrane bound cytoplasmic vacuoles (known as autophagosomes) that sequester cytosolic protein and organelles, and deliver them to lysosomes for proteolytic degradation. Through this

process, autophagy promotes a dynamic and tightly regulated balance between the formation and degradation of proteins and organelles in the maintenance of normal cell growth and development. Additionally, it can promote cellular survival during starvation by maintaining cellular energy levels through the recycling of redundant proteins and organelles (Benavides et al., 2013; Singh and Cuervo, 2011). In this manner it is thought that by recycling damaged organelles and redundant proteins, the pool of available energy for synthesis of new proteins and organelles within the cell increases, thus allowing DRG axons and cells to survive and grow (Ashrafi et al., 2014; Gumy et al., 2010; Heo et al., 2015; Verma et al., 2005). However, while the intricacies of the autophagy process and function are still being studied, little is still known about how its modulation can help in neuropathic diseases.

Taking into consideration both the effects of peripheral neuropathies on the peripheral axons, and the mechanisms that control endogenous autophagic nutrient homeostasis, this study sought to determine the effects of autophagy on adult DRG neuron survival and neurite growth in normal and metabolically challenged conditions. Here we investigated endogenous LC3B (microtubule-associated protein 1A/1B light chain 3B, MAP1LC3B, or more commonly LC3B) to study autophagy within axons; previous studies have employed GFP-LC3B transgenic mice and have described constitutive autophagy and formation of autophagosomes in DRG neurons (Maday and Holzbaur, 2014; Maday et al., 2012; Mizushima et al., 2004). In addition, we utilized the autophagic pharmacological modulators rapamycin and 3-methyladenine in conjunction with normal and metabolically challenged conditions. Rapamycin is an autophagic activator that inhibits the activity of mTOR, while 3-methyladenine is an autophagic inhibitor that inhibits the function of Vps34, a class III PI3-kinase involved in autophagosome formation. Our results demonstrate a reduction in adult DRG neuron survival, axon growth and axon

branching complexity with the inhibition of autophagy in conjunction with nutrient deprivation-induced cellular stress. Overall, the data provide further insights into how autophagy influences DRG neuronal cell survival and growth.

### **4.3 Materials and Methods**

#### **4.3.1 Reagents and Antibodies**

F12 media, HBSS (Hanks Balanced Salt solution) +  $\text{Ca}^{2+}/\text{Mg}^{2+}$ , HBSS without  $\text{Ca}^{2+}$  or  $\text{Mg}^{2+}$ , B27 supplement, collagenase type II and natural mouse laminin were purchased from Invitrogen (Burlington, ON, CAN). Cytosine  $\beta$ -D-arabinofuranoside hydrochloride (AraC), 5-fluoro-2'-deoxyuridine 5'-monophosphate sodium salt (FdU), 3-methyladenine (3-MA), bafilomycin-A1 (BA1), rapamycin (Rapa), trypsin, phenazine methosulfate (PMS) and deoxyribonuclease I (DNase) were purchased from Sigma-Aldrich Canada Ltd. (Oakville, ON, CAN). The pharmacologic phosphatidylinositol 3-kinase (PI3K) inhibitor LY294002 was purchased from Millipore Canada Ltd. (Etobicoke, ON, CAN). BCA protein assay solutions, Blot® 4-12% Bis-Tris Plus Gels, immunoblot reagents, immunoblot membranes, SuperSignal® West Pico Chemiluminescent Substrate were purchased from ThermoFisher Scientific (Nepean, ON, CAN). Cell Titer 96® Aqueous MTS Reagent Powder was purchased from Promega (Madison, WI, USA). The protease inhibitor, ovomucoid was obtained from Worthington Biochemical Corp. (Lakewood, NJ, USA). AErrane (isoflurane) was purchased from Baxter Corp. (Mississauga, ON, CAN). Primary and secondary antibodies used in this study are outlined in Table 4.1.

**Table 4.1: List of primary and secondary antibodies, with experimental dilutions, used either for immunoblotting (IB) or immunocytochemistry (ICC).**

<b>Antibody</b>	<b>Method</b>	<b>Dilution</b>	<b>Company</b>	<b>Cat. #</b>
Rabbit anti- $\beta$ -Actin	IB	1:500	Sigma-Aldrich	A2066
Rabbit anti-LC3B	IB ICC	1:1000 1:100	Cell Signaling Technology	2775
Rabbit anti-p70S6 kinase $\alpha$ (C-18)	IB	1:1000	Santa Cruz Biotechnology	SC-230
Rabbit anti-phospho-p70S6 kinase $\alpha$ (Thr421/Ser424)	IB	1:1000	Santa Cruz Biotechnology	SC-7984-R
Rabbit anti-mTOR (7C10)	IB	1:1000	Cell Signaling Technology	2983
Rabbit anti-phospho-mTOR (Ser2448)	IB	1:1000	Cell Signaling Technology	2971
Mouse anti-Neuronal Class III $\beta$ -Tubulin (Tuj1)	ICC	1:100	Covance	MMS-435P
Dylight <sup>TM</sup> 405-conjugated AffiniPure Donkey anti-Mouse IgG (H&L)	ICC	1:500	Jackson ImmunoResearch	715-475-150
Alexa Fluor <sup>®</sup> 488-conjugated AffiniPure Donkey anti-Rabbit IgG (H&L)	ICC	1:500	Jackson ImmunoResearch	711-545-152

### **4.3.2 Ethics Statement**

Animal procedures were approved by the Institutional Animal Care Committee (IACC) of Memorial University of Newfoundland in accordance with the Canadian Council on Animal Care (CCAC). The approved protocol is ACP#KM-14-07.

### **4.3.3 DRG Isolation and Plating**

DRG neuronal dissociation and plating were carried out according to our established protocols (Fudge and Mearow, 2013; Tucker et al., 2005b; Williams et al., 2005). Briefly, 4-5 week old male Sprague-Dawley rats were anaesthetized using isoflurane, and then sacrificed by rapid decapitation. Spinal columns were then removed, cut along the sagittal plane of the spinal column, and individual dorsal root ganglia were removed. Pooled dorsal root ganglia were subjected to enzymatic and mechanical dissociation. Dissociated cells were suspended in serum-free DRG medium (F12, 2% B27 supplement, 1% AraC/0.1% FdU), and plated on pre-coated (2X poly-D-lysine and 2X 25ng/ $\mu$ L laminin) 12-well plates, 96-well plates, or 16-well slides. The cells were then allowed to attach for 24 hr at 37°C, in an atmosphere of air and 5% CO<sub>2</sub>, before treatments were added. For immunoblotting or survival experiments, we utilized three rats per 12-well plate or three rats per 96-well plate. Each experiment we performed was replicated a minimum of three times. For the experiments using 16-well culture slides, 3-6 slides were used for each experiment, with 1-2 slide/time point. We attempted to do all the conditions concomitantly in any one experiment. The number of replicates/experiment ranged from 4-6 different platings. For neurite growth analyses cells were plated at a low density to enable individual cellular and neurite analyses.

#### **4.3.4 MTS Cell Viability Assay**

DRG neurons were cultured on poly-D-lysine and laminin coated 96-well plates at ~1000 cells/well for 24 hr. Culture media was then removed and replaced with HBSS  $\text{Ca}^{2+}/\text{Mg}^{2+}$  and treated for 3 hr, 16 hr or 24 hr. In conjunction with HBSS  $\text{Ca}^{2+}/\text{Mg}^{2+}$ , the autophagy modulators 3-MA (10mM), Rapa (200nM), BA1 (200nM) and LY294002 (10 $\mu$ M) were added over the same time frames. Cell viability was quantified by the MTS colorimetric technique using the Cell Titer 96® AQueous MTS Reagent and PMS. This procedure was carried out as per the manufacturer's protocol (See Appendix E), with absorbance recording of the plates read at 490nm using a VICTOR™ X5 Multilabel Plate Reader (PerkinElmer Office, Woodbridge, ON, CAN). Results are presented as fractions of viable cells relative to untreated controls.

#### **4.3.5 Isolation and Biochemical Analysis of Protein Fractions**

Protein extraction and western blot analyses were carried out according to our established protocols (Clarke and Mearow, 2013; Tucker et al., 2005a; Williams et al., 2005). Briefly, DRG neurons were grown on poly-D-lysine and laminin coated 12-well plates at  $\sim 1 \times 10^6$  cells/well for 24 hr. Culture media was then removed and replaced with fresh normal medium or HBSS  $\text{Ca}^{2+}/\text{Mg}^{2+}$  and treated for 3 hr, 16 hr or 24 hr. In conjunction with HBSS  $\text{Ca}^{2+}/\text{Mg}^{2+}$ , the autophagy modulators 3-MA (10mM) and rapamycin (200nM) were added over the same time frames. Immediately after treatments, plates were placed on ice, and cells were scraped with a rubber policeman, quickly collected and centrifuged at 4°C to pellet the cells. The medium was removed and the pellet was lysed with ice-cold lysis buffer (10% glycerol, 1% NP40, 1 complete protease inhibitor cocktail tablet, 1.0mM sodium vanadate, 1.0mM sodium fluoride, 0.025% sodium dodecyl sulfate and TBS). All samples for a given experiment were collected at the

same time. Equivalent amounts of protein (10-15 $\mu$ g) were electrophoresed and separated on Bolt® 4-12% Bis-Tris Plus gels, and transferred onto nitrocellulose membranes for further analysis. Nitrocellulose membranes were then blocked with either 3% skim milk or 5% BSA solution, depending on whether phospho-specific antibodies were used or not, incubated overnight at 4°C with primary antibodies (Table 4.1) and developed the following day. Bands were detected using peroxidase-conjugated secondary antibodies and SuperSignal® West Pico Chemiluminescent Substrate.

#### **4.3.6 Immunocytochemistry of DRG Neurons**

DRG neurons were cultured on poly-D-lysine and laminin coated 16-well chamber slides at ~1000 cells/well for 24 hr. Culture media was then removed and replaced with HBSS Ca<sup>2+</sup>/Mg<sup>2+</sup> and treated for 3 hr, 16 hr or 24 hr. In conjunction with HBSS Ca<sup>2+</sup>/Mg<sup>2+</sup>, the autophagy modulators 3-MA (10mM) and rapamycin (200nM) were added over the same time frames. After treatment, cells were fixed immediately with 4% paraformaldehyde in PBS, pH 7.4, for 20 min. Cells were washed twice with PBS and then permeabilized in a solution containing 0.1% Triton X-100 and 10% horse serum in PBS. Cells were then incubated with primary antibodies at appropriate concentrations (Table 4.1) for 16-20 hr at 4°C. After incubation, cells were rinsed with TBST, pH 7.2, and subsequently incubated with fluorophore-conjugated secondary antibodies at appropriate concentrations (Table 4.1) for 1-2 hr. Cells were washed again three times with TBST and cover-slipped with Gelvatol™.

For autophagosomal flux analysis, the autophagy inhibitor BA1 (200nM) was added either alone, or in conjunction with treatments stated above for 3 hr or 16 hr. Using immunocytochemistry, cytosolic autophagic vesicles in the cell soma were counted and

compared to the diameters of the cells analyzed in order to compare the results observed from differently sized DRG neurons.

Images for data analysis were acquired in each of two channels (405nm and 488nm) by laser scanning confocal microscopy with sequential Z-stage scanning (Olympus Fluoview 1000 confocal laser scanning microscope). Image acquisition for the different samples was carried out using similar scanning parameters (laser power, HV PMTs, and number of optical slices). Scanned stacks were compiled as individual images, and composite digital images were prepared using both Imaris software (Bitplane Inc., South Windsor, CT, USA) and Adobe Photoshop CS (Adobe Systems Incorporated, San Jose, CA, USA).

For neurite analyses and quantification of LC3B-positive puncta, confocal images were volume rendered in 3-dimensions (3D) using Imaris software, and the amount of LC3B positive puncta found within the growing neurites were quantified. The Filament Tracer tool within Imaris was also utilized to determine total neurite growth from the cell soma in length ( $\mu\text{m}$ ) and the amount of branching of the growing neurites using the Sholl Analysis calculation within the tool; the Sholl spheres resolution was set at  $20\mu\text{m}$  for analysis.

#### **4.3.7 Densitometric and Statistical Analysis**

Densitometric analyses of triplicate Western immunoblots were carried out using ImageJ and a calibrated grey value scale (NIH, Bethesda, MD, USA); ratios of total and phosphorylated protein expression were compared to each other, while LC3BII expression was compared to LC3I expression.  $\beta$ -Actin was included in the data to correct for loading differences. Statistical analyses were performed using GraphPad Prism 6 (GraphPad Software, San Diego, CA, USA),

with significance determined using one-way ANOVA for column data, and two-way ANOVA for grouped data. All analyses were subjected to post hoc testing via Tukey's test.

## **4.4 Results**

### **4.4.1 Nutrient Deprivation Alters Constitutive Autophagy in DRG Neurons**

To evaluate whether nutrient deprivation or pharmacological treatment could modulate the autophagic process in adult rat DRG neurons, immunocytochemical analysis of LC3B-positive puncta was used. This is a well-established approach to determine if autophagy is occurring and whether its flux is being altered (Barth et al., 2010; Loos et al., 2014). For this experiment, dissociated DRG neurons were grown on laminin-coated 16-well chamber slides for 3, 16 or 24 hr under either untreated (control), or nutrient deprived conditions. Nutrient deprived conditions were obtained by replacing the medium with HBSS (Hanks Balanced Salt Solution). After 3 hr and 16 hr treatment, cultures were fixed and immunostained with anti-LC3B. Analysis of individual DRG neurons in culture demonstrated a distinct LC3B-positive puncta staining (Fig. 4.1A, B), and with nutrient deprivation, there was an apparent increase in these puncta (Fig. 4.1C, D).

Having established that endogenous autophagosomes could be detected by ICC in the neurons, we then asked whether they could also be detected in growing neurites and whether autophagy modulation would show any differences. In this, and subsequent experiments, cells were plated on laminin-coated surfaces and allowed to recover for 24 hr prior to treatments as noted above, along with the use of pharmacological modulators rapamycin (Rapa, autophagy activator) or 3-methyladenine (3-MA, autophagy inhibitor). LC3B-positive puncta in neurites were assessed, and the results showed that 3-MA resulted in a reduction in both control and

HBSS treated conditions (Fig. 4.2). There was no significant difference between the control and rapamycin treated cells and only a transient increase in the HBSS condition (Fig. 4.2).

In order to assess whether autophagic flux was being altered, BA1 was employed in another experimental series. Treatment with BA1 would be expected to result in the accumulation of autophagic vesicles in a greater number than that observed with either nutrient deprivation or the other modulators. BA1 inhibits lysosomal acidification and the fusion of the autophagosome with lysosomes and halts the maturation and recycling of autophagosome (Yamamoto et al., 1998), which is thought to occur predominantly in the cytosol of neurons. Therefore, we analyzed the number of autophagosomes in the cell body in this analysis (Chu et al., 2009). As shown in Fig 4.3, treatment with BA1 resulted in significant increase in puncta in both the control and HBSS conditions. 3-MA resulted in a reduction in both control and HBSS treated conditions, with and without BA1 co-treatment. Rapamycin treatment showed an increase in LC3B-positive puncta in both control and HBSS treated conditions, again with and without BA1 co-treatment (Fig. 4.3).

#### **4.4.2 Autophagy Inhibition Reduces DRG Neuron Viability**

These data showed that autophagy was occurring in DRG neurons and its flux could be modulated by nutrient deprivation with HBSS and pharmacological treatment. The next question assessed was whether modulating autophagy caused any changes in DRG neuron viability. Briefly, dissociated DRG neurons were plated in laminin-coated 96-well plates and were either left untreated (control), or treated with HBSS over time frames of 3 hr, 16 hr and 24 hr. Additionally, in both untreated and HBSS-treated conditions, the DRG neurons were exposed to

**Figure 4.1: Constitutive autophagy in adult DRG neurons can be modulated with nutrient deprivation and pharmacological treatment.**

Adult DRG neurons were cultured on poly-D-lysine and laminin coated 16-well culture slides and treated under nutrient control (norm) (**A and B**) and nutrient deprived conditions (**C and D**) for 3 hr and 16 hr. After treatments, cells were processed for immunocytochemistry using anti-LC3B antibody, followed by fluorescently tagged secondary antibodies. DRG neurons were visualized with confocal microscopy. Scale bar = 10 $\mu$ m. Arrows – indicate cellular staining with LC3B puncta.

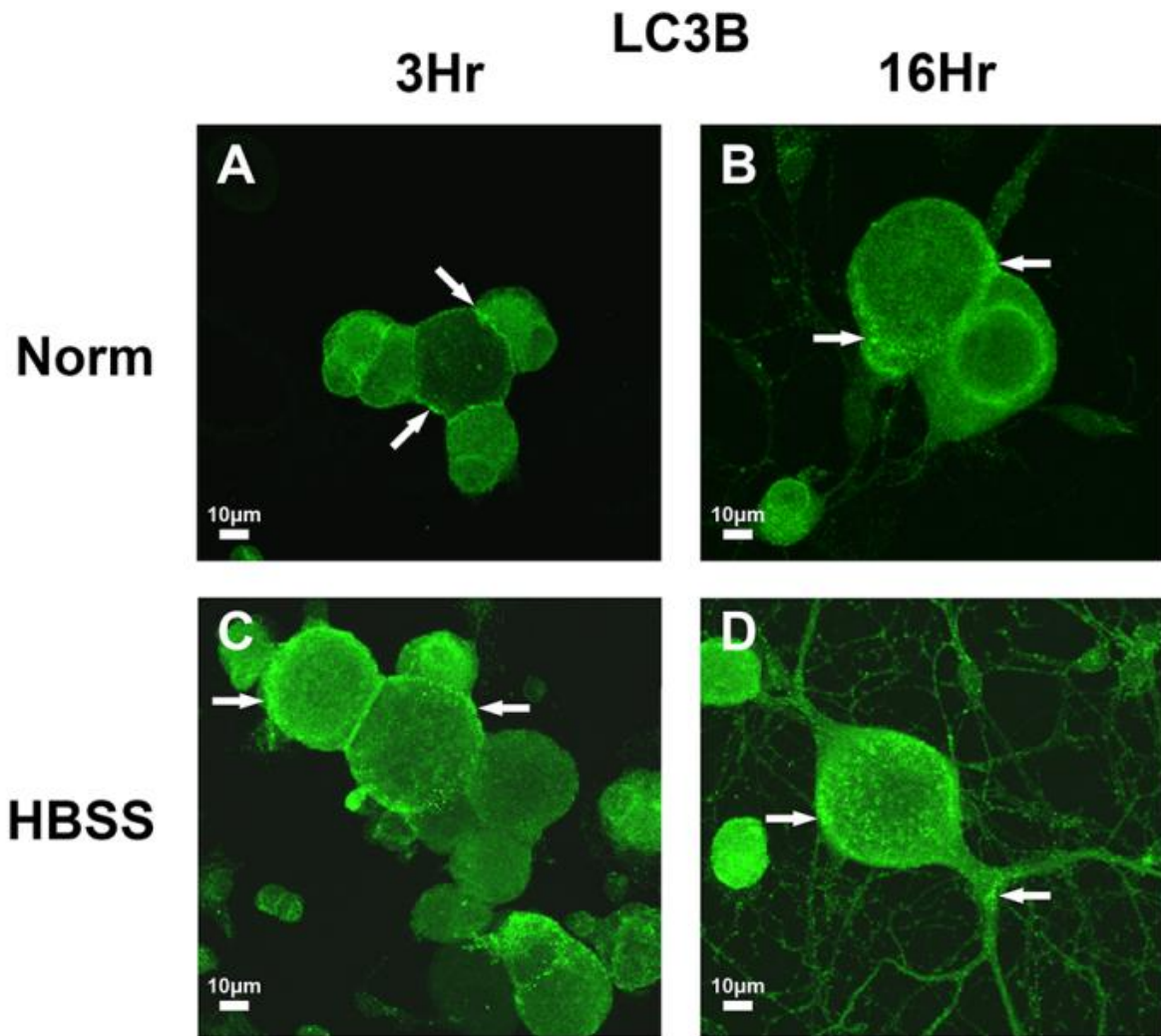
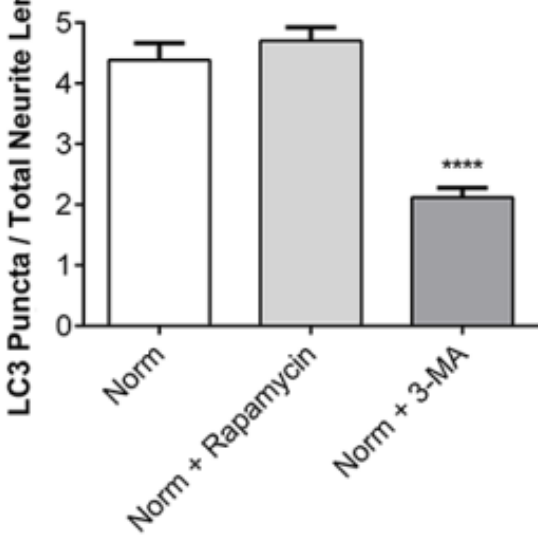


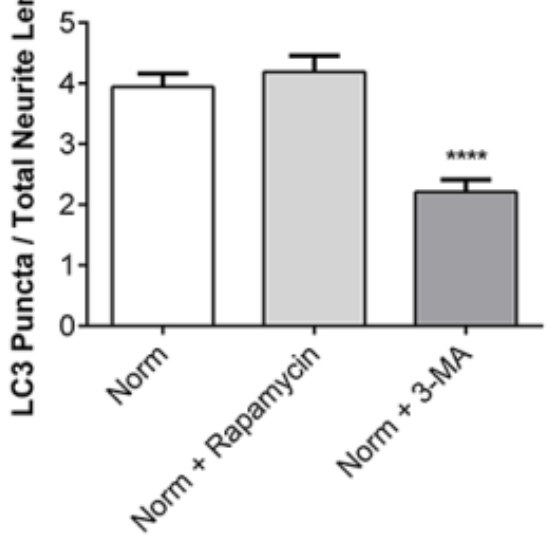
**Figure 4.2: Constitutive autophagy in adult DRG neurons can be modulated with nutrient deprivation and pharmacological treatment.**

Adult DRG neurons were cultured on poly-D-lysine and laminin coated 16-well culture slides and treated under nutrient control (norm) and nutrient deprived conditions for 3 hr and 16 hr. After treatments, cells were processed for immunocytochemistry using anti-LC3B antibody, followed by fluorescently tagged secondary antibodies. DRG neurons were visualized with confocal microscopy and the ratio of total LC3B puncta to total neurite length found in growing neurites with autophagy modulation was assessed. Autophagy was modulated by using either rapamycin (200nM) or 3-methyladenine (3-MA, 10mM). Values are mean  $\pm$  SEM; n = 35 cells per condition, per time-point, with conditions and time-points done in triplicate. Significance of results was determined using a one-way ANOVA with Tukey's *post hoc* test, confirmed using a non-parametric test, comparing samples to the control (norm) condition at each time-point. \* P < 0.05, \*\*\* P < 0.001 and \*\*\*\* P < 0.0001.

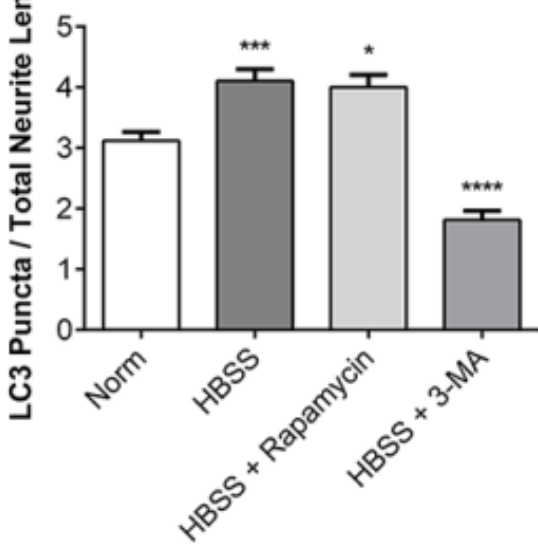
3Hr Norm Condition With Treatments



16Hr Norm Condition With Treatments



3Hr HBSS Condition With Treatments



16Hr HBSS Condition With Treatments

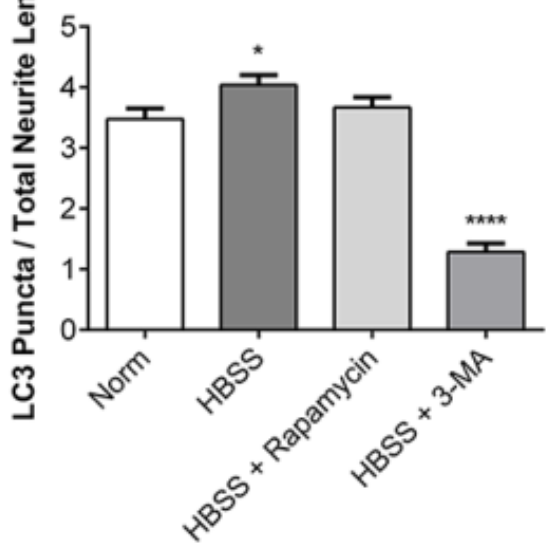
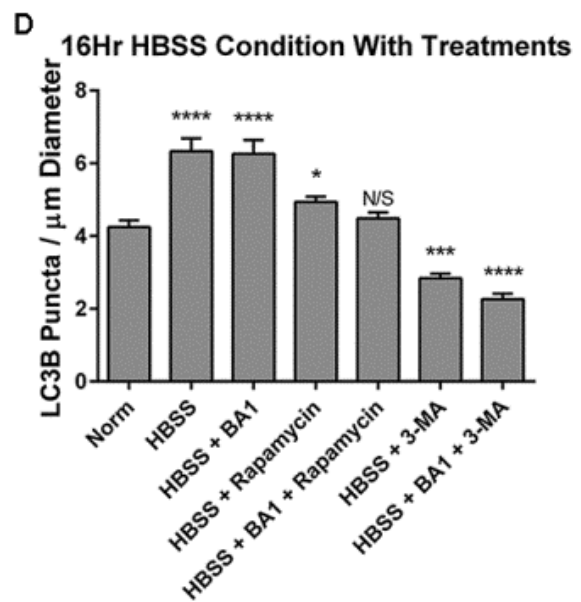
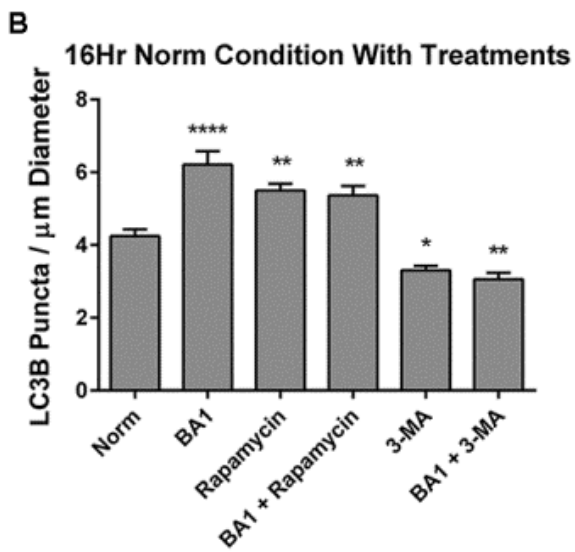
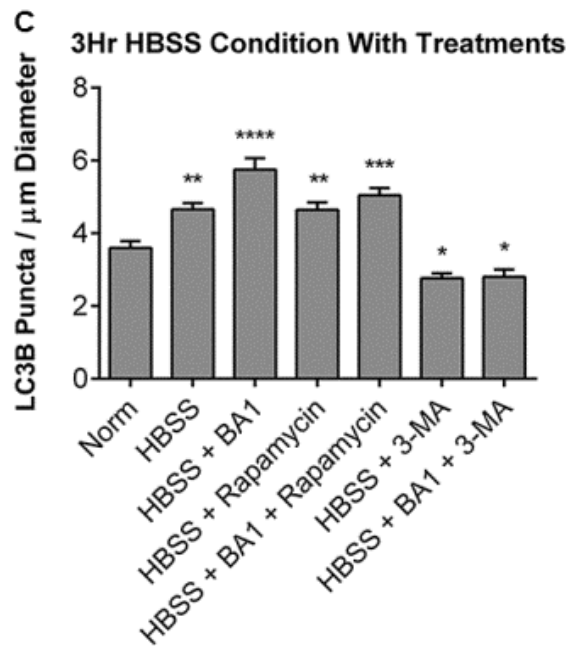
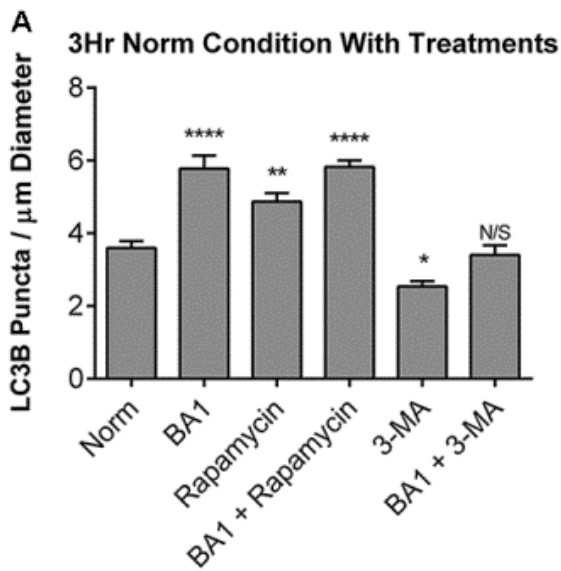


**Figure 4.3: Alterations in constitutive autophagy with nutrient deprivation and pharmacological treatment are a result of changes in autophagic flux**

Adult DRG neurons were cultured on laminin coated 16-well culture slides, and processed for immunocytochemistry using anti-LC3B antibody, followed by fluorescently tagged secondary antibodies. DRG neurons were visualized using confocal microscopy, and the ratio of LC3B puncta per  $\mu\text{m}$  of cell diameter was calculated. Cellular conditions include (**A and B**) nutrient control (norm) and (**C and D**) nutrient deprivation (HBSS) over time periods of 3 hr and 16 hr. rapamycin (200nM) was added as an activator and 3-MA (10mM) as an inhibitor of autophagy. Additionally, autophagic flux was assessed using the autophagosome degradation inhibitor BA1 (200nM). Values are mean  $\pm$  SEM; n = 25 cells per condition, per time-point, with conditions and time-points done in triplicate. Significance of results was determined by using a one-way ANOVA with Tukey's *post hoc* test, confirmed using a non-parametric test, comparing samples to the control (norm) condition at each time-point. \* P < 0.05, \*\* P < 0.01, \*\*\* P < 0.001, \*\*\*\* P < 0.0001.



the autophagy modulators Rapamycin, 3-MA and BA1; LY294002, a PI3-kinase inhibitor, was included as it was previously shown that LY294002 inhibits neurite outgrowth from these neurons in the absence of a significant effect on cell survival at this concentration (Dodge et al., 2002; Tucker et al., 2005a). Cellular viability was determined using a MTS assay, with data being expressed as fractions of viable cells relative to untreated controls, and significance determined by comparing the sample means to control conditions.

Under control conditions, DRG neuron viability did not change throughout the course of the experiment (Fig. 4.4A, B), nor did it differ significantly in the presence of rapamycin or LY29004. In contrast, treatment with 3MA or BA1 resulted in significantly decreased viability by 16 hr (~15%) increasing to 40% by 24 hr.

With HBSS, DRG cell viability gradually decreased over time (~20% decrease by 24 hr), with similar results observed with rapamycin co-treatment (Fig. 4.4C), although there was no significant difference between HBSS and the HBSS + rapamycin conditions. Treatment with the inhibitors (3MA, BA1 and LY29004) resulted in significantly decreased viability over the experimental time period (Fig 4.4C, D).

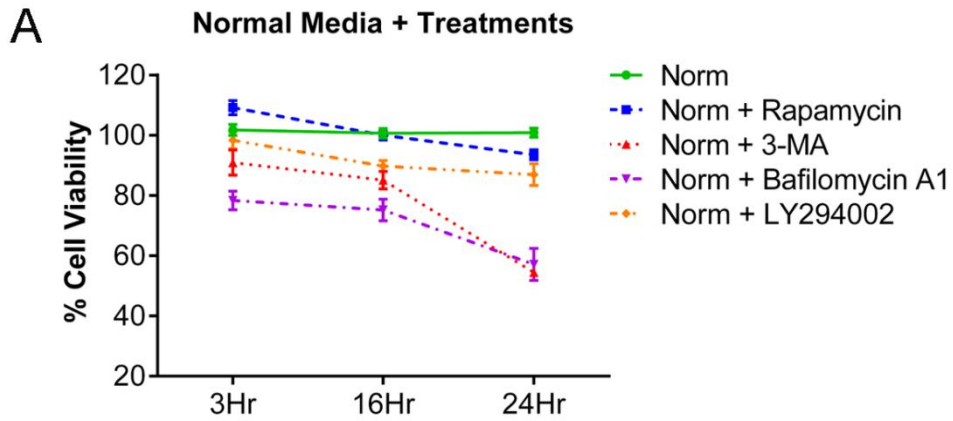
We did not directly assess whether this decreased viability resulted in cell death, although over the course of the experiment, neuron detachment and loss of cells was more noticeable in the presence of the inhibitors and HBSS.

#### **4.4.3 Inhibiting Autophagy Decreases Autophagy Related Proteins in DRG Neurons**

We next investigated alterations in the expression of LC3B and mTOR, as well as p70S6-kinase- $\alpha$  (p70S6K), a downstream target of mTOR. Dissociated DRG neurons were plated in laminin-coated 12-well plates, allowed to recover for 24 hr and subsequently left untreated

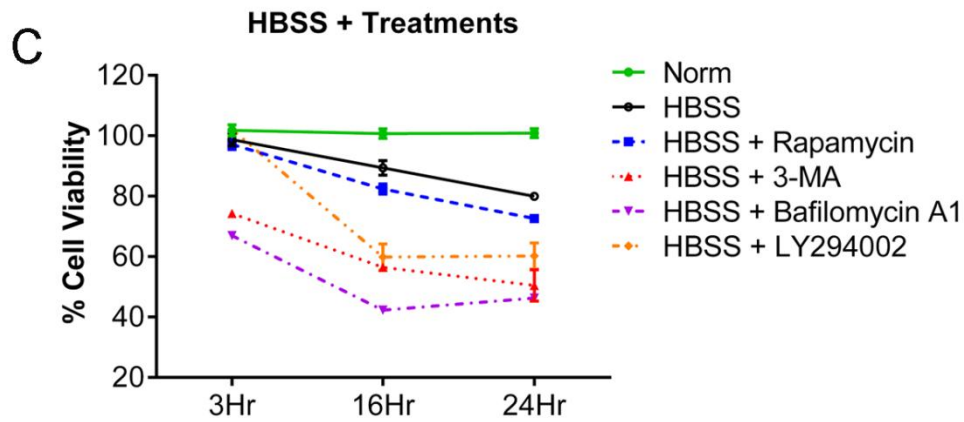
**Figure 4.4: DRG cell viability is reduced with treatment of either 3-MA or BA1 in control and nutrient deprived conditions.**

DRG neurons were cultured on laminin coated 96-well plates at ~1000 cells/well, allowed to recover for 24 hr, and subsequently exposed to the experimental treatments. MTS cell viability assay was employed to analyze DRG neurons survival in (A) nutrient control conditions and (C) nutrient deprived conditions, with and without rapamycin (200nM), 3-MA (10mM), Bafilomycin A1 (200nM) and LY294002 (10 $\mu$ M). Plotted values are mean  $\pm$  SEM; n = minimum of 8 MTS replicates. The significance at each time-point for each sample was determined by using a one way ANOVA with Tukey's *post hoc* test, comparing the data from the specific treatment to the control (norm) condition. \* P < 0.05; \*\* P < 0.01; \*\*\*\* P < 0.0001.



**B**

Compared to Norm	3 hr	16 hr	24 hr
Norm 3 hr	--	NS	NS
Norm vs Norm + Rapamycin	NS	NS	NS
Norm vs Norm + 3 MA	NS	****	****
Norm vs Norm + Bafilomycin A1	****	****	****
Norm vs Norm + LY29004	NS	NS	NS



**D**

Compared to HBSS	3 hr	16 hr	24 hr
HBSS vs Norm	NS	**	****
HBSS vs HBSS	—	*	****
HBSS vs HBSS + Rapamycin	NS	NS	NS
HBSS vs HBSS + 3 MA	****	****	****
HBSS vs HBSS + Bafilomycin A1	****	****	****
HBSS vs HBSS + LY29004	NS	****	****

(control), or nutrient-deprived with HBSS over time frames of 3 hr, 16 hr and 24 hr. As before, both untreated and HBSS-treated cultures were co-treated with either rapamycin or 3-MA. Biochemical changes in the ratio of LC3BII:LC3BI, phospho-p70S6K:p70S6K and phospho-mTOR:mTOR were determined by immunoblotting, as described in the Methods section. LC3B is an essential autophagy-related protein, whose expression can be used as a marker of autophagy modulation, while mTOR is both a key protein in modulating the activity of autophagy, as well as the direct target of inhibition by rapamycin. To determine whether rapamycin had the expected inhibitory effect on mTOR activity, the phosphorylation of the mTOR downstream target protein p70S6K was also analyzed.

In the control (untreated) conditions, the ratio of LC3BII:LC3BI did not change, while co-treatment with 3-MA decreased it (Fig. 4.5A-D). Unlike the 3-MA treatment, there was little change in the LC3BII:LC3BI ratio with rapamycin treatment (Fig. 4.5A-D). However, analysis of the ratios of phospho-mTOR:mTOR (Fig. 4.5A-C, F) and phospho-p70S6K:p70S6K (Fig. 4.5A-C, E) show that rapamycin is having a specific effect on the activation and activity of mTOR, as the phosphorylation of both mTOR and p70S6K were both decreased with rapamycin treatment.

With HBSS treatment, the ratio of LC3BII:LC3BI increased throughout the experiment, supporting induction of autophagy (Fig. 4.6A-D). As in the control conditions, 3-MA caused a clear reduction in the LC3BII:LC3BI, while rapamycin co-treatment with HBSS resulted in an overall increase in the LC3BII:LC3BI ratio compared to control, although it did not differ from the HBSS situation (Fig. 4.6A-D). Again, rapamycin resulted in the decreased activation and activity of mTOR (Fig. 4.6A-C, F) and p70S6K (Fig. 4.6A-C, E) as expected.

**Figure 4.5: Autophagy related proteins are reduced with 3-MA treatment in nutrient control conditions.**

DRG neurons were grown on laminin-coated 12-well plates at  $\sim 1 \times 10^6$  cells/well for 24 hr. The neurons were then treated with 3-MA (10mM) and rapamycin (200nM) for 3 hr, 16 hr or 24 hr. After treatment, protein extracts were collected and immunoblotted as described in the Methods. Western blots were probed with LC3B, p70S6 kinase, phospho-p70S6 kinase (Thr421/Ser424), mTOR, phospho-mTOR (Ser2448) and  $\beta$ -Actin antibodies, with the blots stripped and reprobed after each antibody was analyzed. After each probe, Western blots were scanned and densitometric analysis of bands was carried out using ImageJ and a calibrated gray scale standard. Western blots presented in (A-C) are representative of the densitometric data analysis in (D-F). The bars in (D-F) are mean ROD ( $\pm$  SEM) from each of 3 separate experiments. Significance of results was determined by using a one-way ANOVA with Tukey's *post hoc* test, confirmed using a non-parametric test, comparing samples to the control (norm) condition at each time-point. \* P < 0.05, \*\* P < 0.01, \*\*\* P < 0.001, \*\*\*\* P < 0.0001.

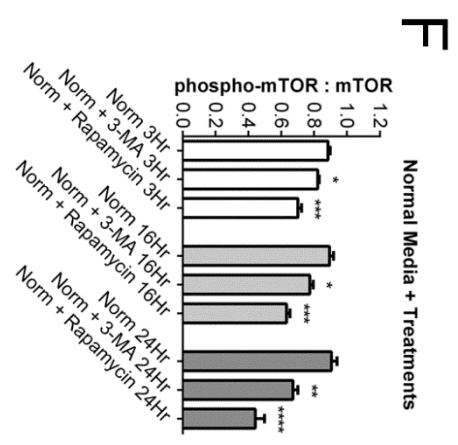
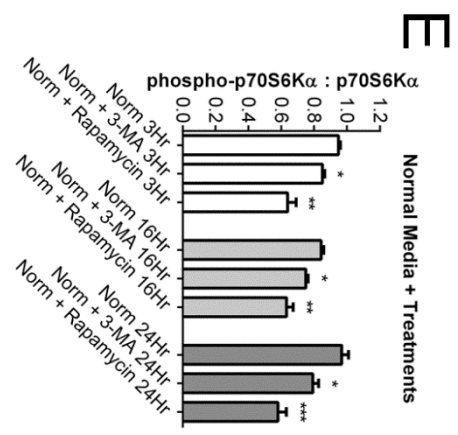
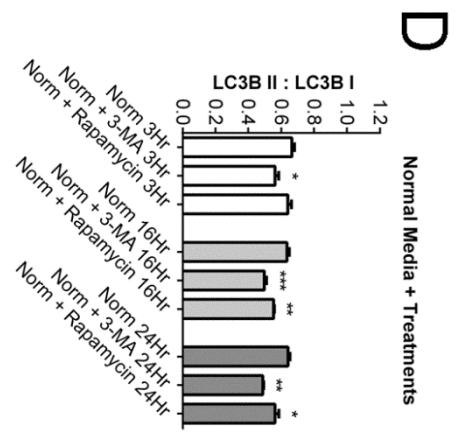
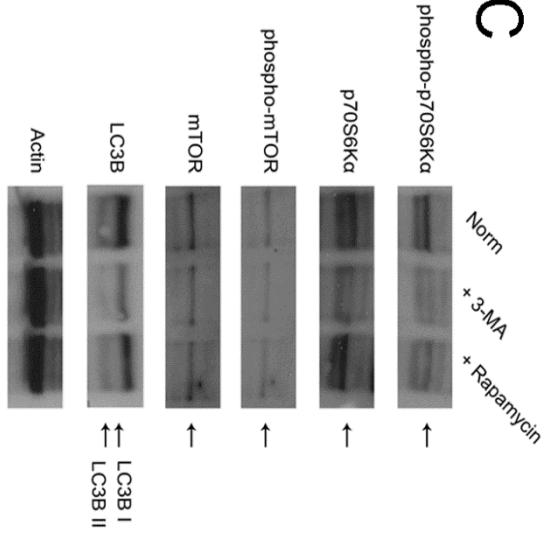
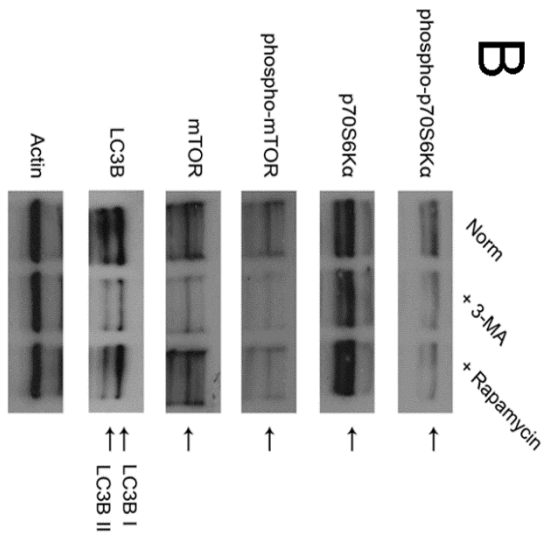
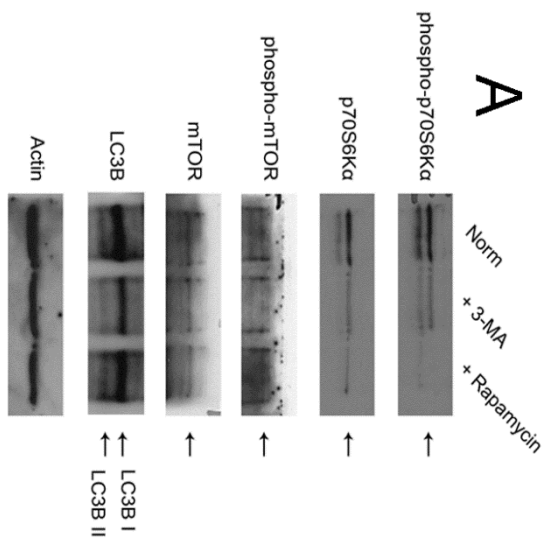
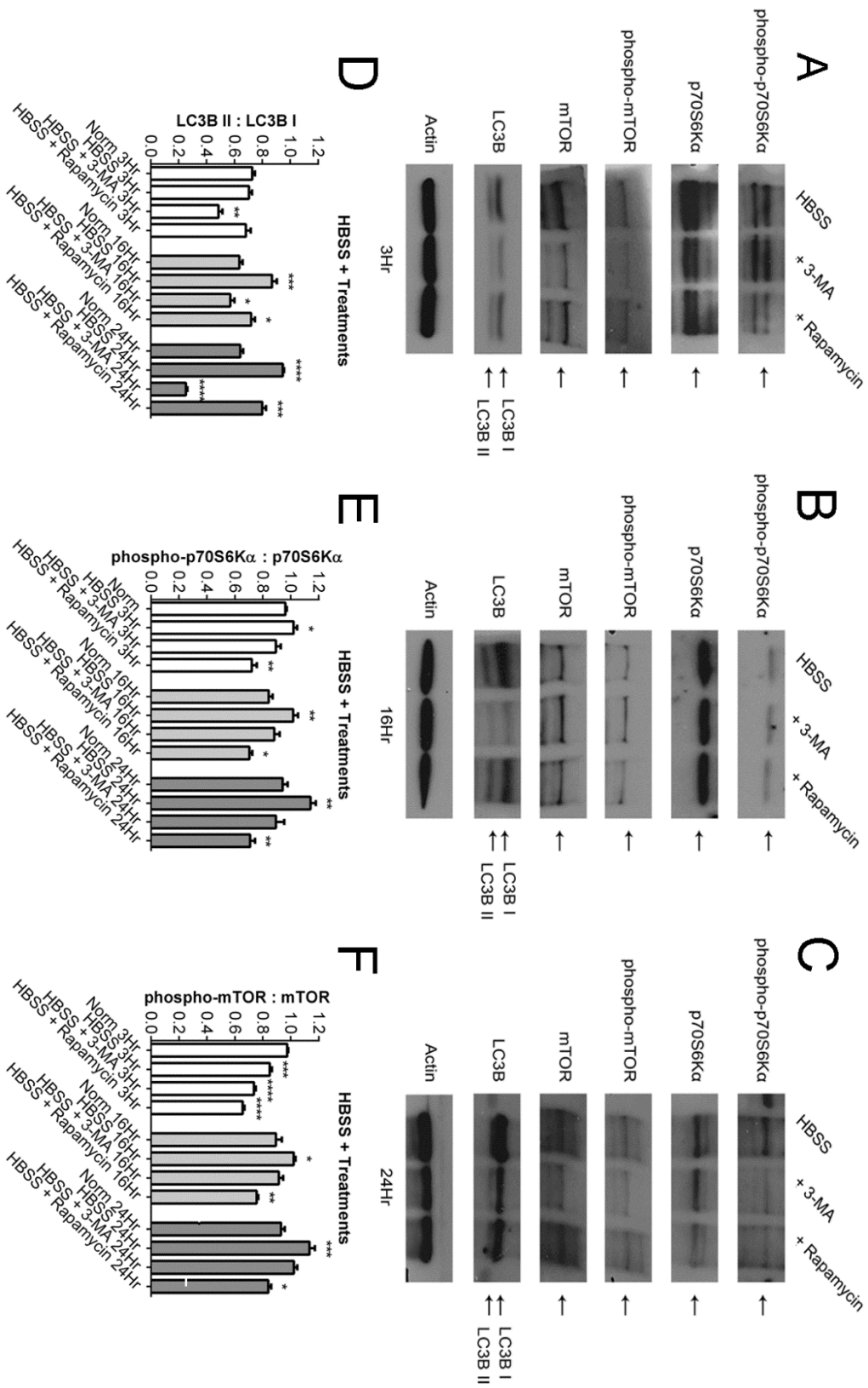


**Figure 4.6: Autophagy is activated by nutrient deprivation conditions, while inhibited with subsequent 3-MA treatment.**

DRG neurons were grown on laminin-coated 12-well plates at  $\sim 1 \times 10^6$  cells/well for 24 hr. Culture media was then removed and replaced with HBSS  $\text{Ca}^{2+}/\text{Mg}^{2+}$  and treated for 3 hr, 16 hr or 24 hr. In conjunction with HBSS  $\text{Ca}^{2+}/\text{Mg}^{2+}$ , 3-MA (10mM) or rapamycin (200nM) were added over the same time frames. DRG protein extracts were collected and immunoblotted as described in the Methods. Western blots were probed with LC3B, p70S6 kinase, phospho-p70S6 kinase (Thr421/Ser424), mTOR, phospho-mTOR (Ser2448) and  $\beta$ -Actin antibodies, with the blots stripped and reprobed after each antibody was analyzed. After each probe, Western blots were scanned and densitometric analysis of bands was carried out using ImageJ and a calibrated gray scale standard. Western blots presented in (A-C) are representative of the densitometric data analysis in (D-F). The bars in (D-F) are mean ROD ( $\pm$  SEM) from each of 3 separate experiments. Significance of results was determined by using a one-way ANOVA with Tukey's *post hoc* test, confirmed using a non-parametric test, comparing samples to the control (norm) condition at each time-point. \*  $P < 0.05$ , \*\*  $P < 0.01$ , \*\*\*  $P < 0.001$ , \*\*\*\*  $P < 0.0001$ .



#### **4.4.4 DRG Growth Morphology Is Negatively Altered With Autophagy Inhibition**

Morphological and growth-associated changes in the neurons with the treatments outlined previously were next evaluated. Immunocytochemistry was carried out using neuron-specific  $\beta$ III-tubulin (for cell and neurite quantitation) and LC3B (for quantitation of autophagosomes) staining. Cells were plated on laminin and allowed to recover for 24 hr. Under these conditions, about 40-60% of the neurons exhibit neurite growth, ranging from those with relatively short processes to those with more extensive growth (Tucker et al., 2005a, 2006). Cultures were imaged using confocal microscopy, and DRG neurite growth, neurite branching complexity and autophagosome puncta were analyzed with Imaris imaging software, as outlined in the Methods section. In these experiments, only neurons that displayed neurite growth were analyzed.

While neurite growth increased in the control conditions, 3-MA treatment resulted in a decreased amount of growth over the course of the experiment (Fig. 4.7A and 4.8). Treatment with HBSS resulted in a reduction in growth by 24 hr, with rapamycin showing a similar decrease as HBSS (Fig. 4.9A and 4.10); 3-MA treatment resulted in a further decrease over the experimental time course (Fig. 4.9A and 4.10). There was little difference in growth detected in the presence of rapamycin in the control medium, but a decrease was observed in the HBSS+rapamycin situation. Given that there was already growth present when the cells were treated, it is likely that the apparent decrease in neurite length is due to a combination of attenuated extension and neurite retraction. Neurite blebbing and terminal collapse was observed particularly in the 3 MA treated cells (Fig 4.8C, F, I and Fig 4.10C, F, I) as well as in the HBSS + rapamycin conditions (Fig 4.10E, H).

The changes in neurite branching complexity were also assessed using Sholl analysis. There was little difference in the neurite complexity in the control or rapamycin treated neurons over

24 hr, while 3-MA resulted in reduced branching by 24 hr (Fig. 4.7B-D). Treatment with HBSS resulted in decreased branching compared to the controls by 24 hr, while HBSS with rapamycin did not differ from HBSS alone (Fig. 4.9B-D); 3-MA treatment, however, effectively suppressed neurite branching over the 24 hr period (Fig. 4.9B-D).

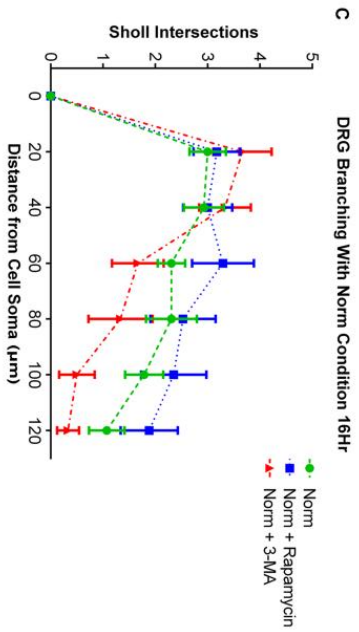
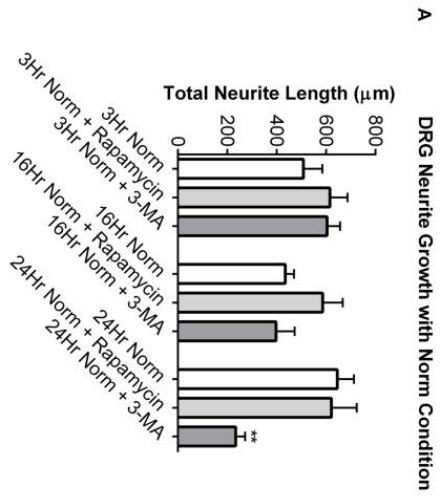
With changes in neurite growth and branching complexity observed, we assessed whether there was any correlation with the presence of autophagosomal puncta in the neurites that might relate to the growth alterations. Under control and rapamycin treated conditions the number of LC3B-positive puncta in neurites increased over the experiment, with a sharp increase found at 3 hr after rapamycin (Fig. 4.11A), while with 3-MA treatment LC3B puncta decreased over time (Fig. 4.11A). With HBSS, LC3B-positive puncta initially increased at 3 hr, and maintained this increase through 16 hr, but decreased sharply by 24 hr (Fig. 4.11B). Treatment with rapamycin resulted in a reduction in LC3B-positive puncta at 24 hr only, while 3-MA treatment caused an overall reduction in puncta throughout the experiment (Fig. 4.11B). These results suggest that 3-MA treatment alters either autophagosome formation or transport. Alteration of autophagosome formation by 3-MA may be the main cause of reduction, since autophagosome aggregation, which would suggest transport malfunction, was not generally observed.

The ratio of the number of LC3B puncta/100 $\mu$ m neurite length under each condition was also determined. The puncta/100 $\mu$ m neurite length ratio increased gradually over time in both the control and the rapamycin-treated cultures (Fig. 4.11C), while there was a significant reduction with 3-MA (Fig. 4.11C). HBSS treatment caused an initial increase in the ratio that eventually decreased over time (Fig. 4.11D), while with rapamycin co-treatment the ratio remained elevated compared to HBSS (Fig. 4.11D). As in the control situation, 3-MA treatment resulted in significantly reduced numbers of puncta/neurite (Fig. 4.11D).

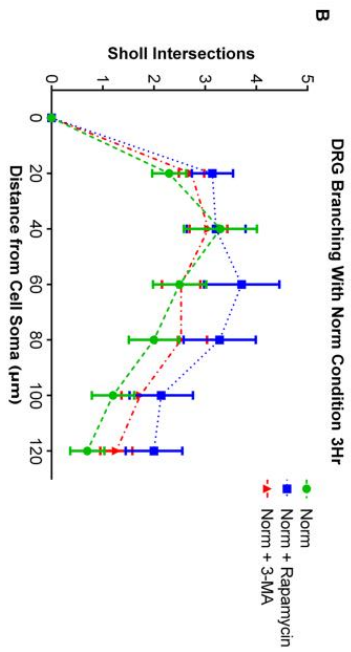
**Figure 4.7: DRG neurite length and branching complexity are reduced with autophagy inhibition in nutrient control conditions.**

DRG neurons were grown on laminin-coated 16-well culture slides for 24 hr. The neurons were then treated with 3-MA (10mM) and rapamycin (200nM) for 3, 16 and 24 hr. After treatment, the slides were processed for immunocytochemistry using antibodies directed against LC3B and  $\beta$ III-Tubulin, followed by fluorescently tagged secondary antibodies, as described in the Methods. Neurons were visualized with confocal microscopy, and **(A)** total neurite growth in length ( $\mu$ m) from the cell soma was assessed. Values are mean  $\pm$  SEM; n = 10 field of view replicates from 3 separate experiments/plating. Sholl intersection analysis was also performed at 3 **(B)**, 16 **(C)** and 24 hr **(D)** using the Filament Tracer tool in Imaris, described in the Methods. Sholl spheres resolution was set at 20 $\mu$ m for analysis. Values are mean  $\pm$  SEM; 20 cells were analyzed per condition, per time-point. The significance at each Sholl spheres resolution was determined by comparing the data from the specific treatment to the control (norm) condition.

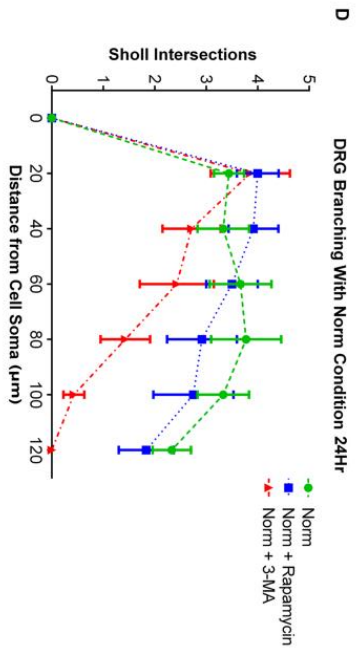
\* P < 0.05, \*\* P < 0.01, with a two-way ANOVA with Tukey's *post hoc* test.



Norm + Rapamycin	NS								
Norm + 3-MA	NS								



Norm + Rapamycin	NS								
Norm + 3-MA	NS								



Norm + Rapamycin	NS								
Norm + 3-MA	NS	NS	NS	NS	NS	*	**	**	**

**Figure 4.8: DRG neurite growth is reduced after 3, 16 and 24 hr treatment with 3-MA in nutrient control conditions.**

DRG neurons were grown on laminin-coated 16-well culture slides for 24 hr and subsequently treated with 3-MA (10mM) and rapamycin (200nM) for 3, 16 and 24 hr. After treatment, the slides were processed for immunocytochemistry using an antibody directed against  $\beta$ III-Tubulin, followed by a fluorescently tagged secondary antibody, as described in the Methods. DRG neurons were visualized with confocal microscopy. Panels: A-C – 3 hr treatment; D-F – 16 hr treatment; G-I – 24 hr treatment. Note neurite blebbing as well as terminal collapse in cells treated with 3-MA (arrowheads, C, F, I). Scale bar = 50  $\mu$ m.

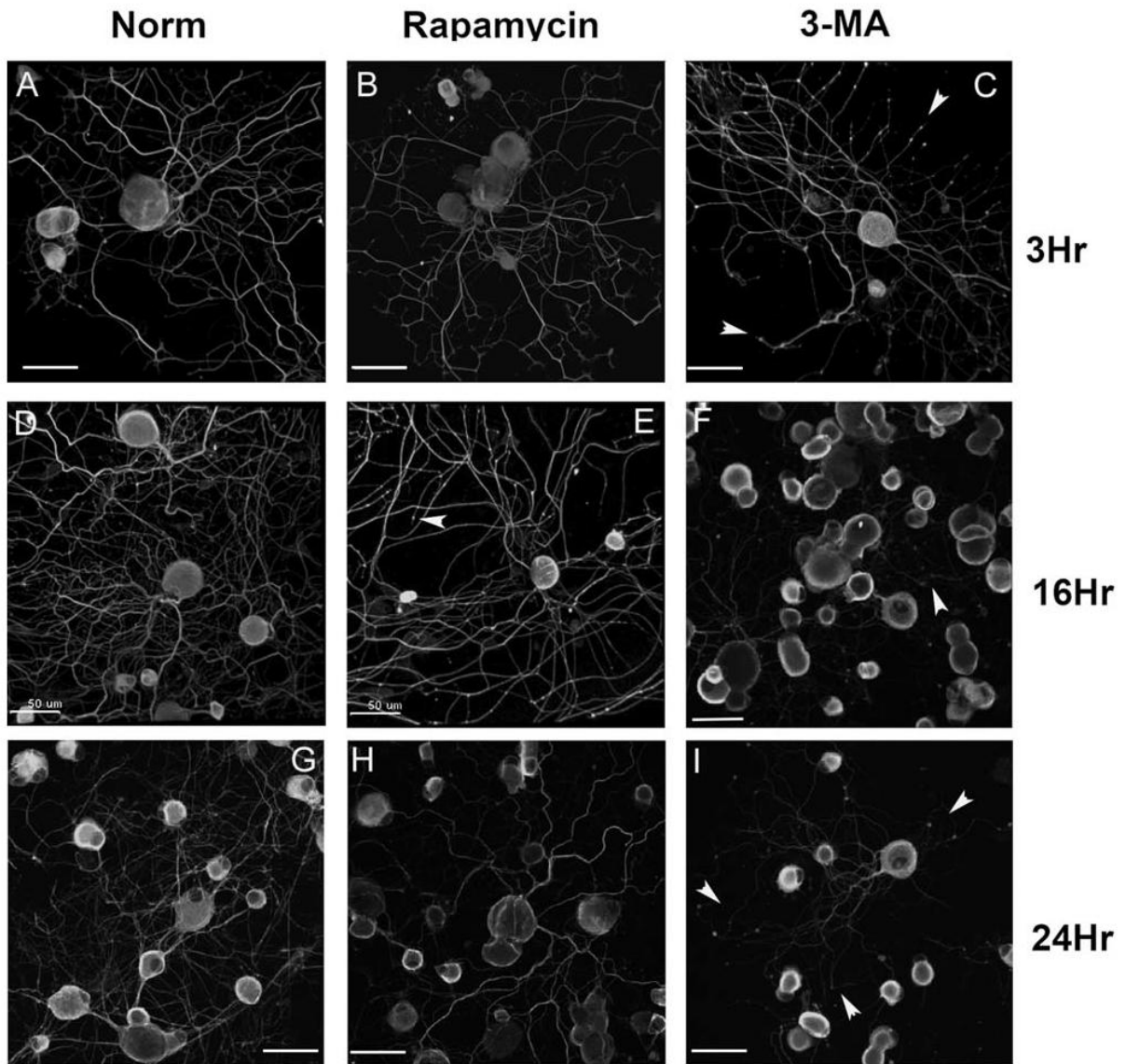
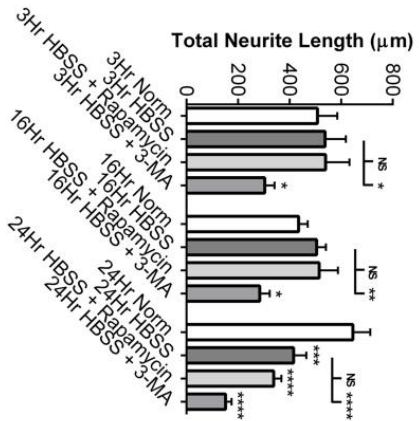


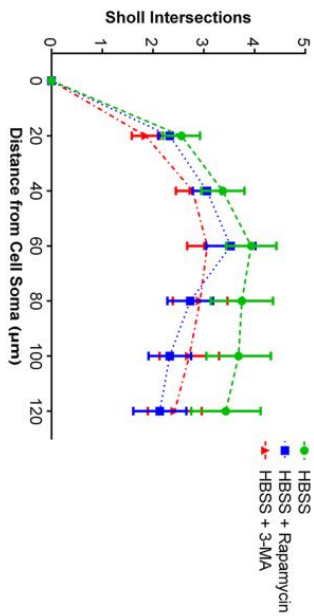
**Figure 4.9: DRG neurite length and branching complexity are reduced with autophagy inhibition in nutrient deprived (HBSS) conditions.**

DRG neurons were grown on poly-D-lysine and laminin-coated 16-well culture slides for 24 hr. Culture media was then removed and replaced with HBSS  $\text{Ca}^{2+}/\text{Mg}^{2+}$  and treated for 3, 16 and 24 hr. In conjunction with HBSS  $\text{Ca}^{2+}/\text{Mg}^{2+}$ , the autophagy modulators 3-MA (10mM) and rapamycin (200nM) were added over the same time frame. Cells were immunostained to detect LC3B and  $\beta$ III-Tubulin, as previously noted. DRG neurons were visualized with confocal microscopy, and (A) total neurite growth in length ( $\mu\text{m}$ ) from the cell soma was assessed. Values are mean  $\pm$  SEM; n = 10 field of view replicates from 3 separate experiments/platings. Sholl intersection analysis was also performed at 3 (B), 16 (C) and 24 hr (D) using the Filament Tracer tool in Imaris, described in the Methods. Sholl spheres resolution was set at  $20\mu\text{m}$  for analysis. Values are mean  $\pm$  SEM; 20 cells were analyzed per condition, per time-point. The significance at each Sholl spheres resolution was determined by comparing the data from the specific treatment to the control (norm) condition. \*  $P < 0.05$ , \*\*  $P < 0.01$ , \*\*\*  $P < 0.001$ , \*\*\*\*  $P < 0.0001$ , with a two-way ANOVA with Tukey's *post hoc* test.

**A** DRG Neurite Growth with HBSS Condition

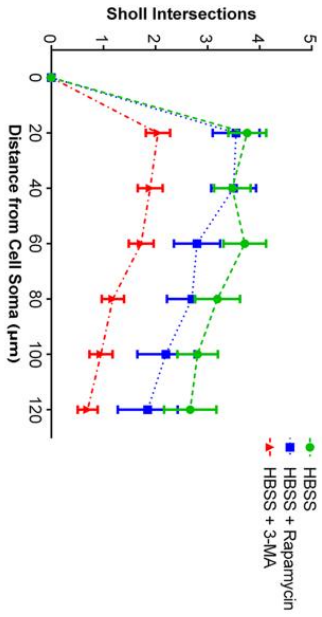


**B** DRG Branching With HBSS Condition 3Hr



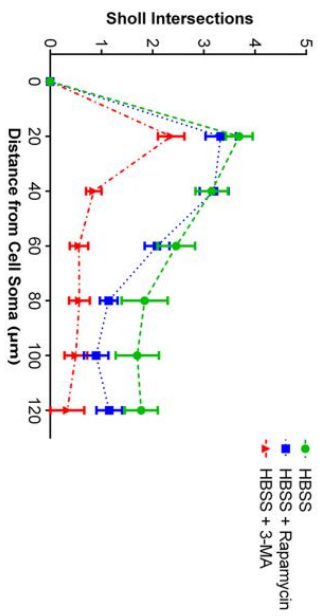
HBSS + Rapamycin	20µm	40µm	60µm	80µm	100µm	120µm
HBSS + 3-MA	NS	NS	NS	NS	NS	NS

**C** DRG Branching With HBSS Condition 16Hr



HBSS + Rapamycin	20µm	40µm	60µm	80µm	100µm	120µm
HBSS + 3-MA	NS	NS	NS	NS	NS	NS

**D** DRG Branching With HBSS Condition 24Hr



HBSS + Rapamycin	20µm	40µm	60µm	80µm	100µm	120µm
HBSS + 3-MA	NS	NS	NS	NS	NS	NS

**Figure 4.10: DRG neurite growth is reduced after 3, 16 and 24 hr treatment with 3-MA in nutrient deprived (HBSS) conditions.**

DRG neurons were grown on poly-D-lysine and laminin-coated 16-well culture slides for 24 hr. Culture media was then removed and replaced with HBSS  $\text{Ca}^{2+}/\text{Mg}^{2+}$  and treated for 3, 16 and 24 hr, plus or minus 3-MA (10mM) or rapamycin (200nM). Cells were immunostained to detect LC3B and  $\beta$ III-Tubulin, and neurons were visualized with confocal microscopy. Panels: A-C – 3 hr treatment; D-F – 16 hr treatment; G-I – 24 hr treatment. Note neurite blebbing/swelling as well as terminal collapse in cells treated with 3-MA (arrowheads, C, F, I). Scale bar = 50  $\mu\text{m}$ .

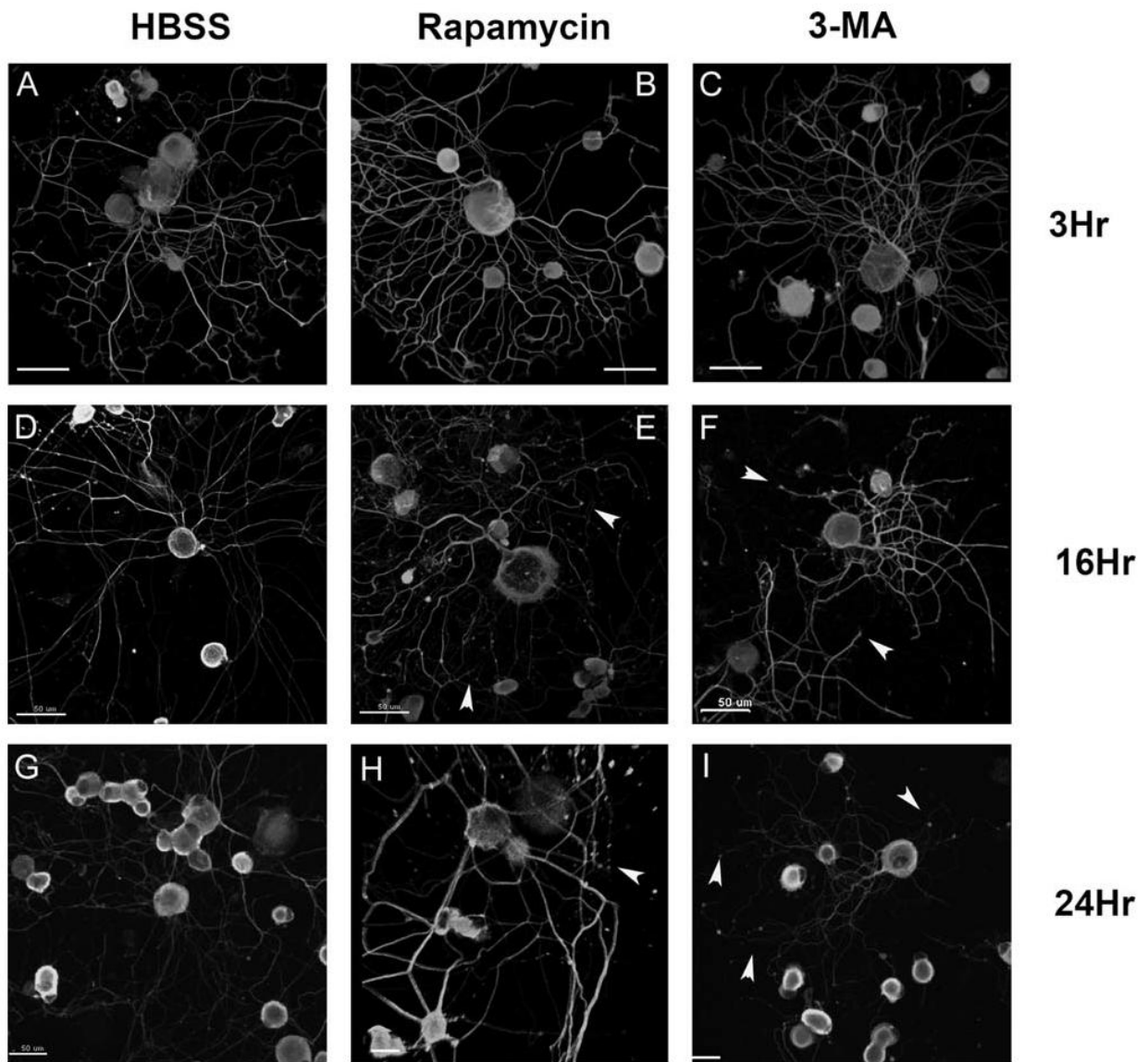
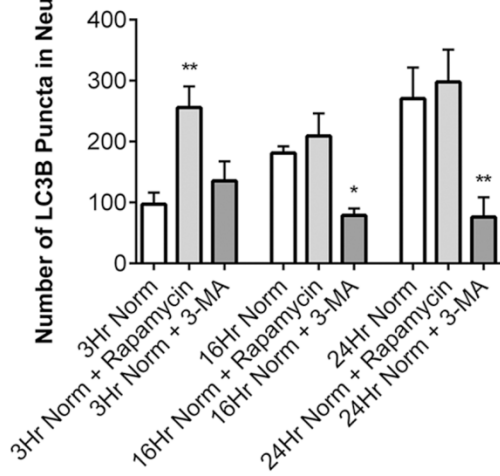


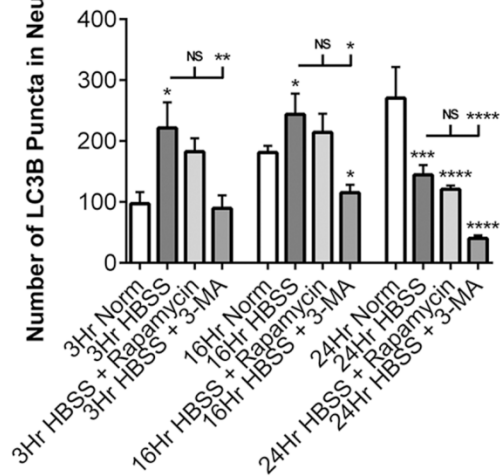
**Figure 4.11: Autophagy inhibition reduces autophagosome occurrence in DRG neurites.**

DRG neurons were grown on poly-D-lysine and laminin-coated 16-well culture slides for 24 hr. The neurons were then treated with 3-MA (10mM) and Rapa (200nM) for 3, 16 and 24 hr. Alternatively, culture media was removed and replaced with HBSS  $\text{Ca}^{2+}/\text{Mg}^{2+}$  and treated for 3, 16 and 24 hr, plus or minus 3-MA (10mM) and Rapa (200nM). Cells were immunostained to detect LC3B and  $\beta$ III-Tubulin, and neurons were visualized with confocal microscopy. The total number of LC3B puncta found in growing DRG neurites with Rapa or 3-MA in (A) nutrient control conditions, and (B) nutrient deprivation conditions was quantitated. Values are mean  $\pm$  SEM; n = 4 replicates. Additionally, the ratio of the number of LC3B puncta per 100 $\mu\text{m}$  neurite length with Rapa or 3-MA in (C) nutrient control conditions, and (D) nutrient deprivation conditions was analyzed. (E) Raw image of neurites showing localization of LC3-positive puncta (green). (F) Imaging software (Imaris, Spots algorithm) was used to highlight “spots” in the LC3 (green) channel (as outlined in the Methods section), and quantitation was then done on selected neurite lengths; the cells were also immunostained for HspB1 (blue), which served to outline the neurites. Scale bar-10  $\mu\text{m}$ . Values are mean  $\pm$  SEM; n = 7 replicates. In all samples, a total of 20 cells were analyzed per condition, per time-point, with conditions and time-points done in triplicate. Significance of results was determined by using a one-way ANOVA with Tukey’s *post hoc* test, confirmed using a non-parametric test, comparing samples to the control (norm) condition at each time-point. \* P < 0.05, \*\* P < 0.01, \*\*\* P < 0.001, and \*\*\*\* P < 0.0001.

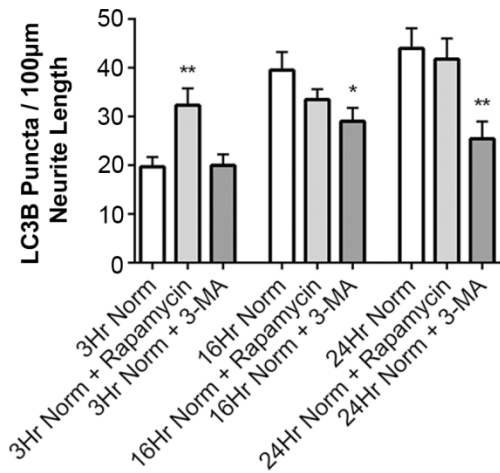
**A Total LC3Puncta Under Control Conditions**



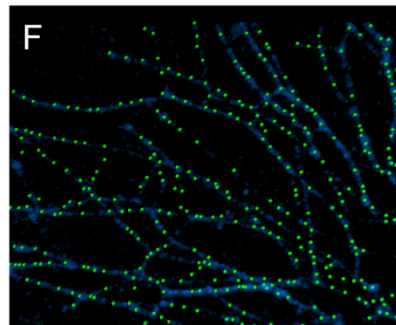
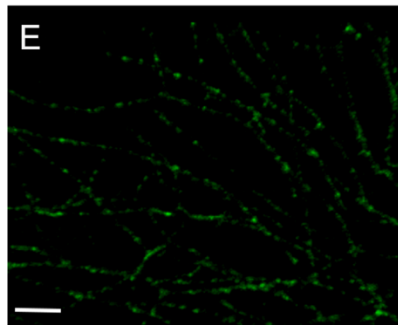
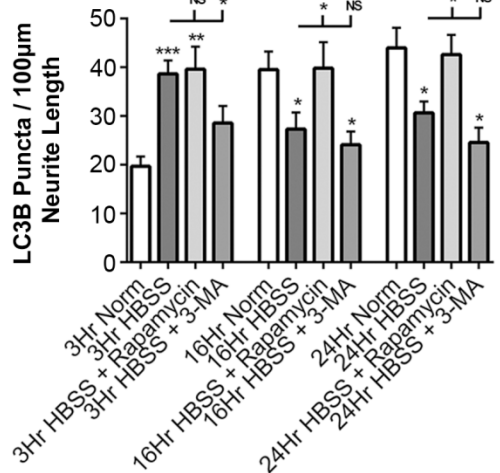
**B Total LC3Puncta Under Nutrient Deprivation**



**C Control Conditions**



**D Nutrient Deprivation**



Overall, a global reduction in neurite growth and branching complexity with HBSS treatment was observed (Fig. 4.9). Additionally, autophagosomal puncta formation was increased with HBSS treatment, but decreased with 3-MA co-treatment (Fig. 4.11B). Interestingly, rapamycin treatment did not increase the ratio beyond what is found with control conditions alone, suggesting that an autophagosome formation threshold had been reached (Fig. 4.11D).

## **4.5 Discussion**

This study investigated the influence of autophagy on adult DRG neuronal cell survival and neurite growth, and has demonstrated that constitutive autophagy in DRG neurons can be modulated using either metabolic challenge or chemical modulators. Inhibition of either constitutive or nutrient deprivation-induced autophagy adversely affected cell survival, neurite growth and neurite branching. Overall, our data provide further insight into how autophagy influences DRG neuron survival and neurite growth.

### **4.5.1 Autophagy and Neuronal Cell Survival**

The process of autophagy has been studied in many cellular systems and within many pathological diseases [reviewed in (Ravikumar et al., 2010)]. The functions of autophagy are to maintain cellular homeostasis, and to degrade long-lived and damaged proteins and organelles, and to recycle nutrients. In particular, endogenous autophagic processes are especially important in neurons, since neurons are post-mitotic cells and are unable to dilute harmful by-products, accumulated through either endogenous mechanisms or through cell stressors, by cell division. The prevailing view is that autophagy is a constitutive process in neurons and that disruption or dysregulation of the process can lead to axonopathies and eventual neurodegeneration (Button et

al., 2015; Chu et al., 2009; Frake et al., 2015; Menzies et al., 2015; Ravikumar et al., 2010; Wong and Holzbaur, 2015; Yang et al., 2013). While autophagic function and modulation has been extensively studied in the CNS, there have been relatively few studies addressing the potential protective effects on survival and axonal maintenance in the PNS (Maday and Holzbaur, 2014; Maday et al., 2012; Marinelli et al., 2014; Mohseni, 2011; Nicks et al., 2014; Rangaraju et al., 2010; Simon et al., 2004).

This current study focused upon whether and how autophagy modulation might affect adult DRG neuron survival and neurite growth, and is among the first to show that constitutive autophagy in adult DRG neurons can be modulated through both nutrient deprivation and pharmacological treatment. Our data show that neuron viability is decreased by inhibiting endogenous autophagy in non-stressed adult DRG neurons. Additionally, stressing adult DRGs with a low nutrient environment, and inhibiting autophagy in parallel, resulted in further decreased cell viability as compared to non-stressed neurons. We did not directly assess whether this decreased viability resulted in cell death, although detachment and loss of cells was more noticeable in the presence of the inhibitors and/or nutrient deprivation.

While cell loss occurred with nutrient deprivation alone, it was not as pronounced as when autophagy was also inhibited, suggesting that endogenous autophagic mechanisms are important in adult DRG neuron survival during stress. The relationship between autophagy and cell death, particularly in neuronal cells, is complex and appears to depend on the type of neuron, the stress and the extent of compromise of cellular constituents (Button et al., 2015; Menzies et al., 2015). In DRG neurons, with their long peripheral axons, constitutive autophagy is likely important in the face of the unique challenges associated with the peripheral innervation fields (e.g., terminal recycling, exposure to thermal and chemical stresses). A role for constitutive autophagy in the

survival of mature DRG neurons is supported by work showing that while the development of sensory neurons in neonatal Atg7-knockout mice was normal, there was significant DRG neuronal loss in older animals (Zhou et al., 2010). In the face of starvation or local injury, increased autophagosome formation and flux might be expected to balance the loss of energy or requirement for increased local protein synthesis. However, at some point there may be a rundown of cellular energy/ATP levels which would not only impair the maturation of the autophagosomes with lysosomes and the degradation process that is necessary for nutrient recycling, but could also lead to eventual cell death. The inhibition of autophagy induction, as with 3-MA, or the blocking of the final fusion process, as with BA1, would enhance this scenario resulting in further cell death. While our data support the contention that inhibition of autophagy with 3-MA negatively influences neuronal survival and neurite growth, it is possible that other pathways may be involved (Ravikumar et al., 2010; Zhou et al., 2010). Although 3-MA is considered to inhibit the formation of autophagosomes via its effects on the Class III PI3-K  $\rightarrow$  beclin complex, it can also inhibit Class I PI3-K and the activation of its downstream target Akt. We have previously shown that PI3-K  $\rightarrow$  Akt pathway is important in both the neurotrophin-independent survival and neurite growth from these DRG neurons (Dodge et al., 2002; Tucker et al., 2005a, 2006, 2008). In the current study, treatment of the cells with LY29004, a selective PI3-K inhibitor, did not result in any significant changes in viability in the normal medium, although in the nutrient deprived conditions there was decreased viability at the longer exposure times, similar to that observed with 3-MA.

#### 4.5.2 Modulation of Autophagy

We employed both ICC and immunoblotting to assess the levels of LC3 under the differing experimental conditions. The presence of LC3-positive puncta signifies that autophagy is occurring, although it does not necessarily indicate overall flux, i.e., the measure of production vs degradation (Barth et al., 2010; Loos et al., 2014). The number of autophagosomes per cell over time can be used to estimate the steady state levels. For example, in the control conditions there is effectively no change in the number of puncta/cell between 3 and 16 hr (Fig. 4.3), supporting the idea of a steady state level. The addition of rapamycin increases the number/cell above the control, but again does not differ between the 2 time points, suggesting that prolonged exposure to rapamycin does not increase above a steady state level. Similarly, the addition of 3MA decreases the number of puncta/cell, but this does not differ with time. With HBSS, there is a difference in the puncta/cell between 3 and 16 hr time, suggesting that the nutrient deprivation continues to drive autophagy. The ratio of LC3BII:LC3I expression is another approach to assessing whether autophagy is occurring, with level of LC3II expression on immunoblots correlating with the number of autophagosomes (Mizushima and Yoshimori, 2007; Mizushima et al., 2010). As in the analyses of autophagosomes at the cellular level, protein expression of both LC3I and LC3BII was observed, with inhibition of autophagy resulting in more consistent changes LC3BII:LC3BI ratio. Similar to the ICC studies, the addition of rapamycin did not appear to significantly influence the ratio compared to the levels observed in the normal medium, which might be considered a threshold level that can be sustained by these neurons. Analysis of the effects of rapamycin on mTOR and p70S6K, indicate that in both the normal and HBSS conditions, rapamycin had the expected inhibitory effect on downstream activation of p70S6K. Our data support a role for constitutive autophagy in the maintenance of

neurons under the ‘control’ conditions that reaches a threshold or steady state level that is not further increased; inhibition or dysregulation of autophagy results in decreased cell viability. Under nutrient-deprived conditions there is an increase in autophagy that might be expected to promote survival but is not sufficient to sustain it at the control levels. It may be that increased autophagosomes represent the cellular response to attempt to deal with a compromised energy balance. Negatively altering this response tips the balance towards cell death.

### **4.5.3 Autophagy and Neurite Growth**

We also quantified LC3B-positive autophagosomes within growing neurites. The neurite analysis approach provided similar with autophagosome formation being reduced with autophagy inhibition, increased with nutrient deprivation and reduced with a combination of both. Interestingly, when rapamycin was used, there was an increase in autophagosome formation early in the experimental paradigm, but this did not go beyond the levels of endogenous autophagy. The same held true with nutrient deprivation, as the level of autophagosome formation with rapamycin added did not increase over the amount found caused by nutrient deprivation alone. As noted above, the lack of change over time may reflect a steady state level of autophagy, especially in the normal medium with or without rapamycin. However, it is possible that the concentration of rapamycin employed did not effectively inhibit mTOR functions, despite the fact that the Western data show the expected inhibitory effects in both the normal and HBSS conditions.

In addition to assessing autophagy in neuronal cell survival, the effects of autophagy on DRG neurite growth were also examined. Elegant studies from the Holzbaur group have shown that autophagosome formation occurs in an ordered and spatially regulated pathway within the distal

tips of DRG axons, and from here are transported back to the cell soma along the microtubule network using retrograde transport mechanisms (Fu et al., 2014; Maday and Holzbaur, 2012, 2014; Maday et al., 2012). They suggest that autophagosome formation within the distal axon tips is required for proper recycling of damaged organelles, as due to an increase in demand for membrane recycling under periods of active axon extension and retraction, organelles within this region may become more susceptible to damage (Maday and Holzbaur, 2014; Maday et al., 2012). One can additionally hypothesize that autophagy allows for the availability of nutrients within the distal axon tips for use in both distal translation of local proteins involved in axon growth (Christie et al., 2010; Gumy et al., 2010; Verma et al., 2005).

We assessed the potential role of autophagy on DRG neurite growth by determining its influence on total neurite length from the DRG cell soma and the degree of neurite branching complexity. We observed that when autophagy had been inhibited, either during nutrient deprivation or in control conditions, neurite growth from the cell soma significantly decreased, with a more pronounced effect observed with prior stress. Further analysis of the neurite branching complexity found a significant reduction in the complexity of branching with autophagy inhibition.

The potential role of autophagy in neurite or axonal growth or maintenance has been the subject of several reviews (Chu et al., 2009; Gumy et al., 2010; Rubinsztein et al., 2015; Yang et al., 2013), but there is little consensus on whether the effects are positive or negative. For example, early neurite outgrowth from cultured cortical neurons is enhanced by inhibition of autophagy with 3-MA (Ban et al., 2013). Optic nerve transection results in retinal ganglion cell death which can be prevented by autophagy induction (Rodriguez-Muela et al., 2012). Transection also results in axonal degeneration, but in contrast to RGC survival, this can be

inhibited by blocking autophagy (Knoferle et al., 2010). Autophagy has also been shown to be important in the maintenance of Purkinje cell axons in Atg7-knock-out mice, where loss of autophagy results in a progression axonal dystrophy and eventual neuronal loss (Komatsu et al., 2006).

Relatively few studies have investigated whether and how autophagy modulation might influence peripheral neurite growth. For example, it has been reported that neurite degeneration induced by NGF-withdrawal in neonatal sympathetic neurons results in axonal autophagy and that inhibition with 3-MA provides some amount of protection from this degeneration (Yang et al., 2007). Amyloid beta exposure of PC12 cells or sympathetic neurons results in increased autophagy. This is also accompanied by neurite retraction or degeneration which can be blocked by increasing autophagy with rapamycin, though inhibition with 3-MA had little effect in this study (Yang et al., 2014). *In vivo* studies of peripheral nerves from hypoglycemic rats noted that the presence of autophagic vacuoles correlated more with the appearance of regenerating axons, than with degenerating ones (Mohseni, 2011).

Although our data indicate that autophagy does influence DRG neurite growth, we did not investigate the mechanism(s) underlying its contribution. Further study is necessary to investigate the signaling pathways that contribute to the regulation of autophagy and how axonal growth can be promoted. A caveat of attributing the effects of 3-MA only to an inhibition of autophagy is the fact that 3-MA may also inhibit PI3-K  $\rightarrow$  Akt pathway (Chu et al., 2009), which is important not only in promoting cell survival but also neurite outgrowth (Tucker et al., 2006, 2008). It is likely that the reduction in total growth reflects a combination of inhibited extension as well as increased retraction or collapse. This could come about due to decreased

autophagosome formation with 3-MA treatment and thus provision of local building blocks, or a potential reduction in local protein synthesis, due to altered mTOR function.

The actions of rapamycin on neuronal and axonal growth and regeneration are quite complex, and the majority of studies have assessed these actions in terms of effects on protein translation or other processes not necessarily related to autophagy. In our experiments, inhibition of mTOR had little detectable effect on neurite growth and branching except in the 24 hr nutrient-deprived condition. Naive DRG neurons (as opposed to those exposed to an *in vivo* conditioning lesion prior to dissociation) tend to exhibit a rather elaborate branching pattern does not require new protein synthesis at least over 24 hr; the subsequent transition to elongated neurites does require a period of protein synthesis (Smith and Skene, 1997). Most of the neurons in our cultures show this type of growth, starting with a relatively rapid elaboration of highly branched neurites, followed by elongation of some neurites. Thus with short term treatment a lack of effect of rapamycin (related to its inhibition of protein synthesis) on neurite growth might be expected. At the later stages, particularly in the situations where there is likely to be an overall decrease in general cellular metabolism, the further inhibition of local protein synthesis could have a negative influence. There have been relatively few studies assessing the role of rapamycin in axonal growth or regeneration in DRG neurons, particularly mature neurons, although the lack of effect of rapamycin on naive (i.e. not subjected to a conditioning lesion prior to plating) has been reported. For example, rapamycin had no effect on axonal elongation in the absence of axotomy, although when added prior to an *in vivo* conditioning lesion, rapamycin decreased overall neurite growth *in vitro*, via inhibition of mTOR and local protein synthesis in the distal axon (Verma et al., 2005). In another study, injury to DRG neurons by nerve ligation resulted in increased

mTOR activation; again, rapamycin treatment of the injured neurons blocked the increased growth although there was no effect on the non-injured naive neurons (Abe et al., 2010).

It has also been suggested in other studies that neurite growth in adult DRG neurons may be moderated by mTOR-independent mechanisms, such as PI3K-GSK3 $\beta$ -Smad1 signaling and PTEN inhibition, and thus mTOR inhibition with rapamycin may have little or no effect (Christie et al., 2010; Saijilafu et al., 2013).

#### **4.6 Conclusion**

Autophagy is a constitutively active process in adult DRG neurons and contributes to neuronal survival and neurite growth and regeneration *in vitro*, although further study is necessary to investigate the signaling pathways that contribute to the regulation of autophagy and how axonal growth can be promoted. A better understanding of the mechanisms involved in autophagy regulation in neurons can inform future experiments and potential therapeutic interventions.

#### **4.7 Acknowledgements**

The technical assistance of F. Nafar and J. B. Williams during the course of this study is gratefully acknowledged.

## **Chapter 5: Autophagy Inhibition in Endogenous and Increased Reactive Oxygen Species Conditions Reduces DRG Neuron Survival and Growth *In Vitro***

### **5.1 Abstract**

Efficient protein and mitochondrial activity in peripheral neuropathies is highly dependent upon proper oxidative stress management. Deviations in oxidative stress management can lead to improper function of homeostatic cellular pathways and a disruption of a stable energetic environment. In order to attenuate the effects of oxidative stress, the process of autophagy has been focused upon as a mechanism to target damaged proteins and mitochondria for proteolytic degradation, thereby prohibiting further cellular damage, and inhibiting an establishment of an oxidative stress environment. This study investigates the influence of autophagy on adult DRG neuron survival and axonal growth in control and increased ROS conditions. Constitutive autophagy was modulated using pharmacological activators (rapamycin) and inhibitors (3-methyladenine, Bafilomycin A1) in conjunction with either a nutrient stable environment (standard culture medium) or an increased ROS environment (H<sub>2</sub>O<sub>2</sub>). The results demonstrate that autophagy inhibition decreased cell viability and reduced neurite growth and branching complexity. While autophagy was upregulated with increased ROS conditions compared to the control, it was not further activated by rapamycin, suggesting a threshold level of autophagy. Overall, both cellular and biochemical approaches have been combined to show the influence of autophagy on adult DRG neuron survival and growth.

### **5.2 Introduction**

Research presented in chapter 4 (Clarke J and Mearow K, J. Neurosci. Res. 2016) demonstrated that negatively modulating autophagy during nutrient deprived stress in DRG

neurons causes decreased survival, growth and neurite branching. Research in other cell types, however, has shown that an increased reactive oxygen species (ROS) environment can also induce autophagy (Wang et al., 2015). This finding is interesting, as the maintenance of oxidative stress is of utmost importance for DRG neuron survival and growth in metabolic diseases, like DPN. Specifically, abnormalities in oxidative stress management in peripheral neuropathies can directly affect protein and mitochondrial activity, thereby leading to further deviations in the proper function of homeostatic cellular pathways and in the maintenance of a stable energetic environment.

Current studies focusing upon DPN have found that increased oxidative stress associated with disease leads to impairment and damage of mitochondria, cytosolic and cytoskeletal proteins, leading to further development of many DPN complications (Babizhayev et al., 2014; Persson et al., 2013). Specifically with regards to mitochondria, this understanding has led to the observation that while there is cellular energy depletion in DPN caused by mitochondria dysfunction, this depletion occurs despite an elevation in the availability of glucose (Roy Chowdhury et al., 2012). Therefore, current research is focused upon strategies to both manage oxidative stress and repair or recycle damaged mitochondria (Arrigo, 2013). As such, autophagy, or specifically mitophagy, is an avenue that could be studied and used to target ROS damaged mitochondria for proteolytic degradation, thereby prohibiting further establishment of oxidative stress from damaged mitochondria.

In continuation of the research presented in chapter 4 (Clarke J and Mearow K, *J. Neurosci. Res.* 2016), the research presented herein assesses whether ROS stress, induced by treating DRG neurons with a high concentration of H<sub>2</sub>O<sub>2</sub>, has similar effects on autophagy and DRG neuron survival, growth and neurite branching as found with nutrient deprivation. The results in this

study demonstrate that H<sub>2</sub>O<sub>2</sub> induces ROS stress in DRG neurons, and the resulting ROS stress reduces adult DRG neuron survival, axon growth and axon branching complexity. In addition, results show that by inhibiting autophagy in conjunction with an increased ROS environment, DRG neuron survival, axon growth and axon branching complexity are further attenuated compared to ROS stress alone. Overall, the data presented in this study provide further insights into how autophagy influences DRG neuronal cell survival and neurite growth.

### **5.3 Materials and Methods**

#### **5.3.1 Reagents and Antibodies**

F12 media, B27 supplement, collagenase type II and natural mouse laminin were purchased from Invitrogen (Burlington, ON, CAN). AraC, FdU, 3-MA, BA1, Rapa, trypsin, PMS, DNase, H<sub>2</sub>O<sub>2</sub> 30% w/w and menadione were purchased from Sigma-Aldrich Canada Ltd. (Oakville, ON, CAN). The pharmacologic PI3K inhibitor LY294002 was purchased from Millipore Canada Ltd. (Etobicoke, ON, CAN). BCA protein assay solutions, Blot® 4-12% Bis-Tris Plus Gels, immunoblot reagents, immunoblot membranes, SuperSignal® West Pico Chemiluminescent Substrate and CellROX® Green Reagent for oxidative stress detection were purchased from ThermoFisher Scientific (Nepean, ON, CAN). Cell Titer 96® AQueous MTS Reagent Powder was purchased from Promega (Madison, WI, USA). The protease inhibitor, ovomucoid was obtained from Worthington Biochemical Corp. (Lakewood, NJ, USA). AErrane (isoflurane) was purchased from Baxter Corp. (Mississauga, ON, CAN). Primary and secondary antibodies used in this study are outlined in Table 5.1.

**Table 5.1: List of primary and secondary antibodies, with experimental dilutions, used either for immunoblotting (IB) or immunocytochemistry (ICC).**

<b>Antibody</b>	<b>Method</b>	<b>Dilution</b>	<b>Company</b>	<b>Cat. #</b>
Rabbit anti- $\beta$ -Actin	IB	1:500	Sigma-Aldrich	A2066
Rabbit anti-LC3B	IB ICC	1:1000 1:100	Cell Signaling Technology	2775
Mouse anti-Neuronal Class III $\beta$ -Tubulin (Tuj1)	ICC	1:100	Covance	MMS-435P
DAPI	ICC	1:500	ThermoFisher Scientific	D1306
Dylight™ 405-conjugated AffiniPure Donkey anti-Mouse IgG (H&L)	ICC	1:500	Jackson ImmunoResearch	715-475-150
Alexa Fluor® 488-conjugated AffiniPure Donkey anti-Rabbit IgG (H&L)	ICC	1:500	Jackson ImmunoResearch	711-545-152

### **5.3.2 Ethics Statement**

Animal procedures were approved by the Institutional Animal Care Committee (IACC) of Memorial University of Newfoundland in accordance with the Canadian Council on Animal Care (CCAC). The approved protocol is ACP#KM-14-07.

### **5.3.3 DRG Isolation and Plating**

DRG neuronal dissociation and plating were carried out according to our established protocols (Fudge and Mearow, 2013; Tucker et al., 2005b; Williams et al., 2005). Briefly, 4-5 week old male Sprague-Dawley rats were anaesthetized using isoflurane, and then sacrificed by rapid decapitation. Spinal columns were then removed, cut along the sagittal plane of the spinal column, and individual dorsal root ganglia were removed. Pooled dorsal root ganglia were subjected to enzymatic and mechanical dissociation. Dissociated cells were suspended in serum-free DRG medium (F12, 2% B27 supplement, 1% AraC/0.1% FdU), and plated on pre-coated (2X poly-D-lysine and 2X 25ng/ $\mu$ L laminin) 12-well plates, 96-well plates, or 16-well slides. The cells were then allowed to attach for 24 hr at 37°C, in an atmosphere of air and 5% CO<sub>2</sub>, before treatments were added. For immunoblotting or survival experiments, we utilized three rats per 12-well plate or three rats per 96-well plate. Each experiment we performed was replicated a minimum of three times. For the experiments using 16-well culture slides, 3-6 slides were used for each experiment, with 1-2 slide/time point. We attempted to do all the conditions concomitantly in any one experiment. The number of replicates/experiment ranged from 4-6 different platings. For neurite growth analyses cells were plated at a low density to enable individual cellular and neurite analyses.

#### **5.3.4 MTS Cell Viability Assay**

DRG neurons were cultured on poly-D-lysine and laminin coated 96-well plates at ~1000 cells/well for 24 hr. DRG neurons were then treated with hydrogen peroxide ( $H_2O_2$ ; 10mM) for 3 hr, 16 hr and 24 hr. In conjunction with the addition of  $H_2O_2$ , the autophagy modulators 3-MA (10mM), Rapa (200nM), BA1 (200nM) and LY294002 (10 $\mu$ M) were added over the same time frames. Cell viability was quantified by the MTS colorimetric technique using the Cell Titer 96® AQueous MTS Reagent and PMS. This procedure was carried out as per the manufacturer's protocol (See Appendix E), with absorbance recording of the plates read at 490nm using a VICTOR™ X5 Multilabel Plate Reader (PerkinElmer Office, Woodbridge, ON, CAN). Results are presented as fractions of viable cells relative to untreated controls.

#### **5.3.5 Isolation and Biochemical Analysis of Protein Fractions**

Protein extraction and western analyses were carried out according to our established protocols (Clarke and Mearow, 2013; Tucker et al., 2005a; Williams et al., 2005). DRG neurons were grown on poly-D-lysine and laminin coated 12-well plates at  $\sim 1 \times 10^6$  cells/well for 24 hr. DRG neurons were then treated with  $H_2O_2$  (10mM) for 3 hr, 16 hr and 24 hr. In conjunction with the addition of  $H_2O_2$ , the autophagy modulators 3-MA (10mM) and Rapa (200nM) were added over the same time frames. Immediately after treatments, plates were placed on ice, and cells were scraped with a rubber policeman, quickly collected and centrifuged at 4°C to pellet the cells. The medium was removed and the pellet was lysed with ice-cold lysis buffer (10% glycerol, 1% NP40, 1 complete protease inhibitor cocktail tablet, 1.0mM sodium vanadate, 1.0mM sodium fluoride, 0.025% sodium dodecyl sulfate and TBS). All samples for a given experiment were collected at the same time. Equivalent amounts of protein (10-15 $\mu$ g) were

electrophoresed and separated on Bolt® 4-12% Bis-Tris Plus gels, and transferred onto nitrocellulose membranes for further analysis. Nitrocellulose membranes were then blocked with either 3% skim milk or 5% BSA solution, depending on whether phospho-specific antibodies were used or not, incubated overnight at 4°C with primary antibodies (Table 5.1) and developed the following day. Bands were detected using peroxidase-conjugated secondary antibodies and SuperSignal® West Pico Chemiluminescent Substrate.

### **5.3.6 Immunocytochemistry and Oxidative Stress Analysis of DRG Neurons**

DRG neurons were cultured on poly-D-lysine and laminin coated 16-well chamber slides at ~1000 cells/well for 24 hr. DRG neurons were then treated with H<sub>2</sub>O<sub>2</sub> (10mM) for 3 hr, 16 hr and 24 hr. In conjunction with the addition of H<sub>2</sub>O<sub>2</sub>, the autophagy modulators 3-MA (10mM) and Rapa (200nM) were added over the same time frames. After treatment, cells were fixed immediately with 4% paraformaldehyde in PBS, pH 7.4, for 20 min. Cells were washed twice with PBS and then permeabilized in a solution containing 0.1% Triton X-100 and 10% horse serum in PBS. Cells were then incubated with primary antibodies at appropriate concentrations (Table 4.1) for 16-20 hr at 4°C. After incubation, cells were rinsed with TBST, pH 7.2, and subsequently incubated with fluorophore-conjugated secondary antibodies at appropriate concentrations (Table 5.1) for 1-2 hr. Cells were washed again three times with TBST and cover-slipped with Gelvatol™.

To determine whether H<sub>2</sub>O<sub>2</sub> caused an oxidative stress response in DRG neurons, cultures were either treated with H<sub>2</sub>O<sub>2</sub> (10mM), menadione (10µM) or culture media for 30 min, 1 hr, 2 hr and 3 hr. Menadione was used as a positive control to induce an oxidative stress response in DRG neurons as high concentrations of menadione (>2µM) have been shown to generate ROS

through redox cycling (Hu et al., 2016; Jaeger et al., 2010). Immediately after treatments, cultures were further treated with CellROX Green Reagent (5 $\mu$ M) for 30 mins, after which they were prepared for immunocytochemistry and confocal imaging analysis, using DAPI to stain DRG nuclei (See Appendix F.1-F.5). For analysis, confocal images were volume rendered in 3-dimensions (3D) using Imaris software, and the number of cells with CellROX Green Reagent localized within DAPI stained nuclei were quantified (See Appendix F.1-F.5).

Images for data analysis were acquired in each of two channels (405nm and 488nm) by laser scanning confocal microscopy with sequential Z-stage scanning (Olympus Fluoview 1000 confocal laser scanning microscope). Image acquisition for the different samples was carried out using similar scanning parameters (laser power, HV PMTs, and number of optical slices). Scanned stacks were compiled as individual images, and composite digital images were prepared using both Imaris software (Bitplane Inc., South Windsor, CT, USA) and Adobe Photoshop CS (Adobe Systems Incorporated, San Jose, CA, USA).

For neurite analyses and quantification of LC3B-positive puncta, confocal images were volume rendered in 3-dimensions (3D) using Imaris software, and the amount of LC3B positive puncta found within the growing neurites were quantified. The Filament Tracer tool within Imaris was also utilized to determine total neurite growth from the cell soma in length ( $\mu$ m) and the amount of branching of the growing neurites using the Sholl Analysis calculation within the tool; the Sholl spheres resolution was set at 20 $\mu$ m for analysis.

### **5.3.7 Densitometric and Statistical Analysis**

Densitometric analyses of triplicate Western immunoblots were carried out using ImageJ and a calibrated grey value scale (NIH, Bethesda, MD, USA); ratios of total and phosphorylated

protein expression were compared to each other, while LC3BII expression was compared to LC3I expression.  $\beta$ -Actin was included in the data to correct for loading differences. Statistical analyses were performed using GraphPad Prism 6 (GraphPad Software, San Diego, CA, USA), with significance determined using one-way ANOVA for column data, and two-way ANOVA for grouped data. All analyses were subjected to post hoc testing via Tukey's test.

## 5.4 Results

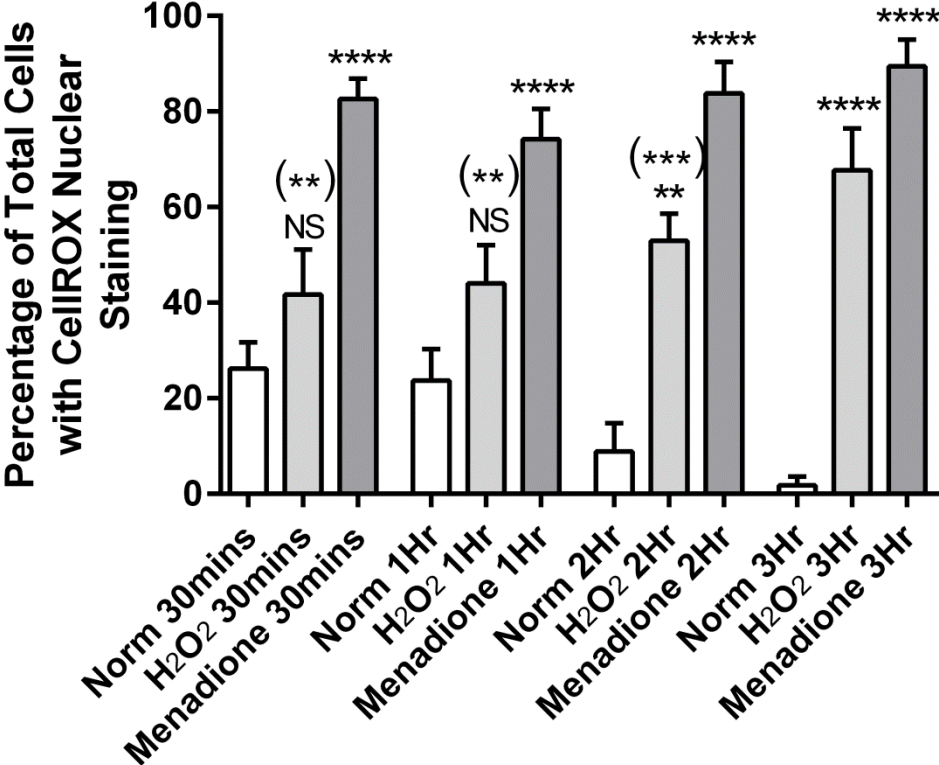
### 5.4.1 $H_2O_2$ Causes Oxidative Stress in DRG Neurons

To test the efficacy of  $H_2O_2$  as an oxidative stress inducer in DRG neurons, dissociated DRG neurons were plated on laminin-coated 16-well slides and were either treated with  $H_2O_2$ , menadione or culture media over time frames of 30 min, 1 hr, 2 hr and 3 hr. Treatment with menadione caused oxidative stress in DRG neurons after 30 mins that was maintained at a constant level throughout the experiment (Fig. 5.1) (See Appendix F.2-F.5). However, treatment with  $H_2O_2$  caused oxidative stress after 2 hr of treatment and increased additionally by 3 hr (Fig. 5.1) (See Appendix F.2-F.5). Analysis of the changes observed in the control (norm) sample throughout the experiment did not indicate significance (Fig. 5.1). It is believed that the initial increase in oxidative stress in the control (norm) sample was due to fluid shear stress caused by the addition of culture media as a negative control. The oxidative stress result found in control (norm) cells at 3 hr is potentially more indicative of a true *in vitro* cellular environment, as the fluid shear stress effect has subsided by this time-point and the cells are now under homeostatic oxidative stress conditions (i.e. small amounts of oxidative stress that are normally produced by the electron transport chain). If it is accepted that the 3 hr results are the true *in vitro* cellular environment, comparing the results to this time-point indicates that treatment with  $H_2O_2$  does in

**Figure 5.1: H<sub>2</sub>O<sub>2</sub> treatment causes oxidative stress in DRG neurons.**

DRG neurons were grown on poly-D-lysine and laminin coated 16-well slides at ~1000 cells/well for 24 hr. Cultures were then treated with H<sub>2</sub>O<sub>2</sub> (10mM), menadione (10μM) or culture media for 30 mins, 1 hr, 2 hr and 3 hr. Cells were further treated with CellROX Green Reagent (5μM) and immunostained with DAPI to stain for DRG nuclei. DRG neurons that had CellROX reagent localized within their nuclei were quantified. Values are mean ± SEM; n = 7 replicates. In all samples, a total of 50 cells were analyzed per condition, per time-point. Significance of results was determined using a one-way ANOVA with Tukey's *post hoc* test, confirmed using a non-parametric test, comparing samples to the control (norm) condition at each time-point and to the control (norm) at 3 hr (see \* in brackets for this comparison). \*\* P < 0.01, \*\*\* P < 0.001 and \*\*\*\* P < 0.0001.

# Measurement of DRG Oxidative Stress With Treatment



fact cause significant oxidative stress throughout the experiment (Fig. 5.1). This further indicates that H<sub>2</sub>O<sub>2</sub> treatment does in fact cause an oxidative stress environment in DRG neurons.

#### **5.4.2 Autophagy Inhibition in Conjunction with H<sub>2</sub>O<sub>2</sub> Treatment Reduces DRG Neuron Viability**

This study next evaluated the effect(s) of autophagy on adult rat DRG neuron survival in cells exposed to an increased reactive oxygen species environment or pharmacological treatment. Briefly, dissociated DRG neurons were plated in laminin-coated 96-well plates and were either left untreated (control), or treated with H<sub>2</sub>O<sub>2</sub> over time frames of 3 hr, 16 hr and 24 hr. Additionally, in both untreated (control) and H<sub>2</sub>O<sub>2</sub>-treated conditions DRG neurons were co-treated with the autophagy modulators Rapa, 3-MA, BA1 and LY294002. Cellular viability was determined using a MTS assay, with data being expressed as fractions of viable cells relative to untreated controls; significance was determined by comparing the sample means to control conditions. To note, the controls used for comparison and analysis for this study are the same as those used in chapter 4 (Clarke J and Mearow K, J. Neurosci. Res. 2016), as the experimentation presented herein was performed in parallel with that study. Therefore, refer to section 4.4.2 for control data and results.

Treatment with H<sub>2</sub>O<sub>2</sub> gradually decreased DRG cell viability (20% decrease, P < 0.0001), with similar results observed with Rapa and LY294002 co-treatment (Fig. 5.2). With H<sub>2</sub>O<sub>2</sub> plus 3-MA or BA1, however, cell viability decreased after 3 hr of treatment and continued to decrease steadily thereafter (with 50% cellular viability, P < 0.0001). While an increased reactive oxygen species environment, as well as Rapa treatment is considered to be an effective inducer of

autophagy, these results suggest that induction of autophagy alone is insufficient to promote cell survival, although inhibition of autophagy appears to have an earlier deleterious influence on cell survival.

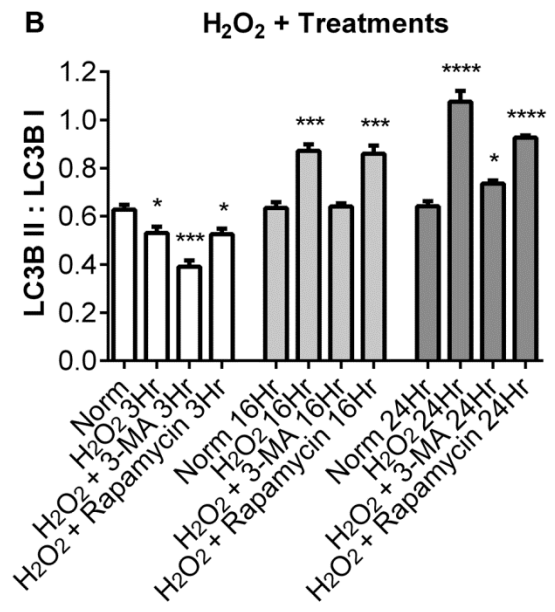
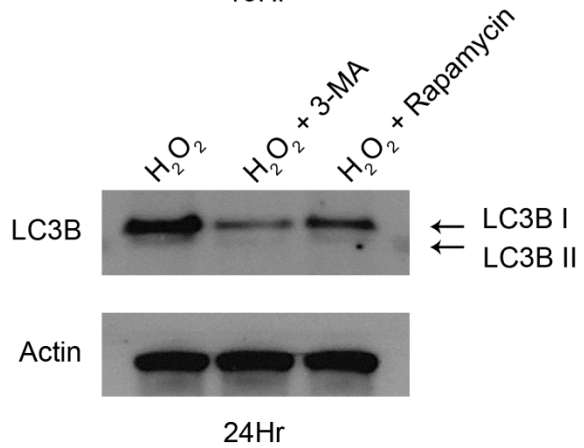
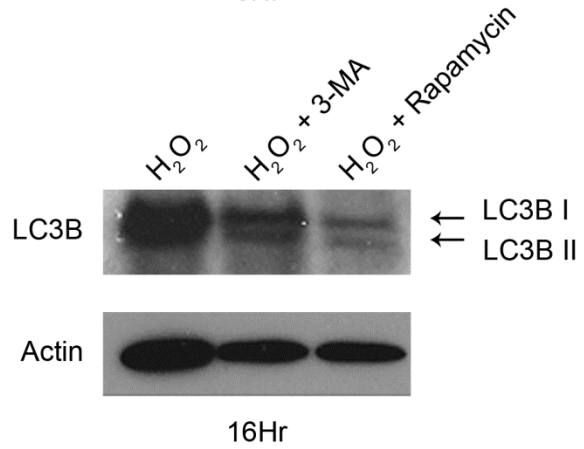
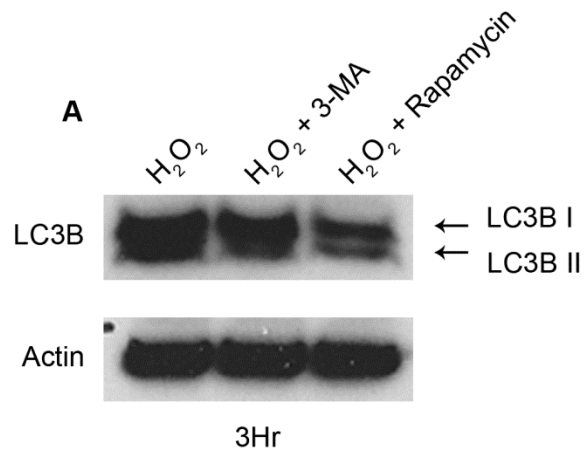
### **5.4.3 Inhibiting Autophagy in Conjunction with H<sub>2</sub>O<sub>2</sub> Treatment Decreases Autophagy Related Proteins in DRG Neurons**

After determining that modulating autophagy resulted in changes in neuron viability based upon a cell survival assay, it was next investigated whether there were corresponding alterations in autophagy related proteins. Dissociated DRG neurons were plated in laminin-coated 12-well plates and were either left untreated (control), or treated with H<sub>2</sub>O<sub>2</sub> over time frames of 3 hr, 16 hr and 24 hr. As before, both untreated and H<sub>2</sub>O<sub>2</sub>-treated cultures were co-treated with either Rapa or 3-MA. Biochemical changes in the ratio of LC3BII:LC3BI were determined by immunoblotting, as described in the Methods section. Again, refer to section 4.4.3 for control data and results.

With H<sub>2</sub>O<sub>2</sub> treatment, the ratio of LC3BII:LC3BI increased throughout the experiment, which would suggest the induction of autophagy (Fig. 5.3). As in the control conditions (Fig. 4.4), 3-MA caused a clear reduction in the LC3BII:LC3BI, while Rapa co-treatment with H<sub>2</sub>O<sub>2</sub> also resulted in an overall increase in the LC3BII:LC3BI ratio compared to control, although it did not differ from the H<sub>2</sub>O<sub>2</sub> situation (Fig. 5.3).

**Figure 5.2: Autophagy is activated with increased reactive oxygen species, and inhibited with 3-MA treatment.**

DRG neurons were grown on poly-D-lysine and laminin coated 12-well plates at  $\sim 1 \times 10^6$  cells/well for 24 hr. Culture media was then treated with  $H_2O_2$  (10mM) for 3 hr, 16 hr or 24 hr. In conjunction with  $H_2O_2$ , the autophagy modulators 3-MA (10mM) and Rapa (200nM) were added over the same time frames. DRG neuronal protein extracts were collected and Western immunoblotted as described in the Methods. Western blots were probed with LC3B antibody, and then stripped and reprobed for  $\beta$ -Actin. After each probe, Western blots were scanned and densitometric analysis of bands was carried out using ImageJ and a calibrated gray scale standard. Western blots presented in **(A)** are representative of the densitometric data analysis in **(B)**. The bars in **(B)** are mean ROD ( $\pm$  SEM) from each of 3 separate experiments. \*  $P < 0.05$ , \*\*  $P < 0.01$ , \*\*\*  $P < 0.001$ , \*\*\*\*  $P < 0.0001$ , with a one-way ANOVA with Tukey's *post hoc* test, confirmed using a non-parametric test.



#### **5.4.4 DRG Growth Morphology Is Negatively Altered With Autophagy Inhibition in Conjunction with H<sub>2</sub>O<sub>2</sub> Treatment**

Morphological and growth-associated changes in the neurons with the treatments outlined previously were next examined. Immunocytochemistry was carried out using neuron-specific  $\beta$ III-tubulin staining (for cell and neurite quantitation) and LC3B (for quantitation of autophagosomes). Cultures were imaged using confocal microscopy and DRG neurite growth, neurite branching complexity and autophagosome puncta were analyzed with Imaris imaging software, as outlined in the Methods section. Refer to section 4.4.4 for control data and results.

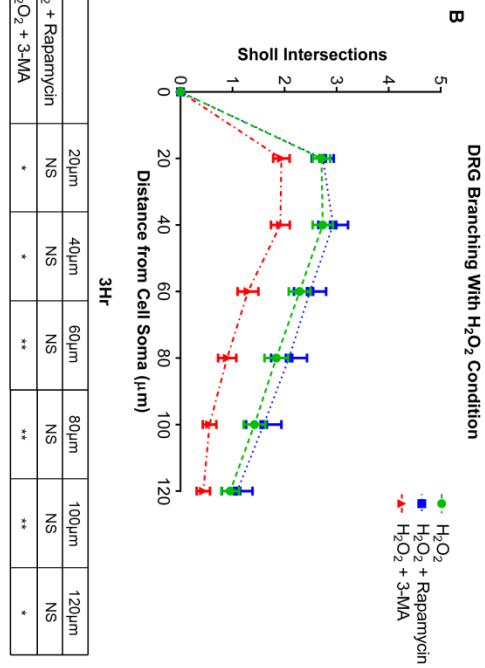
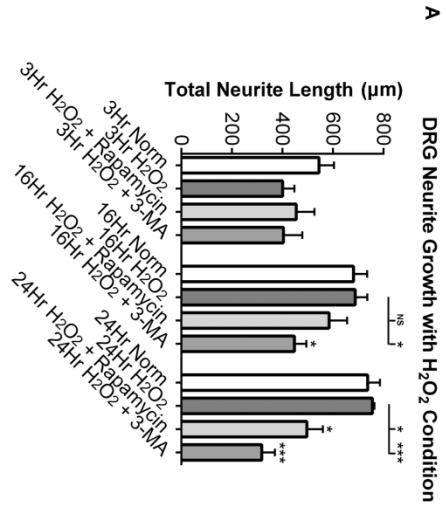
Neurite growth was evaluated by quantitating the combined total neurite length ( $\mu$ m) of all neurites extending from the cell soma. Treatment with H<sub>2</sub>O<sub>2</sub> did not affect neurite growth by 24 hr, while co-treatment with Rapa or 3-MA resulted in a reduction in growth by 24 hr (Fig. 5.4A, 5.5). However, unlike Rapa, growth reduction with 3-MA began earlier, as there was a significant reduction in growth by 16 hr with 3-MA treatment (Fig. 5.4A, 5.5).

Changes in neurite branching complexity using Sholl analysis were also assessed. Treatment with H<sub>2</sub>O<sub>2</sub> resulted in decreased branching compared to the controls at 3 hr and 16 hr, but recovered to control levels at 24 hr post-treatment (Fig. 5.4B-D). H<sub>2</sub>O<sub>2</sub> plus Rapa did not differ from H<sub>2</sub>O<sub>2</sub> alone, while 3-MA treatment suppressed neurite branching over the 24 hr period (Fig. 5.4B-D).

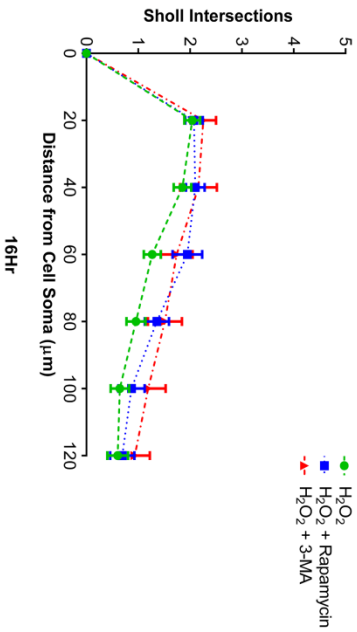
With changes in neurite growth and branching complexity observed, we assessed whether there was any correlation with the presence of autophagosomal puncta in the neurites that might related to the growth alterations. With H<sub>2</sub>O<sub>2</sub> treatment, LC3B-positive puncta initially increased at 3 hr, and this was maintained through 24 hr (Fig. 5.6A). Treatment with Rapa resulted in a

**Figure 5.3: DRG neurite length and branching complexity are reduced with autophagy inhibition in increased reactive oxygen species conditions.**

DRG neurons were grown on poly-D-lysine and laminin coated 16-well culture slides for 24 hr. Culture media was then treated with H<sub>2</sub>O<sub>2</sub> (10mM) for 3 hr, 16 hr or 24 hr. In conjunction with H<sub>2</sub>O<sub>2</sub>, the autophagy modulators 3-MA (10mM) and Rapa (200nM) were added over the same time frame. Cells were immunostained to detect LC3B and  $\beta$ III-Tubulin, as previously noted. DRG neurons were visualized with confocal microscopy, and (A) total neurite growth in length ( $\mu$ m) from the cell soma was assessed. Values are mean  $\pm$  SEM; n = 10 field of view replicates. Sholl intersection analysis was also performed at 3 (B), 16 (C) and 24 hr (D) using the Filament Tracer tool in Imaris, described in the Methods. Sholl spheres resolution was set at 20 $\mu$ m for analysis. Values are mean  $\pm$  SEM; 20 cells were analyzed per condition, per time-point. The significance at each Sholl spheres resolution was determined by comparing the data from the specific treatment to the control (norm) condition. \* P < 0.05, \*\* P < 0.01, \*\*\* P < 0.001, \*\*\*\* P < 0.0001, with a two-way ANOVA with Tukey's *post hoc* test.

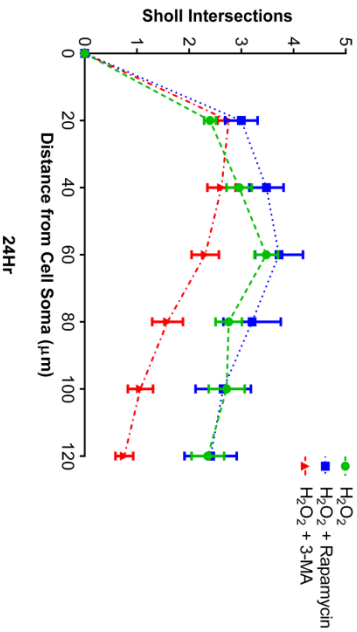


**C** DRG Branching With H<sub>2</sub>O<sub>2</sub> Condition



	20µm	40µm	60µm	80µm	100µm	120µm
H <sub>2</sub> O <sub>2</sub> + Rapamycin	NS	NS	NS	NS	NS	NS
H <sub>2</sub> O <sub>2</sub> + 3-MA	NS	NS	NS	NS	NS	NS

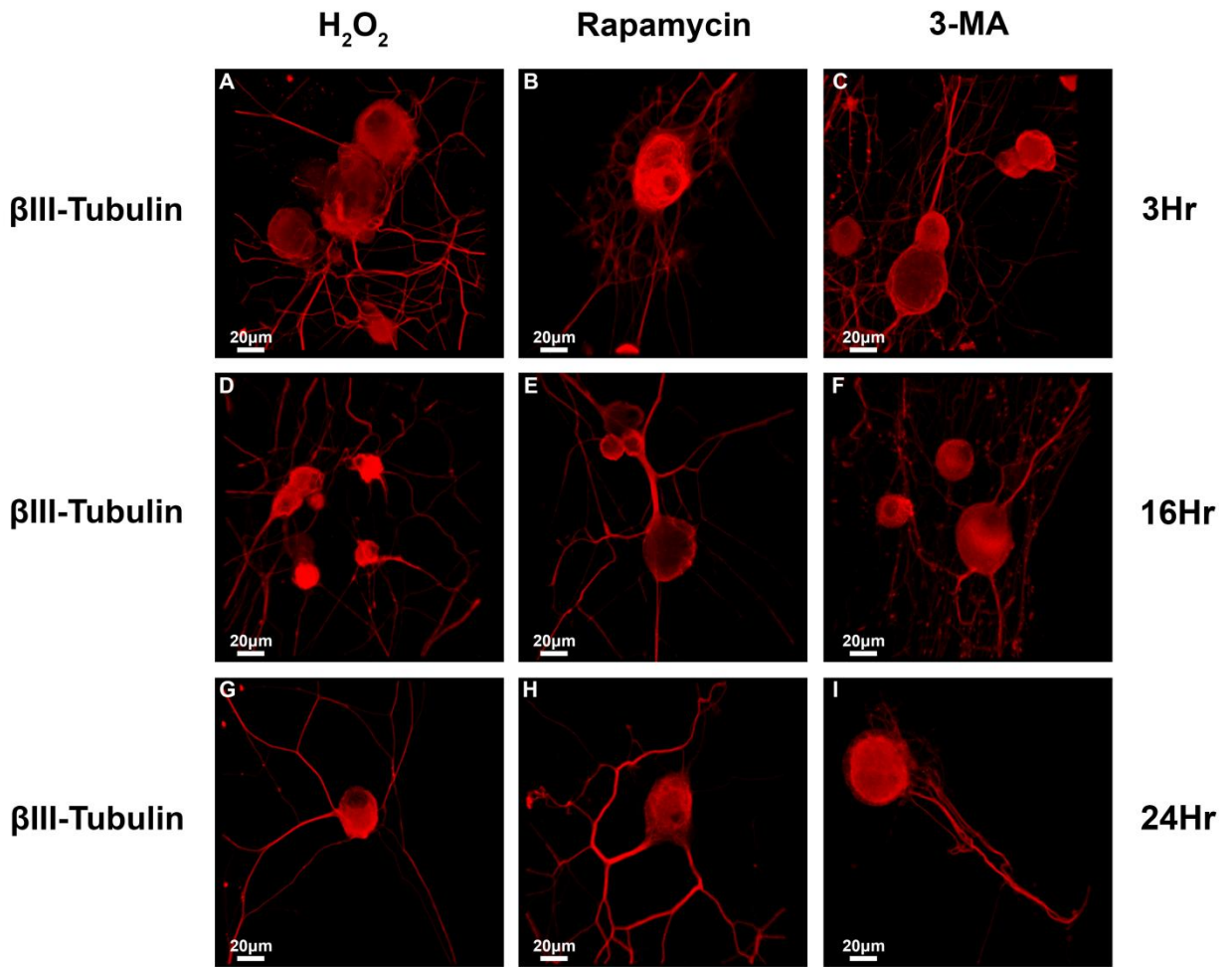
**D** DRG Branching With H<sub>2</sub>O<sub>2</sub> Condition



	20µm	40µm	60µm	80µm	100µm	120µm
H <sub>2</sub> O <sub>2</sub> + Rapamycin	NS	NS	NS	NS	NS	NS
H <sub>2</sub> O <sub>2</sub> + 3-MA	NS	NS	*	*	***	**

**Figure 5.4: DRG neurite growth is reduced after 3, 16 and 24 hr treatment with 3-MA in increased reactive oxygen species conditions.**

DRG neurons were grown on poly-D-lysine and laminin coated 16-well culture slides for 24 hr. Culture media was then treated with H<sub>2</sub>O<sub>2</sub> (10mM) and treated for 3, 16 and 24 hr, plus or minus 3-MA (10mM) or Rapa (200nM). Cells were immunostained to detect LC3B and  $\beta$ III-Tubulin, and neurons were visualized with confocal microscopy. Scale bar = 20  $\mu$ m. Panels: A-C – 3 hr treatment; D-F – 16 hr treatment; G-I – 24 hr treatment.



reduction in LC3B-positive puncta at 24 hr only, while 3-MA treatment caused an overall reduction starting at 3 hr and continuing through to 24 hr (Fig. 5.6A).

The ratio of the number of LC3B puncta/100µm neurite length under each condition was also determined. H<sub>2</sub>O<sub>2</sub> treatment caused an initial significant increase in the ratio that eventually decreased over time, while Rapa co-treatment had similar results as H<sub>2</sub>O<sub>2</sub> treatment alone (Fig. 5.6B). As in the control situation (Fig. 4.10), 3-MA treatment resulted in significantly reduced numbers of puncta/neurite (Fig. 5.6B).

Overall, a global reduction in neurite growth and branching complexity that recovered back to normal levels after 24 hr with H<sub>2</sub>O<sub>2</sub> treatment was observed (Fig. 5.4A). Additionally, autophagosomal puncta formation was increased with H<sub>2</sub>O<sub>2</sub> treatment, but decreased with 3-MA co-treatment (Fig. 5.6A). Interestingly, comparing the LC3B puncta/100µm neurite length ratio of control conditions with H<sub>2</sub>O<sub>2</sub> and Rapa co-treatment the Rapa treatment did not increase the ratio beyond what is found with control conditions alone, again suggesting that an autophagosome formation threshold had been reached (Fig. 5.6B).

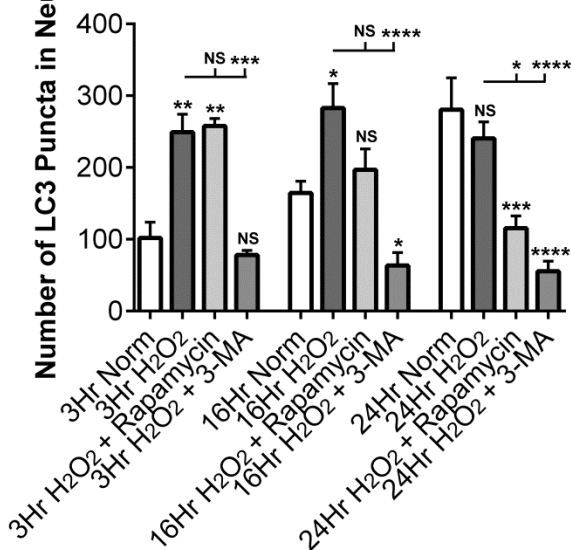
## 5.5 Discussion

Like the study presented in chapter 4 (Clarke J and Mearow K, J. Neurosci. Res. 2016), this study also investigated the influence of autophagy on adult DRG neuronal cell survival and neurite growth, and has demonstrated that in addition to a metabolic challenge, as presented in chapter 4 (Clarke J and Mearow K, J. Neurosci. Res. 2016), constitutive autophagy in DRG neurons can also be modulated by ROS stress caused by H<sub>2</sub>O<sub>2</sub> treatment. Inhibition of ROS stress-induced autophagy adversely affected cell survival, neurite growth and neurite branching.

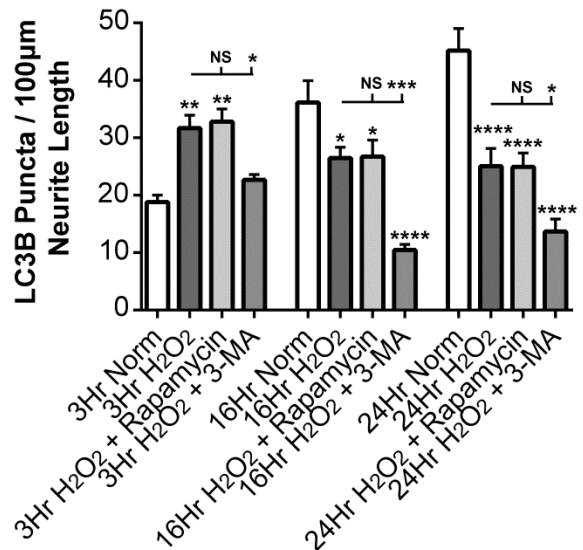
**Figure 5.5: Autophagy inhibition reduces autophagosome occurrence in DRG neurites.**

DRG neurons were grown on poly-D-lysine and laminin coated 16-well culture slides for 24 hr. The neurons were treated with H<sub>2</sub>O<sub>2</sub> (10mM) for 3, 16 and 24 hr, plus or minus 3-MA (10mM) and Rapa (200nM). Cells were immunostained to detect LC3B and  $\beta$ III-Tubulin, and neurons were visualized with confocal microscopy. The total number of LC3B puncta found in growing DRG neurites with Rapa or 3-MA in nutrient control conditions (see Figure 4.10), and H<sub>2</sub>O<sub>2</sub> conditions was quantitated. Values are mean  $\pm$  SEM; n = 4 replicates. Additionally, the ratio of the number of LC3B puncta per 100 $\mu$ m neurite length with Rapa or 3-MA in nutrient control (see Figure 4.10) conditions, and H<sub>2</sub>O<sub>2</sub> conditions was analyzed. Values are mean  $\pm$  SEM; n = 7 replicates. In all samples, a total of 20 cells were analyzed per condition, per time-point. \* P < 0.05, \*\* P < 0.01, \*\*\* P < 0.001, and \*\*\*\* P < 0.0001, with a one-way ANOVA with Tukey's *post hoc* test, confirmed using a non-parametric test.

**A Total LC3 Puncta Under ROS Stress**



**B ROS Stress**



Overall, our data provide further insight into how autophagy influences DRG neuron survival and neurite growth.

### **5.5.1 Autophagy and Neuronal Cell Survival**

The main functions of autophagy are to maintain cellular homeostasis, and to degrade long-lived and damaged proteins and organelles. During non-stressed conditions, autophagy fulfills those functions without issue. However, it is during episodes of cellular stress when the proper functioning of autophagy is of most importance. Data from this study demonstrate that when adult DRG neurons undergo ROS stress with H<sub>2</sub>O<sub>2</sub> treatment (Fig. 5.1) (See Appendix F.2-F.5), there is a subsequent decrease in cell viability, as compared to non-stressed neurons (Fig. 5.2). When autophagy was inhibited in parallel, however, cell viability decreased further, thus suggesting that proper endogenous autophagic function is important in adult DRG neuron survival during ROS stress (Fig. 5.2).

To measure whether autophagy was activated with ROS stress we further examined the protein expression of the autophagic specific protein LC3B. Using Western immunoblotting we demonstrate that ROS stress increases the LC3BII:LC3BI protein ratio, indicating an increase in autophagosome formation, while upon introduction of 3-MA the ratio decreased (Fig. 5.3). Additional analysis of autophagosomes in the neurites of DRG neurons showed a similar trend, as autophagosome formation was reduced with 3-MA treatment (Fig. 5.6), increased with H<sub>2</sub>O<sub>2</sub> treatment (Fig. 5.6) and reduced with a combination of both (Fig. 5.6). A previous study from the Elazar group supports the observations we have documented, as they have shown that low levels of ROS formed under starvation conditions act as a signaling molecule that leads to the activation of autophagy in transfected cell lines (Scherz-Shouval et al., 2007). Interestingly,

similar to the data demonstrated in chapter 4, rapamycin co-treatment with H<sub>2</sub>O<sub>2</sub> showed an early increase in autophagosome formation, but this increase did not increase over the amount found caused by H<sub>2</sub>O<sub>2</sub> treatment alone (Fig. 5.6). Again, as in chapter 4, this suggests that autophagy activation in DRG neurons may not go beyond an endogenous set-point, or threshold, even with positive autophagic modulation in presence of cellular stress.

### **5.5.2 Autophagy and Neurite Growth**

In addition to assessing autophagy in neuronal cell survival, the effects of autophagy on DRG neurite growth were also examined. Current studies have found that ROS stress leads to impairment and damage of mitochondria, cytosolic and cytoskeletal proteins, leading to further complications with neurite growth (Arrigo, 2013; Babizhayev et al., 2014; Persson et al., 2013). Therefore, by studying autophagy as an avenue to specifically target ROS damaged mitochondria, and other damaged cytosolic and cytoskeletal proteins, one could potentially prevent the complications with neurite growth associated with ROS stress.

In this study, we demonstrate that when autophagy was inhibited during ROS stress, neurite growth from the cell soma significantly decreased, with a more pronounced effect observed with prior stress (Fig. 5.4, 5.5). Similarly, analysis of neurite branching complexity demonstrated a significant reduction in the complexity of branching with autophagy inhibition, again with a more pronounced effect observed with prior stress (Fig. 5.4, 5.5). These results suggest that while inhibition of autophagy induces a negative effect on neurite growth and branching complexity, the addition of H<sub>2</sub>O<sub>2</sub> stress further exacerbates the negative effects observed. Overall, these results suggest that while ROS stress induces complications in neurite growth, proper autophagic function prevents further complications from occurring.

## **5.6 Conclusion**

Disruption or inhibition of autophagy in adult DRG neurons can result in adverse effects on neuronal survival, neurite growth and branching. In continuation of previous research, this study demonstrates that in conjunction with an increased ROS environment, DRG neuron survival, neurite growth and neurite branching is reduced. Additionally, this study shows that ROS stress induces autophagy in adult DRG neurons, with more severe survival and neurite growth effects found when ROS induced autophagy is inhibited. Although the mechanisms of how an increased ROS environment induces autophagy are unknown, overall, the data presented in this study provide further insights into how autophagy influences DRG neuronal cell survival and neurite growth.

## **5.7 Acknowledgements**

The technical assistance of F. Nafar and J. B. Williams during the course of this study is gratefully acknowledged.

## **Chapter 6: Autophagy Inhibition Alters DRG Neurite Growth Initiation *In Vitro***

### **6.1 Abstract**

Proper neurite initiation and regrowth after episodes of cell stress is a key determinate in the survival of neurons. Recently, autophagy has been studied as a potential target for improving axonal survival and growth. This study investigates whether autophagy modulation influences neurite initiation in DRG neurons, and whether the differential neurite initiation found in the subtypes of DRG neurons is influenced by autophagy. Neurite initiation was stimulated in quiescent DRG neurons via the addition of soluble laminin, and autophagy was modulated using pharmacological activators (rapamycin) and inhibitors (3-methyladenine, Bafilomycin A1). The results demonstrate that autophagy inhibition attenuates adult DRG neurite initiation, neurite growth and neurite branching complexity. Furthermore, results demonstrate that autophagy induction influences the neurite initiation from the sub-populations of DRG neurons. Overall, both cellular and biochemical approaches have been combined to show that autophagy is indispensable in DRG neurite growth.

### **6.2 Introduction**

As stated previously, peripheral neuropathy in DRG neurons causes axonal disassembly and granular degeneration, also known as axonal dieback or Wallerian degeneration, and ultimately cell death (Raff et al., 2002; Wang et al., 2012). Mature DRG neurons, however, are able to robustly regenerate damaged axons, and there are many studies reporting on strategies to promote axonal regrowth in DRG neurons (Averill et al., 2004; Karamoysoyli et al., 2008; Lindsay, 1988; Plantman et al., 2008; Tucker et al., 2005a, 2006; Williams et al., 2005; Zhu et al., 2010).

Again, as stated previously, the influence of autophagy in promoting axonal regrowth is an interesting strategy that is being studied. The ability of autophagy to bulk recycle damaged proteins and organelles, and to maintain a homeostatic energy environment during cellular stress make this process an intriguing target in axonal regrowth. As a result, a number of studies have attempted to determine how this process can help manage axonal degeneration in neuropathic diseases that affect the PNS (Babizhayev et al., 2014; Kosacka et al., 2013).

Chapters 4 and 5 focused upon how the modulation of endogenous autophagy during cellular stress affects DRG neuron survival, neurite growth and neurite branching. While novel, the research presented in those chapters described the response of neurons in conditions where they were initially allowed to grow neurites under favorable conditions and then were subjected to the treatment paradigms outlined in those studies. Alternatively, it is also interesting to investigate how autophagy influences the initiation of new neurites from damaged DRG neurons as a further understanding of this process has implications into potentially promoting the regrowth of neurites in other neuron types that typically do not regrow neurites after their loss (i.e. CNS neurons). Furthermore, it is of interest to investigate how autophagy influences the initiation of new neurites in the different sub-populations of DRG neurons, as it has been previously shown that neurite initiation in all DRG neurons is not uniform, and occurs differentially depending on the DRG neuron sub-type (Tucker et al., 2006). Therefore, determining whether autophagy is involved in the differential neurite initiation seen can lead to a better understanding of how the overall process works, and whether modulating autophagy can influence it.

This study sought to determine whether autophagy modulation influences neurite initiation in DRG neurons, and whether the differential neurite initiation found in the sub-types of DRG neurons is influenced by autophagy. This study employed an experimental paradigm that allows

for the study of neurite initiation via the stimulation of quiescent cells with the addition of soluble laminin, and has investigated how the modulation of autophagy influences neurite initiation. The results demonstrate that the inhibition of autophagy attenuates adult DRG neurite initiation, neurite growth and neurite branching. Furthermore, results indicate that autophagy induction influences the neurite initiation from the sub-populations of DRG neurons. Overall, this study indicates that autophagy is indispensable in DRG neurite growth.

## **6.3 Materials and Methods**

### **6.3.1 Reagents and Antibodies**

F12 media, B27 supplement, collagenase type II and natural mouse laminin were purchased from Invitrogen (Burlington, ON, CAN). AraC, FdU, 3-MA, BA1, Rapa, trypsin, PMS, DNase, and *Bandeiraea simplicifolia* (*Griffonia simplicifolia*) were purchased from Sigma-Aldrich Canada Ltd. (Oakville, ON, CAN). The pharmacologic PI3K inhibitor LY294002 was purchased from Millipore Canada Ltd. (Etobicoke, ON, CAN). BCA protein assay solutions, Blot® 4-12% Bis-Tris Plus Gels, immunoblot reagents, immunoblot membranes, SuperSignal® West Pico Chemiluminescent Substrate and CellROX® Green Reagent for oxidative stress detection were purchased from ThermoFisher Scientific (Nepean, ON, CAN). Cell Titer 96® AQueous MTS Reagent Powder was purchased from Promega (Madison, WI, USA). The protease inhibitor, ovomucoid was obtained from Worthington Biochemical Corp. (Lakewood, NJ, USA). AErrane (isoflurane) was purchased from Baxter Corp. (Mississauga, ON, CAN). Primary and secondary antibodies used in this study are outlined in Table 6.1.

**Table 6.1: List of primary and secondary antibodies, with experimental dilutions, used either for immunoblotting (IB) or immunocytochemistry (ICC).**

<b>Antibody</b>	<b>Method</b>	<b>Dilution</b>	<b>Company</b>	<b>Cat. #</b>
Rabbit anti- $\beta$ -Actin	IB	1:500	Sigma-Aldrich	A2066
Rabbit anti-LC3B	IB ICC	1:1000 1:100	Cell Signaling Technology	2775
Mouse anti-Neuronal Class III $\beta$ -Tubulin (Tuj1)	ICC	1:100	Covance	MMS-435P
Dylight <sup>TM</sup> 405-conjugated AffiniPure Donkey anti-Mouse IgG (H&L)	ICC	1:500	Jackson ImmunoResearch	715-475-150
Alexa Fluor <sup>®</sup> 488-conjugated AffiniPure Donkey anti-Rabbit IgG (H&L)	ICC	1:500	Jackson ImmunoResearch	711-545-152
Isolectin B <sub>4</sub> , biotin-conjugated	ICC	1:50	Sigma-Aldrich	L2140
NeutrAvidin <sup>TM</sup> , DyLight <sup>TM</sup> 649-conjugated	ICC	1:250	ThermoFisher Scientific	22845

### **6.3.2 Ethics Statement**

Animal procedures were approved by the Institutional Animal Care Committee (IACC) of Memorial University of Newfoundland in accordance with the Canadian Council on Animal Care (CCAC). The approved protocol is ACP#KM-14-07.

### **6.3.3 DRG Isolation, Plating and Immunocytochemistry**

DRG neurons were cultured on poly-D-lysine coated 16-well chamber slides at ~1000 cells/well for 24 hr. Under these conditions, these neurons are allowed to recover from the dissociation protocol and there is little to no neurite growth on poly-lysine (Tucker et al., 2005a, 2006; Williams et al., 2005). Subsequently, DRG neurons were treated with 50ng/ $\mu$ L of soluble laminin for 2 hr, 4 hr or 6 hr to allow for neurite growth initiation before further treatments were added, as it has previously been reported that this treatment stimulates neurite initiation in these neurons (Williams et al., 2005). After incubation with soluble laminin, the autophagy modulators 3-MA (10mM), Rapa (200nM) and BA1 (200nM) were added and the treated cells were left for an additional 16 hr before analysis. In the case of control conditions, where no autophagy modulators were added, fresh culture medium was added at 2 hr, 4 hr or 6 hr.

After treatment, cells were fixed immediately, permeabilized and then incubated with primary antibodies at appropriate concentrations, followed by incubation with fluorophore-conjugated secondary antibodies (Table 6.1). Additionally, DRG neurons were stained with isolectin B<sub>4</sub> (IB<sub>4</sub>) (Tucker et al., 2005b). Briefly, cells that had been initially stained with secondary antibodies were washed with PBS and then incubated with lectin binding buffer (0.1mM calcium chloride, 0.1mM magnesium chloride, 0.1mM manganese chloride, and dH<sub>2</sub>O) for 30 min. After incubation, lectin binding buffer was replaced with biotinylated-IB<sub>4</sub> (20 $\mu$ g/mL in PBS) for

30 min. Following this incubation, the cells were washed once with PBS and DyLight™ 649-conjugated NeutrAvidin™ was added for 45 min. After incubation, the cells were washed and cover-slipped with Gelvatol™.

Images for data analysis were acquired in each of two channels (405nm and 488nm) by laser scanning confocal microscopy with sequential Z-stage scanning (Olympus Fluoview 1000 confocal laser scanning microscope). Image acquisition for the different samples was carried out using similar scanning parameters (laser power, HV PMTs, and number of optical slices). Scanned stacks were compiled as individual images, and composite digital images were prepared using both Imaris software (Bitplane Inc., South Windsor, CT, USA) and Adobe Photoshop CS (Adobe Systems Incorporated, San Jose, CA, USA).

For neurite analyses and quantification of LC3B-positive puncta, confocal images were volume rendered in 3-dimensions (3D) using Imaris software, and the amount of LC3B positive puncta found within the growing neurites were quantified. The Filament Tracer tool within Imaris was also utilized to determine total neurite growth from the cell soma in length ( $\mu\text{m}$ ) and the amount of branching of the growing neurites using the Sholl Analysis calculation within the tool; the Sholl spheres resolution was set at  $20\mu\text{m}$  for analysis.

## **6.4 Results**

### **6.4.1 Inhibition of Autophagy Suppresses DRG Neurite Growth Initiation**

Previous data presented in chapters 4 and 5 indicate that by inhibiting autophagy with 3-MA induced significant morphological changes in neurite growth, branching complexity and autophagosome formation after neurites had already extended from the cell soma. This effect on growth could potentially be either an inhibition or decrease in extension, or potentially a

retraction of neurites (Gumy et al., 2010; Verma et al., 2005). This could be tested and distinguished by using similar treatments with live-cell imaging (not performed in this study), as this technique would allow for a more concise interpretation into how growth is modulated in real-time.

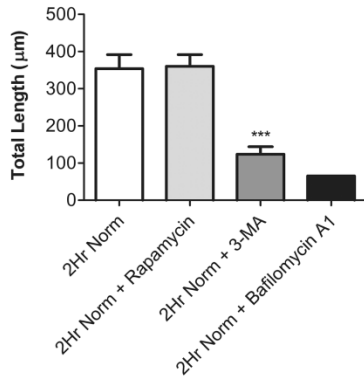
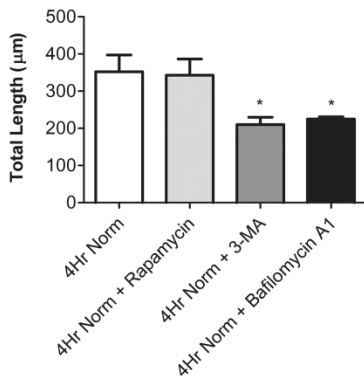
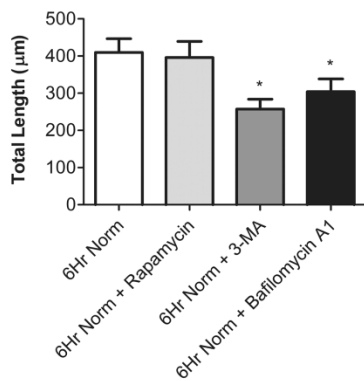
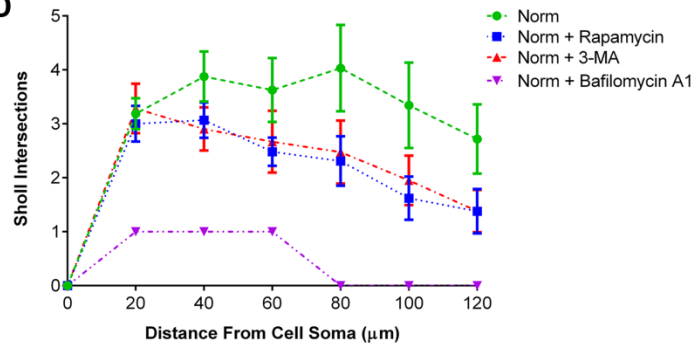
In this study I sought to determine whether autophagy modulation also influenced neurite growth initiation from DRG cells. To accomplish this, dissociated DRG neurons were cultured on poly-D-lysine coated 16-well slides for 2 4hr in control medium. The cultures were then incubated with 50 ng/ $\mu$ L of soluble laminin for 2 hr, 4 hr or 6 hr. After treatment, cultures were further incubated for 16 hr with soluble laminin alone, or co-treated with either Rapa, 3-MA or BA1. After 16 hr, immunocytochemistry was carried out using neuron-specific  $\beta$ III-tubulin (for cell and neurite quantitation) and LC3B (for quantitation of autophagosomes). Cultures were imaged using confocal microscopy, and DRG neurite growth, neurite branching complexity and autophagosome puncta were analyzed with Imaris imaging software, as outlined in the Methods.

In control and Rapa-treated conditions, neurite initiation gradually increased with longer exposures to soluble laminin (Fig. 6.1A-C and 6.2B, J and R). With 3-MA or BA1 treatment, however, initiation was reduced compared to control conditions with all treatments of soluble laminin, but did gradually recovered with longer laminin treatment albeit not to the same level as control or Rapa treated cells (Fig. 6.1A-C and 6.2C, D, K, L, S and T). In the case of branching complexity, control conditions showed an overall decrease in neurite branching with longer exposures to soluble laminin (Fig. 6.1D-F and 6.2A, I and Q).

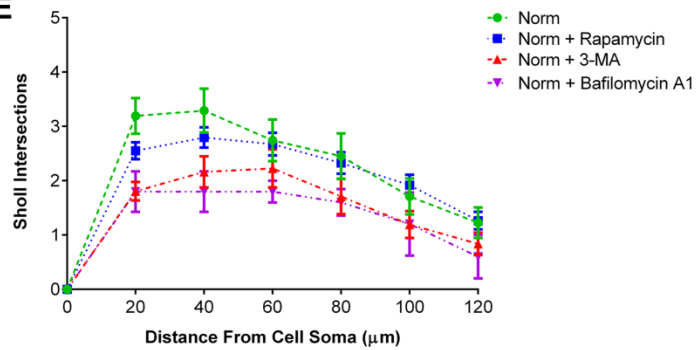
The amount of LC3B-positive puncta in neurites was also quantified and the data demonstrate that treatment with either 3-MA or BA1 significantly reduced puncta (Fig. 6.3A). To assess whether there was any correlation between puncta and neurite growth, the ratio of LC3B

**Figure 6.1: DRG neurite initiation and branching complexity are reduced with autophagy inhibition.**

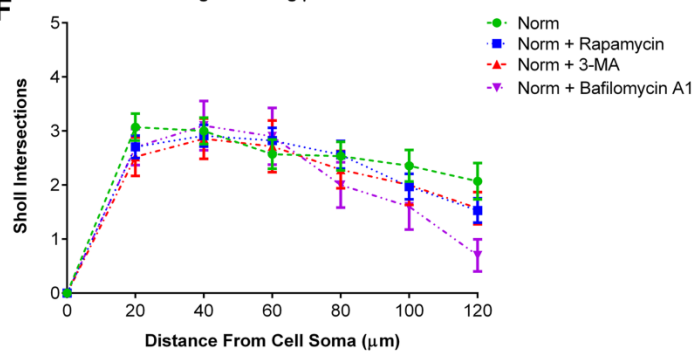
**1) Left Panels.** Total neurite growth in length ( $\mu\text{m}$ ) from the cell soma at 2 hr, 4 hr and 6 hr post soluble laminin treatment, with and without the modulation of autophagy using 3-MA (10mM), BA1 (200nM) or Rapa (200nM) for 16 hr. Values are mean  $\pm$  SEM; n = 10 replicates, with a total of 20 cells analyzed per condition, per time-point. Note: n = 1 for BA1 at 2 hr, as there was zero growth observed with BA1 treatment. \* P < 0.05, \*\*\* P < 0.001, with a one-way ANOVA with Tukey's *post hoc* test; confirmed using a non-parametric test. **2) Right Panels.** Sholl intersection analysis was performed after 3-MA, BA1 or Rapamycin treatment using the Filament Tracer tool in Imaris. Values are mean  $\pm$  SEM; 20 cells were analyzed per condition, per time-point. The significance at each time-point for each sample was determined by comparing the data from the specific treatment to the control (norm) condition. \* P < 0.05, \*\*\* P < 0.001, with a two-way ANOVA with Tukey's *post hoc* test.

**A**DRG Growth With 50ng/ $\mu$ L Soluble Laminin**B**DRG Growth With 50ng/ $\mu$ L Soluble Laminin**C**DRG Growth With 50ng/ $\mu$ L Soluble Laminin**D**DRG Branching With 50ng/ $\mu$ L Soluble Laminin 2Hr

	20 $\mu$ m	40 $\mu$ m	60 $\mu$ m	80 $\mu$ m	100 $\mu$ m	120 $\mu$ m
Norm + Rapamycin	NS	NS	NS	*	*	*
Norm + 3-MA	NS	NS	NS	NS	NS	*
Norm + Bafilomycin	NS	NS	NS	NS	NS	NS

**E**DRG Branching With 50ng/ $\mu$ L Soluble Laminin 4Hr

	20 $\mu$ m	40 $\mu$ m	60 $\mu$ m	80 $\mu$ m	100 $\mu$ m	120 $\mu$ m
Norm + Rapamycin	NS	NS	NS	NS	NS	NS
Norm + 3-MA	***	*	NS	NS	NS	NS
Norm + Bafilomycin	*	*	*	NS	NS	NS

**F**DRG Branching With 50ng/ $\mu$ L Soluble Laminin 6Hr

	20 $\mu$ m	40 $\mu$ m	60 $\mu$ m	80 $\mu$ m	100 $\mu$ m	120 $\mu$ m
Norm + Rapamycin	NS	NS	NS	NS	NS	NS
Norm + 3-MA	NS	NS	NS	NS	NS	NS
Norm + Bafilomycin	NS	NS	NS	NS	NS	*

**Figure 6.2: DRG neurite growth initiation is reduced after 24 hr treatment with 3-MA or BA1.**

DRG neurons were cultured on poly-D-lysine coated 16-well culture slides for 24 hr and subsequently incubated with soluble laminin for 2, 4 or 6 hr. After treatment, cultures were further incubated with either 3-MA (10mM), BA1 (200nM) or Rapa (200nM) for an additional 16 hr. After treatment, the slides were processed for immunocytochemistry using an antibody directed against  $\beta$ III-Tubulin, followed by a fluorescently tagged secondary antibody. Additionally, neurons were stained with IB<sub>4</sub> in order to characterize if stained cells for IB<sub>4</sub> were growing or not. DRG neurons were visualized with confocal microscopy. Scale bar = 20  $\mu$ m. Panels: A-H – 2 hr treatment; I-P – 4 hr treatment; Q-X – 6 hr treatment. Arrows illustrate IB<sub>4</sub> stained cells. Arrowheads illustrate neurite blebbing.

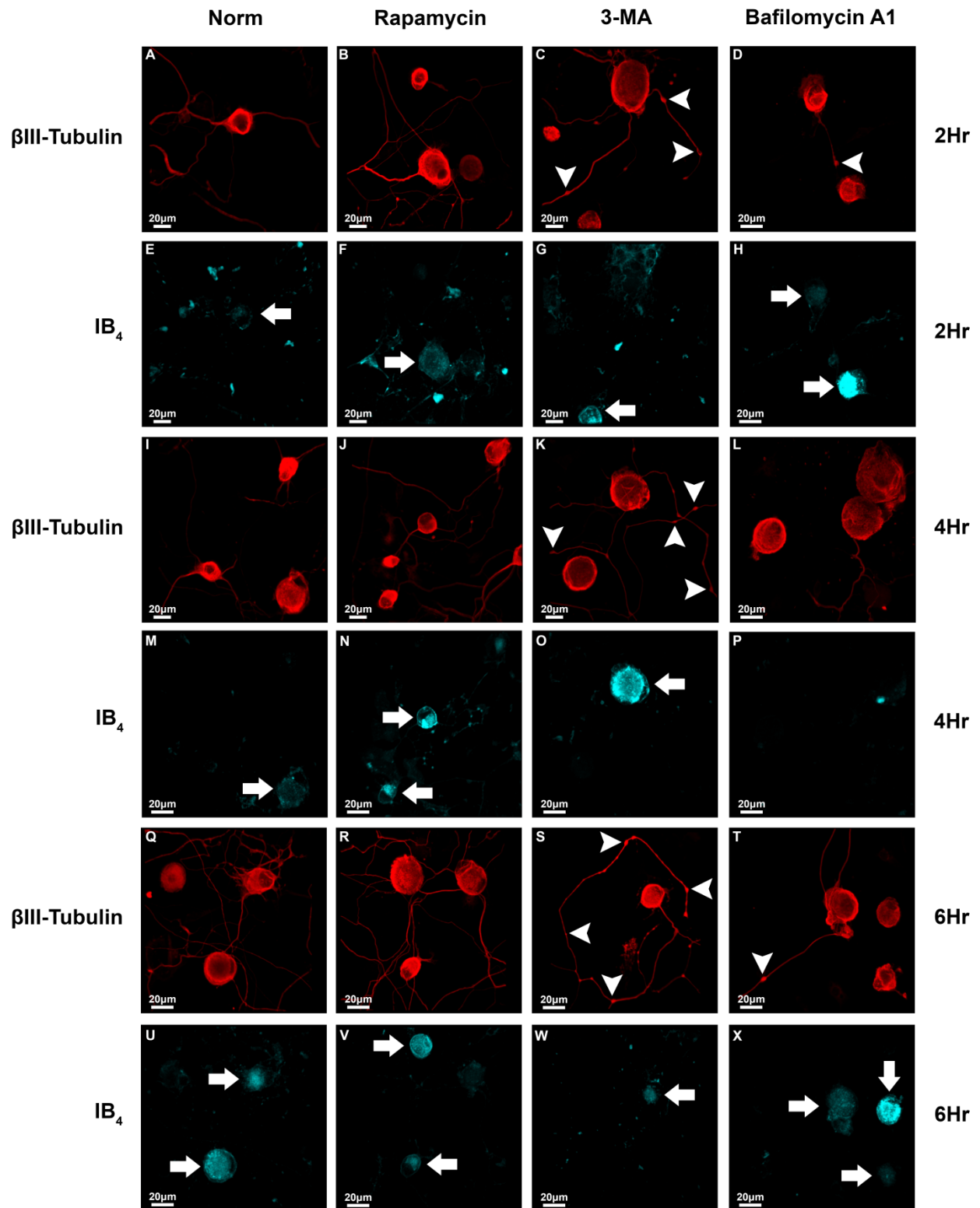


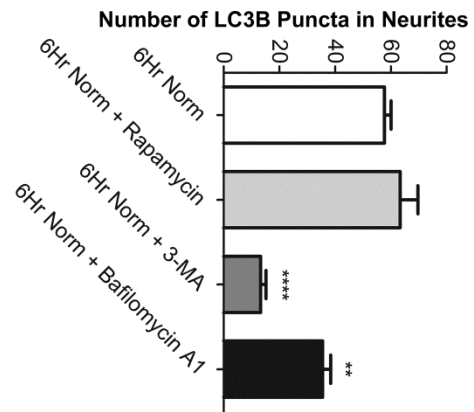
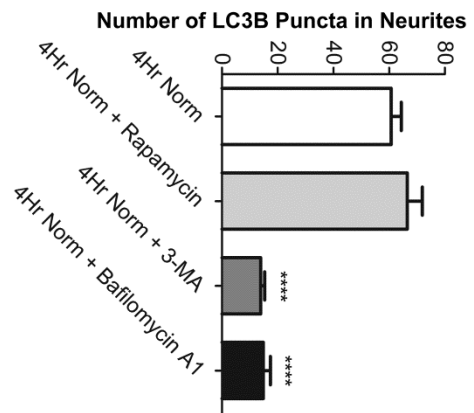
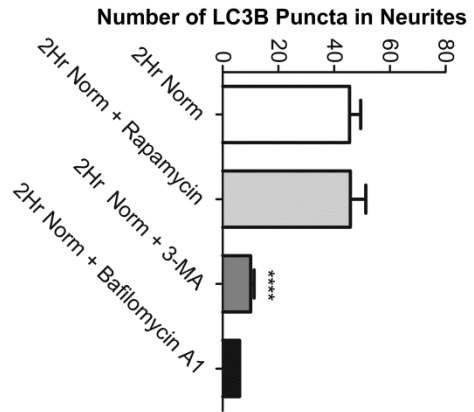
**Figure 6.3: Autophagy inhibition reduces autophagosomes in DRG neurites.**

DRG neurons were cultured on poly-D-lysine coated 16-well culture slides for 24 hr and subsequently incubated with soluble laminin for 2, 4 or 6 hr. After treatment, cultures were further incubated with either 3-MA (10mM), BA1 (200nM) or Rapa (200nM) for an additional 16 hr. After treatment, the slides were processed for immunocytochemistry using antibodies directed against  $\beta$ III-Tubulin and LC3B, and neurons were visualized with confocal microscopy.

**(A)** The total number of LC3B puncta found in growing DRG neurites with soluble laminin, plus and minus 3-MA, BA1 or Rapa were quantified. **(B)** Additionally, the ratio of the number of LC3B puncta per 100 $\mu$ m neurite length with soluble laminin, plus and minus 3-MA, BA1 or Rapa was analyzed. In all analyses, values are mean  $\pm$  SEM; n = 10 replicates, with a total of 20 cells analyzed per condition, per time-point. Note: n =1 for BA1 at 2 hr, as there was zero growth observed with BA1 treatment. \* P < 0.05, \*\* P < 0.01, \*\*\* P < 0.001, and \*\*\*\* P < 0.0001, with a one-way ANOVA with Tukey's *post hoc* test, confirmed using a non-parametric test.

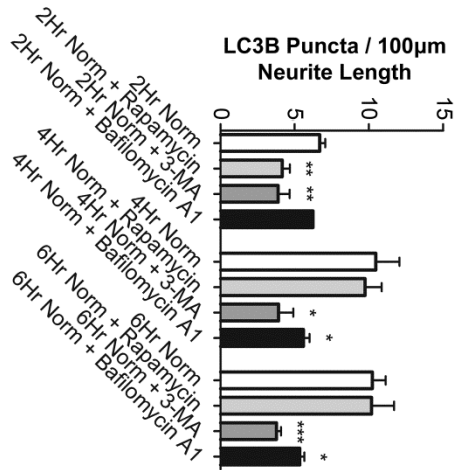
A

Total LC3B Puncta With 50ng/ $\mu$ L Soluble Laminin



B

Control Conditions



puncta/100 $\mu$ m neurite length was calculated. In control and Rapa treated conditions, LC3B puncta significantly decrease with 2 hr soluble laminin treatment, but had no effect at later time points (Fig. 6.3B). Co-treatment with 3-MA or BA1, however, showed an overall significant decrease in LC3B puncta at all time points (Fig. 6.3B). The differences found in the LC3B puncta/100 $\mu$ m neurite length ratio with treatments demonstrate that autophagy modulation affects neurite initiation from the cell soma.

#### **6.4.2 Autophagy Inhibition Reduces IB<sub>4</sub>-Positive DRG Neurite Growth**

After showing that autophagy inhibition with 3-MA or BA1 caused a significant reduction in DRG neurite initiation, this study further investigated this effect on the different sub-populations of DRG neurons. In particular, the nociceptive small diameter DRG neurons were analyzed in order to determine if they showed differences in neurite initiation and outgrowth related to both basal and modulated levels of autophagy. Nociceptive small diameter DRG neurons are thought to be the first affected neurons in peripheral neuropathies associated with loss in pain and temperature modalities, and thus are essential targets to protect against Wallerian degeneration. To accomplish this, DRG neurons were stained with the lectin IB<sub>4</sub>, a marker to distinguish between peptidergic (non-IB<sub>4</sub> positive) and non-peptidergic (IB<sub>4</sub> positive) nociceptive small diameter neurons (Averill et al., 1995; Tucker et al., 2005b, 2006), and then analyzed for the total amount of neurite growth. Additionally, the types of cells that grew neurites, regardless of IB<sub>4</sub> staining, were qualitatively assessed based upon the diameter of the neurons, with small neurons having a cell diameter <30 $\mu$ m, medium neurons a diameter of 30-40 $\mu$ m, and large neurons with a diameter >40 $\mu$ m (Tucker et al., 2005b). Further, the degree of neurite blebbing in

the cell cultures was also recorded, as neurite blebbing is a morphological indication of cytoskeletal breakdown in neurites (Duncan and Goldstein, 2006).

Results demonstrate that neurite growth from large, medium and small (IB<sub>4</sub> and non-IB<sub>4</sub> stained) DRG neurons increased with longer exposures to soluble laminin (Fig. 6.4, 6.5). There was an increased initiation with Rapa co-treatment, while 3-MA caused a reduction and BA1 inhibited initiation (Fig. 6.4, 6.5). Interestingly, Rapa treatment only affected non-IB<sub>4</sub> neurite growth after 4 hr of laminin treatment (Fig. 6.4). Further observations demonstrated that both 3-MA and BA1 progressively increased the amount of neurite blebbing in the growing neurites, while no blebbing occurred in control or Rapa treated conditions (Fig. 6.2).

## **6.5 Discussion**

Previous work in CNS neurons has demonstrated that autophagy is induced under stress conditions and affects axonal growth, while studies in PNS neurons have predominantly focused upon the functionality of the process during disease [see chapter 4 and 5; (Ban et al., 2013; Maday and Holzbaaur, 2014; Maday et al., 2012; Wang et al., 2006a)]. What those studies have not investigated is how autophagy may also influence neurite growth initiation once environmentally favorable conditions are present, and therefore it was the aim of this study to investigate that aspect of autophagy on DRG neurite growth.

Results indicated that inhibition of basal autophagy with 3-MA or BA1 caused a significant reduction in both neurite initiation and branching (Fig. 6.1 and 6.2). Typically, DRG neurites will initiate and grow with soluble laminin treatment, with non-peptidergic small diameter DRG neurons growing neurites at a much slower rate than their peptidergic counterparts (Tucker et al., 2006). Additionally, prior reports have shown that non-peptidergic small DRG neurons need

**Figure 6.4: Qualitative measurement of neurite growth in soluble laminin treated IB<sub>4</sub> and non-IB<sub>4</sub> DRG neurons.**

DRG neurons were cultured on poly-D-lysine coated 16-well culture slides for 24 hr and subsequently incubated with soluble laminin for 2, 4 or 6 hr. After treatment, cultures were further incubated with either 3-MA (10mM), BA1 (200nM) or Rapa (200nM) for an additional 16 hr. After treatment, the slides were processed for immunocytochemistry using an antibody directed against  $\beta$ III-Tubulin, followed by a fluorescently tagged secondary antibody. Additionally, neurons were stained with IB<sub>4</sub> in order to characterize sub-populations of DRG neurons (IB<sub>4</sub> vs. non-IB<sub>4</sub>). DRG neurons were visualized with confocal microscopy and were qualitatively counted based upon whether they exhibited neurite growth or not. The percentage of DRG neurons with neurite growth compared to all DRG neurons counted was then graphically represented.

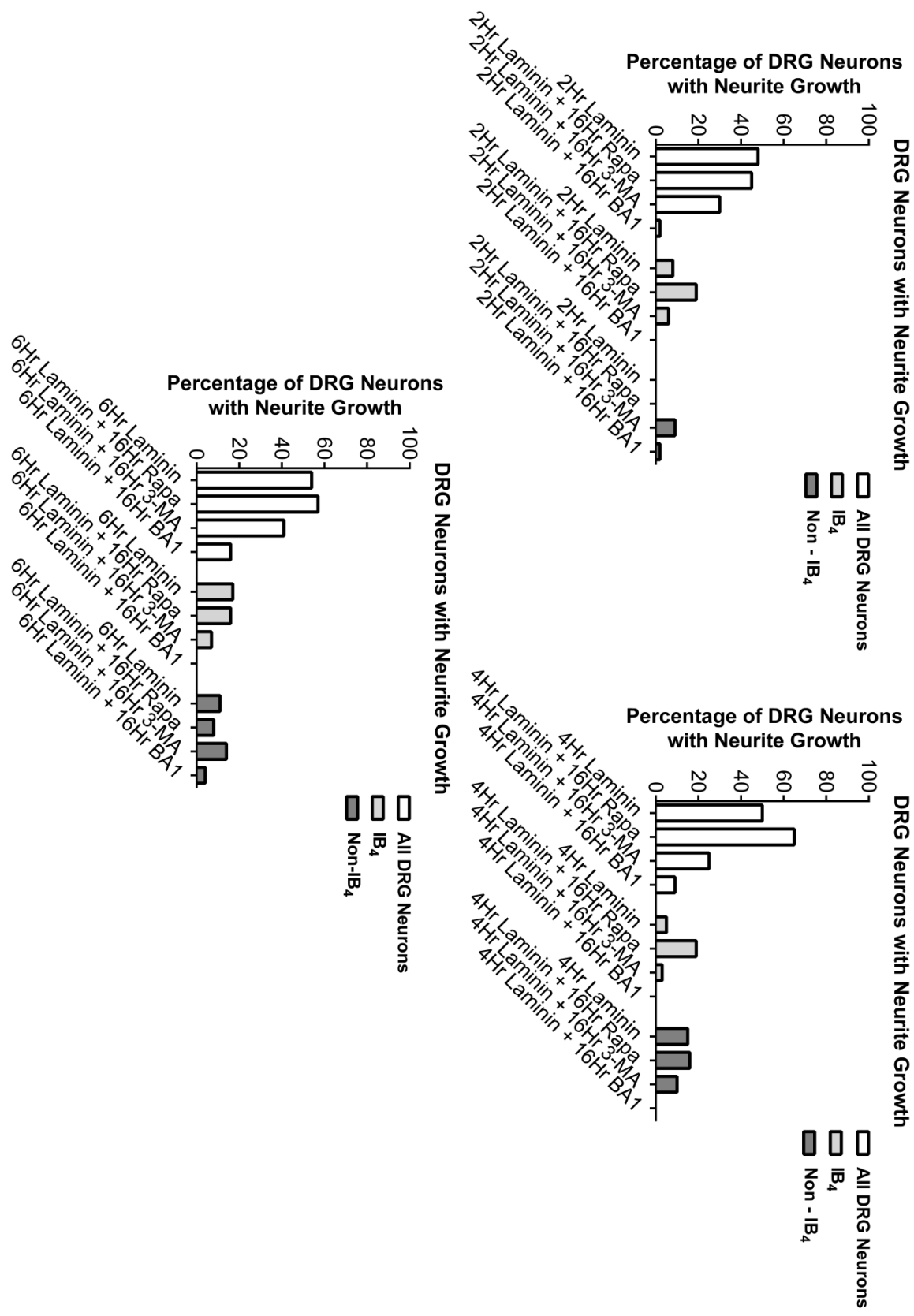
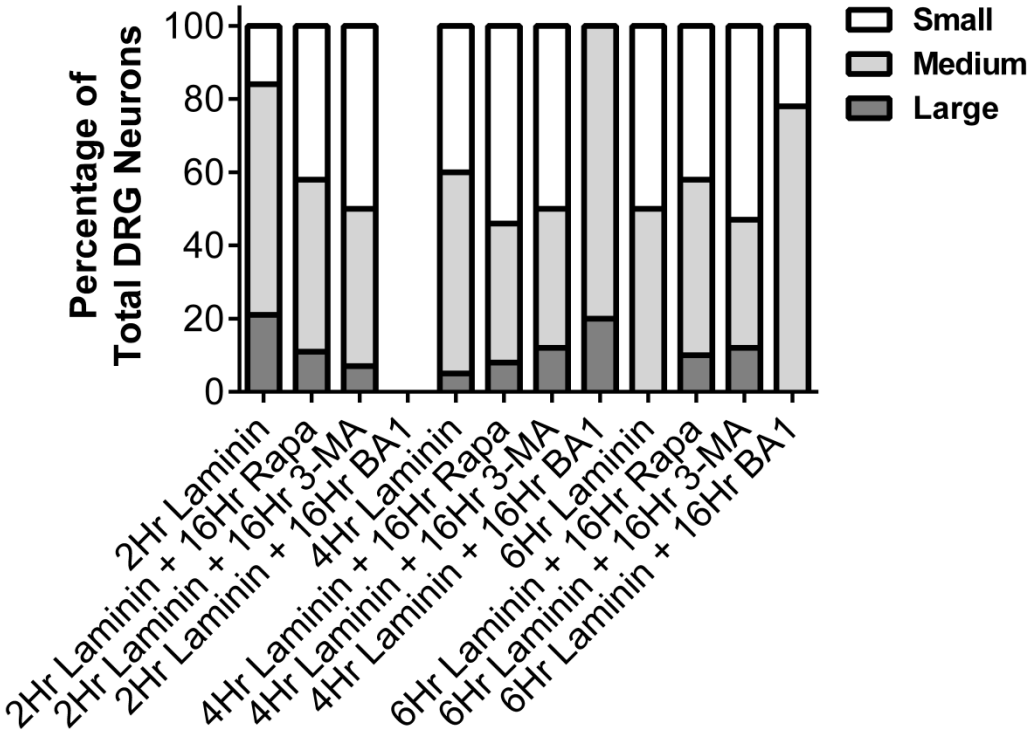


**Figure 6.5: Qualitative measurement of neurite growth characteristics in soluble laminin treated small, medium and large DRG neurons.**

DRG neurons were cultured on poly-D-lysine coated 16-well culture slides for 24 hr and subsequently incubated with soluble laminin for 2, 4 or 6 hr. After treatment, cultures were further incubated with either 3-MA (10mM), BA1 (200nM) or Rapa (200nM) for an additional 16 hr. After treatment, the slides were processed for immunocytochemistry using an antibody directed against  $\beta$ III-Tubulin, followed by a fluorescently tagged secondary antibody. DRG neurons were visualized with confocal microscopy and were qualitatively counted based upon the DRG neuron sub-type (i.e. small, medium or large) that exhibited neurite growth. The percentage of DRG neurons with neurite growth compared to all DRG neurons counted was then graphically represented.

### Growing DRG Neuron Sub-Type



additional neurotrophin support in order to stimulate their growth capacity, while peptidergic neurons do not, although they will respond with greater outgrowth in the presence of NGF (Tucker et al., 2006). Since inhibition of autophagy attenuated neurite initiation, this would suggest that autophagy plays a role in DRG neurite growth initiation characteristics.

Previous research has shown that mTOR is expressed in all DRG neuronal subtypes, with nociceptive non-peptidergic (IB<sub>4</sub> positive) and peptidergic (substance P positive; non-IB<sub>4</sub>) small DRG neurons expressing more mTOR than their medium and large neuron counterparts (Xu et al., 2010). Therefore, it is possible that rapamycin added to small nociceptive DRG neurons could affect mTOR signaling in those cells than in medium or large neurons, and thus in turn may have a larger effect on autophagy and neurite growth if autophagy is mTOR-dependent in these neurons. If rapamycin does not have an effect on autophagic flux and neurite growth in those neurons, however, then it could be reasoned that autophagy may be mTOR-independent and may function via another intracellular pathway. Results from this study showed that rapamycin treatment increased neurite growth initiation from small nociceptive DRG neurons compared to controls at early time-points (Fig. 6.4). The total percentage of small nociceptive DRG neurons with neurite growth at any time-point, however, was not more abundant than their medium and large neurons counterparts (Fig. 6.4). These observations could suggest that while activation of autophagy with rapamycin may induce changes in neurite growth in small nociceptive DRG neurons early after initial treatment, either a sustained activation of autophagy, or further neurotrophin support may be needed to maintain and enhance neurite growth. Additionally, since mTOR also affects mRNA transcription/translation, cell proliferation, lipid synthesis, microtubule organization and mitochondrial function, inhibiting it with rapamycin

may also be having other effects in addition to promoting autophagy that may also contribute to the observed effects on neurite growth (Morita et al., 2015).

An additional observation from this study was the increased amount of neurite blebbing observed with 3-MA. This observation could suggest that in addition to inhibiting autophagosome formation, 3-MA might also directly or indirectly influence cytoskeletal dynamics, as neurite blebbing is indicative of neurite cytoskeletal breakdown and damage, and thus vesicular, autophagosome and organelle transport disruption. Specifically, the presence of neurite blebbing with 3-MA could be a response to its modulation on proteins involved in cytoskeletal maintenance. Alternatively, the cause of the neurite blebbing may also be a direct result of autophagy modulation, as a study found that the loss of function of the ATG5 protein, which is involved in the lipidation of LC3B, lead to swelling of Purkinje neuron axons and lead to progressive neurodegeneration (Nishiyama et al., 2007).

## **6.6 Conclusion**

This study demonstrates that DRG neurite growth initiation in environmentally favorable conditions is reduced with autophagy inhibition, and may suggest that autophagy directly influences the neurite growth process. Although the mechanisms of how autophagy may influence neurite growth initiation are unknown, overall, the data presented in this study provide further insights into how autophagy may influence DRG neuronal cell survival and neurite growth.

## **6.7 Acknowledgements**

The technical assistance of F. Nafar and J. B. Williams during the course of this study is gratefully acknowledged.

## **Chapter 7: Discussion and Future Directions**

### **7.1 Research Outcomes and Future Directions**

The main goal of the research presented in this thesis was to investigate the cellular stress responses of the heat shock response and autophagy in neurons and to determine how they influence neuronal cell survival and neurite growth. Previous work in the Mearow lab demonstrating the role HspB1 plays in the survival and growth of DRG neurons formed the basis of this investigation, while the inclusion of autophagy stemmed from a hypothesis that HspB1 may be involved in its process. Autophagy was further explored in DRG neurons to determine whether this process is influential in the characteristic survival and neurite regrowth nature of mature DRG neurons.

The objectives of this study were three-fold: determine whether endogenous HspB1 interacts with filamentous actin and whether phosphorylation influences this interaction; determine whether a link between HspB1, Daxx, Bcl-2 and autophagic activity exists; and determine whether autophagy plays a role in DRG neuron survival and neurite growth. To summarize and discuss results of this study, as well as elaborate on future directions for each experimental focus, each experimental finding has been placed into 3 separate categories discussed below.

#### **7.1.1 The effect(s) of stress induced HspB1 phosphorylation on its interaction(s) with filamentous actin**

Previous research has clearly shown that HspB1 plays a protective role in neuron survival, and that its positive cellular effects can be attributed to its specific abilities to act as a chaperone protein involved in inhibiting apoptosis and stabilizing the cellular cytoskeleton. Studies have demonstrated that HspB1 can interact with actin, tubulin, tau and several types of intermediate

filaments, including neurofilaments, glial fibrillary acidic protein, vimentin and nestin (Jia et al., 2010; Perng et al., 1999; Shimura et al., 2004). With regards to actin, it has been suggested that HspB1 could interact with either globular or filamentous actin, ultimately inhibiting the polymerization of actin by either sequestering globular actin or directly stabilizing the actin filament through a capping interaction (Benndorf et al., 1994; During et al., 2007; Guay et al., 1997; Lavoie et al., 1995; Pichon et al., 2004). Although numerous reports have described an interaction between actin and HspB1 *in vitro*, using either purified solutions of each or labeled overexpression mutants of phosphorylated HspB1, there has been less evidence of such an interaction in an endogenous cellular system. Additionally, with regards to labeled overexpression mutants, a recent study has suggested that the addition of fluorescent protein markers on the N-terminus and C-terminus of HspB1 affects its oligomeric structure, chaperone activity and its ability to form hetero-oligomers with other Hsp proteins (Datskevich and Gusev, 2014). The results from this study suggest that data obtained with fluorescently labeled HspB1 expressed in cells should be interpreted cautiously (Datskevich and Gusev, 2014).

As a consequence of the data reliability of using labeled overexpression mutants of HspB1, and a limitation in the amount of data for native HspB1 known, the goal of this research was to determine whether a direct interaction between HspB1 and actin occurs in an endogenous cellular model, and to determine the effect(s) that stress activated phosphorylation of HspB1 has on this interaction. Research presented in this study is the first to demonstrate that endogenous HspB1 interacts directly with filamentous actin, and that this interaction can be modified in response to cell stress. Further, this research is also the first to show that endogenously phosphorylated HspB1 weakly interacts with filamentous actin, while after a cell stress has occurred, this interaction becomes more pronounced. The design of this study, however, did not

allow for the interpretation into how phosphorylated HspB1 interacts with filamentous actin, and thus further studies are still needed to assess this interaction. Yet, others have suggested that phosphorylated HspB1 may act either as an actin filament side binding protein, improving the stability and preventing the depolymerization of filamentous actin during cell stress, or may influence other signaling pathways that can modulate actin stability (Doshi et al., 2009; Graceffa, 2011).

In continuation of this study, assessing how phosphorylated HspB1 interacts with filamentous actin is the next important question to be addressed in order to fully understand the influence HspB1 has on filamentous actin stability. As the research presented in this study was able to isolate endogenous actin filaments, one could use this methodology to further determine whether phosphorylated HspB1 interacts as an actin side binding protein or not. To elaborate, *in vitro* one could incubate the recombinant F-actin capping protein CapZ with recombinant F-actin and then assess the association between F-actin and CapZ using F-actin pull-down and protein immunoblotting. Next, using the same procedure, recombinant phospho-HspB1 mutants could then be added to the solution after CapZ has been first incubated with F-actin. After pull-down and protein immunoblotting, one could then assess which phospho-HspB1 mutant binds as a side binding protein or as a capping protein. Theoretically, if CapZ is observed after pull-down and immunoblotting, and its amount is unchanged from the non-HspB1 treated samples, then any phosphorylated HspB1 observed could be theorized to bind to other portions of the actin filament. However, if the amount of CapZ found after pull-down and immunoblotting changes significantly from the control then the phosphorylated HspB1 species could be theorized to bind as a capping protein. While simplistic, this experimentation could further the understanding of how phosphorylated and non-phosphorylated HspB1 interacts with F-actin. Another

methodology that could be used in conjunction with *in vitro* experimentation is immuno-electron microscopy, as this would allow for the visualization of the interaction between the recombinant phospho-HspB1 mutants and F-actin.

The importance of the work presented in this study is highlighted by the fact that through a further understanding of how HspB1 interacts with cytoskeletal proteins, we can then attempt to develop strategies to use HspB1 to treat or prevent neurodegenerative diseases. For example, in the neurodegenerative diseases of Alzheimer's, Huntington's, DPN and amyotrophic lateral sclerosis, anterograde and retrograde transport mechanisms become disrupted, along with the formation of axonal swellings and axonal loss [reviewed in (Yang et al., 2007)]. Based upon studies showing that HspB1 helps maintain the integrity of cytoskeletal morphology, it is reasonable to suggest that HspB1 could at least help prevent axonal swellings and loss, as both are tied to the disruption of the cytoskeletal network. A caveat to this, however, is the fact that most neurons do not endogenously express HspB1, and thus cannot normally regulate the disruption of the cytoskeletal network through the activity of HspB1. An interesting fact, however, is that non-neuronal cells, such as astrocytes, schwann cells, oligodendrocytes and microglia, do express HspB1, and in recent studies have shown that HspB1 is released into the extracellular environment during cell stress (Komiya et al., 2010; Smith and Skene, 1997; Tian et al., 2010). As a result of this, it is reasonable to suggest that though the further understanding of endocytotic mechanisms used by neurons, in parallel to understanding the mechanisms behind how HspB1 influences neuron survival, we can develop a method in which extracellular HspB1, released endogenously from non-neuronal cells during stress, can be uptaken by neurons in order to help them survive.

### **7.1.2 The potential role HspB1 has on the process of autophagy**

Stemming from the research investigating the interaction between HspB1 and filamentous actin, this study next focused upon determining the potential interactions HspB1 has with other cellular proteins, and how these interactions may influence endogenous stress activated cellular survival processes. Specifically, this study focused upon the interaction between HspB1 and Daxx, and how this interaction may potentially modify autophagy in DRG neurons. The idea for this study initially stemmed from three published studies, whereby two *in vitro* studies initially discovered that HspB1 can interact with Daxx and prohibited its activation of cellular apoptosis during cell stress (Charette and Landry, 2000; Charette et al., 2000), while another other study found that Daxx acts as a transcriptional co-repressor of Bcl-2 (Li et al., 2000). Neither study was functionally linked, nor has any other study published since has tried to functionally link both ideas. Therefore, the potential discovery of a link was a new opportunity to further understand the role HspB1 has in cell survival. In addition, looking at the functional link between both experimental ideas in DRG neurons was a way to potentially further understand the innate process of DRG axonal regeneration, and if successful, could suggest a new avenue of research to help modulate the effects of peripheral neurodegenerative diseases.

Although experimentation did not suggest a link that could form a control mechanism of autophagy, as qRT-PCR showed changes in RNA transcription of HspB1, Daxx and Bcl-2 after cell stress had occurred, and cellular localization and protein expression showed trends that agree with already published material regarding Daxx and HspB1, additional work is still required to prove if a link exists. Therefore, through further experimentation, and an adjusted experimental paradigm, it may be possible to accomplish such a task. For instance, the use of different stress conditions that specifically activate autophagy would be an initial experimental paradigm that

could be changed, as high glucose did not appear to affect autophagy in these mature neurons, as determined by protein immunoblotting. Again, taking into consideration the conditions in which the DRG neurons were cultured and treated, we cannot rule out the fact that hyperglycemia and hyperinsulinemia may have been occurring well before treatments were carried out, and may be influencing the results obtained in this study. Therefore, a change to the DRG culture protocol, as well as the use of different stress conditions could yield more reliable results.

Other cell stressors that could be used are either nutrient deprivation or increased ROS stress, as these have been shown to activate autophagy in other cell types; this study has also shown these stimuli also activate autophagy in DRG neurons. Additionally, the use of RNA interference (RNAi) toward Daxx and HspB1 could give a better idea into whether either is involved in the transcription of Bcl-2, and/or the overall process of autophagy. Small interfering RNA (siRNA) were used to knock down expression of Daxx and HspB1 in this study, but results were unreliable to be included as DRG neurons were difficult to transfect, and resulted in substantial cell loss after transfection. Furthermore, with cells that did survive transfection, a knock down in RNA expression was not experimentally apparent. With an improvement in the transfection procedure, or through the use of a different transfection technique, such as viral vectors with short hairpin RNA (shRNA), one could improve the survivability of the mature neurons and could get functional RNAi.

As with the first study, the importance of the work presented in this study is highlighted by the fact that through a further understanding of how HspB1 interacts with and influences cellular proteins, during both cellular stress and cellular homeostasis, we can then attempt to develop strategies to use HspB1 to treat or prevent neurodegenerative diseases. In the case of HspB1 potentially influencing autophagy through its interaction with Daxx, this does pose an

interestingly new avenue in neurodegenerative disease treatment. For instance, Daxx, Bcl-2, and HMGB1 are all expressed in neurons, unlike HspB1 (Abe et al., 2010; Towns et al., 2008a; Towns et al., 2005). If a link between the proteins and the activation of autophagy is found, however, this new knowledge could help to develop strategies to influence neurodegenerative disease through autophagic activity. For instance, as referred to previously, if we can develop a method in which extracellular HspB1, released endogenously from non-neuronal cells during cell stress, can be uptaken by neurons, we can then potentially use this to both influence cytoskeletal dynamics and modulate autophagy in neighboring stressed neurons.

### **7.1.3 The effects of autophagy on DRG neuron survival and neurite growth**

The study of autophagy in the peripheral nervous system is a relatively new topic, and its effects and mechanisms within that system are still being explored. Therefore, it was the intent of this study to further our understanding of autophagy in adult DRG neurons, and to help determine its effect on neuron survival and neurite growth during cellular stress.

Adult DRG neurons were specifically chosen for this study for two reasons: cell stress in adult DRG neurons more accurately mimics an endogenous cellular system, and adult DRG neurons do not require additional neurotrophic support for survival and neurite growth. A confounding factor in using either embryonic or neonatal DRG neurons over adult neurons is the fact that they do require additional neurotrophic support in order to survive and grow neurites (Lindsay, 1988; Tucker and Mearow, 2008). The potential issue with this is that neurotrophins could induce autophagy through the activation of JNK, as shown in other neuronal cell types, and thus would complicate the interpretation of how autophagy affects DRG neuron survival and neurite growth (Florez-McClure et al., 2004).

In addition to using adult DRG neurons, the stress induction models of nutrient deprivation and increased ROS stress were also chosen for this study. These stress models have been shown to occur in DPN, and been shown to induce autophagy in other cellular models. Therefore, it was our goal to both demonstrate that those stressors induce autophagy in adult DRG neurons, and that stress induced autophagy efficiency helps maintain cell survival and axonal maintenance and regeneration. Additionally, the stress models were chosen in order to correlate any similarities/differences in the autophagic response due to either model and determine whether there were any associated differences found in DRG neuron survival and neurite growth. In conjunction with the nutrient deprivation and increased ROS stress treatment paradigms, pharmacological agents were also used to alter autophagy and to monitor its change in flux. Overall, the work in this study demonstrated that endogenous autophagy in adult DRG neurons is up-regulated in response to both nutrient deprivation and increased ROS stress, and that inhibition of either autophagosome initiation or autophagosome degradation has a negative effect on DRG neuron survival, neurite growth and neurite growth initiation. Taken together, these results suggest that negative alterations in autophagy have detrimental effects the survival and morphology of DRG neurons. Previous publications agree with this data, as it has been shown that the modulation of autophagy in other neuronal cell models alters their survival and neurite growth (Caccamo et al., 2010; Radad et al., 2015; Ravikumar et al., 2004). Additionally, studies have shown that autophagy occurs in peripheral neuropathy, with its occurrence suggested to help improve the state of the peripheral nerves, either through an increase in damaged protein and organelle recycling, or through an increase in nutrient availability (Kosacka et al., 2013; Mohseni, 2011; Osman et al., 2015; Shi et al., 2013; Towns et al., 2005).

Although the mechanism(s) underlying autophagy are not completely understood, this study does allow for further analysis into how autophagy may be involved in peripheral neuron diseases. Experimental models that could be used to further assess autophagy in peripheral neuron diseases are either a streptozotocin (STZ) induced type 1 diabetic peripheral neuropathy model in rats, or alternatively an animal model that induces type 2 diabetic peripheral neuropathy, such as the db/db mouse model (Towns et al., 2008b). The streptozotocin treated rat model causes the necrosis of pancreatic beta cells, producing an animal model of hyperglycemia, while in the case of the db/db mouse model these mice lose leptin receptor activity due to a mutation in the gene for the leptin receptor. Both models have been used to study DPN, as both models induce the effects seen on peripheral neurons during DPN (i.e. loss of axonal conduction velocity, increased axonal swellings and disruption of axonal transportation, and Wallerian degeneration of axons). Using either model, one could utilize similar experiments that have been presented in this study and assess the effect(s) that *in vivo* diabetes has on autophagy in DRG neurons. In particular, these models would be of interest to determine whether autophagy is modulated by *in vivo* hyperglycemia, and to determine what its effects are on *in vivo* neurite growth. In this experimental design, one could obtain transected nerve samples from the animal models and then determine if there are changes in the amount of autophagosome formation, either via protein analysis or visually using immunocytochemical confocal microscopy. In addition to using streptozotocin and db/db animal models, one could apply the same methodology using developed transgenic mouse models that expresses either GFP-LC3B or RFP-EGFP-LC3B, which would allow for a better analysis of autophagic flux (Mizushima et al., 2004).

Similar to the studies I have suggested above, research has been done using similar models, with results suggesting that there may be a differential regulation of endogenous autophagy depending on whether type 1 or type 2 diabetes is present, and that stress activated autophagy may have an effect on the symptomatic outcome of individuals with DPN (Guo et al., 2015; Osman et al., 2015). Additionally, studies have observed that the presence of endogenous autophagic vesicles in peripheral nerves correlated more with the presence of regenerating axons, and that the overall process of autophagy may protect peripheral nerves from neuropathy, based upon an altered metabolic syndrome animal model (Kosacka et al., 2013; Mohseni, 2011). Furthermore, it has been demonstrated that proper constitutive autophagy influences the survival of DRG neurons in a mouse ATG7-knockout model, as older animals with ATG7 knockout illustrated significant DRG neuronal loss (Zhou et al., 2010).

The work I have presented in this study, along with other studies previously published in the same area, highlight the importance of further understanding how homeostatic and stress induced autophagy works in the PNS. For example, by following autophagic activity throughout the course of peripheral nerve disease, we can potentially use this information as a tool to detect early adverse changes in disease in order to develop treatments that can influence the establishment or outcome of the disease. Furthermore, through this approach, we can also study the potential positive and negative effects that autophagy modulation has on disease etiology, and further characterize peripheral nerve diseases based upon autophagic function.

## **7.2 Conclusion**

In summary, the major findings of this thesis are as follows:

- HspB1 directly interacts with F-actin in a cellular model and that both endogenously phosphorylated and non-phosphorylated HspB1 are found to be present in F-actin complexes.
- DRG neurons constitutively express Daxx, Bcl-2, HMGB1 and the autophagy related protein LC3B, and high glucose stress alters the RNA expression and cellular localization of HspB1 and Daxx.
- Inhibition of constitutive autophagy in mature DRG neurons negatively affects neuron survival, neurite growth, branching and initiation, with these effects becoming more pronounced with the addition of cell stress, such as nutrient deprivation or increased ROS.
- Overall, the research in this study presents new data and ideas into how the cellular stress responses of heat shock, in relation to HspB1, and autophagy influence neuronal cell survival and neurite growth during cell stress.

## References

- Abe, N., Borson, S.H., Gambello, M.J., Wang, F., and Cavalli, V. (2010). Mammalian target of rapamycin (mTOR) activation increases axonal growth capacity of injured peripheral nerves. *J Biol Chem* 285, 28034-28043.
- Acosta-Jaquez, H.A., Keller, J.A., Foster, K.G., Ekim, B., Soliman, G.A., Feener, E.P., Ballif, B.A., and Fingar, D.C. (2009). Site-specific mTOR phosphorylation promotes mTORC1-mediated signaling and cell growth. *Mol Cell Biol* 29, 4308-4324.
- Almeida-Souza, L., Asselbergh, B., d'Ydewalle, C., Moonens, K., Goethals, S., de Winter, V., Azmi, A., Irobi, J., Timmermans, J.P., Gevaert, K., *et al.* (2011). Small heat-shock protein HSPB1 mutants stabilize microtubules in Charcot-Marie-Tooth neuropathy. *The Journal of neuroscience : the official journal of the Society for Neuroscience* 31, 15320-15328.
- Ao, X., Zou, L., and Wu, Y. (2014). Regulation of autophagy by the Rab GTPase network. *Cell Death Differ* 21, 348-358.
- Aquilina, J.A., Shrestha, S., Morris, A.M., and Ecroyd, H. (2013). Structural and functional aspects of hetero-oligomers formed by the small heat shock proteins alphaB-crystallin and HSP27. *J Biol Chem* 288, 13602-13609.
- Arrigo, A.P. (2012). Pathology-dependent effects linked to small heat shock proteins expression: an update. *Scientifica (Cairo)* 2012, 185641.
- Arrigo, A.P. (2013). Human small heat shock proteins: protein interactomes of homo- and hetero-oligomeric complexes: an update. *FEBS letters* 587, 1959-1969.
- Arrigo, A.P., and Gibert, B. (2012). HspB1 dynamic phospho-oligomeric structure dependent interactome as cancer therapeutic target. *Current molecular medicine* 12, 1151-1163.
- Arrigo, A.P., Suhan, J.P., and Welch, W.J. (1988). Dynamic changes in the structure and intracellular locale of the mammalian low-molecular-weight heat shock protein. *Mol Cell Biol* 8, 5059-5071.
- Arrigo, A.P., Viot, S., Chaufour, S., Firdaus, W., Kretz-Remy, C., and Diaz-Latoud, C. (2005). Hsp27 consolidates intracellular redox homeostasis by upholding glutathione in its reduced form and by decreasing iron intracellular levels. *Antioxidants & redox signaling* 7, 414-422.
- Arrigo, A.P., and Welch, W.J. (1987). Characterization and purification of the small 28,000-dalton mammalian heat shock protein. *J Biol Chem* 262, 15359-15369.
- Ashford, T.P., and Porter, K.R. (1962). Cytoplasmic components in hepatic cell lysosomes. *The Journal of cell biology* 12, 198-202.

Ashrafi, G., Schlehe, J.S., LaVoie, M.J., and Schwarz, T.L. (2014). Mitophagy of damaged mitochondria occurs locally in distal neuronal axons and requires PINK1 and Parkin. *J Cell Biol* 206, 655-670.

Averill, S., McMahon, S.B., Clary, D.O., Reichardt, L.F., and Priestley, J.V. (1995). Immunocytochemical localization of trkA receptors in chemically identified subgroups of adult rat sensory neurons. *The European journal of neuroscience* 7, 1484-1494.

Averill, S., Michael, G.J., Shortland, P.J., Leavesley, R.C., King, V.R., Bradbury, E.J., McMahon, S.B., and Priestley, J.V. (2004). NGF and GDNF ameliorate the increase in ATF3 expression which occurs in dorsal root ganglion cells in response to peripheral nerve injury. *Eur J Neurosci* 19, 1437-1445.

Baba, M., Takeshige, K., Baba, N., and Ohsumi, Y. (1994). Ultrastructural analysis of the autophagic process in yeast: detection of autophagosomes and their characterization. *The Journal of cell biology* 124, 903-913.

Babizhayev, M.A., Stokov, I.A., Nosikov, V.V., Savel'yeva, E.L., Sitnikov, V.F., Yegor, E.Y., and Lankin, V.Z. (2014). The Role of Oxidative Stress in Diabetic Neuropathy: Generation of Free Radical Species in the Glycation Reaction and Gene Polymorphisms Encoding Antioxidant Enzymes to Genetic Susceptibility to Diabetic Neuropathy in Population of Type I Diabetic Patients. *Cell Biochem Biophys*.

Ban, B.K., Jun, M.H., Ryu, H.H., Jang, D.J., Ahmad, S.T., and Lee, J.A. (2013). Autophagy negatively regulates early axon growth in cortical neurons. *Mol Cell Biol* 33, 3907-3919.

Barth, S., Glick, D., and Macleod, K.F. (2010). Autophagy: assays and artifacts. *J Pathol* 221, 117-124.

Benavides, G.A., Liang, Q., Dodson, M., Darley-Usmar, V., and Zhang, J. (2013). Inhibition of autophagy and glycolysis by nitric oxide during hypoxia-reoxygenation impairs cellular bioenergetics and promotes cell death in primary neurons. *Free Radic Biol Med* 65, 1215-1228.

Benn, S.C., Perrelet, D., Kato, A.C., Scholz, J., Decosterd, I., Mannion, R.J., Bakowska, J.C., and Woolf, C.J. (2002). Hsp27 upregulation and phosphorylation is required for injured sensory and motor neuron survival. 36, 45-56.

Benndorf, R., Hayess, K., Ryazantsev, S., Wieske, M., Behlke, J., and Lutsch, G. (1994). Phosphorylation and supramolecular organization of murine small heat shock protein HSP25 abolish its actin polymerization-inhibiting activity. *J Biol Chem* 269, 20780-20784.

Biazik, J., Yla-Anttila, P., Vihinen, H., Jokitalo, E., and Eskelinen, E.L. (2015). Ultrastructural relationship of the phagophore with surrounding organelles. *Autophagy* 11, 439-451.

Bierer, B.E., Mattila, P.S., Standaert, R.F., Herzenberg, L.A., Burakoff, S.J., Crabtree, G., and Schreiber, S.L. (1990). Two distinct signal transmission pathways in T lymphocytes are inhibited by complexes formed between an immunophilin and either FK506 or rapamycin. *Proceedings of the National Academy of Sciences of the United States of America* 87, 9231-9235.

- Brown, N.F., Stefanovic-Racic, M., Sipula, I.J., and Perdomo, G. (2007). The mammalian target of rapamycin regulates lipid metabolism in primary cultures of rat hepatocytes. *Metabolism* 56, 1500-1507.
- Bruey, J.M., Ducasse, C., Bonniaud, P., Ravagnan, L., Susin, S.A., Diaz-Latoud, C., Gurbuxani, S., Arrigo, A.P., Kroemer, G., Solary, E., and Garrido, C. (2000a). Hsp27 negatively regulates cell death by interacting with cytochrome c. *Nature cell biology* 2, 645-652.
- Bruey, J.M., Paul, C., Fromentin, A., Hilpert, S., Arrigo, A.P., Solary, E., and Garrido, C. (2000b). Differential regulation of HSP27 oligomerization in tumor cells grown in vitro and in vivo. *Oncogene* 19, 4855-4863.
- Bryantsev, A.L., Kurchashova, S.Y., Golyshev, S.A., Polyakov, V.Y., Wunderink, H.F., Kanon, B., Budagova, K.R., Kabakov, A.E., and Kampinga, H.H. (2007). Regulation of stress-induced intracellular sorting and chaperone function of Hsp27 (HspB1) in mammalian cells. *Biochem J* 407, 407-417.
- Bryantsev, A.L., Loktionova, S.A., Ilyinskaya, O.P., Tararak, E.M., Kampinga, H.H., and Kabakov, A.E. (2002). Distribution, phosphorylation, and activities of Hsp25 in heat-stressed H9c2 myoblasts: a functional link to cytoprotection. *Cell Stress Chaperones* 7, 146-155.
- Button, R.W., Luo, S., and Rubinsztein, D.C. (2015). Autophagic activity in neuronal cell death. *Neurosci Bull* 31, 382-394.
- Caccamo, A., Majumder, S., Richardson, A., Strong, R., and Oddo, S. (2010). Molecular interplay between mammalian target of rapamycin (mTOR), amyloid-beta, and Tau: effects on cognitive impairments. *J Biol Chem* 285, 13107-13120.
- Calero, M., Gomez-Ramos, A., Calero, O., Soriano, E., Avila, J., and Medina, M. (2015). Additional mechanisms conferring genetic susceptibility to Alzheimer's disease. *Frontiers in cellular neuroscience* 9, 138.
- Carlioni, S., Girelli, S., Scopa, C., Buonocore, G., Longini, M., and Balduini, W. (2010). Activation of autophagy and Akt/CREB signaling play an equivalent role in the neuroprotective effect of rapamycin in neonatal hypoxia-ischemia. *Autophagy* 6, 366-377.
- Caro, L.H., Plomp, P.J., Wolvetang, E.J., Kerkhof, C., and Meijer, A.J. (1988). 3-Methyladenine, an inhibitor of autophagy, has multiple effects on metabolism. *European journal of biochemistry / FEBS* 175, 325-329.
- Charette, S.J., and Landry, J. (2000). The interaction of HSP27 with Daxx identifies a potential regulatory role of HSP27 in Fas-induced apoptosis. *Ann N Y Acad Sci* 926, 126-131.
- Charette, S.J., Lavoie, J.N., Lambert, H., and Landry, J. (2000). Inhibition of Daxx-mediated apoptosis by heat shock protein 27. *Mol Cell Biol* 20, 7602-7612.

- Chavez Zobel, A.T., Lambert, H., Theriault, J.R., and Landry, J. (2005). Structural instability caused by a mutation at a conserved arginine in the alpha-crystallin domain of Chinese hamster heat shock protein 27. *Cell Stress Chaperones* 10, 157-166.
- Chen, J., Zheng, X.F., Brown, E.J., and Schreiber, S.L. (1995). Identification of an 11-kDa FKBP12-rapamycin-binding domain within the 289-kDa FKBP12-rapamycin-associated protein and characterization of a critical serine residue. *Proceedings of the National Academy of Sciences of the United States of America* 92, 4947-4951.
- Cheng, S.W., Fryer, L.G., Carling, D., and Shepherd, P.R. (2004). Thr2446 is a novel mammalian target of rapamycin (mTOR) phosphorylation site regulated by nutrient status. *J Biol Chem* 279, 15719-15722.
- Chiou, Y.W., Hwu, W.L., and Lee, Y.M. (2008). Hsp27 decreases inclusion body formation from mutated GTP-cyclohydrolase I protein. *Biochimica et biophysica acta* 1782, 169-179.
- Choi, S., Oh, J.H., Kim, H., Nam, S.H., Shin, J., and Park, J.S. (2015). Protective Effect of Tat PTD-Hsp27 Fusion Protein on Tau Hyperphosphorylation Induced by Okadaic Acid in the Human Neuroblastoma Cell Line SH-SY5Y. *Cell Mol Neurobiol*.
- Choo, A.Y., Yoon, S.O., Kim, S.G., Roux, P.P., and Blenis, J. (2008). Rapamycin differentially inhibits S6Ks and 4E-BP1 to mediate cell-type-specific repression of mRNA translation. *Proceedings of the National Academy of Sciences of the United States of America* 105, 17414-17419.
- Chretien, P., and Landry, J. (1988). Enhanced Constitutive Expression of the 27-Kda Heat-Shock Proteins in Heat-Resistant Variants from Chinese-Hamster Cells. *J Cell Physiol* 137, 157-166.
- Christie, K.J., Webber, C.A., Martinez, J.A., Singh, B., and Zochodne, D.W. (2010). PTEN inhibition to facilitate intrinsic regenerative outgrowth of adult peripheral axons. *J Neurosci* 30, 9306-9315.
- Chu, C.T., Plowey, E.D., Dagda, R.K., Hickey, R.W., Cherra, S.J., 3rd, and Clark, R.S. (2009). Autophagy in neurite injury and neurodegeneration: in vitro and in vivo models. *Methods Enzymol* 453, 217-249.
- Clarke, J.P., and Mearow, K.M. (2013). Cell stress promotes the association of phosphorylated HspB1 with F-actin. *PloS one* 8, e68978.
- Conway, M., Nafar, F., Straka, T., and Mearow, K. (2014). Modulation of amyloid-beta protein precursor expression by HspB1. *Journal of Alzheimer's disease : JAD* 42, 435-450.
- Cordonnier, T., Bishop, J.L., Shiota, M., Nip, K.M., Thaper, D., Vahid, S., Heroux, D., Gleave, M., and Zoubeydi, A. (2015). Hsp27 regulates EGF/beta-catenin mediated epithelial to mesenchymal transition in prostate cancer. *International journal of cancer Journal international du cancer* 136, E496-507.

Costigan, M., Mannion, R.J., Kendall, G., Lewis, S.E., Campagna, J.A., Coggeshall, R.E., Meridith-Middleton, J., Tate, S., and Woolf, C.J. (1998). Heat shock protein 27: developmental regulation and expression after peripheral nerve injury. *The Journal of neuroscience : the official journal of the Society for Neuroscience* 18, 5891-5900.

Cuervo, A.M., and Wong, E. (2014). Chaperone-mediated autophagy: roles in disease and aging. *Cell Res* 24, 92-104.

Cuesta, R., Laroia, G., and Schneider, R.J. (2000). Chaperone hsp27 inhibits translation during heat shock by binding eIF4G and facilitating dissociation of cap-initiation complexes. *Genes Dev* 14, 1460-1470.

Datskevich, P.N., and Gusev, N.B. (2014). Structure and properties of chimeric small heat shock proteins containing yellow fluorescent protein attached to their C-terminal ends. *Cell Stress Chaperones* 19, 507-518.

Datskevich, P.N., Mymrikov, E.V., and Gusev, N.B. (2012). Utilization of fluorescent chimeras for investigation of heterooligomeric complexes formed by human small heat shock proteins. *Biochimie* 94, 1794-1804.

Dent, E.W., Gupton, S.L., and Gertler, F.B. (2011). The growth cone cytoskeleton in axon outgrowth and guidance. *Cold Spring Harb Perspect Biol* 3.

Deter, R.L., Baudhuin, P., and De Duve, C. (1967). Participation of lysosomes in cellular autophagy induced in rat liver by glucagon. *The Journal of cell biology* 35, C11-16.

Deter, R.L., and De Duve, C. (1967). Influence of glucagon, an inducer of cellular autophagy, on some physical properties of rat liver lysosomes. *The Journal of cell biology* 33, 437-449.

Devor, M. (1999). Unexplained peculiarities of the dorsal root ganglion. *Pain Suppl* 6, S27-35.

Dodge, M.E., Rahimtula, M., and Mearow, K.M. (2002). Factors contributing to neurotrophin-independent survival of adult sensory neurons. *Brain Res* 953, 144-156.

Dodge, M.E., Wang, J., Guy, C., Rankin, S., Rahimtula, M., and Mearow, K.M. (2006). Stress-induced heat shock protein 27 expression and its role in dorsal root ganglion neuronal survival. *Brain Res* 1068, 34-48.

Doshi, B.M., Hightower, L.E., and Lee, J. (2009). The role of Hsp27 and actin in the regulation of movement in human cancer cells responding to heat shock. *Cell Stress Chaperones* 14, 445-457.

Doshi, B.M., Hightower, L.E., and Lee, J. (2010). HSPB1, actin filament dynamics, and aging cells. *Ann N Y Acad Sci* 1197, 76-84.

Duncan, J.E., and Goldstein, L.S. (2006). The genetics of axonal transport and axonal transport disorders. *PLoS genetics* 2, e124.

Dunn, W.A., Jr. (1990). Studies on the mechanisms of autophagy: formation of the autophagic vacuole. *The Journal of cell biology* 110, 1923-1933.

During, R.L., Gibson, B.G., Li, W., Bishai, E.A., Sidhu, G.S., Landry, J., and Southwick, F.S. (2007). Anthrax lethal toxin paralyzes actin-based motility by blocking Hsp27 phosphorylation. *EMBO J* 26, 2240-2250.

Ecsedy, J.A., Michaelson, J.S., and Leder, P. (2003). Homeodomain-interacting protein kinase 1 modulates Daxx localization, phosphorylation, and transcriptional activity. *Mol Cell Biol* 23, 950-960.

Egan, D., Kim, J., Shaw, R.J., and Guan, K.L. (2011a). The autophagy initiating kinase ULK1 is regulated via opposing phosphorylation by AMPK and mTOR. *Autophagy* 7, 643-644.

Egan, D.F., Shackelford, D.B., Mihaylova, M.M., Gelino, S., Kohnz, R.A., Mair, W., Vasquez, D.S., Joshi, A., Gwinn, D.M., Taylor, R., *et al.* (2011b). Phosphorylation of ULK1 (hATG1) by AMP-activated protein kinase connects energy sensing to mitophagy. *Science* 331, 456-461.

Ehrensperger, M., Graber, S., Gaestel, M., and Buchner, J. (1997). Binding of non-native protein to Hsp25 during heat shock creates a reservoir of folding intermediates for reactivation. *EMBO J* 16, 221-229.

Ehrensperger, M., Lilie, H., Gaestel, M., and Buchner, J. (1999). The dynamics of Hsp25 quaternary structure. Structure and function of different oligomeric species. *J Biol Chem* 274, 14867-14874.

Ekins, S., Litterman, N.K., Arnold, R.J., Burgess, R.W., Freundlich, J.S., Gray, S.J., Higgins, J.J., Langley, B., Willis, D.E., Notterpek, L., *et al.* (2015). A brief review of recent Charcot-Marie-Tooth research and priorities. *F1000Research* 4, 53.

Evgrafov, O.V., Mersyanova, I., Irobi, J., Van Den Bosch, L., Dierick, I., Leung, C.L., Schagina, O., Verpoorten, N., Van Impe, K., Fedotov, V., *et al.* (2004). Mutant small heat-shock protein 27 causes axonal Charcot-Marie-Tooth disease and distal hereditary motor neuropathy. *Nature genetics* 36, 602-606.

Fabrizi, G.M., Cavallaro, T., Angiari, C., Cabrini, I., Taioli, F., Malerba, G., Bertolasi, L., and Rizzuto, N. (2007). Charcot-Marie-Tooth disease type 2E, a disorder of the cytoskeleton. *Brain* 130, 394-403.

Feng, M., Li, J., Wang, J., Ma, C., Jiao, Y., Wang, Y., Zhang, J., Sun, Q., Ju, Y., Gao, L., and Zhao, Y. (2014). High glucose increases LPS-induced DC apoptosis through modulation of ERK1/2, AKT and Bax/Bcl-2. *BMC gastroenterology* 14, 98.

Florez-McClure, M.L., Linseman, D.A., Chu, C.T., Barker, P.A., Bouchard, R.J., Le, S.S., Laessig, T.A., and Heidenreich, K.A. (2004). The p75 neurotrophin receptor can induce autophagy and death of cerebellar Purkinje neurons. *The Journal of neuroscience : the official journal of the Society for Neuroscience* 24, 4498-4509.

- Fragoso, G., Robertson, J., Athlan, E., Tam, E., Almazan, G., and Mushynski, W.E. (2003). Inhibition of p38 mitogen-activated protein kinase interferes with cell shape changes and gene expression associated with Schwann cell myelination. *Experimental neurology* 183, 34-46.
- Franklin, T.B., Krueger-Naug, A.M., Clarke, D.B., Arrigo, A.P., and Currie, R.W. (2005). The role of heat shock proteins Hsp70 and Hsp27 in cellular protection of the central nervous system. *Int J Hyperthermia* 21, 379-392.
- Fu, M.M., and Holzbaur, E.L. (2014). MAPK8IP1/JIP1 regulates the trafficking of autophagosomes in neurons. *Autophagy* 10, 2079-2081.
- Fu, M.M., Nirschl, J.J., and Holzbaur, E.L. (2014). LC3 binding to the scaffolding protein JIP1 regulates processive dynein-driven transport of autophagosomes. *Dev Cell* 29, 577-590.
- Fudge, N.J., and Mearow, K.M. (2013). Extracellular matrix-associated gene expression in adult sensory neuron populations cultured on a laminin substrate. *BMC neuroscience* 14, 15.
- Fulda, S., Gorman, A.M., Hori, O., and Samali, A. (2010). Cellular stress responses: cell survival and cell death. *International journal of cell biology* 2010, 214074.
- Fulga, T.A., Elson-Schwab, I., Khurana, V., Steinhilb, M.L., Spires, T.L., Hyman, B.T., and Feany, M.B. (2007). Abnormal bundling and accumulation of F-actin mediates tau-induced neuronal degeneration in vivo. *Nature cell biology* 9, 139-148.
- Gavazzi, I., Kumar, R.D., McMahon, S.B., and Cohen, J. (1999). Growth responses of different subpopulations of adult sensory neurons to neurotrophic factors in vitro. *The European journal of neuroscience* 11, 3405-3414.
- Gibert, B., Eckel, B., Gonin, V., Goldschneider, D., Fombonne, J., Deux, B., Mehlen, P., Arrigo, A.P., Clezardin, P., and Diaz-Latoud, C. (2012). Targeting heat shock protein 27 (HspB1) interferes with bone metastasis and tumour formation in vivo. *British journal of cancer* 107, 63-70.
- Goldbaum, O., Riedel, M., Stahnke, T., and Richter-Landsberg, C. (2009). The small heat shock protein HSP25 protects astrocytes against stress induced by proteasomal inhibition. *Glia* 57, 1566-1577.
- Goldshmit, Y., Kanner, S., Zacs, M., Frisca, F., Pinto, A.R., Currie, P.D., and Pinkas-Kramarski, R. (2015). Rapamycin increases neuronal survival, and reduces inflammation and astrocyte proliferation after spinal cord injury. *Molecular and cellular neurosciences* 68, 82-91.
- Graceffa, P. (2011). Hsp27-actin interaction. *Biochemistry research international* 2011, 901572.
- Greene, L.A., and Tischler, A.S. (1976). Establishment of a noradrenergic clonal line of rat adrenal pheochromocytoma cells which respond to nerve growth factor. *Proceedings of the National Academy of Sciences of the United States of America* 73, 2424-2428.

- Guay, J., Lambert, H., Gingras-Breton, G., Lavoie, J.N., Huot, J., and Landry, J. (1997). Regulation of actin filament dynamics by p38 map kinase-mediated phosphorylation of heat shock protein 27. *Journal of cell science* 110 ( Pt 3), 357-368.
- Gumy, L.F., Tan, C.L., and Fawcett, J.W. (2010). The role of local protein synthesis and degradation in axon regeneration. *Exp Neurol* 223, 28-37.
- Guo, J.S., Jing, P.B., Wang, J.A., Zhang, R., Jiang, B.C., Gao, Y.J., and Zhang, Z.J. (2015). Increased autophagic activity in dorsal root ganglion attenuates neuropathic pain following peripheral nerve injury. *Neuroscience letters* 599, 158-163.
- Guo, K., Gan, L., Zhang, S., Cui, F.J., Cun, W., Li, Y., Kang, N.X., Gao, M.D., and Liu, K.Y. (2012). Translocation of HSP27 into liver cancer cell nucleus may be associated with phosphorylation and O-GlcNAc glycosylation. *Oncology reports* 28, 494-500.
- Gwinn, D.M., Shackelford, D.B., Egan, D.F., Mihaylova, M.M., Mery, A., Vasquez, D.S., Turk, B.E., and Shaw, R.J. (2008). AMPK phosphorylation of raptor mediates a metabolic checkpoint. *Mol Cell* 30, 214-226.
- Hannan, K.M., Brandenburger, Y., Jenkins, A., Sharkey, K., Cavanaugh, A., Rothblum, L., Moss, T., Poortinga, G., McArthur, G.A., Pearson, R.B., and Hannan, R.D. (2003). mTOR-dependent regulation of ribosomal gene transcription requires S6K1 and is mediated by phosphorylation of the carboxy-terminal activation domain of the nucleolar transcription factor UBF. *Mol Cell Biol* 23, 8862-8877.
- Haslbeck, M., Franzmann, T., Weinfurter, D., and Buchner, J. (2005). Some like it hot: the structure and function of small heat-shock proteins. *Nat Struct Mol Biol* 12, 842-846.
- Hayes, D., Napoli, V., Mazurkie, A., Stafford, W.F., and Graceffa, P. (2009). Phosphorylation dependence of hsp27 multimeric size and molecular chaperone function. *J Biol Chem* 284, 18801-18807.
- He, C., Zhu, H., Li, H., Zou, M.H., and Xie, Z. (2013). Dissociation of Bcl-2-Beclin1 complex by activated AMPK enhances cardiac autophagy and protects against cardiomyocyte apoptosis in diabetes. *Diabetes* 62, 1270-1281.
- Head, M.W., Corbin, E., and Goldman, J.E. (1994). Coordinate and independent regulation of alpha B-crystallin and hsp27 expression in response to physiological stress. *J Cell Physiol* 159, 41-50.
- Heo, J.M., Ordureau, A., Paulo, J.A., Rinehart, J., and Harper, J.W. (2015). The PINK1-PARKIN Mitochondrial Ubiquitylation Pathway Drives a Program of OPTN/NDP52 Recruitment and TBK1 Activation to Promote Mitophagy. *Mol Cell* 60, 7-20.
- Hightower, L.E. (1991). Heat shock, stress proteins, chaperones, and proteotoxicity. *Cell* 66, 191-197.

- Hoeffler, C.A., Tang, W., Wong, H., Santillan, A., Patterson, R.J., Martinez, L.A., Tejada-Simon, M.V., Paylor, R., Hamilton, S.L., and Klann, E. (2008). Removal of FKBP12 enhances mTOR-Raptor interactions, LTP, memory, and perseverative/repetitive behavior. *Neuron* 60, 832-845.
- Hollenbach, A.D., McPherson, C.J., Mientjes, E.J., Iyengar, R., and Grosveld, G. (2002). Daxx and histone deacetylase II associate with chromatin through an interaction with core histones and the chromatin-associated protein Dek. *Journal of cell science* 115, 3319-3330.
- Hosokawa, N., Hara, T., Kaizuka, T., Kishi, C., Takamura, A., Miura, Y., Iemura, S., Natsume, T., Takehana, K., Yamada, N., *et al.* (2009). Nutrient-dependent mTORC1 association with the ULK1-Atg13-FIP200 complex required for autophagy. *Mol Biol Cell* 20, 1981-1991.
- Houlden, H., Laura, M., Wavrant-De Vrieze, F., Blake, J., Wood, N., and Reilly, M.M. (2008). Mutations in the HSP27 (HSPB1) gene cause dominant, recessive, and sporadic distal HMN/CMT type 2. *Neurology* 71, 1660-1668.
- Hsiao, V.C., Tian, R., Long, H., Der Perng, M., Brenner, M., Quinlan, R.A., and Goldman, J.E. (2005). Alexander-disease mutation of GFAP causes filament disorganization and decreased solubility of GFAP. *Journal of cell science* 118, 2057-2065.
- Hu, G., Gong, X., Wang, L., Liu, M., Liu, Y., Fu, X., Wang, W., Zhang, T., and Wang, X. (2016). Triptolide Promotes the Clearance of alpha-Synuclein by Enhancing Autophagy in Neuronal Cells. *Molecular neurobiology*.
- Huot, J., Houle, F., Spitz, D.R., and Landry, J. (1996). HSP27 phosphorylation-mediated resistance against actin fragmentation and cell death induced by oxidative stress. *Cancer research* 56, 273-279.
- Huot, J., Lambert, H., Lavoie, J.N., Guimond, A., Houle, F., and Landry, J. (1995). Characterization of 45-kDa/54-kDa HSP27 kinase, a stress-sensitive kinase which may activate the phosphorylation-dependent protective function of mammalian 27-kDa heat-shock protein HSP27. *European journal of biochemistry / FEBS* 227, 416-427.
- Inoki, K., Li, Y., Xu, T., and Guan, K.L. (2003a). Rheb GTPase is a direct target of TSC2 GAP activity and regulates mTOR signaling. *Genes Dev* 17, 1829-1834.
- Inoki, K., Zhu, T., and Guan, K.L. (2003b). TSC2 mediates cellular energy response to control cell growth and survival. *Cell* 115, 577-590.
- Jacinto, E., Loewith, R., Schmidt, A., Lin, S., Ruegg, M.A., Hall, A., and Hall, M.N. (2004). Mammalian TOR complex 2 controls the actin cytoskeleton and is rapamycin insensitive. *Nature cell biology* 6, 1122-1128.
- Jaeger, P.A., Pickford, F., Sun, C.H., Lucin, K.M., Masliah, E., and Wyss-Coray, T. (2010). Regulation of amyloid precursor protein processing by the Beclin 1 complex. *PloS one* 5, e11102.

- Jakob, U., Gaestel, M., Engel, K., and Buchner, J. (1993). Small heat shock proteins are molecular chaperones. *J Biol Chem* 268, 1517-1520.
- Jia, Y., Wu, S.L., Isenberg, J.S., Dai, S., Sipes, J.M., Field, L., Zeng, B., Bandle, R.W., Ridnour, L.A., Wink, D.A., *et al.* (2010). Thiolutin inhibits endothelial cell adhesion by perturbing Hsp27 interactions with components of the actin and intermediate filament cytoskeleton. *Cell Stress Chaperones* 15, 165-181.
- Jiang, P., and Mizushima, N. (2015). LC3- and p62-based biochemical methods for the analysis of autophagy progression in mammalian cells. *Methods* 75, 13-18.
- Jog, N.R., Jala, V.R., Ward, R.A., Rane, M.J., Haribabu, B., and McLeish, K.R. (2007). Heat shock protein 27 regulates neutrophil chemotaxis and exocytosis through two independent mechanisms. *Journal of immunology* 178, 2421-2428.
- Jovceviski, B., Kelly, M.A., Rote, A.P., Berg, T., Gastall, H.Y., Benesch, J.L., Aquilina, J.A., and Ecroyd, H. (2015). Phosphomimics destabilize Hsp27 oligomeric assemblies and enhance chaperone activity. *Chemistry & biology* 22, 186-195.
- Kampinga, H.H., Hageman, J., Vos, M.J., Kubota, H., Tanguay, R.M., Bruford, E.A., Cheetham, M.E., Chen, B., and Hightower, L.E. (2009). Guidelines for the nomenclature of the human heat shock proteins. *Cell Stress Chaperones* 14, 105-111.
- Kanagasabai, R., Karthikeyan, K., Vedam, K., Qien, W., Zhu, Q., and Ilangovan, G. (2010). Hsp27 protects adenocarcinoma cells from UV-induced apoptosis by Akt and p21-dependent pathways of survival. *Molecular cancer research : MCR* 8, 1399-1412.
- Kang, R., Livesey, K.M., Zeh, H.J., Loze, M.T., and Tang, D. (2010). HMGB1: a novel Beclin 1-binding protein active in autophagy. *Autophagy* 6, 1209-1211.
- Karamoysoyli, E., Burnand, R.C., Tomlinson, D.R., and Gardiner, N.J. (2008). Neuritin mediates nerve growth factor-induced axonal regeneration and is deficient in experimental diabetic neuropathy. *Diabetes* 57, 181-189.
- Kato, K., Shinohara, H., Goto, S., Inaguma, Y., Morishita, R., and Asano, T. (1992). Copurification of Small Heat-Shock Protein with Alpha-B Crystallin from Human Skeletal-Muscle. *Journal of Biological Chemistry* 267, 7718-7725.
- Kim, K.K., Kim, R., and Kim, S.H. (1998). Crystal structure of a small heat-shock protein. *Nature* 394, 595-599.
- Kim, M., and Lee, J.H. (2015). Identification of an AMPK Phosphorylation Site in *Drosophila* TSC2 (gigas) that Regulate Cell Growth. *Int J Mol Sci* 16, 7015-7026.
- Kim, S.A., Yoon, J.H., Lee, S.H., and Ahn, S.G. (2005). Polo-like kinase 1 phosphorylates heat shock transcription factor 1 and mediates its nuclear translocation during heat stress. *J Biol Chem* 280, 12653-12657.

King, M., Nafar, F., Clarke, J., and Mearow, K. (2009). The small heat shock protein Hsp27 protects cortical neurons against the toxic effects of beta-amyloid peptide. *Journal of neuroscience research* 87, 3161-3175.

Kirbach, B.B., and Golenhofen, N. (2011). Differential expression and induction of small heat shock proteins in rat brain and cultured hippocampal neurons. *Journal of neuroscience research* 89, 162-175.

Kirisako, T., Baba, M., Ishihara, N., Miyazawa, K., Ohsumi, M., Yoshimori, T., Noda, T., and Ohsumi, Y. (1999). Formation process of autophagosome is traced with Apg8/Aut7p in yeast. *The Journal of cell biology* 147, 435-446.

Klionsky, D.J., and Codogno, P. (2013). The mechanism and physiological function of macroautophagy. *J Innate Immun* 5, 427-433.

Knoferle, J., Koch, J.C., Ostendorf, T., Michel, U., Planchamp, V., Vutova, P., Tonges, L., Stadelmann, C., Bruck, W., Bahr, M., and Lingor, P. (2010). Mechanisms of acute axonal degeneration in the optic nerve in vivo. *Proceedings of the National Academy of Sciences of the United States of America* 107, 6064-6069.

Kobayashi, R., Tawata, M., and Field, J.B. (1982). Actin in Triton-insoluble cytoskeleton of thyroid. *Metabolism* 31, 133-138.

Komatsu, M., Waguri, S., Chiba, T., Murata, S., Iwata, J., Tanida, I., Ueno, T., Koike, M., Uchiyama, Y., Kominami, E., and Tanaka, K. (2006). Loss of autophagy in the central nervous system causes neurodegeneration in mice. *Nature* 441, 880-884.

Komiya, K., Uchida, T., Ueno, T., Koike, M., Abe, H., Hirose, T., Kawamori, R., Uchiyama, Y., Kominami, E., Fujitani, Y., and Watada, H. (2010). Free fatty acids stimulate autophagy in pancreatic beta-cells via JNK pathway. *Biochemical and biophysical research communications* 401, 561-567.

Korngut, L., Ma, C.H., Martinez, J.A., Toth, C.C., Guo, G.F., Singh, V., Woolf, C.J., and Zochodne, D.W. (2012). Overexpression of human HSP27 protects sensory neurons from diabetes. *Neurobiology of disease* 47, 436-443.

Kosacka, J., Nowicki, M., Blucher, M., Baum, P., Stockinger, M., Toyka, K.V., Kloting, I., Stumvoll, M., Serke, H., Bechmann, I., and Kloting, N. (2013). Increased autophagy in peripheral nerves may protect Wistar Ottawa Karlsburg W rats against neuropathy. *Experimental neurology* 250, 125-135.

Kostenko, S., and Moens, U. (2009). Heat shock protein 27 phosphorylation: kinases, phosphatases, functions and pathology. *Cell Mol Life Sci* 66, 3289-3307.

Lambert, H., Charette, S.J., Bernier, A.F., Guimond, A., and Landry, J. (1999). HSP27 multimerization mediated by phosphorylation-sensitive intermolecular interactions at the amino terminus. *J Biol Chem* 274, 9378-9385.

- Landry, J., and Huot, J. (1995). Modulation of actin dynamics during stress and physiological stimulation by a signaling pathway involving p38 MAP kinase and heat-shock protein 27. *Biochem Cell Biol* 73, 703-707.
- Landry, J., and Huot, J. (1999). Regulation of actin dynamics by stress-activated protein kinase 2 (SAPK2)-dependent phosphorylation of heat-shock protein of 27 kDa (Hsp27). *Biochem Soc Symp* 64, 79-89.
- Landry, J., Lambert, H., Zhou, M., Lavoie, J.N., Hickey, E., Weber, L.A., and Anderson, C.W. (1992). Human HSP27 is phosphorylated at serines 78 and 82 by heat shock and mitogen-activated kinases that recognize the same amino acid motif as S6 kinase II. *J Biol Chem* 267, 794-803.
- Lavoie, J.N., Gingras-Breton, G., Tanguay, R.M., and Landry, J. (1993). Induction of Chinese hamster HSP27 gene expression in mouse cells confers resistance to heat shock. HSP27 stabilization of the microfilament organization. *J Biol Chem* 268, 3420-3429.
- Lavoie, J.N., Lambert, H., Hickey, E., Weber, L.A., and Landry, J. (1995). Modulation of cellular thermoresistance and actin filament stability accompanies phosphorylation-induced changes in the oligomeric structure of heat shock protein 27. *Mol Cell Biol* 15, 505-516.
- Lazarou, M., Sliter, D.A., Kane, L.A., Sarraf, S.A., Wang, C., Burman, J.L., Sideris, D.P., Fogel, A.I., and Youle, R.J. (2015). The ubiquitin kinase PINK1 recruits autophagy receptors to induce mitophagy. *Nature* 524, 309-314.
- Lee, G.J., Roseman, A.M., Saibil, H.R., and Vierling, E. (1997). A small heat shock protein stably binds heat-denatured model substrates and can maintain a substrate in a folding-competent state. *EMBO J* 16, 659-671.
- Lee, J.H., Sun, D., Cho, K.J., Kim, M.S., Hong, M.H., Kim, I.K., Lee, J.S., and Lee, J.H. (2007). Overexpression of human 27 kDa heat shock protein in laryngeal cancer cells confers chemoresistance associated with cell growth delay. *J Cancer Res Clin Oncol* 133, 37-46.
- Lee, J.W., Park, S., Takahashi, Y., and Wang, H.G. (2010). The association of AMPK with ULK1 regulates autophagy. *PLoS one* 5, e15394.
- Lelj-Garolla, B., and Mauk, A.G. (2006). Self-association and chaperone activity of Hsp27 are thermally activated. *J Biol Chem* 281, 8169-8174.
- Lewis, S.E., Mannion, R.J., White, F.A., Coggeshall, R.E., Beggs, S., Costigan, M., Martin, J.L., Dillmann, W.H., and Woolf, C.J. (1999). A role for HSP27 in sensory neuron survival. *The Journal of neuroscience : the official journal of the Society for Neuroscience* 19, 8945-8953.
- Li, R., Pei, H., Watson, D.K., and Papas, T.S. (2000). EAP1/Daxx interacts with ETS1 and represses transcriptional activation of ETS1 target genes. *Oncogene* 19, 745-753.

- Li, T., Ying, L., Wang, H., Li, N., Fu, W., Guo, Z., and Xu, L. (2012a). Microcystin-LR induces ceramide to regulate PP2A and destabilize cytoskeleton in HEK293 cells. *Toxicol Sci* 128, 147-157.
- Li, W.W., Li, J., and Bao, J.K. (2012b). Microautophagy: lesser-known self-eating. *Cell Mol Life Sci* 69, 1125-1136.
- Lindsay, R.M. (1988). Nerve growth factors (NGF, BDNF) enhance axonal regeneration but are not required for survival of adult sensory neurons. *J Neurosci* 8, 2394-2405.
- Lipinski, M.M., Zheng, B., Lu, T., Yan, Z., Py, B.F., Ng, A., Xavier, R.J., Li, C., Yankner, B.A., Scherzer, C.R., and Yuan, J. (2010). Genome-wide analysis reveals mechanisms modulating autophagy in normal brain aging and in Alzheimer's disease. *Proceedings of the National Academy of Sciences of the United States of America* 107, 14164-14169.
- Liu, S., Sarkar, C., Dinizo, M., Faden, A.I., Koh, E.Y., Lipinski, M.M., and Wu, J. (2015). Disrupted autophagy after spinal cord injury is associated with ER stress and neuronal cell death. *Cell Death Dis* 6, e1582.
- Long, X., Lin, Y., Ortiz-Vega, S., Yonezawa, K., and Avruch, J. (2005a). Rheb binds and regulates the mTOR kinase. *Curr Biol* 15, 702-713.
- Long, X., Ortiz-Vega, S., Lin, Y., and Avruch, J. (2005b). Rheb binding to mammalian target of rapamycin (mTOR) is regulated by amino acid sufficiency. *J Biol Chem* 280, 23433-23436.
- Loos, B., du Toit, A., and Hofmeyr, J.H. (2014). Defining and measuring autophagosome flux-concept and reality. *Autophagy* 10, 2087-2096.
- Maday, S., and Holzbaur, E.L. (2012). Autophagosome assembly and cargo capture in the distal axon. *Autophagy* 8, 858-860.
- Maday, S., and Holzbaur, E.L. (2014). Autophagosome biogenesis in primary neurons follows an ordered and spatially regulated pathway. *Dev Cell* 30, 71-85.
- Maday, S., Wallace, K.E., and Holzbaur, E.L. (2012). Autophagosomes initiate distally and mature during transport toward the cell soma in primary neurons. *J Cell Biol* 196, 407-417.
- Maejima, Y., Kyoji, S., Zhai, P., Liu, T., Li, H., Ivessa, A., Sciarretta, S., Del Re, D.P., Zablocki, D.K., Hsu, C.P., *et al.* (2013). Mst1 inhibits autophagy by promoting the interaction between Beclin1 and Bcl-2. *Nature medicine* 19, 1478-1488.
- Marinelli, S., Nazio, F., Tinari, A., Ciarlo, L., D'Amelio, M., Pieroni, L., Vacca, V., Urbani, A., Cecconi, F., Malorni, W., and Pavone, F. (2014). Schwann cell autophagy counteracts the onset and chronification of neuropathic pain. *Pain* 155, 93-107.
- McDonald, P.C., Oloumi, A., Mills, J., Dobрева, I., Maidan, M., Gray, V., Wederell, E.D., Bally, M.B., Foster, L.J., and Dedhar, S. (2008). Rictor and integrin-linked kinase interact and regulate Akt phosphorylation and cancer cell survival. *Cancer research* 68, 1618-1624.

- Mearow, K.M., Dodge, M.E., Rahimtula, M., and Yegappan, C. (2002). Stress-mediated signaling in PC12 cells - the role of the small heat shock protein, Hsp27, and Akt in protecting cells from heat stress and nerve growth factor withdrawal. *Journal of neurochemistry* 83, 452-462.
- Mehlen, P., and Arrigo, A.P. (1994). The serum-induced phosphorylation of mammalian hsp27 correlates with changes in its intracellular localization and levels of oligomerization. *European journal of biochemistry / FEBS* 221, 327-334.
- Mehlen, P., Mehlen, A., Guillet, D., Preville, X., and Arrigo, A.P. (1995). Tumor necrosis factor- $\alpha$  induces changes in the phosphorylation, cellular localization, and oligomerization of human hsp27, a stress protein that confers cellular resistance to this cytokine. *Journal of cellular biochemistry* 58, 248-259.
- Menzies, F.M., Fleming, A., and Rubinsztein, D.C. (2015). Compromised autophagy and neurodegenerative diseases. *Nat Rev Neurosci* 16, 345-357.
- Michaelson, J.S., Bader, D., Kuo, F., Kozak, C., and Leder, P. (1999). Loss of Daxx, a promiscuously interacting protein, results in extensive apoptosis in early mouse development. *Genes Dev* 13, 1918-1923.
- Miron, T., Vancompernelle, K., Vandekerckhove, J., Wilchek, M., and Geiger, B. (1991). A 25-kD inhibitor of actin polymerization is a low molecular mass heat shock protein. *The Journal of cell biology* 114, 255-261.
- Mizui, T., Yamashina, S., Tanida, I., Takei, Y., Ueno, T., Sakamoto, N., Ikejima, K., Kitamura, T., Enomoto, N., Sakai, T., *et al.* (2010). Inhibition of hepatitis C virus replication by chloroquine targeting virus-associated autophagy. *J Gastroenterol* 45, 195-203.
- Mizushima, N., Yamamoto, A., Hatano, M., Kobayashi, Y., Kabeya, Y., Suzuki, K., Tokuhisu, T., Ohsumi, Y., and Yoshimori, T. (2001). Dissection of autophagosome formation using Apg5-deficient mouse embryonic stem cells. *The Journal of cell biology* 152, 657-668.
- Mizushima, N., Yamamoto, A., Matsui, M., Yoshimori, T., and Ohsumi, Y. (2004). In vivo analysis of autophagy in response to nutrient starvation using transgenic mice expressing a fluorescent autophagosome marker. *Mol Biol Cell* 15, 1101-1111.
- Mizushima, N., Yoshimori, T., and Levine, B. (2010). Methods in mammalian autophagy research. *Cell* 140, 313-326.
- Mohseni, S. (2011). Autophagy in insulin-induced hypoglycaemic neuropathy. *Pathology* 43, 254-260.
- Morita, M., Gravel, S.P., Chenard, V., Sikstrom, K., Zheng, L., Alain, T., Gandin, V., Avizonis, D., Arguello, M., Zakaria, C., *et al.* (2013). mTORC1 controls mitochondrial activity and biogenesis through 4E-BP-dependent translational regulation. *Cell metabolism* 18, 698-711.

- Morita, M., Gravel, S.P., Hulea, L., Larsson, O., Pollak, M., St-Pierre, J., and Topisirovic, I. (2015). mTOR coordinates protein synthesis, mitochondrial activity and proliferation. *Cell cycle* 14, 473-480.
- Mortimore, G.E., and Schworer, C.M. (1977). Induction of autophagy by amino-acid deprivation in perfused rat liver. *Nature* 270, 174-176.
- Mounier, N., and Arrigo, A.P. (2002). Actin cytoskeleton and small heat shock proteins: how do they interact? *Cell Stress Chaperones* 7, 167-176.
- Muromoto, R., Sugiyama, K., Takachi, A., Imoto, S., Sato, N., Yamamoto, T., Oritani, K., Shimoda, K., and Matsuda, T. (2004). Physical and functional interactions between Daxx and DNA methyltransferase 1-associated protein, DMAP1. *Journal of immunology* 172, 2985-2993.
- Mymrikov, E.V., Seit-Nebi, A.S., and Gusev, N.B. (2011). Large potentials of small heat shock proteins. *Physiol Rev* 91, 1123-1159.
- Mymrikov, E.V., Seit-Nebi, A.S., and Gusev, N.B. (2012). Heterooligomeric complexes of human small heat shock proteins. *Cell Stress Chaperones* 17, 157-169.
- Narumi, T., Shishido, T., Otaki, Y., Kadowaki, S., Honda, Y., Funayama, A., Honda, S., Hasegawa, H., Kinoshita, D., Yokoyama, M., *et al.* (2015). High-mobility group box 1-mediated heat shock protein beta 1 expression attenuates mitochondrial dysfunction and apoptosis. *Journal of molecular and cellular cardiology* 82, 1-12.
- Nemes, Z., Devreese, B., Steinert, P.M., Van Beeumen, J., and Fesus, L. (2004). Cross-linking of ubiquitin, HSP27, parkin, and alpha-synuclein by gamma-glutamyl-epsilon-lysine bonds in Alzheimer's neurofibrillary tangles. *FASEB journal : official publication of the Federation of American Societies for Experimental Biology* 18, 1135-1137.
- Nicks, J., Lee, S., Harris, A., Falk, D.J., Todd, A.G., Arredondo, K., Dunn, W.A., Jr., and Notterpek, L. (2014). Rapamycin improves peripheral nerve myelination while it fails to benefit neuromuscular performance in neuropathic mice. *Neurobiol Dis* 70, 224-236.
- Nishiyama, J., Miura, E., Mizushima, N., Watanabe, M., and Yuzaki, M. (2007). Aberrant membranes and double-membrane structures accumulate in the axons of Atg5-null Purkinje cells before neuronal death. *Autophagy* 3, 591-596.
- Nixon, R.A., Wegiel, J., Kumar, A., Yu, W.H., Peterhoff, C., Cataldo, A., and Cuervo, A.M. (2005). Extensive involvement of autophagy in Alzheimer disease: an immuno-electron microscopy study. *J Neuropathol Exp Neurol* 64, 113-122.
- Nollen, E.A.A., Kabakov, A.E., Brunsting, J.F., Kanon, B., Höhfeld, J., and Kampinga, H.H. (2001). Modulation of in Vivo HSP70 Chaperone Activity by Hip and Bag-1. *Journal of Biological Chemistry* 276, 4677-4682.

- Nomura, N., Nomura, M., Sugiyama, K., and Hamada, J. (2007). Phorbol 12-myristate 13-acetate (PMA)-induced migration of glioblastoma cells is mediated via p38MAPK/Hsp27 pathway. *Biochem Pharmacol* 74, 690-701.
- O'Callaghan-Sunol, C., Gabai, V.L., and Sherman, M.Y. (2007). Hsp27 modulates p53 signaling and suppresses cellular senescence. *Cancer research* 67, 11779-11788.
- O'Shaughnessy, R.F., Welti, J.C., Cooke, J.C., Avilion, A.A., Monks, B., Birnbaum, M.J., and Byrne, C. (2007). AKT-dependent HspB1 (Hsp27) activity in epidermal differentiation. *J Biol Chem* 282, 17297-17305.
- Ochaba, J., Lukacsovich, T., Csikos, G., Zheng, S., Margulis, J., Salazar, L., Mao, K., Lau, A.L., Yeung, S.Y., Humbert, S., *et al.* (2014). Potential function for the Huntingtin protein as a scaffold for selective autophagy. *Proceedings of the National Academy of Sciences of the United States of America* 111, 16889-16894.
- Ojha, J., Karmegam, R.V., Masilamoni, J.G., Terry, A.V., and Cashikar, A.G. (2011a). Behavioral defects in chaperone-deficient Alzheimer's disease model mice. *PLoS one* 6, e16550.
- Ojha, J., Masilamoni, G., Dunlap, D., Udoff, R.A., and Cashikar, A.G. (2011b). Sequestration of toxic oligomers by HspB1 as a cytoprotective mechanism. *Mol Cell Biol* 31, 3146-3157.
- Okada, M., Hatakeyama, T., Itoh, H., Tokuta, N., Tokumitsu, H., and Kobayashi, R. (2004). S100A1 Is a Novel Molecular Chaperone and a Member of the Hsp70/Hsp90 Multichaperone Complex. *Journal of Biological Chemistry* 279, 4221-4233.
- Oshiro, N., Yoshino, K., Hidayat, S., Tokunaga, C., Hara, K., Eguchi, S., Avruch, J., and Yonezawa, K. (2004). Dissociation of raptor from mTOR is a mechanism of rapamycin-induced inhibition of mTOR function. *Genes Cells* 9, 359-366.
- Osman, A.A., Dahlin, L.B., Thomsen, N.O., and Mohseni, S. (2015). Autophagy in the posterior interosseous nerve of patients with type 1 and type 2 diabetes mellitus: an ultrastructural study. *Diabetologia* 58, 625-632.
- Pankiv, S., Clausen, T.H., Lamark, T., Brech, A., Bruun, J.A., Outzen, H., Overvatn, A., Bjorkoy, G., and Johansen, T. (2007). p62/SQSTM1 binds directly to Atg8/LC3 to facilitate degradation of ubiquitinated protein aggregates by autophagy. *J Biol Chem* 282, 24131-24145.
- Parcellier, A., Schmitt, E., Gurbuxani, S., Seigneurin-Berny, D., Pance, A., Chantome, A., Plenchette, S., Khochbin, S., Solary, E., and Garrido, C. (2003). HSP27 is a ubiquitin-binding protein involved in I-kappaBalpha proteasomal degradation. *Mol Cell Biol* 23, 5790-5802.
- Parzych, K.R., and Klionsky, D.J. (2014). An overview of autophagy: morphology, mechanism, and regulation. *Antioxidants & redox signaling* 20, 460-473.
- Pasta, S.Y., Raman, B., Ramakrishna, T., and Rao Ch, M. (2004). The IXI/V motif in the C-terminal extension of alpha-crystallins: alternative interactions and oligomeric assemblies. *Mol Vis* 10, 655-662.

- Pattingre, S., Tassa, A., Qu, X., Garuti, R., Liang, X.H., Mizushima, N., Packer, M., Schneider, M.D., and Levine, B. (2005). Bcl-2 antiapoptotic proteins inhibit Beclin 1-dependent autophagy. *Cell* 122, 927-939.
- Paul, C., Manero, F., Gonin, S., Kretz-Remy, C., Viot, S., and Arrigo, A.P. (2002). Hsp27 as a negative regulator of cytochrome C release. *Mol Cell Biol* 22, 816-834.
- Pedersen, J.T., and Sigurdsson, E.M. (2015). Tau immunotherapy for Alzheimer's disease. *Trends in molecular medicine*.
- Pei, B., Zhao, M., Miller, B.C., Vela, J.L., Bruinsma, M.W., Virgin, H.W., and Kronenberg, M. (2015). Invariant NKT Cells Require Autophagy To Coordinate Proliferation and Survival Signals during Differentiation. *Journal of immunology*.
- Perng, M.D., Cairns, L., van den, I.P., Prescott, A., Hutcheson, A.M., and Quinlan, R.A. (1999). Intermediate filament interactions can be altered by HSP27 and alphaB-crystallin. *Journal of cell science* 112 ( Pt 13), 2099-2112.
- Perrin, V., Regulier, E., Abbas-Terki, T., Hassig, R., Brouillet, E., Aebischer, P., Luthi-Carter, R., and Deglon, N. (2007). Neuroprotection by Hsp104 and Hsp27 in lentiviral-based rat models of Huntington's disease. *Molecular therapy : the journal of the American Society of Gene Therapy* 15, 903-911.
- Persson, A.K., Kim, I., Zhao, P., Estacion, M., Black, J.A., and Waxman, S.G. (2013). Sodium channels contribute to degeneration of dorsal root ganglion neurites induced by mitochondrial dysfunction in an in vitro model of axonal injury. *The Journal of neuroscience : the official journal of the Society for Neuroscience* 33, 19250-19261.
- Petruska, J.C., Napaporn, J., Johnson, R.D., Gu, J.G., and Cooper, B.Y. (2000). Subclassified acutely dissociated cells of rat DRG: histochemistry and patterns of capsaicin-, proton-, and ATP-activated currents. *Journal of neurophysiology* 84, 2365-2379.
- Pfaffl, M.W. (2001). A new mathematical model for relative quantification in real-time RT-PCR. *Nucleic acids research* 29, e45.
- Pichon, S., Bryckaert, M., and Berrou, E. (2004). Control of actin dynamics by p38 MAP kinase - Hsp27 distribution in the lamellipodium of smooth muscle cells. *Journal of cell science* 117, 2569-2577.
- Pickford, F., Masliah, E., Britschgi, M., Lucin, K., Narasimhan, R., Jaeger, P.A., Small, S., Spencer, B., Rockenstein, E., Levine, B., and Wyss-Coray, T. (2008). The autophagy-related protein beclin 1 shows reduced expression in early Alzheimer disease and regulates amyloid beta accumulation in mice. *J Clin Invest* 118, 2190-2199.
- Piotrowicz, R.S., Hickey, E., and Levin, E.G. (1998). Heat shock protein 27 kDa expression and phosphorylation regulates endothelial cell migration. *FASEB journal : official publication of the Federation of American Societies for Experimental Biology* 12, 1481-1490.

- Pivovarova, A.V., Chebotareva, N.A., Chernik, I.S., Gusev, N.B., and Levitsky, D.I. (2007). Small heat shock protein Hsp27 prevents heat-induced aggregation of F-actin by forming soluble complexes with denatured actin. *FEBS J* 274, 5937-5948.
- Pivovarova, A.V., Mikhailova, V.V., Chernik, I.S., Chebotareva, N.A., Levitsky, D.I., and Gusev, N.B. (2005). Effects of small heat shock proteins on the thermal denaturation and aggregation of F-actin. *Biochemical and biophysical research communications* 331, 1548-1553.
- Plantman, S., Patarroyo, M., Fried, K., Domogatskaya, A., Tryggvason, K., Hammarberg, H., and Cullheim, S. (2008). Integrin-laminin interactions controlling neurite outgrowth from adult DRG neurons in vitro. *Mol Cell Neurosci* 39, 50-62.
- Polleux, F., and Snider, W. (2010). Initiating and growing an axon. *Cold Spring Harb Perspect Biol* 2, a001925.
- Portovedo, M., Ignacio-Souza, L.M., Bombassaro, B., Coope, A., Reginato, A., Razolli, D.S., Torsoni, M.A., Torsoni, A.S., Leal, R.F., Velloso, L.A., and Milanski, M. (2015). Saturated Fatty Acids Modulate Autophagy's Proteins in the Hypothalamus. *PloS one* 10, e0119850.
- Pourhamidi, K., Dahlin, L.B., Boman, K., and Rolandsson, O. (2011). Heat shock protein 27 is associated with better nerve function and fewer signs of neuropathy. *Diabetologia* 54, 3143-3149.
- Preville, X., Salvemini, F., Giraud, S., Chaufour, S., Paul, C., Stepien, G., Ursini, M.V., and Arrigo, A.P. (1999). Mammalian small stress proteins protect against oxidative stress through their ability to increase glucose-6-phosphate dehydrogenase activity and by maintaining optimal cellular detoxifying machinery. *Experimental cell research* 247, 61-78.
- Priestley, J.V., Michael, G.J., Averill, S., Liu, M., and Willmott, N. (2002). Regulation of nociceptive neurons by nerve growth factor and glial cell line derived neurotrophic factor. *Can J Physiol Pharmacol* 80, 495-505.
- Qi, S., Xin, Y., Qi, Z., Xu, Y., Diao, Y., Lan, L., Luo, L., and Yin, Z. (2014a). HSP27 phosphorylation modulates TRAIL-induced activation of Src-Akt/ERK signaling through interaction with beta-arrestin2. *Cellular signalling* 26, 594-602.
- Qi, Z., Shen, L., Zhou, H., Jiang, Y., Lan, L., Luo, L., and Yin, Z. (2014b). Phosphorylation of heat shock protein 27 antagonizes TNF-alpha induced HeLa cell apoptosis via regulating TAK1 ubiquitination and activation of p38 and ERK signaling. *Cellular signalling* 26, 1616-1625.
- Qu, L., Liang, X., Gu, B., and Liu, W. (2014). Quercetin alleviates high glucose-induced Schwann cell damage by autophagy. *Neural Regen Res* 9, 1195-1203.
- Quigley, D.J., Gorman, A.M., and Samali, A. (2003). Heat shock protects PC12 cells against MPP+ toxicity. *Brain Res* 993, 133-139.
- Quinlan, R. (2002). Cytoskeletal competence requires protein chaperones. *Prog Mol Subcell Biol* 28, 219-233.

Quraishe, S., Asuni, A., Boelens, W.C., O'Connor, V., and Wyttenbach, A. (2008). Expression of the small heat shock protein family in the mouse CNS: differential anatomical and biochemical compartmentalization. *Neuroscience* 153, 483-491.

Radad, K., Moldzio, R., and Rausch, W.D. (2015). Rapamycin protects dopaminergic neurons against rotenone-induced cell death in primary mesencephalic cell culture. *Folia neuropathologica / Association of Polish Neuropathologists and Medical Research Centre, Polish Academy of Sciences* 53, 250-261.

Raff, M.C., Whitmore, A.V., and Finn, J.T. (2002). Axonal self-destruction and neurodegeneration. *Science* 296, 868-871.

Ramirez, A.E., Pacheco, C.R., Aguayo, L.G., and Opazo, C.M. (2014). Rapamycin protects against Abeta-induced synaptotoxicity by increasing presynaptic activity in hippocampal neurons. *Biochimica et biophysica acta* 1842, 1495-1501.

Rangaraju, S., Verrier, J.D., Madorsky, I., Nicks, J., Dunn, W.A., Jr., and Notterpek, L. (2010). Rapamycin activates autophagy and improves myelination in explant cultures from neuropathic mice. *J Neurosci* 30, 11388-11397.

Ravikumar, B., Sarkar, S., Davies, J.E., Futter, M., Garcia-Arencibia, M., Green-Thompson, Z.W., Jimenez-Sanchez, M., Korolchuk, V.I., Lichtenberg, M., Luo, S., *et al.* (2010). Regulation of mammalian autophagy in physiology and pathophysiology. *Physiol Rev* 90, 1383-1435.

Ravikumar, B., Vacher, C., Berger, Z., Davies, J.E., Luo, S., Oroz, L.G., Scaravilli, F., Easton, D.F., Duden, R., O'Kane, C.J., and Rubinsztein, D.C. (2004). Inhibition of mTOR induces autophagy and reduces toxicity of polyglutamine expansions in fly and mouse models of Huntington disease. *Nature genetics* 36, 585-595.

Renault, T.T., Floros, K.V., and Chipuk, J.E. (2013). BAK/BAX activation and cytochrome c release assays using isolated mitochondria. *Methods* 61, 146-155.

Rich, K.A., Burkett, C., and Webster, P. (2003). Cytoplasmic bacteria can be targets for autophagy. *Cell Microbiol* 5, 455-468.

Rieber, M., and Rieber, M.S. (2008). Sensitization to radiation-induced DNA damage accelerates loss of bcl-2 and increases apoptosis and autophagy. *Cancer Biol Ther* 7, 1561-1566.

Ritossa, F. (1962). New Puffing Pattern Induced by Temperature Shock and Dnp in *Drosophila*. *Experientia* 18, 571-573.

Roczniak-Ferguson, A., Petit, C.S., Froehlich, F., Qian, S., Ky, J., Angarola, B., Walther, T.C., and Ferguson, S.M. (2012). The transcription factor TFEB links mTORC1 signaling to transcriptional control of lysosome homeostasis. *Sci Signal* 5, ra42.

Rodriguez-Muela, N., Germain, F., Marino, G., Fitze, P.S., and Boya, P. (2012). Autophagy promotes survival of retinal ganglion cells after optic nerve axotomy in mice. *Cell Death Differ* 19, 162-169.

Rogalla, T., Ehrnsperger, M., Preville, X., Kotlyarov, A., Lutsch, G., Ducasse, C., Paul, C., Wieske, M., Arrigo, A.P., Buchner, J., and Gaestel, M. (1999). Regulation of Hsp27 oligomerization, chaperone function, and protective activity against oxidative stress/tumor necrosis factor alpha by phosphorylation. *J Biol Chem* 274, 18947-18956.

Rohn, T.T., Wirawan, E., Brown, R.J., Harris, J.R., Masliah, E., and Vandenabeele, P. (2011). Depletion of Beclin-1 due to proteolytic cleavage by caspases in the Alzheimer's disease brain. *Neurobiology of disease* 43, 68-78.

Rouse, J., Cohen, P., Trigon, S., Morange, M., Alonso-Llamazares, A., Zamanillo, D., Hunt, T., and Nebreda, A.R. (1994). A novel kinase cascade triggered by stress and heat shock that stimulates MAPKAP kinase-2 and phosphorylation of the small heat shock proteins. *Cell* 78, 1027-1037.

Rousseau, S., Houle, F., Kotanides, H., Witte, L., Waltenberger, J., Landry, J., and Huot, J. (2000). Vascular endothelial growth factor (VEGF)-driven actin-based motility is mediated by VEGFR2 and requires concerted activation of stress-activated protein kinase 2 (SAPK2/p38) and geldanamycin-sensitive phosphorylation of focal adhesion kinase. *J Biol Chem* 275, 10661-10672.

Roy Chowdhury, S.K., Smith, D.R., Saleh, A., Schapansky, J., Marquez, A., Gomes, S., Akude, E., Morrow, D., Calcutt, N.A., and Fernyhough, P. (2012). Impaired adenosine monophosphate-activated protein kinase signalling in dorsal root ganglia neurons is linked to mitochondrial dysfunction and peripheral neuropathy in diabetes. *Brain* 135, 1751-1766.

Rui, Y.N., Xu, Z., Patel, B., Chen, Z., Chen, D., Tito, A., David, G., Sun, Y., Stimming, E.F., Bellen, H.J., *et al.* (2015). Huntingtin functions as a scaffold for selective macroautophagy. *Nature cell biology* 17, 262-275.

Russell, R.C., Yuan, H.X., and Guan, K.L. (2014). Autophagy regulation by nutrient signaling. *Cell Res* 24, 42-57.

Sabatini, D.M. (2006). mTOR and cancer: insights into a complex relationship. *Nat Rev Cancer* 6, 729-734.

Sabatini, D.M., Erdjument-Bromage, H., Lui, M., Tempst, P., and Snyder, S.H. (1994). RAFT1: a mammalian protein that binds to FKBP12 in a rapamycin-dependent fashion and is homologous to yeast TORs. *Cell* 78, 35-43.

Saetre, F., Korseberg Hagen, L., Engedal, N., and Seglen, P.O. (2015). Novel steps in the autophagic-lysosomal pathway. *FEBS J*.

Saijilafu, Hur, E.M., Liu, C.M., Jiao, Z., Xu, W.L., and Zhou, F.Q. (2013). PI3K-GSK3 signalling regulates mammalian axon regeneration by inducing the expression of Smad1. *Nat Commun* 4, 2690.

Saleh, A., Roy Chowdhury, S.K., Smith, D.R., Balakrishnan, S., Tessler, L., Martens, C., Morrow, D., Schartner, E., Frizzi, K.E., Calcutt, N.A., and Fernyhough, P. (2013). Ciliary

neurotrophic factor activates NF-kappaB to enhance mitochondrial bioenergetics and prevent neuropathy in sensory neurons of streptozotocin-induced diabetic rodents. *Neuropharmacology* 65, 65-73.

Sarbassov, D.D., Ali, S.M., Kim, D.H., Guertin, D.A., Latek, R.R., Erdjument-Bromage, H., Tempst, P., and Sabatini, D.M. (2004). Rictor, a novel binding partner of mTOR, defines a rapamycin-insensitive and raptor-independent pathway that regulates the cytoskeleton. *Curr Biol* 14, 1296-1302.

Sato, T., Nakashima, A., Guo, L., and Tamanoi, F. (2009). Specific activation of mTORC1 by Rheb G-protein in vitro involves enhanced recruitment of its substrate protein. *J Biol Chem* 284, 12783-12791.

Schafer, C., Clapp, P., Welsh, M.J., Benndorf, R., and Williams, J.A. (1999). HSP27 expression regulates CCK-induced changes of the actin cytoskeleton in CHO-CCK-A cells. *The American journal of physiology* 277, C1032-1043.

Scherz-Shouval, R., Shvets, E., Fass, E., Shorer, H., Gil, L., and Elazar, Z. (2007). Reactive oxygen species are essential for autophagy and specifically regulate the activity of Atg4. *EMBO J* 26, 1749-1760.

Schneider, G.B., Hamano, H., and Cooper, L.F. (1998). In vivo evaluation of hsp27 as an inhibitor of actin polymerization: hsp27 limits actin stress fiber and focal adhesion formation after heat shock. *J Cell Physiol* 177, 575-584.

Schreiber, S.L., and Crabtree, G.R. (1992). The mechanism of action of cyclosporin A and FK506. *Immunol Today* 13, 136-142.

Schworer, C.M., Shiffer, K.A., and Mortimore, G.E. (1981). Quantitative relationship between autophagy and proteolysis during graded amino acid deprivation in perfused rat liver. *J Biol Chem* 256, 7652-7658.

Seit-Nebi, A.S., Datskevich, P., and Gusev, N.B. (2013). Commentary on paper: Small heat shock proteins and the cytoskeleton: an essential interplay for cell integrity? (Wettstein et al.). *Int J Biochem Cell Biol* 45, 344-346.

Shi, G., Shi, J., Liu, K., Liu, N., Wang, Y., Fu, Z., Ding, J., Jia, L., and Yuan, W. (2013). Increased miR-195 aggravates neuropathic pain by inhibiting autophagy following peripheral nerve injury. *Glia* 61, 504-512.

Shi, W.Y., Xiao, D., Wang, L., Dong, L.H., Yan, Z.X., Shen, Z.X., Chen, S.J., Chen, Y., and Zhao, W.L. (2012). Therapeutic metformin/AMPK activation blocked lymphoma cell growth via inhibition of mTOR pathway and induction of autophagy. *Cell Death Dis* 3, e275.

Shi, Y., Mosser, D.D., and Morimoto, R.I. (1998). Molecular chaperones as HSF1-specific transcriptional repressors. *Genes Dev* 12, 654-666.

- Shimizu, S., Honda, S., Arakawa, S., and Yamaguchi, H. (2014). Alternative macroautophagy and mitophagy. *Int J Biochem Cell Biol* 50, 64-66.
- Shimura, H., Miura-Shimura, Y., and Kosik, K.S. (2004). Binding of tau to heat shock protein 27 leads to decreased concentration of hyperphosphorylated tau and enhanced cell survival. *J Biol Chem* 279, 17957-17962.
- Shinohara, H., Inaguma, Y., Goto, S., Inagaki, T., and Kato, K. (1993). Alpha B crystallin and HSP28 are enhanced in the cerebral cortex of patients with Alzheimer's disease. *Journal of the neurological sciences* 119, 203-208.
- Shvets, E., and Elazar, Z. (2008). Autophagy-independent incorporation of GFP-LC3 into protein aggregates is dependent on its interaction with p62/SQSTM1. *Autophagy* 4, 1054-1056.
- Shvets, E., Fass, E., Scherz-Shouval, R., and Elazar, Z. (2008). The N-terminus and Phe52 residue of LC3 recruit p62/SQSTM1 into autophagosomes. *Journal of cell science* 121, 2685-2695.
- Simon, D., Seznec, H., Gansmuller, A., Carelle, N., Weber, P., Metzger, D., Rustin, P., Koenig, M., and Puccio, H. (2004). Friedreich ataxia mouse models with progressive cerebellar and sensory ataxia reveal autophagic neurodegeneration in dorsal root ganglia. *J Neurosci* 24, 1987-1995.
- Singh, R., and Cuervo, A.M. (2011). Autophagy in the cellular energetic balance. *Cell Metab* 13, 495-504.
- Smith, D.S., and Skene, J.H. (1997). A transcription-dependent switch controls competence of adult neurons for distinct modes of axon growth. *The Journal of neuroscience : the official journal of the Society for Neuroscience* 17, 646-658.
- Soliman, G.A., Acosta-Jaquez, H.A., Dunlop, E.A., Ekim, B., Maj, N.E., Tee, A.R., and Fingar, D.C. (2010). mTOR Ser-2481 autophosphorylation monitors mTORC-specific catalytic activity and clarifies rapamycin mechanism of action. *J Biol Chem* 285, 7866-7879.
- Stokoe, D., Engel, K., Campbell, D.G., Cohen, P., and Gaestel, M. (1992). Identification of MAPKAP kinase 2 as a major enzyme responsible for the phosphorylation of the small mammalian heat shock proteins. *FEBS letters* 313, 307-313.
- Straume, O., Shimamura, T., Lampa, M.J., Carretero, J., Oyan, A.M., Jia, D., Borgman, C.L., Soucheray, M., Downing, S.R., Short, S.M., *et al.* (2012). Suppression of heat shock protein 27 induces long-term dormancy in human breast cancer. *Proceedings of the National Academy of Sciences of the United States of America* 109, 8699-8704.
- Su, W.C., Chao, T.C., Huang, Y.L., Weng, S.C., Jeng, K.S., and Lai, M.M. (2011). Rab5 and class III phosphoinositide 3-kinase Vps34 are involved in hepatitis C virus NS4B-induced autophagy. *J Virol* 85, 10561-10571.

- Sudnitsyna, M.V., Mymrikov, E.V., Seit-Nebi, A.S., and Gusev, N.B. (2012). The role of intrinsically disordered regions in the structure and functioning of small heat shock proteins. *Curr Protein Pept Sci* 13, 76-85.
- Sugiyama, Y., Suzuki, A., Kishikawa, M., Akutsu, R., Hirose, T., Waye, M.M., Tsui, S.K., Yoshida, S., and Ohno, S. (2000). Muscle develops a specific form of small heat shock protein complex composed of MKBP/HSPB2 and HSPB3 during myogenic differentiation. *J Biol Chem* 275, 1095-1104.
- Sun, X., Fontaine, J.M., Rest, J.S., Shelden, E.A., Welsh, M.J., and Benndorf, R. (2004). Interaction of human HSP22 (HSPB8) with other small heat shock proteins. *J Biol Chem* 279, 2394-2402.
- Sun, X., Zhou, Z., Fink, D.J., and Mata, M. (2013). HspB1 silences translation of PDZ-RhoGEF by enhancing miR-20a and miR-128 expression to promote neurite extension. *Molecular and cellular neurosciences* 57, 111-119.
- Sun, Y., Meng, G.M., Guo, Z.L., and Xu, L.H. (2011). Regulation of heat shock protein 27 phosphorylation during microcystin-LR-induced cytoskeletal reorganization in a human liver cell line. *Toxicol Lett* 207, 270-277.
- Suzuki, K., Kirisako, T., Kamada, Y., Mizushima, N., Noda, T., and Ohsumi, Y. (2001). The pre-autophagosomal structure organized by concerted functions of APG genes is essential for autophagosome formation. *EMBO J* 20, 5971-5981.
- Tang, D., Kang, R., Livesey, K.M., Kroemer, G., Billiar, T.R., Van Houten, B., Zeh, H.J., 3rd, and Lotze, M.T. (2011). High-mobility group box 1 is essential for mitochondrial quality control. *Cell metabolism* 13, 701-711.
- Theriault, J.R., Lambert, H., Chavez-Zobel, A.T., Charest, G., Lavigne, P., and Landry, J. (2004). Essential role of the NH2-terminal WD/EPF motif in the phosphorylation-activated protective function of mammalian Hsp27. *J Biol Chem* 279, 23463-23471.
- Tian, F., Deguchi, K., Yamashita, T., Ohta, Y., Morimoto, N., Shang, J., Zhang, X., Liu, N., Ikeda, Y., Matsuura, T., and Abe, K. (2010). In vivo imaging of autophagy in a mouse stroke model. *Autophagy* 6, 1107-1114.
- Tissieres, A., Mitchell, H.K., and Tracy, U.M. (1974). Protein synthesis in salivary glands of *Drosophila melanogaster*: relation to chromosome puffs. *J Mol Biol* 84, 389-398.
- Tosaki, T., Kamiya, H., Yasuda, Y., Naruse, K., Kato, K., Kozakae, M., Nakamura, N., Shibata, T., Hamada, Y., Nakashima, E., *et al.* (2008). Reduced NGF secretion by Schwann cells under the high glucose condition decreases neurite outgrowth of DRG neurons. *Exp Neurol* 213, 381-387.
- Toth, M.E., Szegedi, V., Varga, E., Juhasz, G., Horvath, J., Borbely, E., Csibrany, B., Alfoldi, R., Lenart, N., Penke, B., and Santha, M. (2013). Overexpression of Hsp27 ameliorates symptoms of Alzheimer's disease in APP/PS1 mice. *Cell Stress Chaperones* 18, 759-771.

- Towns, R., Guo, C., Shangguan, Y., Hong, S., and Wiley, J.W. (2008a). Type 2 diabetes with neuropathy: autoantibody stimulation of autophagy via Fas. *Neuroreport* 19, 265-269.
- Towns, R., Kabeya, Y., Yoshimori, T., Guo, C., Shangguan, Y., Hong, S., Kaplan, M., Klionsky, D.J., and Wiley, J.W. (2005). Sera from patients with type 2 diabetes and neuropathy induce autophagy and colocalization with mitochondria in SY5Y cells. *Autophagy* 1, 163-170.
- Towns, R., Pietropaolo, M., and Wiley, J.W. (2008b). Stimulation of autophagy by autoantibody-mediated activation of death receptor cascades. *Autophagy* 4, 715-716.
- Tucker, B.A., and Mearow, K.M. (2008). Peripheral sensory axon growth: from receptor binding to cellular signaling. *The Canadian journal of neurological sciences Le journal canadien des sciences neurologiques* 35, 551-566.
- Tucker, B.A., Rahimtula, M., and Mearow, K.M. (2005a). Integrin activation and neurotrophin signaling cooperate to enhance neurite outgrowth in sensory neurons. *The Journal of comparative neurology* 486, 267-280.
- Tucker, B.A., Rahimtula, M., and Mearow, K.M. (2005b). A procedure for selecting and culturing subpopulations of neurons from rat dorsal root ganglia using magnetic beads. *Brain research Brain research protocols* 16, 50-57.
- Tucker, B.A., Rahimtula, M., and Mearow, K.M. (2006). Laminin and growth factor receptor activation stimulates differential growth responses in subpopulations of adult DRG neurons. *The European journal of neuroscience* 24, 676-690.
- Tucker, B.A., Rahimtula, M., and Mearow, K.M. (2008). Src and FAK are key early signalling intermediates required for neurite growth in NGF-responsive adult DRG neurons. *Cell Signal* 20, 241-257.
- van Montfort, R., Slingsby, C., and Vierling, E. (2001a). Structure and function of the small heat shock protein/alpha-crystallin family of molecular chaperones. *Adv Protein Chem* 59, 105-156.
- van Montfort, R.L., Basha, E., Friedrich, K.L., Slingsby, C., and Vierling, E. (2001b). Crystal structure and assembly of a eukaryotic small heat shock protein. *Nat Struct Biol* 8, 1025-1030.
- Van Why, S.K., Mann, A.S., Ardito, T., Thulin, G., Ferris, S., Macleod, M.A., Kashgarian, M., and Siegel, N.J. (2003). Hsp27 associates with actin and limits injury in energy depleted renal epithelia. *Journal of the American Society of Nephrology : JASN* 14, 98-106.
- Verma, P., Chierzi, S., Codd, A.M., Campbell, D.S., Meyer, R.L., Holt, C.E., and Fawcett, J.W. (2005). Axonal protein synthesis and degradation are necessary for efficient growth cone regeneration. *J Neurosci* 25, 331-342.
- Verschuure, P., Croes, Y., van den, I.P.R., Quinlan, R.A., de Jong, W.W., and Boelens, W.C. (2002). Translocation of small heat shock proteins to the actin cytoskeleton upon proteasomal inhibition. *Journal of molecular and cellular cardiology* 34, 117-128.

- Vigilanza, P., Aquilano, K., Rotilio, G., and Ciriolo, M.R. (2008). Transient cytoskeletal alterations after SOD1 depletion in neuroblastoma cells. *Cell Mol Life Sci* 65, 991-1004.
- Vinik, A.I., Nevoret, M.L., Casellini, C., and Parson, H. (2013). Diabetic neuropathy. *Endocrinol Metab Clin North Am* 42, 747-787.
- Vollrath, J.T., Sechi, A., Dreser, A., Katona, I., Wiemuth, D., Vervoorts, J., Dohmen, M., Chandrasekar, A., Prause, J., Brauers, E., *et al.* (2014). Loss of function of the ALS protein SigR1 leads to ER pathology associated with defective autophagy and lipid raft disturbances. *Cell Death Dis* 5, e1290.
- Vos, M.J., Hageman, J., Carra, S., and Kampinga, H.H. (2008). Structural and functional diversities between members of the human HSPB, HSPH, HSPA, and DNAJ chaperone families. *Biochemistry* 47, 7001-7011.
- Wang, J.T., Medress, Z.A., and Barres, B.A. (2012). Axon degeneration: molecular mechanisms of a self-destruction pathway. *The Journal of cell biology* 196, 7-18.
- Wang, Q.J., Ding, Y., Kohtz, D.S., Mizushima, N., Cristea, I.M., Rout, M.P., Chait, B.T., Zhong, Y., Heintz, N., and Yue, Z. (2006a). Induction of autophagy in axonal dystrophy and degeneration. *The Journal of neuroscience : the official journal of the Society for Neuroscience* 26, 8057-8068.
- Wang, T., Wang, Q., Song, R., Zhang, Y., Zhang, K., Yuan, Y., Bian, J., Liu, X., Gu, J., and Liu, Z. (2015). Autophagy Plays a Cytoprotective Role During Cadmium-Induced Oxidative Damage in Primary Neuronal Cultures. *Biol Trace Elem Res*.
- Wang, X., Khaleque, M.A., Zhao, M.J., Zhong, R., Gaestel, M., and Calderwood, S.K. (2006b). Phosphorylation of HSF1 by MAPK-activated protein kinase 2 on serine 121, inhibits transcriptional activity and promotes HSP90 binding. *J Biol Chem* 281, 782-791.
- Watson, D.F., Nachtman, F.N., Kuncl, R.W., and Griffin, J.W. (1994). Altered neurofilament phosphorylation and beta tubulin isotypes in Charcot-Marie-Tooth disease type 1. *Neurology* 44, 2383-2387.
- Welsh, M.J., and Gaestel, M. (1998). Small heat-shock protein family: function in health and disease. *Ann N Y Acad Sci* 851, 28-35.
- Wettstein, G., Bellaye, P.S., Kolb, M., Hammann, A., Crestani, B., Soler, P., Marchal-Somme, J., Hazoume, A., Gaudie, J., Gunther, A., *et al.* (2013). Inhibition of HSP27 blocks fibrosis development and EMT features by promoting Snail degradation. *FASEB journal : official publication of the Federation of American Societies for Experimental Biology* 27, 1549-1560.
- Wettstein, G., Bellaye, P.S., Micheau, O., and Bonniaud, P. (2012). Small heat shock proteins and the cytoskeleton: an essential interplay for cell integrity? *Int J Biochem Cell Biol* 44, 1680-1686.

- Wild, P., Farhan, H., McEwan, D.G., Wagner, S., Rogov, V.V., Brady, N.R., Richter, B., Korac, J., Waidmann, O., Choudhary, C., *et al.* (2011). Phosphorylation of the autophagy receptor optineurin restricts Salmonella growth. *Science* 333, 228-233.
- Wilhelmus, M.M., Boelens, W.C., Otte-Holler, I., Kamps, B., de Waal, R.M., and Verbeek, M.M. (2006a). Small heat shock proteins inhibit amyloid-beta protein aggregation and cerebrovascular amyloid-beta protein toxicity. *Brain Res* 1089, 67-78.
- Wilhelmus, M.M., Otte-Holler, I., Wesseling, P., de Waal, R.M., Boelens, W.C., and Verbeek, M.M. (2006b). Specific association of small heat shock proteins with the pathological hallmarks of Alzheimer's disease brains. *Neuropathology and applied neurobiology* 32, 119-130.
- Williams, K.L., and Mearow, K.M. (2011). Phosphorylation status of heat shock protein 27 influences neurite growth in adult dorsal root ganglion sensory neurons in vitro. *Journal of neuroscience research* 89, 1160-1172.
- Williams, K.L., Rahimtula, M., and Mearow, K.M. (2005). Hsp27 and axonal growth in adult sensory neurons in vitro. *BMC neuroscience* 6, 24.
- Williams, K.L., Rahimtula, M., and Mearow, K.M. (2006). Heat shock protein 27 is involved in neurite extension and branching of dorsal root ganglion neurons in vitro. *Journal of neuroscience research* 84, 716-723.
- Wu, R., Kausar, H., Johnson, P., Montoya-Durango, D.E., Merchant, M., and Rane, M.J. (2007). Hsp27 regulates Akt activation and polymorphonuclear leukocyte apoptosis by scaffolding MK2 to Akt signal complex. *J Biol Chem* 282, 21598-21608.
- Wytenbach, A., Sauvageot, O., Carmichael, J., Diaz-Latoud, C., Arrigo, A.P., and Rubinsztein, D.C. (2002). Heat shock protein 27 prevents cellular polyglutamine toxicity and suppresses the increase of reactive oxygen species caused by huntingtin. *Human molecular genetics* 11, 1137-1151.
- Xie, Z., He, C., and Zou, M.H. (2011). AMP-activated protein kinase modulates cardiac autophagy in diabetic cardiomyopathy. *Autophagy* 7, 1254-1255.
- Xie, Z., Nair, U., and Klionsky, D.J. (2008). Atg8 controls phagophore expansion during autophagosome formation. *Mol Biol Cell* 19, 3290-3298.
- Xu, J.T., Zhao, X., Yaster, M., and Tao, Y.X. (2010). Expression and distribution of mTOR, p70S6K, 4E-BP1, and their phosphorylated counterparts in rat dorsal root ganglion and spinal cord dorsal horn. *Brain research* 1336, 46-57.
- Yadav, R.B., Burgos, P., Parker, A.W., Iadevaia, V., Proud, C.G., Allen, R.A., O'Connell, J.P., Jeshtadi, A., Stubbs, C.D., and Botchway, S.W. (2013). mTOR direct interactions with Rheb-GTPase and raptor: sub-cellular localization using fluorescence lifetime imaging. *BMC Cell Biol* 14, 3.

- Yamamoto, A., Tagawa, Y., Yoshimori, T., Moriyama, Y., Masaki, R., and Tashiro, Y. (1998). Bafilomycin A1 prevents maturation of autophagic vacuoles by inhibiting fusion between autophagosomes and lysosomes in rat hepatoma cell line, H-4-II-E cells. *Cell Struct Funct* 23, 33-42.
- Yang, X., Khosravi-Far, R., Chang, H.Y., and Baltimore, D. (1997). Daxx, a novel Fas-binding protein that activates JNK and apoptosis. *Cell* 89, 1067-1076.
- Yang, Y., Chen, S., Zhang, J., Li, C., Sun, Y., Zhang, L., and Zheng, X. (2014). Stimulation of autophagy prevents amyloid-beta peptide-induced neuritic degeneration in PC12 cells. *Journal of Alzheimer's disease : JAD* 40, 929-939.
- Yang, Y., Fukui, K., Koike, T., and Zheng, X. (2007). Induction of autophagy in neurite degeneration of mouse superior cervical ganglion neurons. *The European journal of neuroscience* 26, 2979-2988.
- Yip, C.K., Murata, K., Walz, T., Sabatini, D.M., and Kang, S.A. (2010). Structure of the human mTOR complex I and its implications for rapamycin inhibition. *Mol Cell* 38, 768-774.
- Yunoki, T., Tabuchi, Y., Hayashi, A., and Kondo, T. (2013). Inhibition of polo-like kinase 1 promotes hyperthermia sensitivity via inactivation of heat shock transcription factor 1 in human retinoblastoma cells. *Invest Ophthalmol Vis Sci* 54, 8353-8363.
- Zhao, Y., Huang, Q., Yang, J., Lou, M., Wang, A., Dong, J., Qin, Z., and Zhang, T. (2010). Autophagy impairment inhibits differentiation of glioma stem/progenitor cells. *Brain Res* 1313, 250-258.
- Zheng, S., Clabough, E.B., Sarkar, S., Futter, M., Rubinsztein, D.C., and Zeitlin, S.O. (2010). Deletion of the huntingtin polyglutamine stretch enhances neuronal autophagy and longevity in mice. *PLoS genetics* 6, e1000838.
- Zhou, X., Wang, L., Hasegawa, H., Amin, P., Han, B.X., Kaneko, S., He, Y., and Wang, F. (2010). Deletion of PIK3C3/Vps34 in sensory neurons causes rapid neurodegeneration by disrupting the endosomal but not the autophagic pathway. *Proceedings of the National Academy of Sciences of the United States of America* 107, 9424-9429.
- Zhu, N., Li, M.G., Guan, Y.J., Schreyer, D.J., and Chen, X.B. (2010). Effects of laminin blended with chitosan on axon guidance on patterned substrates. *Biofabrication* 2, 045002.
- Zochodne, D.W., Ramji, N., and Toth, C. (2008). Neuronal targeting in diabetes mellitus: a story of sensory neurons and motor neurons. *Neuroscientist* 14, 311-318.
- Zou, J., Guo, Y., Guettouche, T., Smith, D.F., and Voellmy, R. (1998). Repression of heat shock transcription factor HSF1 activation by HSP90 (HSP90 complex) that forms a stress-sensitive complex with HSF1. *Cell* 94, 471-480.

## Appendix

### Appendix A: Cytoskeleton, Inc. *In vitro* actin binding protein assay biochemistry kit: G- and F-actin preparation protocol.

See <http://www.cytoskeleton.com/actin/kits> for a full protocol with additional background material.

Abbreviated Protocol:

F-actin preparation

1. Thaw out one 100 $\mu$ L aliquot of 100mM ATP stock and place on ice.
2. Dilute thawed ATP aliquot to 10mM ATP with 900 $\mu$ L of cold sterile water.
3. Aliquot 250 $\mu$ L of general actin buffer (5mM Tris-HCl, pH 8.0, and 0.2mM CaCl<sub>2</sub>) and supplement with 5 $\mu$ L of 10mM ATP to give a final concentration of 0.2mM ATP.
4. Thaw one 250 $\mu$ g aliquot of actin in a room temperature bath and transfer to ice immediately after the protein has thawed.
5. Dilute the actin to 1mg/mL with 225 $\mu$ L of ATP supplemented general actin buffer, and completely resuspend by pipetting.
6. Leave on ice for 30mins.
7. Defrost one aliquot of actin polymerization buffer (500mM KCl, 20mM MgCl<sub>2</sub>, 10mM ATP, 10X solution) and keep on ice. Use within 4 hr after thawing.
8. Pipette 25 $\mu$ L of actin polymerization buffer into the actin protein solution, and mix well by pipetting.
9. Incubate the actin protein solution at room temperature (~24°C) for 1 hr. This is an F-actin stock of 21 $\mu$ M actin.

G-actin preparation

1. Thaw out one 100 $\mu$ L aliquot of 100mM ATP stock and place on ice.
2. Dilute thawed ATP aliquot to 10mM ATP with 900 $\mu$ L of cold sterile water.
3. Aliquot 250 $\mu$ L of general actin buffer (5mM Tris-HCl, pH 8.0, and 0.2mM CaCl<sub>2</sub>) and supplement with 5 $\mu$ L of 10mM ATP to give a final concentration of 0.2mM ATP.
4. Thaw one 250 $\mu$ g aliquot of actin in a room temperature bath and transfer to ice immediately after the protein has thawed.
5. Dilute the actin to 1mg/mL with 225 $\mu$ L of ATP supplemented general actin buffer, and completely resuspend by pipetting.
6. Leave on ice for 30 mins.
7. Add an additional 25 $\mu$ L of ATP supplemented general actin buffer, and mix well by pipetting.
8. Leave on ice for 1 hr. This is a G-actin stock at 21 $\mu$ M actin

## Appendix B: Qiagen RNeasy® Plus Micro kit: cellular RNA isolation protocol.

See <https://www.qiagen.com/ca/shop/sample-technologies/rna/rna-preparation/rneasy-micro-kit#resources> for a full protocol with additional background material.

Abbreviated Protocol:

Before starting

- Add either 10µL β-mercaptoethanol, or 20µL 2M dithiothreitol, to 1mL buffer RLT before use if purifying RNA from cell lines or tissues rich in RNases.
  - For a working buffer RPE solution add 4 volumes of ethanol (96-100%).
  - When preparing DNase I stock solution, dissolve lyophilized DNase I in 550µL RNase-free water, and mix gently by inverting the vial. Store DNase I as single-use aliquots at -20°C for up to 9 months. Do not refreeze after thawing.
1. Harvest a maximum of  $5 \times 10^5$  cells as a pellet, or by direct lysis in the cell culture vessel. Add 350µL buffer RLT and homogenize. Centrifuge the lysates for 3 min at maximum speed. Carefully remove the supernatant by pipetting and use for step 2.
  2. Add 1 volume of 70% ethanol to the lysates and mix well by pipetting. Do not centrifuge.
  3. Transfer the sample, with any precipitate, to an RNeasy MinElute spin column in a 2mL collection tube. Close the lid and centrifuge for 15 sec at  $\geq 8000 \times g$ . Discard the flow-through
  4. Add 350µL buffer RW1 to the RNeasy MinElute spin column. Close the lid and centrifuge for 15 sec at  $\geq 8000 \times g$ . Discard the flow-through
  5. Add 10µL DNase I stock solution to 70µL buffer RDD. Mix by inverting the tube. Add the DNase I incubation mix (80µL) directly to the RNeasy MinElute spin column membrane. Place on the benchtop at room temperature (20-30°C) for 15 min. Add

350µL buffer RW1 to the RNeasy MinElute spin column. Close the lid and centrifuge for 15 sec at  $\geq 8000 \times g$ . Discard the collection tube.

6. Place the RNeasy MinElute spin column in a new 2mL collection tube. Add 500µL buffer RPE to the spin column. Close the lid and centrifuge for 15 sec at  $\geq 8000 \times g$ . Discard the flow-through.
7. Add 500µL of 80% ethanol to the RNeasy MinElute spin column. Close the lid and centrifuge for 2 min at  $\geq 8000 \times g$ . Discard the collection tube.
8. Place the RNeasy MinElute spin column in a new 2mL collection tube. Open the lid of the spin column and centrifuge at full speed for 5 min to dry the membrane. Discard the flow-through and collection tube.
9. Place the RNeasy MinElute spin column in a new 1.5mL collection tube. Add 14µL RNase-free water directly to the center of the spin column membrane. Close the lid gently and centrifuge for 1 min at full speed to elute the RNA.

## Appendix C: Agilent 6000 Nano kit: RNA integrity determination protocol.

See <http://www.genomics.agilent.com/en/product.jsp?cid=AG-PT-105&tabId=AG-PR-1172&requestid=78375> for a full protocol with additional background material.

Abbreviated Protocol:

Storage Conditions

- Freeze unopened RNA ladder at -20°C. Prepared ladder aliquots need to be stored at -70°C. Keep all other reagents and reagent mixes refrigerated at 4°C when not in use to avoid poor results caused by reagent decomposition.
- Protect dye and dye mixtures from light. Remove light covers only when pipetting. Dye decomposes when exposed to light.

Setting up the Chip Priming Station

1. Replace the syringe:
  - a. Unscrew the old syringe from the lid of the chip priming station.
  - b. Release the old syringe from the clip and discard the old syringe.
  - c. Remove the plastic cap of the new syringe and insert it into the clip
  - d. Slide it into the hole of the luer lock adapter and screw it tightly to the chip priming station
2. Adjust the base plate:
  - a. Open the chip priming station by pulling the latch.
  - b. Using a screwdriver, open the screw at the underside of the base plate
  - c. Lift the base plate and insert it again in position, and retighten the screw.
3. Adjust the syringe clip:
  - a. Release the lever of the clip and slide it up to the top position.

### Essential measurement practices

- Heat denature all RNA samples and RNA ladder before use for 2 min at 70°C and keep them on ice.
- Use loaded chips within 5 min after preparation. Reagents might evaporate, leading to poor results.

### Preparing the RNA Ladder

1. Spin the ladder down and pipette in an RNase-free vial.
2. Heat denature the ladder for 2 min at 70°C, and immediately cool the vial on ice.
3. Prepare aliquots in 0.5mL RNase-free vials with the required amount for typical daily use.
4. Store aliquots at -70°C. After initial heat denaturation, the frozen aliquots should not require repeated heat denaturation.
5. Before use, thaw ladder aliquots on ice, and avoid extensive warming.

### Preparing the Gel

1. Pipette 550µL of RNA gel matrix into a spin filter.
2. Centrifuge at 1500 x g for 10 min at room temperature
3. Aliquot 65µL filtered gel into 0.5 mL RNase- free microcentrifuge tubes. Use filtered gel within 4 weeks. Store at 4°C.

### Preparing the Gel-Dye Mix

1. Allow the RNA dye concentrate to equilibrate to room temperature for 30 min.
2. Vortex RNA dye concentrate for 10 sec, spin down and add 1µL of dye into a 65µL aliquot of filtered gel.

3. Vortex solution well. Spin tube at 13000 x g for 10min at room temperature. Use prepared gel-dye mix within one day.

#### Loading the Gel-Dye Mix

1. Put a new RNA chip on the chip priming station.
2. Pipette 9 $\mu$ L of gel-dye mix in the well marked (G).
3. Make sure that the plunger is positioned at 1mL and then close the chip priming station.
4. Press plunger until it is held by the clip.
5. Wait for exactly 30 sec then release clip.
6. Wait for 5sec. Slowly pull back plunger to 1mL position.
7. Open the chip priming station and pipette 9 $\mu$ L of gel-dye mix in the wells marked (ladder).
8. Discard the remaining gel-dye mix.

#### Loading the Marker

1. Pipette 5  $\mu$ L of RNA marker in all 12 sample wells and in the well marked (ladder).

#### Loading the Ladder and Samples

1. Pipette 1 $\mu$ L of prepared ladder in well marked (ladder).
2. Pipette 1 $\mu$ L of sample in each of the 12 sample wells. Pipette 1 $\mu$ L of RNA Marker in each unused sample well.
3. Put the chip horizontally in the IKA vortexer and vortex for 1min at 2400 rpm.
4. Run the chip in the Agilent 2100 Bioanalyzer instrument within 5 min.

**Appendix D: Invitrogen SuperScript® III First-Strand Synthesis System: complimentary DNA (cDNA) reaction protocol.**

See <https://www.thermofisher.com/order/catalog/product/18080051> for a full protocol with additional background material.

Abbreviated Protocol:

First-Strand cDNA Synthesis

- The following procedure is designed to convert 1pg - 5µg of total RNA into first-strand cDNA
1. Combine the following in a 0.2 or 0.5mL tube:

Component	Amount
Up to 5µg total RNA	<i>n</i> µL
Primer (50ng/µL random hexamers)	1µL
10mM dNTP mix	1µL
DEPC-treated water	Up to 10µL

2. Incubate the tube at 65°C for 5 min, then place on ice for at least 1 min.
3. Prepare the following cDNA synthesis mix , adding each component in the indicated order:

Component	1 Reaction	10 Reactions
10X RT buffer	2µL	20µL
25mM MgCl <sub>2</sub>	4µL	40µL
0.1 dithiothreitol	2µL	20µL
RNaseOUT™ (40U/µL)	1µL	10µL
SuperScript® III RT (200U/ µL)	1µL	10µL

4. Add 10µL of cDNA synthesis mix to each RNA/primer mixture, mix gently, and collect by brief centrifuge. Incubate as follows:
  - o Random hexamer primed: 10 min at 25°C, followed by 50 min at 50°C.
5. Terminate the reactions at 85°C for 5 min. Chill on ice.

6. Collect the reactions by brief centrifugation. Add 1 $\mu$ L of RNase H to each tube and incubate the tubes for 20 min at 37°C.
7. cDNA synthesis reactions can be stored at -30°C to -10°C or used for PCR immediately.

**Appendix E: Promega Cell Titer 96® AQueous MTS Reagent and PMS: Cell viability quantification using the MTS colorimetric technique.**

See <http://www.promega.ca/products/cell-health-and-metabolism/cell-viability-assays/celltiter-96-aqueous-non-radioactive-cell-proliferation-assay- mts /> for a full protocol with additional background material.

Abbreviated Protocol:

Background

The MTS tetrazolium compound is bio-reduced by cells into a colored formazan product that is soluble in tissue culture medium. This conversion is presumably accomplished by NADPH or NADH produced by dehydrogenase enzymes in metabolically active cells. Assays are performed by adding a small amount of the CellTiter 96® AQueous MTS Reagent with PMS directly into culture wells, incubating for 1-4 hr and then recording the absorbance at 490nm with a 96-well plate reader. The quantity of formazan product as measured by absorbance at 490nm is directly proportional to the number of living cells in culture.

General protocol

1. Thaw one aliquot of CellTiter 96® AQueous MTS Reagent and one aliquot of PMS. It should take approximately 90 minutes at room temperature, or 10 minutes in a water bath at 37°C, to completely thaw.
2. Mix the thawed CellTiter 96® AQueous MTS Reagent and PMS, and pipet 20µl of the mix into each well of the 96-well assay plate containing the cell samples in culture medium.
3. Incubate the plate at 37°C for 1–4 hr in a humidified, 5% CO<sub>2</sub> atmosphere.

4. Record the absorbance at 490nm using a 96-well plate reader. Note: the higher the absorbance detected, the more formazan product is present, indicating more metabolically active cells.

## **Appendix F.1: ThermoFisher Scientific CellROX® Green Reagent for oxidative stress detection: Oxidative stress quantification protocol.**

See <https://www.thermofisher.com/order/catalog/product/C10444> for a full protocol with additional background material.

Abbreviated Protocol:

Background

CellROX® Green oxidative stress reagent is a cell-permeable reagent that is non-fluorescent or very weakly fluorescent in a reduced state. Upon oxidation, CellROX® green binds to DNA and exhibits a strong fluorescent signal. Its signal is primarily localized in the nucleus and mitochondria; the signals for CellROX® Deep Red and CellROX® Orange, however, are localized primarily in the cytoplasm. Fluorescence signal expression can be measured by traditional fluorescence microscopy, with the presence of oxidative stress being measured by counting cells that have positive nuclear staining for CellROX® Green and comparing them to cells that do not have any nuclear staining.

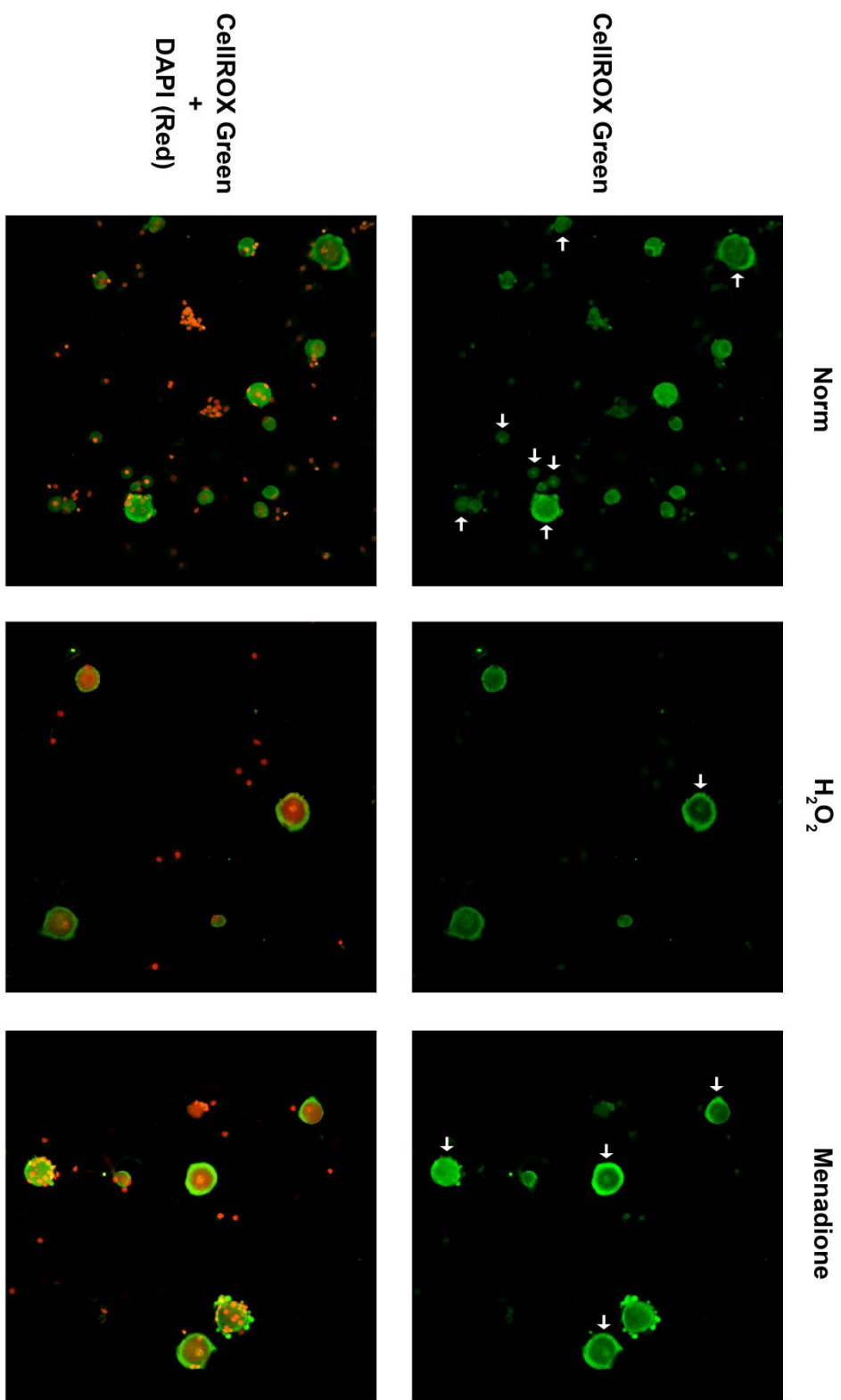
General Protocol

1. Treat cells with the test compound or drug and incubate for recommended or experimental time-frame.
2. Add CellROX® Green reagent at a final concentration of 5µM to the cells and incubate for 30 mins at 37°C.
3. Remove all medium and wash cells three times with PBS
4. Prepare cells for immunocytochemistry, using DAPI as a nuclear stain.

5. Visualize cells using fluorescence microscopy, counting total cell numbers, and comparing cells with positive nuclear CellROX® Green staining to those without nuclear staining.

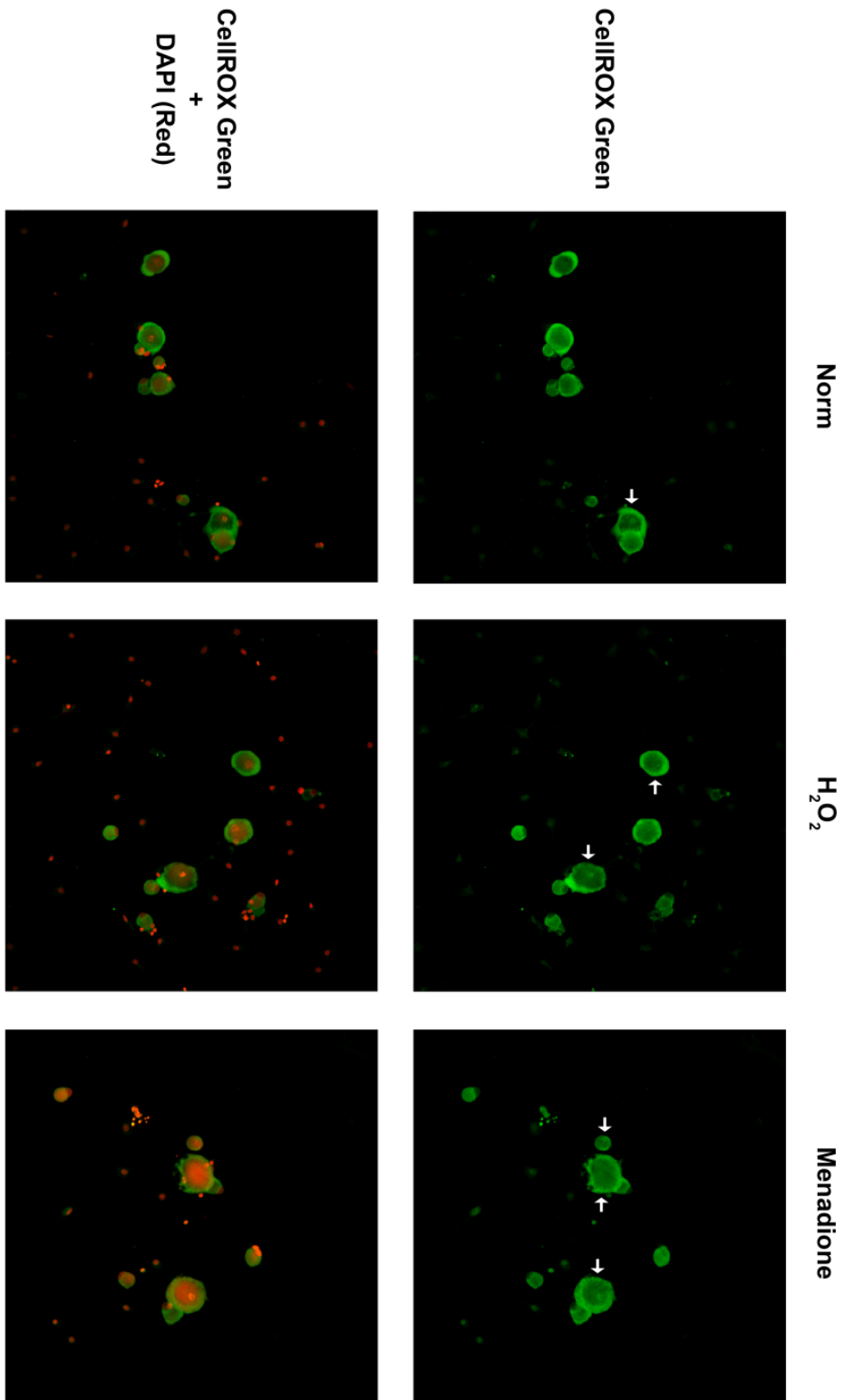
**Appendix G.2: ThermoFisher Scientific CellROX® Green Reagent for oxidative stress detection: DRG neuron images showing that H<sub>2</sub>O<sub>2</sub> causes oxidative stress after 30 mins of treatment.**

DRG neurons were grown on poly-D-lysine and laminin coated 16-well slides at ~1000 cells/well for 24 hr. Cultures were then treated with H<sub>2</sub>O<sub>2</sub> (10mM), menadione (10μM) or culture media for 30 mins. Cells were further treated with CellROX® Green Reagent (5μM) and immunostained with DAPI (red) to stain for DRG nuclei. DRG neurons that had CellROX® reagent localized within their nuclei were quantified. Arrows indicate DRG neurons that have a positive nuclear stain for both CellROX® Green and DAPI (red).



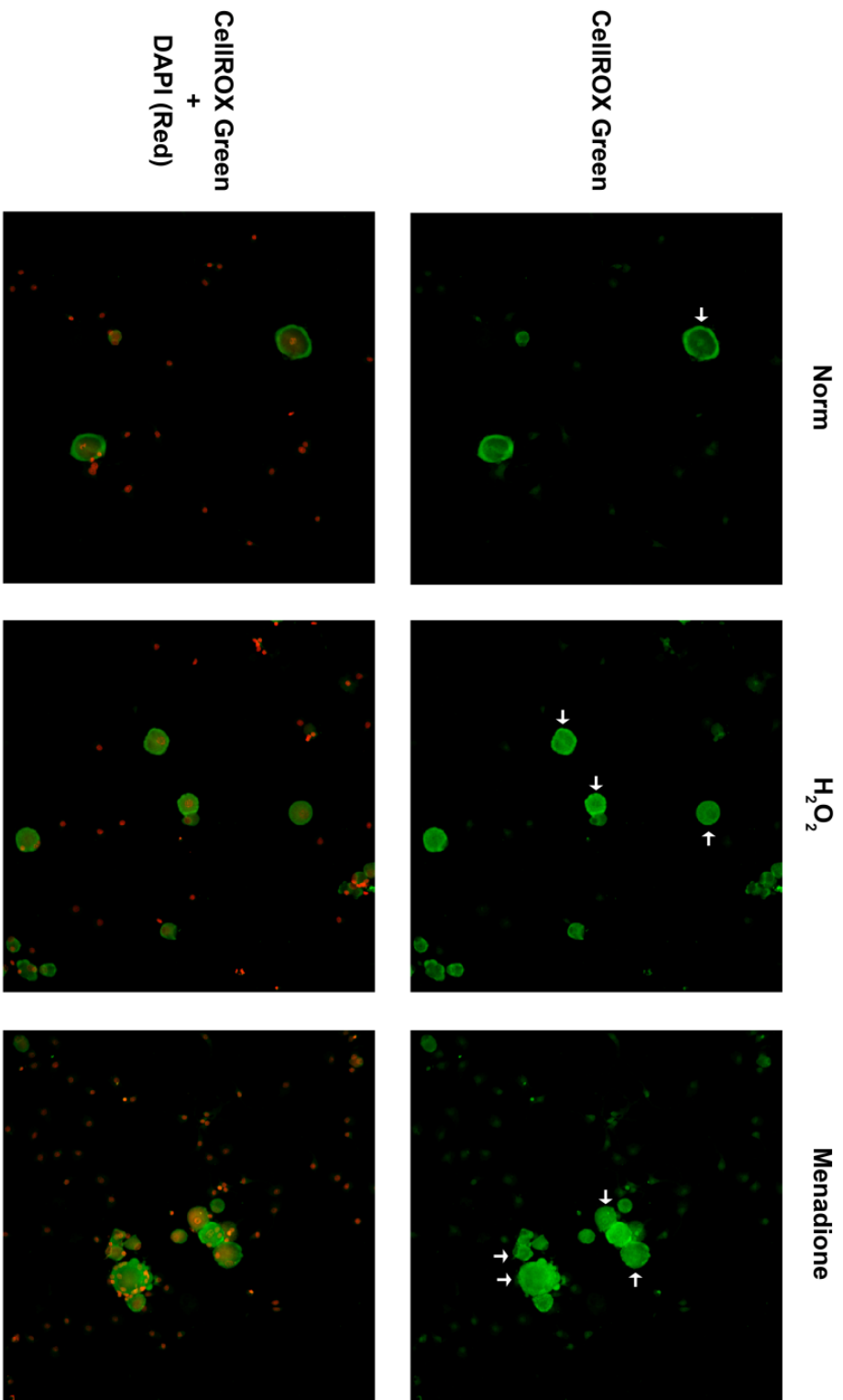
**Appendix H.3: ThermoFisher Scientific CellROX® Green Reagent for oxidative stress detection: DRG neuron images showing that H<sub>2</sub>O<sub>2</sub> causes oxidative stress after 1 hr of treatment.**

DRG neurons were grown on poly-D-lysine and laminin coated 16-well slides at ~1000 cells/well for 24 hr. Cultures were then treated with H<sub>2</sub>O<sub>2</sub> (10mM), menadione (10μM) or culture media for 1 hr. Cells were further treated with CellROX® Green Reagent (5μM) and immunostained with DAPI (red) to stain for DRG nuclei. DRG neurons that had CellROX® reagent localized within their nuclei were quantified. Arrows indicate DRG neurons that have a positive nuclear stain for both CellROX® Green and DAPI (red).



**Appendix I.4: ThermoFisher Scientific CellROX® Green Reagent for oxidative stress detection: DRG neuron images showing that H<sub>2</sub>O<sub>2</sub> causes oxidative stress after 2 hr of treatment.**

DRG neurons were grown on poly-D-lysine and laminin coated 16-well slides at ~1000 cells/well for 24 hr. Cultures were then treated with H<sub>2</sub>O<sub>2</sub> (10mM), menadione (10μM) or culture media for 2 hr. Cells were further treated with CellROX® Green Reagent (5μM) and immunostained with DAPI (red) to stain for DRG nuclei. DRG neurons that had CellROX® reagent localized within their nuclei were quantified. Arrows indicate DRG neurons that have a positive nuclear stain for both CellROX® Green and DAPI (red).



**Appendix J.5: ThermoFisher Scientific CellROX® Green Reagent for oxidative stress detection: DRG neuron images showing that H<sub>2</sub>O<sub>2</sub> causes oxidative stress after 3 hr of treatment.**

DRG neurons were grown on poly-D-lysine and laminin coated 16-well slides at ~1000 cells/well for 24 hr. Cultures were then treated with H<sub>2</sub>O<sub>2</sub> (10mM), menadione (10μM) or culture media for 3 hr. Cells were further treated with CellROX® Green Reagent (5μM) and immunostained with DAPI (red) to stain for DRG nuclei. DRG neurons that had CellROX® reagent localized within their nuclei were quantified. Arrows indicate DRG neurons that have a positive nuclear stain for both CellROX® Green and DAPI (red).

